Investigations into the pharmacological action of vioprolide A on inflammatory and angiogenic processes in endothelial cells

Dissertation

zur Erlangung des Doktorgrades
der Naturwissenschaften

vorgelegt beim Fachbereich 14
der Johann Wolfgang Goethe-Universität
in Frankfurt am Main

von

Luisa Dominique Burgers

aus Bad Dürkheim

Frankfurt (2021)

(D 30)

vom Fachbereich Biochemie, Chemie und Pharmazie (FB 14) der

Johann Wolfgang Goethe-Universität als Dissertation angenommen.

Dekan: Prof. Dr. Clemens Glaubitz

1. Gutachter: Prof. Dr. Robert Fürst

2. Gutachter: Prof. Dr. Rolf Marschalek

Datum der Disputation: 10.03.2022

With deep gratitude and love dedicated to my family

Zoals het klokje thuis tikt, tikt het nergens

TABLE OF CONTENTS

Abbreviations

Table 1: List of abbreviations

Abbreviation	Full name
4E-BP	Eukaryotic translation initiation factor 4E-binding protein
aa-tRNA	Aminoacyl transfer ribonucleic acid
ALL	Acute lymphocytic leukemia
AML	Acute monocytic leukemia
ANOVA	Analysis of variance
APAF1	Apoptotic protease activating factor 1
APC	Adenomatous polyposis coli
APS	Ammonium persulfate
A-site	Acceptor site
ASK1	Apoptosis-signal-regulating kinase 1
ATP	Adenosine triphosphate
Bak	B cell lymphoma antagonist/killer
Bax	B cell lymphoma-associated X protein
BCA	Bicinchoninic acid
Bcl-2	B cell lymphoma 2
bFGF	Basic fibroblast growth factor
BMDM	Bone marrow derived macrophage
BrdU	Bromodeoxyuridine
BSA	Bovine serum albumin
CAM	Cell adhesion molecule
CAPS	3-(Cyclohexylamino)-1-propanesulfonic acid
CAS	Cellular apoptosis susceptibility
CD99	Cluster of differentiation
cDNA	Copy deoxyribonucleic acid
CETSA	Cellular thermal shift assay
CHX	Cycloheximide
CNV	Choroidal neovascularization

Abbreviation	Full name
CTGF	Connective tissue growth factor
Cyr61	Cysteine-rich angiogenic inducer 61
DAMP	Damage/danger-associated molecular pattern
Dll4	Delta-like ligand 4
DMSO	Dimethyl sulfoxide
DNA	Deoxyribonucleic acid
Doxo	Doxorubicin
DTT	1,4-Dithiothreitol
E-cadherin	Epithelial cadherin
ECGM	Endothelial cell growth medium
ECL	Enhanced chemiluminescent solution
EDTA	Ethylenediaminetetraacetic acid
eEF	Eukaryotic elongation factor
EGF	Epidermal growth factor
EGFR	Epidermal growth factor receptor
EGTA	Ethylene Glycol-bis-(beta-aminoethylether)-N,N,N‘,N‘-tetraacetic acid
eIF	Eukaryotic initiation factor
eNOS	Endothelial nitric oxide synthase
eRF	Eukaryotic release factor
ERK	Extracellular-signal regulated kinase
E-site	Entry site
EV	Extracellular vesicle
FCS	Foetal calf serum
FFA	Fundus fluorescein angiography
FGFR	Fibroblast growth factor receptor
GPCR	G-protein-coupled receptor
GTP	Guanosine triphosphate
HFS	Hypotonic fluorescent solution
HIF	Hypoxia-inducible factor

Abbreviation	Full name
HMEC	Human dermal microvascular endothelial cell
HRP	Horseradish peroxidase
HS	Heparan sulfate
HUVEC	Human umbilical vein endothelial cell
IB4	Isolectin B4
Iba1	Ionized calcium binding adaptor molecule 1
IBB	Importin beta binding
ICAM-1	Intracellular adhesion molecule 1
IκBα	Inhibitor of nuclear factor kappa B
IKK	Inhibitor of nuclear factor kappa B kinase
IL	Interleukin
iNOS	Inducible nitric oxide synthase
JNK	c-Jun N-terminal kinase
KDR	Kinase insert domain receptor
KPN	Karyopherin
LATS1/2	Large tumour suppressor kinase 1/2
LDH	Lactate dehydrogenase
LFA-1	Lymphocyte function-associated antigen 1
LSM	Lymphocyte separation medium
Mac-1	Macrophage-1 antigen
MAML	Mastermind like transcriptional coactivator
MAPK	Mitogen-activated protein kinase
MAPKK	MAPK kinase
MAPKKK	MAPK kinase kinase
MAZ	Trans-(2*S*, 4*R*)-4-methylazetidinecarboxylic acid
Mcl-1	Myeloid cell leukemia 1
MDM2	Mouse double minute 2 homolog
Met-tRNA	Methionyl-transfer ribonucleic acid
MMP	Matrix metalloproteinase

Abbreviation	Full name
MNK	Mitogen-activated protein kinase-interacting kinase
MRE	microRNA response element
mRNA	Messenger ribonucleic acid
MST1/2	Mammalian STE20-like protein kinase 1/2
mTOR	Mammalian target of rapamycin
NAD	Nicotinamide adenine dinucleotide
NADH	Reduced nicotinamide adenine dinucleotide
NEMO	Nuclear factor kappa B essential modulator
NES	Nuclear export sequence
NF-κB	Nuclear factor kappa B
NLS	Nuclear localization sequence
NO	Nitric oxide
NOP14	Nucleolar protein 14
NPC	Nuclear pore complex
OPP	O-propargyl-puromycin
PAMP	Pathogen-associated molecular pattern
PARP	Poly ADP ribose polymerase
PBMC	Peripheral blood mononuclear cell
PBS	Phosphate-buffered saline
PCR	Polymerase chain reaction
PDGF	Platelet derived growth factor
PECAM-1	Platelet endothelial cell adhesion molecule 1
PH	Pleckstrin homology
PI	Propidium iodide
PI3K	Phosphoinositide 3 kinase
PIP_3	Phosphatidylinositol-3,4,5-triphosphate
PL	Primary lymphocyte
PlGF	Placental growth factor
PMSF	Phenylmethylsufonyl fluoride

Abbreviation	Full name
PSGL-1	P-selectin glycoprotein ligand 1
P-site	Peptidyl site
PTEN	Phosphatase and tensin homolog
RA	Rheumatoid arthritis
RHD	Rel homology domain
RNA	Ribonucleic acid
ROCK	Ras homolog gene family kinase
ROS	Reactive oxygen species
RPE	Retinal pigment epithelium
rRNA	Ribosomal ribonucleic acid
RSK	Ribosomal S6 kinase
RTK	Receptor tyrosine kinase
SAM	S-adenosylmethionine
Scl	Stem cell leukemia
SDF-1	Stromal cell-derived factor 1
SDS	Sodium dodecylsulfate
SDS-PAGE	Sodium dodecylsulfate polyacrylamide gel electrophoresis
SEM	Standard error of the mean
siRNA	Small interfering ribonucleic acid
snoRNA	Small nucleolar ribonucleic acid
TACE	Tumour necrosis factor-α converting enzyme
T_{agg}	Aggregation temperature
TAK1	Transforming growth factor beta-activated kinase 1
TAZ	Transcriptional coactivator with PDZ-binding motif
TBS	Tris-buffered saline
TC	Ternary complex
TEAD	TEA DNA binding domain
TEMED	Tetramethylethylenediamine
TFPI	Tissue factor pathway inhibitor

Abbreviation	Full name
TGF	Transforming growth factor
Tie2	Tyrosine kinase with immunoglobulin-like and EGF-like domains 2
TKI	Tyrosine kinase inhibitor
TNF	Tumour necrosis factor
TNFR	Tumour necrosis factor receptor
tRNA	Transfer ribonucleic acid
UPR	Unfolded protein response
UTR	Untranslated region
VCAM-1	Vascular cell adhesion molecule 1
VE-cadherin	Vascular endothelial cadherin
VEGF	Vascular endothelial growth factor
VEGFR	Vascular endothelial growth factor receptor
VioA	Vioprolide A
VLA-4	Very late antigen 4
VSMC	Vascular smooth muscle cell
vWF	von Willebrand factor
YAP	Yes-associated protein

List of figures

List of tables

I SUMMARY

The vascular endothelium is a monolayer of endothelial cells that builds the inner lining of the blood vessels and constitutes a regulatory organ within the physiological system to sustain homeostasis. Endothelial cells participate in physiological processes including inflammation and angiogenesis. Dysregulation of these processes, however, can evoke or maintain pathological disorders, including cardiovascular and chronic inflammatory diseases or cancer. Although pathological inflammation and angiogenesis represent treatable conditions, current pharmacotherapeutic approaches are frequently not satisfying since their long-term application can evoke therapy resistance and thus reduced clinical efficacy. Consequently, there is an ongoing demand for the discovery of new therapeutic targets and drug leads. Considering that endothelial cells play a critical role in both angiogenesis and inflammation, the vascular endothelium represents a promising target for the treatment of diseases.

Vioprolide A is a secondary metabolite isolated from the myxobacterium *Cystobacter violaceus* Cb. vi35. Recently, vioprolide A was identified to interact with NOP14, a nucleolar protein involved in ribosome biogenesis. Ribosome biogenesis is an indispensable cellular event that ensures adequate homeostasis. Abnormal alterations in the ribosome biogenesis, referred to as ribosomopathies, however, can lead to an overall increase in the risk of developing cancer. Accordingly, several studies have outlined the involvement of NOP14 in cancer progression and metastasis, and vioprolide A has been demonstrated to exert anti-cancer effects *in vitro*. However, the impact of vioprolide A and NOP14 on the endothelium has been neglected so far, although endothelial cells are crucially involved in inflammation and angiogenesis under both physiological and pathological conditions.

In the present study, the effect of vioprolide A on inflammatory and angiogenic actions was analysed. *In vivo*, the laser-induced choroidal neovascularization (CNV) assay outlined a strong inhibitory effect of vioprolide A on both inflammation and angiogenesis. Furthermore, intravital microscopy of the cremaster muscle in mice revealed that vioprolide A strongly impaired the TNF-induced leukocyte-endothelial cell interaction *in vivo*.

In further experiments, the specific effect of vioprolide A on activation processes of primary human umbilical vein endothelial cells (HUVECs) was examined. According to the *in vivo* results, vioprolide A decreased the leukocyte-endothelial cell interaction *in vitro* through downregulating the cell surface expression and total protein expression of ICAM-1, VCAM-1 and E-selectin. Vioprolide A evoked its anti-inflammatory actions via a dual mechanism: On the one hand, the expression of pro-inflammatory proteins, including TNFR1 and cell adhesion molecules, was lowered through a general downregulation of *de novo* protein synthesis. The inhibition of *de novo* protein synthesis is most likely linked to the interaction with and inhibition of NOP14 by vioprolide A in HUVECs. On the other hand, the natural product prevented the nuclear translocation and promotor activity of the pro-inflammatory transcription factor NF-κB. Interestingly, most anti-inflammatory compounds that interfere with the NF-κB signaling

pathway prevent NF-κB nuclear translocation through recovering or stabilizing the inhibitory IκB proteins. Vioprolide A, however, decreased rather than stabilized the IκB proteins and prevented NF-κB nuclear translocation through interfering with its importin-dependent nuclear import. By performing siRNA-mediated knockdown experiments, we evaluated the role of NOP14 in inflammatory processes in HUVECs and could establish a causal link between the anti-inflammatory actions of vioprolide A and the deletion of NOP14.

Besides exerting anti-inflammatory actions, we found that vioprolide A potently decreased the angiogenic key features proliferation, migration and sprouting of endothelial cells. Mechanistically, the natural product interfered with pro-angiogenic signaling pathways. Vioprolide A reduced the protein level of growth factor receptors, including VEGFR2, which is the most prominent receptor responsible for angiogenic signaling in endothelial cells. This effect was based on the general inhibition of *de novo* protein synthesis by the natural product. Downregulation of growth factor receptors impaired the activation of downstream signaling intermediates, including the MAPKs ERK, JNK and p38. To our surprise, however, activation of Akt, another downstream effector of VEGFR2, was increased rather than decreased. Furthermore, vioprolide A lowered the nuclear translocation of the transcriptional coactivator TAZ, which is regulated by the evolutionary conserved Hippo signaling pathway. Interestingly, however, and in contrast to NF-κB, TAZ nuclear translocation in mammalian cells seems to be independent of importins. In this context, we found that vioprolide A reduced both the protein level and nuclear localization of MAML1, which is needed to retain TAZ in the nucleus after its successful translocation.

Although ribosome biogenesis is a fundamental cellular mechanism and its inhibition has been shown to induce apoptosis, vioprolide A induced pro-survival effects in HUVECs by hampering caspase-3 activation. This effect was mediated by an upregulation of the pro-survival kinase Akt and through impeding DNA damage-induced activation of p53 and expression of its apoptosis-mediating target genes NOXA and APAF1.

Taken together, this study presents vioprolide A as dual inhibitor of both inflammatory and angiogenic actions in endothelial cells and provides first insights into the underlying modes of action including the discovery of a cell-type specific activation of pro-survival signaling. Considering that crosstalk between inflammation and angiogenesis is regularly observed and that pathological conditions like rheumatoid arthritis and psoriasis are characterized by mutual reinforcement of both processes, vioprolide A represents a unique compound with an innovative cellular target that could serve as promising experimental approach for the treatment of diseases characterized by excessive angiogenesis and inflammation without harming normal, healthy cells.

II ZUSAMMENFASSUNG

Endothelzellen bilden die innerste Wand der Blutgefäße und sind in einer Einzelschicht entlang der gesamten Grenzfläche zwischen Blut und Gewebe angeordnet, vom Herz bis zur kleinsten Kapillare. Als endokrines Organ übt das Endothel vielfältige Aufgaben im physiologischen System aus, um die Homöostase aufrechtzuerhalten und Änderungen der Umgebung zu verarbeiten. Physiologische Funktionen des Endothels umfassen die Regulation der Hämostase, des Gefäßtonus und der vaskulären Permeabilität. Weiterhin vermittelt das Endothel die selektive Extravasation von Leukozyten aus dem Blut in das umliegende Gewebe und ist somit maßgeblich an Entzündungsreaktionen beteiligt. Endothelzellen spielen außerdem eine Schlüsselrolle bei der Gefäßneubildung, der sogenannten Angiogenese. Da das Endothel eine zentrale Rolle bei vielfältigen physiologischen Prozessen spielt, ist es nicht verwunderlich, dass Fehlfunktionen gravierende Folgen für den gesamten Organismus haben und zu pathologischen Veränderung führen können, die mit chronischen Entzündungen, kardiovaskulären Erkrankungen, Diabetes und Krebs assoziiert sind.

Akute Entzündungen werden als Reaktion auf Infektionen und Verletzungen ausgelöst. Im geschädigten Gewebe freigesetzte Botenstoffen rufen typische Symptome einer Entzündung wie Schwellung und Rötung hervor und locken weitere Immunzellen an, die zur Beseitigung der Entzündungsursache beitragen. Endothelzellen vermitteln den Austritt der angelockten Leukozyten aus dem Blut in das umliegende Gewebe über einen mehrstufigen Prozess, der als Leukozytendiapedese bezeichnet wird. Dabei wird zunächst durch Integrine und Adhäsionsmoleküle auf der Zelloberfläche eine feste Bindung zwischen Leukozyten und Endothelzellen ausgebildet. Anschließend wandern die Leukozyten parazellulär oder transzellulär durch das Endothel hindurch in das Gewebe. Unter normalen Bedingungen klingt die Entzündung rechtzeitig ab und es kommt zu einer Wiederherstellung der Homöostase. Kann die Entzündungsreaktion auf Grund von Fehlfunktionen nicht beendet werden, kommt es zu chronisch-pathologischen Reaktionen, die langfristig Gewebsschäden hervorrufen und die Entstehung von Krebs begünstigen. Diese chronischen Entzündungsreaktionen sind häufig durch eine krankhafte Überaktivierung des Endothels und eine damit verbundene permanente Leukozytendiapedese in das Gewebe gekennzeichnet.

Das kardiovaskuläre System spielt eine entscheidende Rolle in der Versorgung des Gewebes mit Sauerstoff und Nährstoffen und im Abtransport von Stoffwechselprodukten. Die Entstehung erster primitiver Blutgefäße aus endothelialen Vorläuferzellen wird als Vaskulogenese bezeichnet. Angiogenese hingegen beschreibt die Bildung von neuen Blutgefäßen aus bereits vorhandenen Gefäßstrukturen, was der Erweiterung sowie Modifikation des vaskulären Systems dient. Im ausgewachsenen Organismus befindet sich das Endothel zumeist im Ruhezustand und muss zunächst durch bestimmte Signalmoleküle aktiviert werden. Physiologisch ist dies beispielsweise der Fall während des Menstruationszyklus, der Schwangerschaft und der Wundheilung. Das wichtigste angiogene Signalmolekül ist der

vaskuläre endotheliale Wachstumsfaktor (VEGF). VEGF bindet an membranständige Rezeptoren mit Tyrosinkinase-Aktivität, die VEGF-Rezeptoren 1-3 (VEGFR1-3). Insbesondere der VEGFR2 ist durch seine hohe Enzym-Aktivität maßgeblich an der Induktion nachgeschalteter, intrazellulärer, angiogener Prozesse beteiligt, die zur Aussprossung, Migration und Proliferation von Endothelzellen und somit zur Entstehung neuer Blutgefäße führen. Fehlfunktionen dieser endothelialen Prozesse stellen wichtige Faktoren für die Entstehung, Aufrechterhaltung und das Fortschreiten zahlreicher Krankheiten dar wie kardiovaskuläre Erkrankungen, altersbedingte Makuladegeneration, Diabetes und Krebs.

Obwohl sowohl entzündliche Prozesse als auch krankhafte Gefäßneubildungen behandelbar sind, weisen viele Therapieoptionen Nachteile wie Resistenzentwicklung und verminderte Behandlungseffizienz bei Langzeitgabe auf. Daher spielen die Entdeckung und Charakterisierung neuer zellulärer Angriffspunkte und Arzneistoff-Leitstrukturen weiterhin eine große Rolle in der Forschung.

Naturstoffe sind eine wichtige Quelle für die Entdeckung neuer potenzieller Leitstrukturen. Zu den effektivsten Produzenten bioaktiver Naturstoffe zählen die Myxobakterien. Bekannte Sekundär-Metabolite aus Myxobakterien sind zum Beispiel das Mikrotubuli-destabilisierende Tubulysin oder der Aktin-Binder Chrondramid. Vioprolid A ist ein Metabolit aus dem Myxobakterium *Cystobacter violaceus*. Strukturell handelt es sich um ein Depsipeptid aus mehreren Aminosäuren sowie einer sehr seltenen trans-(2*S*, 4*R*)-4-Methylazetidcarbonsäure. Kürzlich wurde entdeckt, dass Vioprolid A in Krebszellen mit dem nucleolären Protein NOP14 interagiert. NOP14 ist an der Biogenese der kleinen ribosomalen 40S-Untereinheit beteiligt. Die Ribosom-Biogenese und die nachgeschaltete Proteinsynthese an den ausgereiften Ribosomen stellen wesentliche Faktoren für die Aufrechterhaltung der zellulären Homöstase dar. Immer häufiger wird allerdings von Funktionsstörungen der Ribosomen-Biogenese, sogenannten Ribosomopathien, berichtet, die zu einem erhöhten Krebs-Risiko führen. In diesem Zusammenhang konnte gezeigt werden, dass Vioprolid A das Wachstum von Krebszellen in vitro effizient verringern kann.

Obwohl Endothelzellen maßgeblich an physiologischen und pathologischen Prozessen beteiligt sind, wurde der Einfluss von Vioprolid A und NOP14 auf das Endothel bisher vernachlässigt. Aus diesem Grund war das Ziel der vorliegenden Arbeit, die Effekte von Vioprolid A und NOP14 auf inflammatorische und angiogene Prozesse im Endothel zu untersuchen und die zugrundeliegenden Wirkmechanismen aufzuklären.

Um einen ersten Einblick in die Effekte von Vioprolid A auf inflammatorische und angiogene Prozesse zu erhalten, wurden In-vivo-Experimente durchgeführt. In der Laser-induzierten choroidalen Neovascularisation (CNV) wird die Bruch-Membran des Auges an definierten Stellen durch einen Laser zerstört. Im Anschluss kann das Ausmaß an Gefäßneubildung sowie die Einwanderung von Immunzellen und Endothelzellen in die zerstörten Bereiche durch

Immunfluoreszenz-Mikroskopie bestimmt werden. Eine Behandlung des Auges mit Vioprolid A führte zu einer signifikanten Reduktion der Gefäßneubildung sowie der Einwanderung von Mikrogliazellen, Makrophagen und Endothelzellen in die Bereiche um die Laser-Läsionen. Folglich war Vioprolid A in der Lage, sowohl entzündliche als auch angiogene Prozesse in vivo zu unterbinden. Da die Leukozytendiapedese einen wichtigen Schritt in der Rekrutierung von Leukozyten zum Entzündungsort darstellt, wurde in einem weiteren Schritt die Leukozyten-Endothelzell-Interaktion in vivo mittels Intravitalmikroskopie des Mäuse-Kremastermuskels untersucht. Während Vioprolid A das Rollen der Leukozyten auf dem Endothel leicht, aber nicht signifikant, erhöhte, wurden sowohl die Adhäsion der Leukozyten an das Endothel als auch deren Transmigration durch das Endothel hindurch signifikant vermindert.

Basierend auf den Ergebnissen der In-vivo-Studien wurden weitere In-vitro-Experimente mit primären Endothelzellen aus der Nabelschnurvene (HUVECs) durchgeführt, um die Beteiligung von Endothelzellen an den antientzündlichen und antiangiogenen Effekten von Vioprolid A besser beurteilen zu können. Zunächst konnten wir feststellen, dass Konzentrationen bis zu 10 nM Vioprolid A keinen negativen Einfluss auf die Viabilität von HUVECs hatten. Mittels Thermal-Shift-Assay, einer biochemischen Methode zur Untersuchung der Thermostabilität eines Proteins nach Zugabe eines Bindungspartners, konnte weiterhin verifiziert werden, dass NOP14 nicht nur in Jurkat-Zellen sondern auch in HUVECs ein Interaktionspartner von Vioprolid A ist. Da NOP14 an der Ribosomen-Biogenese beteiligt ist, wurde in einem weiteren Schritt bestimmt, ob sich eine Behandlung mit Vioprolid A auf die Protein-de-novo-Synthese auswirkt. In der Tat führte die Gabe von Vioprolid A zu einer konzentrations- und zeitabhängigen Reduktion der sich neu bildenden Polypeptide.

Anschließend wurden die antientzündlichen Effekte von Vioprolide A tiefergehend untersucht. Zelladhäsions- und Transmigrations-Experimente dienten dazu, die Leukozyten-Endothelzell-Interaktion in vitro zu analysiert. Hierfür wurden unterschiedliche primäre leukozytäre Zellen und Zelllinien verwendet. Entsprechend der beobachteten In-vivo-Effekte, reduzierte die Gabe von Vioprolide A die Adhäsion von Leukozyten an und deren Transmigration durch das TNF-aktivierte Endothel auch in vitro. Wir konnten feststellen, dass die verminderte Leukozyten-Adhäsion auf einer Reduktion der Oberflächen- und totalen Expression von Zelladhäsions-molekülen wie ICAM-1, VCAM-1 und E-Selektin auf und in HUVECs beruhte. Obwohl auch die TNF-induzierte Transkription der Zelladhäsionsmoleküle vermindert war, übte Vioprolid A einen stärker inhibierenden Effekt auf das Proteinlevel als auf das mRNA Level von ICAM-1, VCAM-1 und E-Selektin aus. Daraus lässt sich schließen, dass Vioprolid A seine anti-entzündlichen Eigenschaften über einen dualen Mechanismus vermittelt. Zum einen inhibierte der Naturstoff effektiv die Aktivierung des pro-inflammatorischen NF-κB Signalwegs, indem er die Translokation der NF-κB-Untereinheit p65 in den Zellkern sowie die Promotoraktivität des Transkriptionsfaktors NF-κB beeinträchtigte. Die Translation der mRNA, die auf Grund der

Restaktivität des Transkriptionsfaktors trotzdem noch gebildet wurde, konnte wirksam durch die allgemeine Herunterregulierung der Protein-de-novo-Synthese verhindert werden. Die meisten anti-inflammatorischen Substanzen reduzieren die Translokation von NF-κB-Untereinheiten, indem sie den Abbau des inhibitorischen Proteins IκBα verhindern oder zu einer schnellen Erholung des IκBα-Proteinlevels führen. Vioprolid A verringerte jedoch bereits den basalen IκBα-Proteinlevel in Abwesenheit eines Entzündungsstimulus. Daher konnte ein stabilisierender Effekt auf IκBα als Ursache für die verminderte Translokation der NF-κB-Untereinheit ausgeschlossen werden. Vielmehr verringerte Vioprolid A die Translokation von p65 durch ein Eingreifen in den Importin-abhängigen Importmechanismus von p65 durch den Kernporenkomplex in den Zellkern. Interessanterweise führte eine siRNA-induzierte Herunterregulierung von NOP14 in HUVECs zu ähnlichen anti-entzündlichen Effekten wie eine Behandlung mit Vioprolid A. Daraus lässt sich auf einen kausalen Zusammenhang zwischen den Effekten von Vioprolide A und der Interaktion mit NOP14 schließen.

In einem weiteren Schritt wurden die Effekte von Vioprolid A auf angiogene Prozesse in makrovaskulären HUVECs und in der mikrovaskulären humanen Zelllinie HMEC-1 untersucht. Dabei konnte gezeigt werden, dass der Naturstoff alle essenziellen Teilschritte der angiogenen Kaskade, inklusive der Aussprossung, Migration und Proliferation von Endothelzellen, verringerte. Gleichzeitig verursachte Vioprolid A eine Anhäufung von Zellen in der G_0/G_1-Phase des Zellzyklus und eine prozentuale Verringerung der Zellen in der S-Phase. Übereinstimmend damit war auch die DNA-Synthese in HUVECs, die mittels eines Bromdesoxyuridin-Assays ermittelt wurde, stark inhibiert. Im weiteren Verlauf wurde der zugrunde liegende Mechanismus der anti-angiogenen Effekte von Vioprolid A analysiert. In diesem Zusammenhang konnten mehrere Wirkmechanismen identifiziert werden, die (mit)verantwortlich für die Aktivitäten von Vioprolid A sind. Vioprolid A bewirkte über die Inhibition der Protein-de-novo-Synthese eine verminderte Expression der membranständigen Tyrosinkinase-Rezeptoren VEGFR2, EGFR und FGFR1. In der Folge wurde zum einen die Aktivierung des VEGFR2 selbst und zum anderen die Phosphorylierung nachfolgender intrazellulärer Kinasen, wie die MAPKs ERK, JNK und p38, durch Vioprolid A unterbunden. Überraschenderweise führte Vioprolid A gleichzeitig zu einer starken Phosphorylierung der Proteinkinase Akt, ein ebenfalls dem VEGFR2 nachgeschaltetes Protein. Obwohl eine Inhibition der Ribosomen-Biogenese zur Induktion von Apoptose führt, konnte Vioprolid A basierend auf der erhöhten Akt Aktivität sowie einer Inhibition der Caspase-3-Aktivierung zellspezifisch das Überleben von HUVECs fördern, was in Studien mit Krebszellen nicht gezeigt werden konnte.

Da der Einfluss von Vioprolid A auf die MAPKs zwar signifikant, aber nicht außergewöhnlich stark war, lag die Vermutung nahe, dass auch andere angiogene Signalwege in HUVECs durch Vioprolid A beeinflusst werden und das Zusammenspiel aus mehreren Faktoren zu den

stark ausgeprägten Effekten auf die angiogene Kaskade in Endothelzellen führt. Da der evolutionär konservierte Hippo-Signalweg angiogene Prozesse reguliert, wurde die Hypothese aufgestellt, dass er ein zusätzlicher Angriffspunkt von Vioprolid A sein könnte. In der Tat wurde die Translokation des transkriptionellen Co-Aktivators TAZ in den Zellkern und die darauffolgende Transkription von angiogenen Zielgenen wirkungsvoll von Vioprolid A unterbunden, ohne dass das Proteinlevel von TAZ beeinflusst wurde. Während die NF-κB-Untereinheiten über einen Importin-abhängigen Mechanismus in den Zellkern gelangen, nimmt TAZ nicht an diesem klassischen Import-Signalweg teil. Der genaue Mechanismus der Translokation von TAZ in den Zellkern ist bis heute nicht geklärt. Bekannt ist allerdings, dass das nukleäre Protein MAML1 die Menge an TAZ, die bereits in den Zellkern transloziert ist, im Zellkern zurückhält und einen schnellen Export zurück ins Cytosol verhindert. Die Gabe von Vioprolid A führte zu einer starken Reduktion von MAML1 im Zellkern sowie des allgemeinen MAML1-Proteinlevels. Basierend auf diesen Ergebnissen scheint ein Zusammenhang zwischen der reduzierten Translokation von TAZ und dem Einfluss von Vioprolid A auf MAML1 möglich.

Vergleichsstudien mit einer siRNA-induzierten Herunterregulierung von NOP14 in HUVECs führten zu widersprüchlichen Ergebnissen bezüglich der Beteiligung von NOP14 an den anti-angiogenen Effekten von Vioprolid A: Eine Inhibition von NOP14 reduzierte, ähnlich wie Vioprolide A, die Proliferation und Migration von Endothelzellen. Im Gegensatz dazu wurde die Aussprossung von Endothelzellen nach Inhibition von NOP14 verstärkt und nicht, wie bei Gabe von Vioprolid A, verringert. Diese Ergebnisse unterstreichen, dass die Aktivität von Vioprolid A auf das Endothel hochkomplex ist und dass die Interaktion mit NOP14 vermutlich nicht der einzige zugrunde liegende Mechanismus für die beobachteten hoch-potenten Effekte auf angiogene Prozesse ist.

Zusammengefasst konnte die vorliegende Arbeit Vioprolid A als dualen Inhibitor von entzündlichen und angiogenen Prozessen in vivo und im Endothel in vitro identifizieren. Weiterhin wurden erste Einblicke in die zugrundeliegenden Mechanismen gewonnen, die unter anderem einen Einfluss von Vioprolid A auf den VEGFR2- und Hippo-Signalweg sowie eine zellspezifische Erhöhung des Überlebens zeigten. Da Entzündungen und Angiogenese mit vielfältigen Erkrankungen assoziiert und häufig miteinander vergesellschaftet sind, zeigt Vioprolid A ein hoch interessantes pharmakologisches Spektrum. Vioprolid A präsentiert sich als vielversprechender Naturstoff mit innovativem zellulären Interaktionspartner, der in der translationalen Forschung bezüglich seines Nutzens zur Behandlung von Krebs und Krankheiten, die durch chronische Entzündungen oder Angiogenese charakterisiert sind, weiter evaluiert werden sollte.

III INTRODUCTION

1. The vascular endothelium

The vascular endothelium represents a monolayer of endothelial cells, which builds the inner lining of the blood vessels. While the luminal membrane of endothelial cells is directly exposed to blood constituents and blood cells, the basolateral site abuts a glycoprotein basement membrane.[1] Importantly, the vascular endothelium does not simply constitute a passive membrane between blood and tissue but a regulatory organ with highly complex functions in the physiological system serving to maintain homeostasis.[2] Endothelial cells differentiate from so called hemangioblasts, which are precursor cells of mesodermal origin.[3] A schematic overview of the differentiation of hemangioblasts into endothelial cells is given in Figure 1. In this context, endothelial markers such as tyrosine-protein kinase receptor (Tie2), vascular endothelial cadherin (VE-cadherin), CD31 and kinase insert domain receptor (KDR) are upregulated by vascular endothelial growth factor (VEGF) signaling and the expression of the stem cell leukemia (Scl) transcription factor.[4-6]

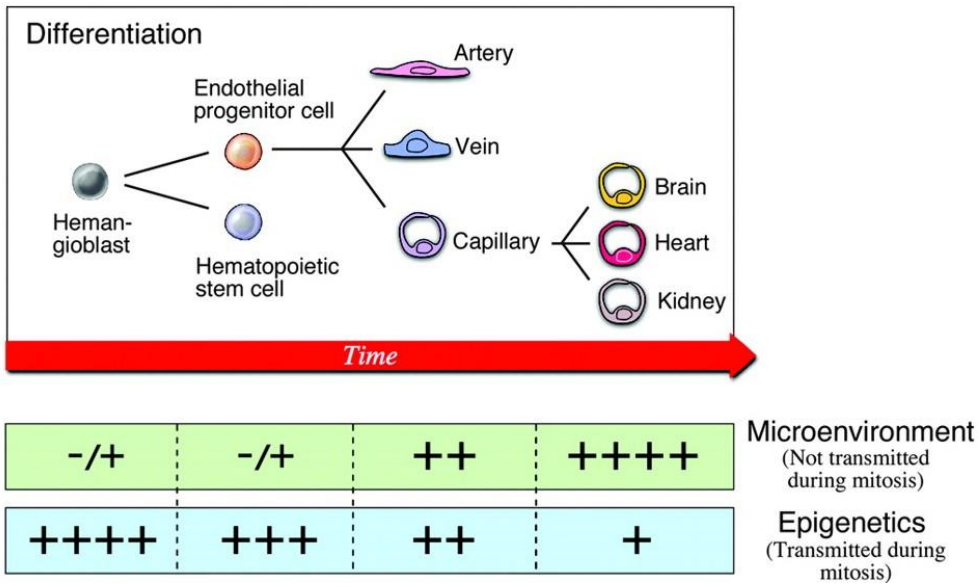

Figure 1: Differentiation of hemangioblasts into endothelial cells. Hemangioblasts can differentiate in endothelial progenitor cells, called angioblasts or hematopoietic stem cells. Through microenvironmental influences and epigenetic regulation mechanisms, angioblasts further differentiate to endothelial cells of arteries, veins and capillaries. The capillaries are further set apart depending on their localization in the brain, heart, or kidney. Reprinted with permission from Wolters Kluwer Health Inc. and Copyright Clearance Center: Wolters Kluwer, Circulation Research, Phenotypic heterogeneity of the endothelium, Aird WC, © 2007.[7]

1.1 Physiological properties of the vascular endothelium

The vascular endothelium is involved in a set of important physiological actions to provide homeostasis, including the regulation of blood fluidity and blood flow and the implementation of a barrier function.

1.1.1 Blood fluidity

Maintenance of blood fluidity by endothelial cells is mainly provided through inhibition of coagulation. On the cell surface, endothelial cells express tissue factor pathway inhibitors (TFPIs), heparan sulfate proteoglycans (HSs) and thrombomodulin. TFPIs hamper the complex of factor VII and tissue factor, thereby halting initiation of coagulation. HSs bind anti-thrombin III, which again captures circulating thrombin molecules generated by the coagulation cascade. Thrombomodulin interacts with thrombin, too and changes its cleavage substrate from pro-coagulating fibrinogen to anti-coagulating protein C.[8-10] Von Willebrand factor (vWF) is another important protein produced by endothelial cells. During physiological coagulation, vWF is secreted and induces the interaction of platelets with the basement membrane. Endothelial cells, however, withhold vWF from secretion through keeping it inside of intracellular storage bodies.[11] These cell surface structures act in concert by regulating the expression, storage and release of each other.[12]

1.1.2 Blood flow

Endothelial cells have a major role in maintaining and regulating the vascular tonus and consequently also modulate blood pressure. Therefore, the tonus of the surrounding vascular smooth muscle cells (VSMCs) is influenced through secretion of vasoactive mediators.[13] The release of these vasoactive mediators is initiated as response to mechanical or pharmacological stimuli.[14, 15] Relaxation of VSMCs and, thus, decreased vessel tone is mediated by vasodilatory factors, such as nitric oxide (NO), prostaglandin I_2 (PGI_2) or endothelium-derived hyperpolarizing factor.[16] Contraction of VSMCs and, thus, increased vessel tone is guided by vasoconstrictors including thromboxane and endothelin-1.[17, 18]

1.1.3 Barrier function and inflammation

Since endothelial cells create the border between the blood and the surrounding tissue, the endothelial monolayer exerts a barrier function, thereby controlling the extravasation of serum proteins and blood cells.[19] In this regard, the permeability of endothelial cells varies based on their anatomical location.[7] Different phenotypes and permeabilities of the vascular endothelium are shown in Figure 2.

Endothelial monolayers with the lowest permeability are found in continuous capillaries in the brain, skin, heart and lung. Here, tight and adherence junctions are integrated in the junctions between adjacent endothelial cells, which holds the cells tightly together. Only small molecules can pass the intercellular gaps between single endothelial cells, while larger molecules rely on an active transport.[20] In the endocrine glands, gastric and intestinal mucosa and glomeruli of the kidney, the permeability of the vascular endothelium is greater but still retains larger

molecules in the blood due to diaphragms in the fenestrae, which act as molecular filter. In the liver, the vascular endothelium is discontinuous without diaphragms also allowing large molecules to pass. In most tissues, the endothelial monolayer is tight enough to form a continuous barrier, which prevents the uncontrolled extravasation of cells and proteins as large as or larger than albumin. To still ensure that the tissue is supplied with larger molecules and cells when needed, endothelial cells can provide a controlled passage via vesicular transport or cell-cell interactions.[21] The endothelial barrier function plays a crucial role during inflammatory processes, where leukocytes from the blood need to reach the tissue site of inflammation.[22, 23] The process of inflammation is described more detailed in section III.2.

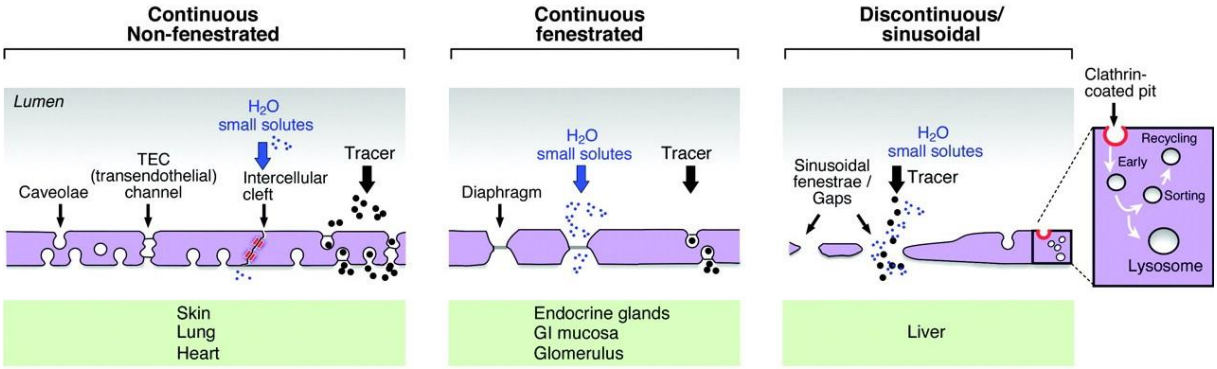

Figure 2: Phenotypes and permeability of the vascular endothelium. The endothelial monolayer executes a barrier function for the controlled extravasation of solutes, fluids and cells. The continuous, non-fenestrated endothelium in the heart, skin and lung only allows water and small solutes to pass, while larger molecules (tracer) are transported through channels or transcytosis. The continuous fenestrated endothelium, present in endocrine glands, gastric and intestinal mucosa and glomeruli of the kidney, provides a greater permeability but still prevents the diffusion of molecules as heavy or heavier as albumin as the diaphragms of the fenestrae function as molecular filter. Discontinuous endothelium is the most permeable form, which contains fenestrae without diaphragms. Here, clathrin-coated pits enable receptor-mediated endocytosis. Reprinted with permission from Wolters Kluwer Health Inc. and Copyright Clearance Center: Wolters Kluwer, Circulation Research, Phenotypic heterogeneity of the endothelium, Aird WC, © 2007.[7]

1.1.4 Angiogenesis

Endothelial cells are key players during the process of angiogenesis, the formation of new blood vessels from preexisting ones. This action is highly important during embryonic development but also during physiological processes in adults.[24, 25] The process of angiogenesis is described more detailed in section III.3.

1.2 Pathological conditions involving the vascular endothelium

Endothelial dysfunctions rise when the endothelial monolayer fails to execute its physiological properties. A schematic overview of the differences between healthy and dysfunctional endothelial cells is provided in Figure 3. Many pathological conditions, including cardiovascular and chronic inflammatory diseases, cancer and viral infections are connected to a dysfunction of the endothelium. Especially cardiovascular risk factors, like aging, smoking, obesity, the

metabolic syndrome, or physical inactivity represent possible causes for endothelial dysfunctions by increasing oxidative stress and impairing the availability of biological mediators, like NO.[26-30]

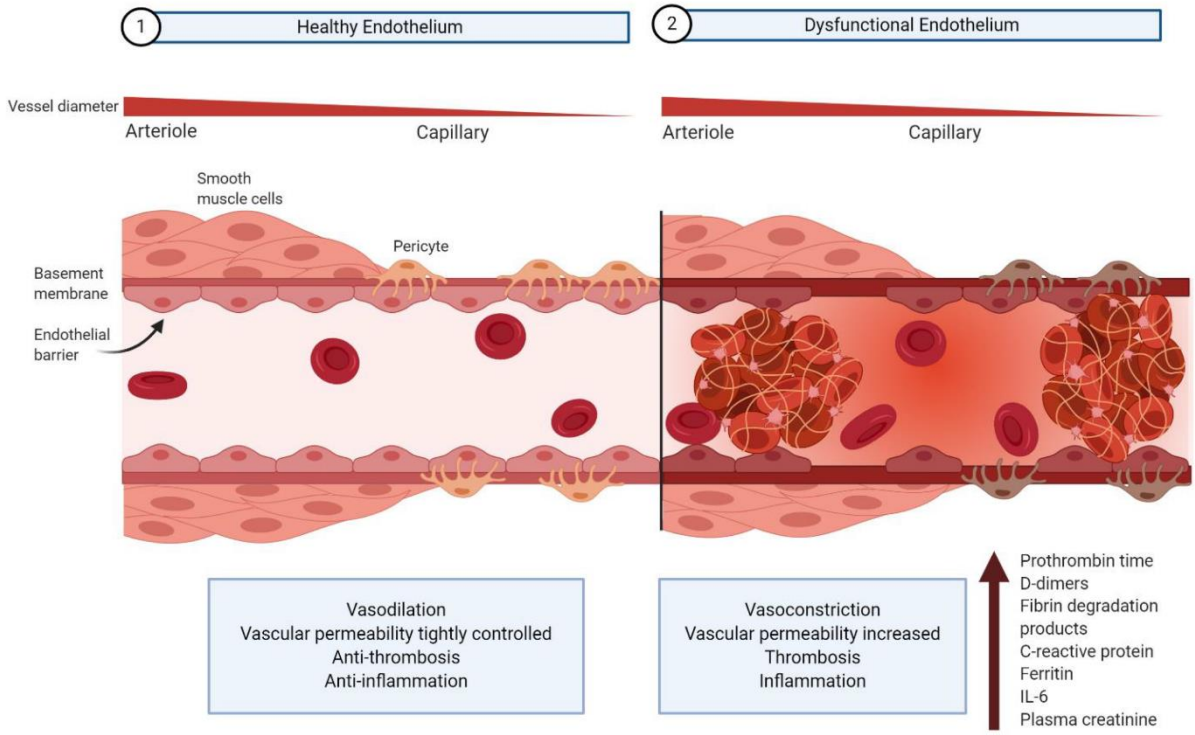

Figure 3: Healthy and dysfunctional vascular endothelium. The healthy endothelium is a thin, intact monolayer of endothelial cells at the border between blood and tissue, which can carry out its physiological functions, including vasodilation, barrier function and control of blood fluidity, in a proper way (left). Disruption of endothelial functions lead to vasoconstriction, increased vascular permeability, coagulation and inflammation (right). The figure was adapted according to the rules of the open access Creative Commons Attribution License (CC BY 4.0) from: Multidisciplinary Digital Publishing Institute (MDPI), Viruses, Endothelium infection and dysregulation by SARS-CoV-2: evidence and caveats in COVID-19, Bernard I *et al*., © 2021.[31]

Given its important role in physiological and pathological conditions, the endothelium represents an auspicious target for the treatment of numerous diseases. To date, various approaches to prevent and reduce cardiovascular risk factors include “endothelial therapy” through diet control, physical exercise, weight control and smoking cessation. On top of this, a diverse pharmacological management aims to reset the hyperactive endothelium back to its physiological quiescent state.[32, 33] In this regard, angiotensin-converting enzyme inhibitors, insulin sensitizers, antioxidants and enhancers of endothelial nitric oxide synthase (eNOS) constitute examples for currently used or investigational medicinal drugs. Furthermore, inhibitors of prominent endothelial signaling pathways and proteins, such as of the Ras homology domain family (Rho) and Akt signaling or of poly(ADP-ribose)-polymerase PARP, have been shown to promote protective actions on the endothelium.[33]

2. Inflammation

Inflammation is a physiological process triggered by infections, tissue injury, tissue stress or malfunctions with the purpose to defend the body and to restore homeostasis. Although acute and controlled inflammation is beneficial, dysregulations can lead to chronic, pathological, and detrimental inflammation. Chronic inflammation is often associated with severe disorders including autoimmune diseases, cardiovascular diseases and cancer.[34] A schematic overview of triggers and outcomes is given in Figure 4.

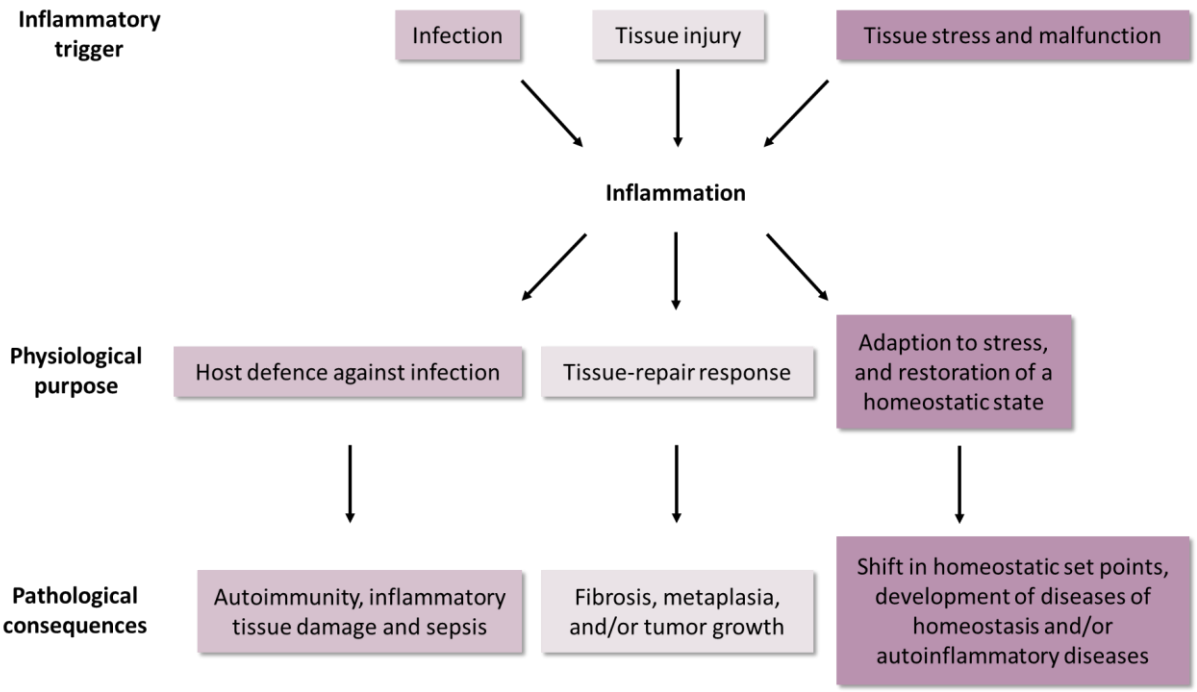

Figure 4: Triggers and outcomes of inflammation. Depending on the origin and type of the inflammatory trigger, different physiological processes are induced by inflammation. Dysregulation of the physiological purpose can lead to pathological consequences and chronic inflammation. Reprinted with permission from Springer Nature and Copyright Clearance Center: Springer Nature, Nature, Origin and physiological roles of inflammation, Medzhitov R, © 2008.[34]

2.1 The physiological function of inflammation

Acute inflammation is the fast and self-limiting response to specific triggers, such as pathogens, damaged tissue or toxic compounds. Typical characteristics of inflammation are heat, swelling, pain, redness, and loss of tissue function. Exogenous inflammatory triggers comprise microbial factors, like pathogen-associated molecular patterns (PAMPs) and virulence factors, and non-microbial factors, including allergens, irritants, foreign bodies, toxic compounds or damage/danger-associated molecular patterns (DAMPs).[35-40] Endogenous inflammatory triggers rise upon stress, tissue damage or tissue malfunctions. Tissue-domiciled macrophages and mast cells initially recognize the inflammatory inducer and thereupon produce and secrete inflammatory mediators.[41, 42] Inflammatory mediators consist of seven

biochemical groups: vasoactive amines like histamine and serotonin, vasoactive peptides like substance P, fragments of complement components including anaphylatoxins, lipid mediators like eicosanoids, cytokines including tumor necrosis factor and interleukins, chemokines and proteolytic enzymes like elastin and cathepsins.[43-45]

Extruded proinflammatory mediators coordinate the subsequent delivery of blood serum and circulating blood cells, especially leukocytes, to the site of inflammation.[46] For this, the inner monolayer of the blood vessels consisting of endothelial cells is activated by the cytokines through inducing intracellular pro-inflammatory signaling pathways, such as nuclear factor kappa B (NF-κB) signaling.[47] Activation of the endothelium enables a direct interaction with leukocytes from the blood, which is mediated by inducible selectins and cell adhesion molecules (CAM) on the surface of endothelial cells and integrins and chemokine receptors on the leukocytes. Upon tight interaction of leukocytes with the endothelium, their subsequent transmigration through the endothelium is initiated. Hence, leukocytes gain access to the site of inflammation in the extravascular tissue.[48, 49]

After their arrival at the site of inflammation, leukocytes are activated through direct contact with the pathogen or through the cytokines secreted by tissue-resident cells. Following this, leukocytes, like neutrophils, eliminate the inflammatory trigger through releasing the toxic content of their intracellular storage granules, consisting of reactive oxygen species (ROS), reactive nitrogen species, proteinase 3, cathepsin G and elastase.[50] As soon as the inflammatory trigger is removed, the resolution of inflammation followed by a repair phase is induced to restore tissue homeostasis. During resolution of inflammation, a switch from the secretion of pro-inflammatory cytokines to anti-inflammatory lipid mediators, such as lipoxins, resolvins and protectins, takes place. Lipid mediators inhibit neutrophil recruitment and attract monocytes, which remove the dead cells and promote tissue remodeling.[51]

2.1.1 The leukocyte-endothelial cell interaction

Both the acute and chronic inflammatory response are conditional on the interaction between leukocytes and endothelial cells.[49] Upon induction of an inflammatory response, released pro-inflammatory mediators activate endothelial cells through initiating pro-inflammatory intracellular signaling pathways.[47] This leads to an upregulated expression of pro-inflammatory genes, including adhesion molecules.[52, 53] Adhesion molecules then convey the establishment of an interaction between endothelial cells and leukocytes, which is a crucial prerequisite for the subsequent extravasation of the leukocytes from the blood towards the site of inflammation. Adhesion molecules are divided into three groups, namely selectins, CAMs and integrins.[54, 55] Selectins like P-selectin and E-selectin are membrane glycoproteins that interact with specific carbohydrate groups, such as glycoprotein ligand 1 (PSGL-1), on leukocytes.[56, 57] Selectins mediate the capturing, tethering and rolling of leukocytes on the

endothelium, thereby establishing an initial contact without being able to promote tight adherence.[58] Considering that selectins are needed for initial lose interactions, these glycoproteins are expressed on the endothelial cell surface rapidly after cell activation. P-selectin is stored in intracellular granules, called Weibel-Palade bodies, and is exocytosed for instance upon histamine release of mast cells.[59] In contrast to P-selectin, E-selectin needs to be expressed *de novo* through gene transcription and protein synthesis, which, however, is accomplished after only 2 to 4 hours.[60] Upon initial tethering and rolling, the leukocytes form a permanent bond with the endothelium through heterophilic interactions of integrins on the leukocyte cell surface with CAMs on the endothelial cell surface. CAMs belong to the immunoglobulin superfamily. The most important CAMs expressed by endothelial cells are the intracellular adhesion molecule 1 (ICAM-1) and the vascular cell adhesion molecule 1 (VCAM-1). Both CAMs need to be expressed *de novo* upon cytokine-induced endothelial cell activation.[49] Typical examples of integrins on the leukocyte cell surface that interact with CAMs are lymphocyte function-associated antigen 1 (LFA-1), macrophage-1 antigen (Mac-1) and very late antigen-4 (VLA-4).[61]

After successful establishment of leukocyte-endothelial cell interactions, the diapedesis of the leukocytes through the endothelium towards the underlying tissue, also referred to as transmigration, is initiated. Therefore, homophilic interactions between molecules on endothelial cells and leukocytes are build. Such molecules are for instance platelet endothelial cell adhesion molecule-1 (PECAM-1) or cluster of differentiation 99 (CD99).[62, 63] Transmigrated leukocytes are then guided to the site of inflammation by chemokines, which form a matrix-associated concentration gradient.[64] The multistep cascade of leukocyte-endothelial cell interaction is depicted in Figure 5.

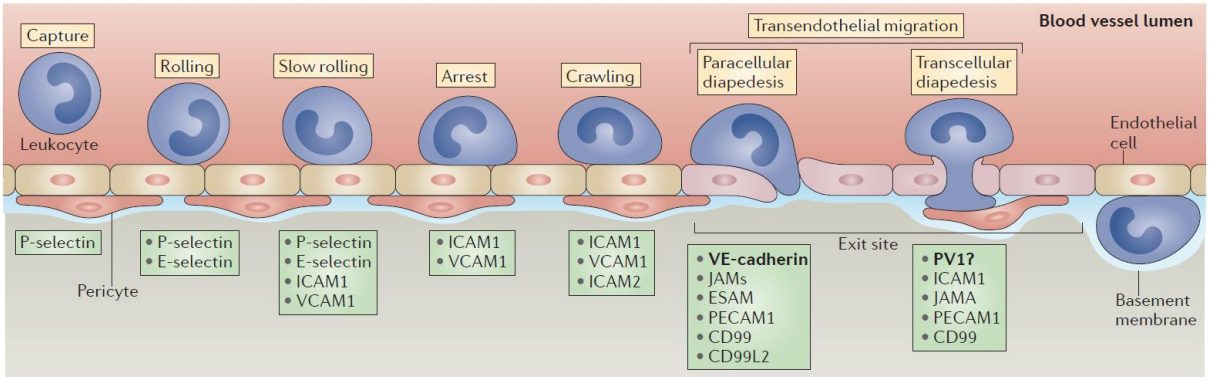

Figure 5: The multistep cascade of leukocyte-endothelial cell interaction. During initial capturing and rolling of the leukocytes on the endothelial cell surface, which is mediated by endothelial selectins, the interaction is still weak. For tight adhesion, endothelial cell adhesion molecules (CAMs) are expressed, which interact with integrins of the leukocyte cell surface. Subsequently, leukocytes migrate through the endothelium towards the underlying tissue (transendothelial migration). Reprinted with permission from Springer Nature and Copyright Clearance Center: Springer Nature, Nat Rev Immunol., How leukocytes cross the vascular endothelium, Vestweber D, © 2015.[65]

2.2 The mechanism of chronic inflammation

Chronic inflammation occurs due to persistent infections, an exaggerated or subnormal inflammatory response or an inappropriate resolution program. Persistent infections have been described for pathogens like *Mycobacterium tuberculosis*, *Heliobacter pylori* or hepatitis viruses.[66-68] While acute inflammation only lasts for a couple of days, chronic inflammation is a slow, long-time type of inflammation, which lasts for months or even years.[69] In general, chronic inflammation is characterized by the excessive production of pro-inflammatory mediators and insufficient release of resolving mediators.[70] These inflammatory mediators hyperactivate endothelial cells and leukocytes and promote ongoing leukocyte diapedesis from the blood to the underlying tissue, which maintains the inflammatory response.[71] Persistent inflammation again leads to aberrant tissue remodeling, irreversible damage and disease symptoms.[72] The pathology of a wide range of human diseases, including cancer, autoimmune, metabolic, cardiovascular and neurodegenerative disorders contributes to pathological inflammation.[34, 73] An overview of triggers and consequences of chronic inflammation is provided in Figure 6.

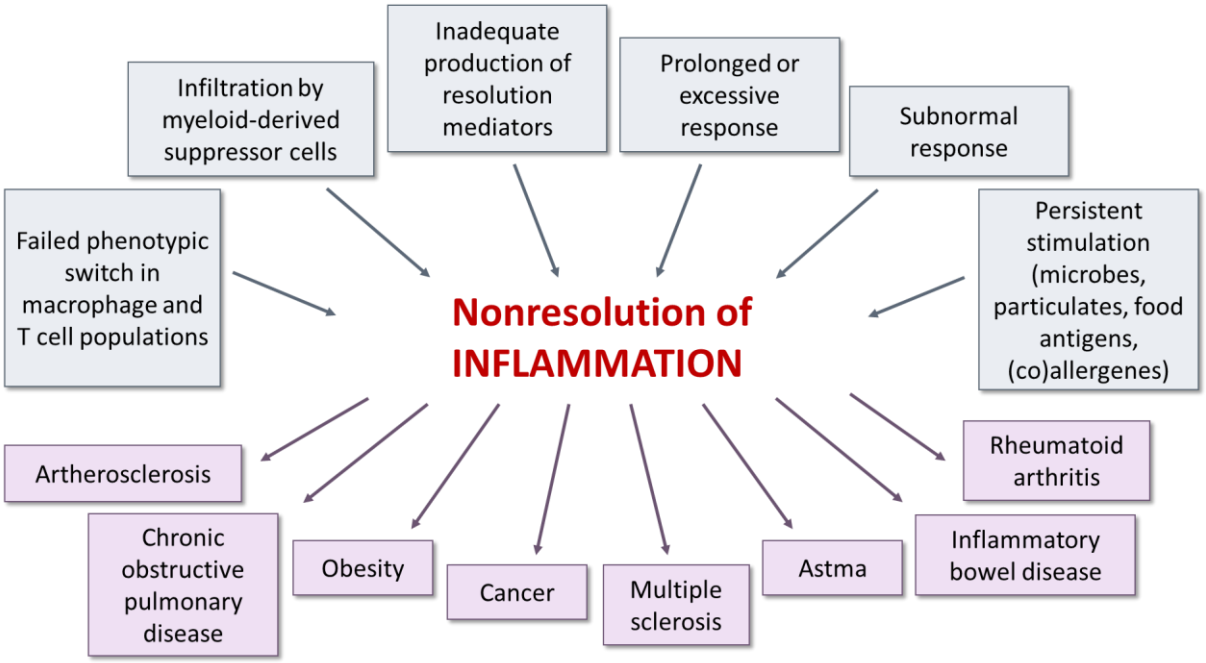

Figure 6: Triggers and pathological consequences of chronic inflammation. Adapted with permission from Elsevier Inc. and Copyright Clearance Center: Elsevier, Cell, Nonresolving inflammation, Nathan C and Ding A, © 2010.[74]

2.3 Inflammatory signaling

Inflammatory signaling intermediates and pathways plays a significant role in the activation of endothelial cells and leukocytes during the inflammatory response.[47] Importantly, various pro-

inflammatory mediators interact with different structures on the cell surface and induce divergent downstream intracellular signaling pathways.[75]

2.3.1 Cytokines and their respective cytokine receptors

Cytokines are important signaling molecules during inflammation and immunity, as they are involved in cell recruitment, cell activation and proliferation, antigen presentation as well as adhesion molecule expression. Major producers of cytokines are antigen-presenting cells (APCs) such as mononuclear phagocytic cells (e.g. monocytes). The most prominent pro-inflammatory cytokines are tumor necrosis factor (TNF) and interleukin 1 (IL-1).[75]

TNF is a member of the TNF superfamily and represents two homologous proteins, called TNF-α and TNF-β. While TNF-α is produced by a wide variety of cells, including mononuclear phagocytes, neutrophils, lymphocytes, endothelial cells and mast cells, TNF-β is mainly secreted by lymphocytes.[76] Initially, TNF-α is a membrane-bound protein, which is cleaved into its soluble form by the TNF-α converting enzyme (TACE).[77, 78] Importantly, only the formation of soluble homotrimers leads to activation of the cytokine.[79] Activated TNF binds to two cell surface receptors, called tumor necrosis factor receptor 1 and 2 (TNFR1/2). While TNFR1 induces proinflammatory activities, including the activation of intracellular signaling pathways like the pro-inflammatory NF-κB pathway, TNFR2 also elicits anti-inflammatory, pro-angiogenic and protective actions.[80, 81]

The IL-1 family consists of 11 members, of which 7 members, including IL-1α and IL-1β, show pro-inflammatory actions and 4 members, including the IL-1 receptor antagonist (IL-1ra), exert anti-inflammatory effects[82] IL-1 is produced by a variety of cells, including mononuclear phagocytes, endothelial cells, keratinocytes, synovial cells, osteoblast, and neutrophils. IL-1 is synthesized as procytokine and is subsequently activated through cleavage by the IL-1 converting enzyme (ICE), also referred to as caspase-1.[83] Active and secreted IL-1 binds to type I and type II IL-1 receptors (IL-1R). While type I IL-1Rs are important for signal transduction and induction of pro-inflammatory biological activities, the type II IL-1Rs are decoy receptors, which capture IL-1 thereby reducing the pro-inflammatory signaling.[84, 85]

2.3.2 The NF-κB signaling pathway

Nuclear factor kappa B (NF-κB) proteins are ubiquitously expressed transcription factors, which are pivotal for inflammatory, immunological and survival signaling.

The NF-κB family comprises five monomeric members, namely p65/RelA, RelB, cRel, p50 and p52. All family members possess a homologous domain with a length of approximately 300 residues near the N terminus, called Rel Homology Domain (RHD), which is responsible for the DNA binding activity of the transcription factor. The monomers form either homo- or

heterodimers, which bind with differential affinities to the promotor region of various genes. The most abundant form of NF-κB is the p50/p65 heterodimer.[86]

The NF-κB signaling pathway is activated by cytokines, like TNF and IL-1, PAMPs or antigen/immune stimulatory signals.[87] These mediators interact with membrane-bound receptors, such as the TNFR1, and activate the canonical NF-κB signaling. In a first step, the regulatory protein NF-κB essential modulator (NEMO), also known as NF-κB kinase subunit gamma (IKKγ), and the catalytic NF-κB kinase subunits alpha and beta (IKKα/β) build an IKK complex.[88] Subsequently, the IKK complex is activated through phosphorylation. Therefore, NEMO either induces trans-autophosphorylation through multimerization of IKK subunits or recruits the IKK complex to upstream kinases, such as transforming growth factor-β-activated kinase 1 (TAK1), which mediate its phosphorylation.[89, 90] Next, the activated IKK complex phosphorylates inhibitor of kappa B (IκB) proteins. IκB proteins are inhibitory proteins, which mask the nuclear localization sequence (NLS) of NF-κB subunits and, thus, hamper their nuclear translocation.[91, 92] Phosphorylated IκB proteins are ubiquitin-dependently degraded by the proteasome, which liberates the NF-κB subunits from their cytosolic retention. Importantly, NF-κB subunits can, due to their molecular weight, not passively diffuse to the nucleus. Therefore, the NLS allows for nuclear translocation via the classical nuclear import pathway (see section III.2.3.3).[93] Once in the nucleus, the NF-κB dimers bind to specific DNA target sites, known as κB sites and enhance subsequent gene expression.[94]

Termination of the NF-κB promotor activity is crucial, for instance during the shift of pro-inflammatory to anti-inflammatory signaling. Negative feedback loops and post-translational ubiquitination of signaling intermediates represent important termination mechanisms. The resynthesis of IκB proteins, which, despite their inhibitory effect, are NF-κB target genes, constitutes one possible feedback loop. Newly synthesized IκB proteins can translocate to the nucleus, interact with NF-κB dimers, thereby inhibiting the promotor activity and shuttling the NF-κB dimers back to the cytosol.[95-97] Key steps of canonical NF-κB signaling are depicted in Figure 7.

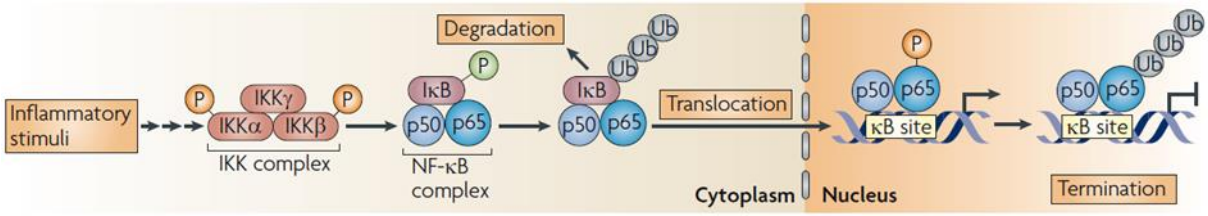

Figure 7: Steps of the canonical NF-κB signaling pathway. Inflammatory triggers lead to the phosphorylation and activation of the IKK complex via a multistep cascade. The IKK complex then evokes the phosphorylation- and ubiquitin-dependent degradation of IκBα, which liberates the NF-κB subunits from their cytosolic retention. NF-κB subunits translocate to the nucleus and bind to the promotor region of pro-inflammatory target genes to induce their expression. Termination of gene transcription is promoted through negative feedback loops or post-translational ubiquitination. Ub, ubiquitin. Reprinted with permission from Springer Nature and Copyright Clearance Center: Springer Nature, Nat Rev Immunol., New regulators of NF-κB in inflammation, Ghosh S and Hayden MS, © 2008.[98]

2.3.3 The classical nuclear import pathway

The classical nuclear import pathway is crucial for nucleocytoplasmic transport of proteins. Especially proteins with a molecular weight higher than 40 kDa rely on an active transport system because the nuclear pore complexes (NPC) at the border between nucleus und cytosol only allows passive diffusion of ions and small molecules.[99, 100] Since the nucleocytoplasmic shuttling is an active process, energy is provided by Ran, a small Ras family GTPase.[101, 102]
The nucleocytoplasmic transport is guided by soluble carrier proteins named karyopherins. Karyopherins involved in nuclear import are termed importins, whereas karyopherins involved in nuclear expert are called exportins. Importantly, however, various carrier proteins participate in both nuclear import and export. Importins comprise the importin alpha and beta family. While for the importin alpha family seven subtypes have been identified, only one importin beta isoform, importin beta 1, is known to recognize and bind importin alpha proteins as adaptors for cargo loading.[103-105] Importin alpha proteins contain three structural domains: the N-terminal domain, called importin beta binding (IBB) domain, is responsible for the interaction with importin beta, the tandemly repeated armadillo (Arm) repeats bind the NLS of the cargo protein, and the C-terminal region is responsible for the export of importin alpha back to the cytosol through interacting with the nuclear export factor cellular apoptosis susceptible gene (CAS).[106-108] Importin beta 1 also contains three structural domains, the N-terminal RanGTP binding site, the NPC binding site, and the C-terminal substrate binding site. In contrast to importin alpha, however, importin beta 1 is not able to bind all three components simultaneously since the binding sites partially overlap.[109]
The first step of nuclear import is the binding of an importin alpha family member to the cargo protein. Therefore, the cargo protein contains an NLS, which consists of one or two sequences of amino acids. Importin alpha proteins, however, do not interact with the NPC. Thus, importin alpha proteins serve as adaptor proteins and establish an additional connection with importin beta 1, creating a trimeric complex. Importin beta 1 mediates the interaction of the trimeric complex with the NPC allowing entry into the nucleus. In the nucleus, RanGTP binds to importin beta 1, which induces a conformational change and releases the cargo from the complex of importin alpha and importin beta. Subsequently, importin alpha dissociates from importin beta and is exported back to the cytosol in a complex with its specific export protein CAS/CSE1L and RanGTP. Importin beta is 1 also recycled back to the cytosol in a RanGTP-dependent mechanism.[105, 110] The process of nucleocytoplasmic transport is depicted in Figure 8.

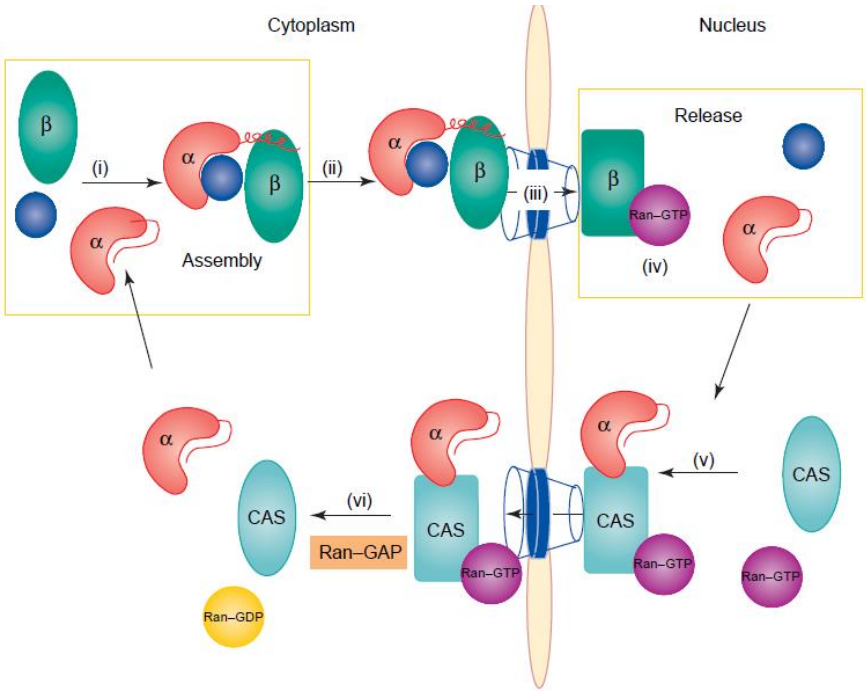

Figure 8: Model of the nuclear import and export system. (**I**) Importin alpha binds on the one hand to the NLS of the cargo protein and establishes on the other hand an interaction with importin beta, thereby creating a trimeric complex. (**II**) Importin beta directs the complex to the nuclear pore complex (NPC) and (**III**) transfers the complex into the nucleus. (**IV**) RanGTP mediates the dissociation of the ternary complex. (**V**) Bindung of importin alpha to its export protein CAS and RanGTP induces the export back to the cytosol. (**VI**) RanGTP is hydrolyzed to RanGDP, which induces complex dissociation and recycles importin alpha for a new nuclear import cycle. The export of importin beta is not shown. Reprinted with permission from Elsevier Inc. and Copyright Clearance Center: Elsevier, Trends in Cell Biology, Importin α: a multipurpose nuclear-transport receptor, Goldfarb DS *et al*., © 2004.[111]

Interestingly, the expression of importin alpha subtypes is cell-type specific and relies on the developmental stage of the cell.[104, 112-114] Furthermore, importin alpha subunits show cargo-specific affinities. In case of the NF-κB subunit p65, importin subunit alpha1 (KPNA2), importin subunit alpha3 (KPNA4) and importin subunit alpha 4 (KPNA3) have been shown to directly interact with its NLS.[115-119]

2.4 Inflammation as therapeutic target

As described in section III.0, chronic inflammation is associated with various human pathologies. Thus, treatment of inflammation is crucial for reducing the risk of cardiovascular and auto-immune diseases. Many treatments available today mainly focus on combatting symptoms of inflammatory diseases, like pain and swelling. Nevertheless, discovering and synthesizing drugs that directly target the underlying causes of inflammatory disorders is an emerging research field. Therefore, however, it is crucial to exploit the molecular mechanism of pathological inflammation. Potential approaches for the disruption of inflammatory processes are the reduction of granulocyte and macrophage growth and production, impairment of the leukocyte-endothelial cell interaction and inhibition of the production, secretion and effects of inflammatory mediators.[120]

Various approaches are known today to address the abovementioned inflammatory actions. Many small molecule inhibitors have been synthesized that inhibit pro-inflammatory signaling pathways, including the mitogen-activated protein kinase (MAPK) p38, phosphatidylinositol 3-kinase (PI3K), signal transducer and activator of transcription 3 (STAT3), NF-κB and Hippo signaling.[121-124] These signaling pathways are often overly activated in inflammatory diseases such as Alzheimer's disease or cancer and induce the production of pro-inflammatory mediators.[125-132] Although small molecule inhibitors of pro-inflammatory pathways reveal promising effects *in vitro* and *in vivo*, unacceptable side effects question the clinical advantage over standard therapies.[123, 133-135]

Besides inhibiting pro-inflammatory signaling pathways, neutralizing antibodies against pro-inflammatory cytokines or blocking antibodies for pro-inflammatory receptors represent a direct approach to target inflammatory processes. Especially mediators against the IL-1 pathway are frequently tested in clinical trials. Three IL-1 targeting agents, including the neutralizing monoclonal anti-IL-1β antibody canakinumab, the soluble decoy receptor rilonacept and the IL-1 receptor antagonist anakinra have been approved as therapeutic drugs.[136] Targeting the cytokine TNF, which triggers immune and endothelial cell activation, pro-inflammatory cytokine production and apoptosis, is another possible approach towards the direct cytokine inhibition. TNF neutralizing antibodies, such as infliximab, adalimumab or golimumab, and the TNF trapping fusion protein etanercept are approved agents for the treatment of cancer, arthritis, psoriasis and many more diseases.[137] Nevertheless, TNF-inhibiting antibodies can also evoke the formation of anti-drug antibodies, which affects drug pharmacokinetics and hampers the clinical response.[138]

3. Angiogenesis

Angiogenesis is the endothelial cell-dependent formation of new blood vessels from preexisting ones with the purpose of expanding the primary capillary plexus, a primary primitive network of embryonic vessels.[139] The primary capillary plexus again is created by vasculogenesis, the *de novo* formation of blood vessels from endothelial precursor cells of mesodermal origin, named angioblasts.[140]

3.1 The physiological function of angiogenesis

The vascular system is formed by a strongly branched network of blood vessels, which ensures the appropriate supply of the tissue with oxygen and nutrients. Consequently, changes in metabolic demands are strong drivers of network expansion.[141] During embryonic development, angiogenesis ensures the formation of the primary vascular tree as well as the

development and growth of vital organs. This enables the supply of the growing embryo with oxygen, nutrients, and metabolites as well as the removal of waste products.[142, 143] In adulthood, physiological angiogenesis is downregulated and mainly serves to maintain homeostasis and tissue integrity. Downregulation of adult angiogenesis is mediated by endogenous matrix and non-matrix derived inhibitors of angiogenesis, including endostatin, angiostatin, vasostatin and more.[144] Nevertheless, selected physiological processes in adults, including the ovarian cycle, pregnancy, and wound healing, heavily depend on blood vessel formation. During the ovarian cycle, blood vessel formation ensures follicular growth and the expansion of the corpus luteum. This is underlined by the finding that inhibition of growth factor signaling suppresses luteal angiogenesis.[145, 146] During wound healing, the formation of new capillaries is essential for providing the wound with nutrients, immune cells and oxygen. At the same time, angiogenesis is involved in tissue formation and remodeling to repair the injured dermis.[147]

3.2 Drivers of angiogenesis

Angiogenesis is controlled by a tight balance between the expression of inducing and negatively regulating angiogenic factors.[148] Thus, to initiate angiogenesis, a so called angiogenic switch is needed, which enhances the expression of pro-angiogenic mediators and reduces the expression of inhibitory molecules.[149] Main inducers of this angiogenic switch constitute hypoxia, nutrient deficiency as well as mechanical forces. Under normoxia, the von Hippel-Lindau tumor suppressor gene product prevents the transcription of genes induced by hypoxia-inducible transcription factors, such as HIF-1α/β and HIF-2α.[150] HIFs are transcription factors with a heterodimeric oxygen-sensitive basic helix-loop-helix structure, which are pivotal for the cellular adaption to low oxygen levels.[151] Following hypoxic tissue conditions, HIFs activate the expression of pro-angiogenic factors like growth factors, growth factor receptors, nitric oxide synthase, neuropilin-1, endothelin-1, interleukin-8 and more. These pro-angiogenic factors either form a well-defined spatial concentration gradient in the tissue, which attracts proliferating and migrating endothelial cells, or directly initiate pro-angiogenic intracellular signaling cascades.[152]

Besides hypoxia, angiogenesis is strongly driven by mechanical factors mediated by the blood flow, such as stretching, tension, compression and shear stress. These mechanical forces lead to changes in cell morphology and physiology, thereby inducing intracellular signaling cascades and selective gene transcription.[153, 154] Furthermore, high wall shear stress causes endothelial cell alignment, thereby reducing the permeability of the endothelial monolayer and increasing cell sprouting.[155, 156] In this context, vascular remodeling is promoted through nitric oxide production and P-selectin expression.[157, 158]

Growing evidence furthermore underlines a vital role of extracellular vesicles (EVs) during angiogenesis. EVs are actively released from cells and contain bioactive messengers, including transcriptional regulators and miRNAs. These messengers are transferred to adjacent or more distant cells, thereby ensuring tight cell-cell communication. Cellular uptake of EVs, which is mediated by tetraspanins, integrins and L-selectin on the vesicle membrane and adhesion molecules on the cell membrane, evokes an upregulation of growth factors, growth factor receptors and vWF. Thus, EVs induce angiogenesis and resistance to apoptosis. Importantly, EVs closely adjust their cargo to changes in the microenvironment. Hence, besides enhancing angiogenesis, EVs can also exert anti-angiogenic actions.[159-161]

In general, inducing mechanisms upregulate the expression of pro-angiogenic mediators. These mediators comprise on the one hand classical factors, including growth factors like vascular endothelial growth factor (VEGF), basic fibroblast growth factor (bFGF) and epidermal growth factor (EGF), transforming growth factor beta 1 (TGF-β1) and platelet derived growth factor B (PDGF-B), and on the other hand non-classical factors.[149] Non-classical factors constitute endogenous peptides with other well-known specific biological activities that are present in the blood and therefore may also influence angiogenesis. Non-classical endogenous angiogenic factors comprise erythropoietin, angiotensin II, endothelin, adrenomodullin, adiponectin, resistin, neuropeptide-Y, vasoactive intestinal peptide (VIP), substance P and more.[162]

3.3 The mechanisms of angiogenesis

In the context of angiogenesis as a process, two distinct types, the sprouting and the non-sprouting or intussusceptive angiogenesis, exist.[163]

Sprouting angiogenesis is characterized by the formation of endothelial sprouts, which in the following elongate in direction of an angiogenic stimulus. Thus, sprouting angiogenesis can install *de novo* blood vessels in formerly poorly perfused tissue sections.[163] The key steps of sprouting angiogenesis are shown in Figure 9.

As outlined in section III.3.2, oxygen and nutrient deprivation as well as mechanical forces can induce sprouting angiogenesis. In a first step, angiogenic factors released from parenchymal cells reset endothelial cells from a quiescent to an active state. In this context, VEGF is the most prominent and crucial proangiogenic factor.[164]

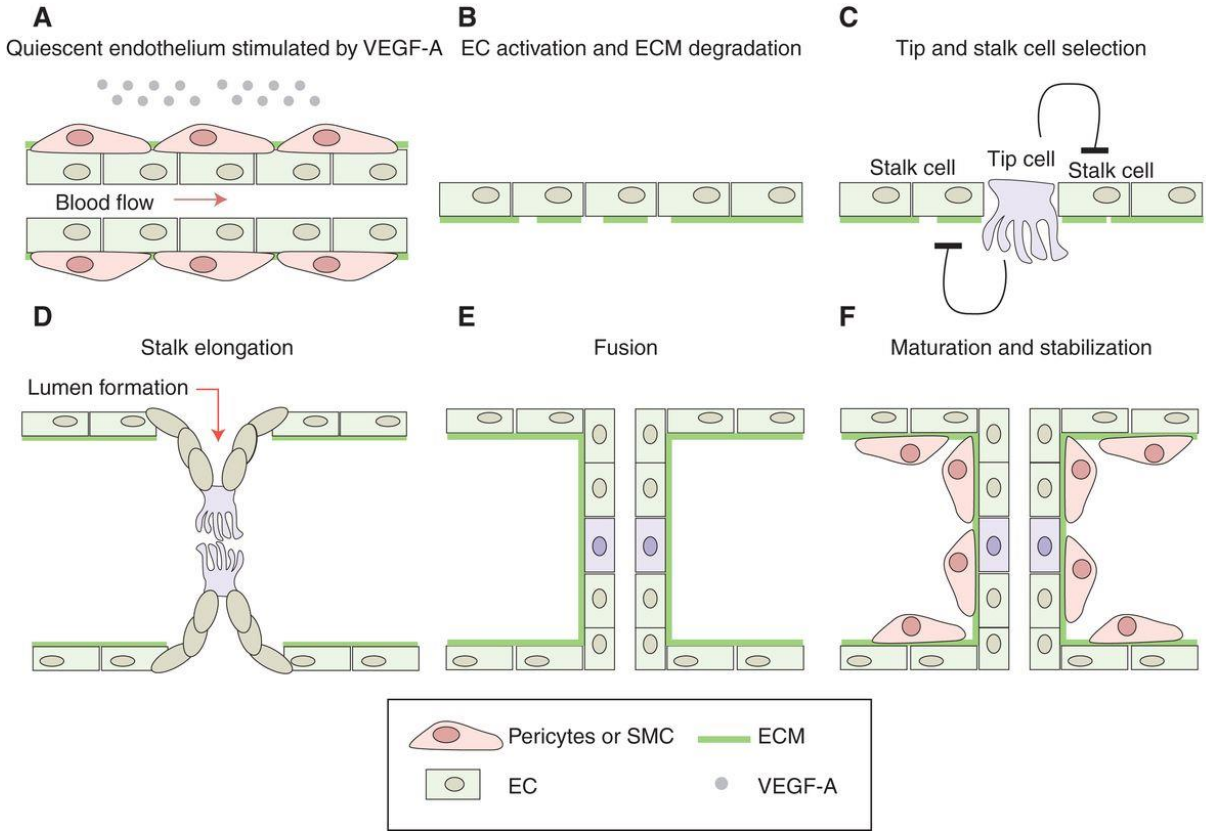

Figure 9: Steps of sprouting angiogenesis. Upon an angiogenic stimulus, growth factors like VEGF are secreted, which interact with endothelial cells and switch their state from a quiescent to an active one (**A**). Subsequently, the extracellular matrix (ECM) is degraded through MMPs and angiopoietin-2 (**B**). Tip cells initiate sprouting and migration, while they at the same time inhibit adjacent cells, which turn into stalk cells (**C**). Stalk cells proliferate to elongate the sprouts and start to form a lumen (**D**). At the origin of the angiogenic stimulus, tip cells can fuse together to create a continuous lumen (**E**). Finally, the new blood vessels maturate and are stabilized by mural cells (**F**). Reprinted with permission from Cold Spring Harbor Laboratory Press: Cold Spring Harbor, Cold Spring Harbor Perspectives in Medicine, VEGF and Notch in tip and stalk cell selection, Blanco R and Gerhardt H, © 2013.[165]

Endothelial cells exposed to the highest VEGF concentration turn into so-called tip cells. Tip cells guide the developing capillary sprout through the extracellular matrix towards the source of the angiogenic stimulus.[166] Typically, tip cells express long and thin cytoplasmic extensions, named filopodia, which secret high amounts of matrix metalloproteinases (MMPs) and angiopoietin-2 that enzymatically degrade the extracellular basolateral basement membrane.[167, 168] Moreover, filopodia are highly enriched in membrane-bound VEGF receptor 2 (VEGFR2), which allows to sense differences in VEGF concentrations. Through actin filament contraction, the filopodia align with the chemotactic gradient towards the angiogenic stimulus.

Tip cell selection is achieved by inhibition of adjacent cells.[169] Therefore, the existing pool of tip cells secrets Delta-like-4 (Dll4), which binds to and activates the notch receptors on neighboring cells. Activation of the notch signaling prevents VEGFR2 production. Thus, these cells, so called stalk cells, are less prone to sensing VEGF concentrations and gradients.[170] Endothelial stalk cells have fewer sprouting and migratory capacity compared to tip cells but

are needed to elongate the capillary sprout through cell proliferation.[165] A schematic overview of the tip and stalk cell selection is provided in Figure 10.

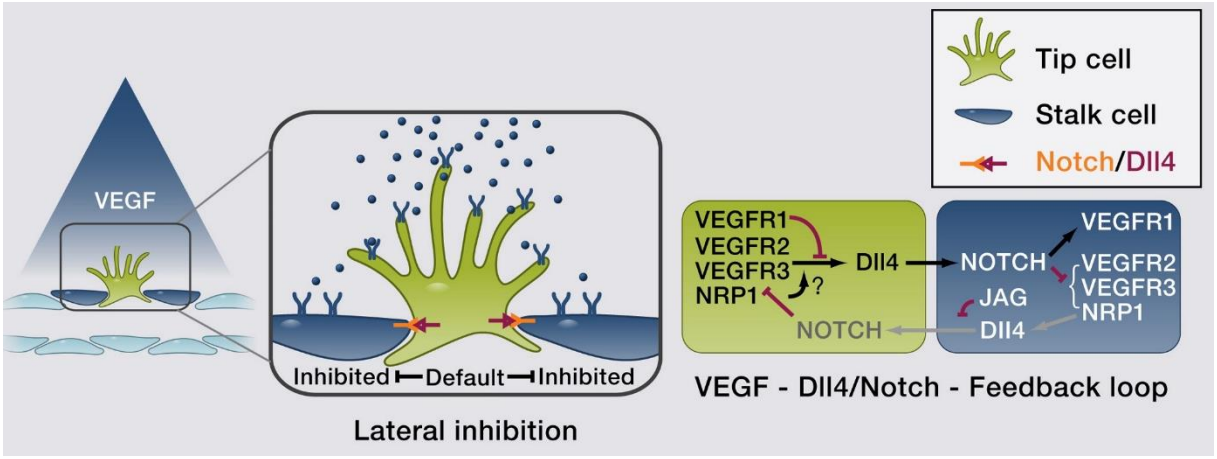

Figure 10: Tip and stalk cell determination during sprouting angiogenesis. VEGFR2 and Notch signaling mediate the specification of tip cells and stalk cells in the vascular endothelium. Upon binding of VEGF to the VEGFR2 of quiescent cells, Dll4 expression is upregulated. Dll4 binds in the following to Notch receptors on neighboring cells, thereby inducing Notch signaling. In the following, the VEGFR2 expression is lowered and the expression of the VEGFR1 as well as Notch target genes is enhanced. Reprinted with permission from Elsevier Inc.and Copyright Clearance Centre: Elsevier, Cell, Basic and therapeutic aspects of angiogenesis, Potente M *et al*., © 2011.[171]

Subsequently, several neighboring stalk cells start to form a lumen through vacuole development and coalescence. At the origin of the angiogenic stimulus, tip cells of different sprouts can fuse together, thereby creating a continuous lumen that allows the flow of oxygenated blood.[172] In the final step of maturation, PDGFs are secreted. On the one hand, PDGFs interact with PDGF receptors on the endothelial cell surface, thereby decreasing cell proliferation and VEGF sensitivity. On the other hand, PDGFs activate and recruit mural cells like pericytes and smooth muscle cells that are needed for the stabilization of the newly formed vessel.[173] Angiopoietin-1 promotes the interaction between endothelial cells and pericytes/VSMC.[174] The more new blood vessels are built, the less proangiogenic factors are secreted by the tissue. Finally, when the tissue is sufficiently supplied with blood, oxygen and nutrients, the endothelium changes back to a quiescent state.

Non-sprouting angiogenesis is characterized by splitting of already existing blood vessels into two new ones.[175] This form of angiogenesis might be advantageous at some points compared to sprouting angiogenesis: Blood vessel volume and surface area are significantly increased in a relatively short period without the need of proliferation and extracellular matrix degradation, which makes this type of angiogenesis more economical.[176, 177] Nevertheless, the mechanism of intussusceptive angiogenesis is less well defined compared to sprouting angiogenesis, which makes it challenging to decipher its molecular regulations and physiological role.

3.4 Angiogenic signaling

3.4.1 Growth factors and their respective growth factor receptors

Vascular endothelial growth factors (VEGFs) are heterodimeric glycoproteins that belong to the cysteine-knot superfamily of growth factors. The family of VEGFs consists of VEGF-A, VEGF-B, VEGF-C, VEGF-D, VEGF-E, VEGF-F, endocrine gland-derived VEGF (EG-VEGF) and placental growth factor (PlGF). Various isoforms of each family member are created by alternative splicing and proteolytical processing.[178] VEGF-A constitutes one of the most fundamental stimulators of angiogenesis and is, inter alia, secreted in response to oxygen deprivation. Isoforms of VEGF-A are named according to the number of amino acids in the mature protein and comprise $VEGFA_{111}$, $VEGFA_{121}$, $VEGFA_{145}$, $VEGFA_{148}$, $VEGFA_{162}$, $VEGFA_{165}$, $VEGFA_{183}$, $VEGFA_{189}$ and $VEGFA_{206}$. $VEGFA_{121}$, $VEGFA_{165}$ and $VEGFA_{189}$ are the most frequently expressed ones, and $VEGFA_{165}$ is the most active one.[179] VEGFs interact with membrane-bound tyrosine kinase receptors named VEGF receptor 1-3 (VEGFR1-3).[180, 181] VEGFRs consist of a VEGF-binding extracellular domain, which is arranged in seven immunoglobulin (Ig)-like folds, a transmembrane domain, a juxtamembrane domain, an intracellular domain with tyrosine kinase activity and a C-terminal tail.[182] Upon binding of VEGF to the Ig-like extracellular domain, the receptors form homo- or heterodimers, which are further stabilized by the transmembrane and juxtamembrane domains.[183] Through dimerization, a conformational change of the receptor is induced that enables tyrosine kinase activity. Consequently, various tyrosine residues of the intracellular receptor domain are auto-phosphorylated and initiate downstream signaling processes.[184] A schematic overview of the VEGFR activation cascade is provided in Figure 11.

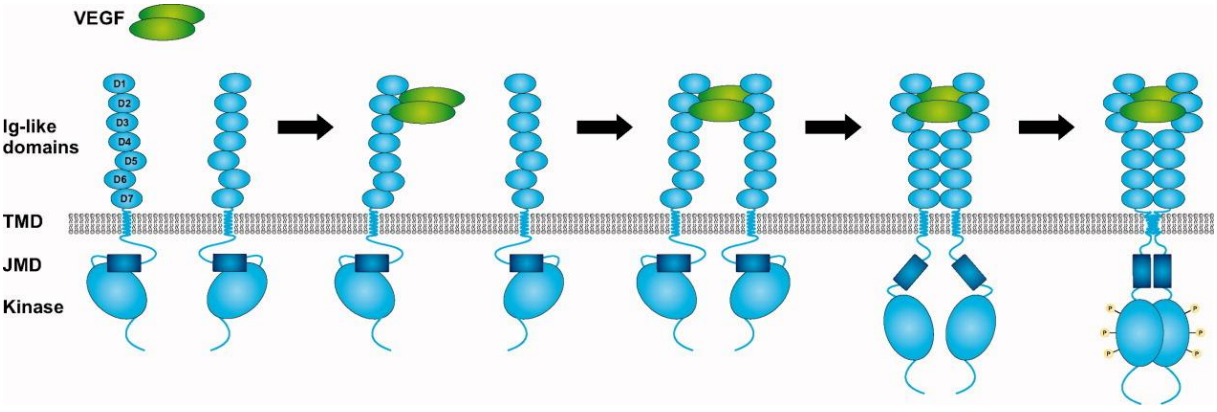

Figure 11: Activation cascade of the VEGFRs. VEGFRs comprise an Ig-like extracellular VEGF-binding domain, a transmembrane domain (TMD), a juxtamembrane domain (JMD) and an intracellular kinase domain. Activated VEGF-dimers bind to the VEGFR causing receptor homo- or heterodimerization. Subsequently, the kinase domain is activated, and the receptor is autophosphorylated at several tyrosine residues, thereby initiating downstream signaling pathways. Reprinted with permission from John Wiley and Sons and Copyright Clearance Center: John Wiley and Sons, IUBMB Life, Structure and function of VEGF receptors, Ballmer-Hofer K and Stuttfeld E, © 2009.[185]

Although the affinity of VEGFR1 to VEGF-A is 10-times higher compared to VEGFR2, its tyrosine kinase activity is rather weak. On top, alternative splicing can create a soluble receptor form (sVEGFR1), which is solely composed of the extracellular Ig-like domain and, thus, does not show any tyrosine kinase activity. Hence, the VEGFR1 and its soluble form might exert an anti-angiogenic effect through intercepting VEGF-A and preventing its interaction with the VEGFR2.[186] VEGFR2 is the predominant tyrosine kinase receptor in endothelial cells and is principally involved in the development and expansion of the vascular system as well as in cell survival.[187] VEGFR3 mediates the establishment of the lymphatic vessel network during embryogenesis and lymphangiogenesis in adults.[188]

Besides the VEGF/VEGFR signaling axis, many more growth factors and receptor tyrosine kinases are known. Amongst them are the epidermal growth factor (EGF) and heparin-binding EGF-like growth factor (HB-EGF), which bind to receptor tyrosine kinases of the ErbB family including the EGF receptor (EGFR). Like the VEGFRs, the EGFR forms homo- or heterodimers, is activated by intrinsic tyrosine kinase activity and mediates physiological pro-angiogenic actions such as cell proliferation and motility. Members of the ErbB receptor family, however, also play a prominent role in carcinogenesis.[189] In a similar way, bFGF and its FGF receptor 1 (FGFR1), PDGF and its PDGF receptor (PDGFR) and angiopoietin and its tyrosine kinase with immunoglobulin-like and EGF-like domains 2 (Tie2) mediate pro-angiogenic cell functions like migration, proliferation, differentiation and survival, which are important for development, metabolism, and tissue homeostasis.[190-192]

Connective tissue growth factor (CTGF) is a cysteine-rich matricellular protein, which is involved in various regulatory processes, including signal transduction, mediating the binding to cytokines to their cell-surface receptors, extracellular matrix turnover and crosstalk between signaling pathways. Compared to growth factors described above, however, CTGF mainly binds to integrin receptors. While CTGF is highly expressed during embryogenesis, the protein level in adults is rather low. Nevertheless, external stimuli like mechanical tension or endogenous factors like ROS, transcription factors like SMAD2/3 and transcriptional coactivators including YAP/TAZ, enhance CTGF expression. CTGF plays an important role during development, cell adhesion and motility, cell survival and tissue remodeling.[193]

3.4.2 Mitogen-activated protein kinase signaling

Mitogen-activated protein kinases (MAPKs) consists of three families of serine/threonine kinases, namely extracellular signal-regulated kinase 1/2 (ERK1/2), c-Jun N-terminal kinase (JNK; also known as stress-activated protein kinase 1 (SAPK)) and p38 MAPK. MAPK signaling is involved in key cellular processes including cell growth, proliferation, differentiation, migration, metabolism and apoptosis.[194] Each of the MAPK signaling pathways relies on a triple kinase cascade composed of the MAPK, a MAPK activator (MAPK kinase (MAPKK or

MAP2K)) and a MAPK kinase activator (MAPKK kinase (MAPKKK or MAP3K)). Upon activation of cell surface receptors, downstream G proteins are initiated, which in turn activate MAP3Ks. In the following, MAP3Ks double-phosphorylate MAP2Ks, and the activated MAP2Ks finally phosphorylate the MAPK. MAPKs induce the activity of various transcription factors located in the cytosol and nucleus, thereby initiating target gene expression for the biological response to a specific stimulus.[195, 196] All MAPKs are inactivated through dephosphorylation mediated by MAPK phosphatases, tyrosine phosphatases or serine/threonine phosphatases.[197] A schematic overview of the MAPK activation cascade is provided in Figure 12.

ERK1 and ERK2 are activated by mitogens and growth factors through tyrosine kinase receptors, G protein coupled receptors (GPCRs) and integrins, which in turn activate small GTPases like Ras and Rap. Ras and Rap recruit MAP3Ks, including Raf family members, Mos and Tpl2, to the cell membrane and mediates their activation.[198] These MAP3Ks phosphorylate their MAP2K substrates MEK1 and MEK2, which finally phosphorylate ERK1/2 at threonine 185 and tyrosine 187. Activated ERK1/2 translocate to the nucleus and activate transcription factors like Ets, Elk-1, Myc and Fos.[199] In total, more than 200 substrates of ERK1/2 are known to date, which also outlines the critical role of ERK1/2 deregulation in cancer and other pathological conditions.[200]

The stress-activated protein kinase family members JNK1, JNK2 and JNK3 are activated by environmental stresses like DNA damage or oxidative stress as well as inflammatory cytokines. They phosphorylate the N-terminus of the transcription factor c-Jun.[201] MAP3K involved in JNK activation comprise MEKK1, MEKK4, MLK2, MLK3, ASK1, TAK1 and Tpl2, and MAP2K for the JNK module are MKK4 and MKK7. MAP2Ks induce dual phosphorylation of JNK members at threonine 183 and tyrosine 185.[202] Deregulation of JNK is associated with neurodegenerative diseases, autoimmune disorders, diabetes, cancer and asthma.[203, 204]

The p38 MAPK exists as four isoforms (p38α-δ) and is, like JNK, induced by environmental stresses and inflammatory cytokines. Interestingly, the p38 dependent cellular response varies depending on cell type and stimulus. In one group of cell types, p38 promotes cell death, while in another group of cell types the MAPK enhances survival, growth and proliferation. MAP3Ks like MLK2/3, ASK1, TAK1, Tlp2, TAO1/2 and DLZ1 as well as the MAP2Ks MEK3/6 are majorly responsible for the phosphorylation of p38 at threonine 180 and tyrosine 182.[205] Based on the wide distribution of the MAPK throughout the body, p38 activation is frequently altered in abnormal cellular conditions. As evaluated in section III.2.4, p38 is therefore commonly investigated as target for the treatment of various diseases including rheumatoid arthritis and Crohn’s disease.[206]

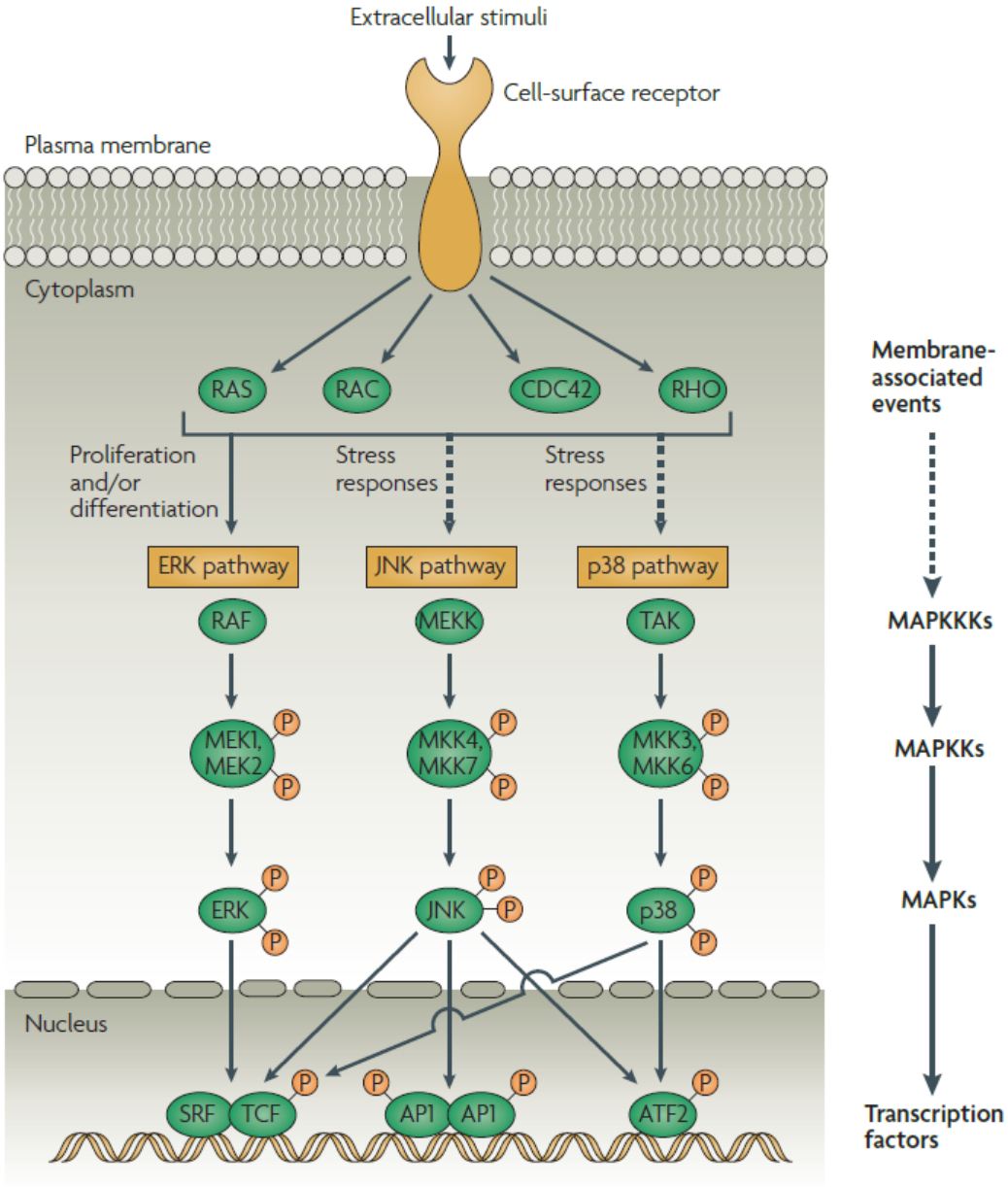

Figure 12: Overview of the MAPKs ERK, JNK and p38 and their respective activation mechanism. Cell-surface receptors are activated by extracellular stimuli and induce membrane-associated events, which then activate MAPKKKs via phosphorylation. MAPKKKs then phosphorylate MAPKKs, which in turn activate the MAPKs. MAPKs translocate to the nucleus, where they activate transcription factors and initiate the expression of target genes. Reprinted with permission from Springer Nature and Copyright Clearance Center: Springer Nature, Nat Rev Immunol., MAPK phosphatases – regulating the immune response, Lui Y *et al.*, © 2007.[207]

3.4.3 The Akt signaling pathway

The serine and threonine kinase Akt is a pivotal regulator of divergent cellular functions like cell metabolism, proliferation, growth, migration and survival as well as protein synthesis and immune cell function.[208-211]

Through initiation of receptor tyrosine kinases and GPCRs, phosphatidylinositol 3-kinase (PI3K) is recruited to and activated at the cell membrane. PI3K catalyzes the formation of the lipid second messenger phosphatidylinositol-3,4,5-triphosphate (PIP_3), which in turn guides

proteins with a pleckstrin homology (PH)-domain like Akt and phosphoinositide-dependent protein kinase 1 (PDPK1) to the cell membrane.[212, 213] PDPK1 phosphorylates Akt at threonine 308 (T308) in the activation loop of its catalytic center.[214] Growing evidence, however, indicates that Akt is also activated in other subcellular compartments. To reach maximum kinase activity, Akt is additionally phosphorylated at serine 473 (S473) in its hydrophobic motif by mammalian target of rapamycin C2 (mTORC2), DNA-dependent protein kinase catalytic subunit (DNA-PKcs) or integrin-linked kinase (ILK).[215-217] Phosphorylation at S473 stabilizes the T308 phosphorylation. Various phosphatases can terminate the phosphorylation of Akt. The 3'-lipid phosphatase and tensin-like protein (PTEN) or the 4'-lipid phosphatase inositol polyphosphate-4-phosphatase (INPP4B) remove PIP_3, which decreases the membrane recruitment and activation of Akt.[218] The PH-domain leucine-rich repeat protein phosphatase (PHLPP1/2) and the protein phosphatase 2A (PP2A) directly dephosphorylate Akt at S473 or T308.[219] The key steps of Akt activation are shown in Figure 13.

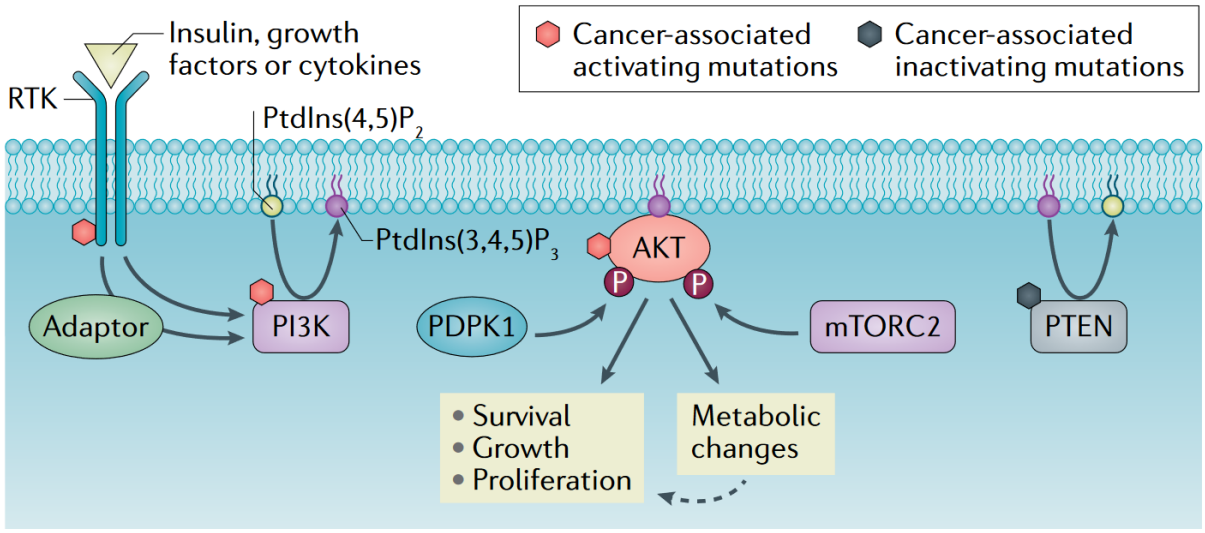

Figure 13: Activation and downstream processes of Akt. Phosphorylation of receptor tyrosine kinases creates binding sites for the lipid kinase phosphoinositide 3-kinase (PI3K) at the plasma membrane. PI3K subsequently produces phosphatidylinositol 3,4,5-triphosphate (PIP_3) from phosphatidylinositol 4,5-diphosphate (PIP_2). The phosphatase and tensin homologue (PTEN) can reverse this process and dephosphorylate PIP_3 back to PIP_2. PIP_3 recruits Akt to the cell membrane, where dual phosphorylation by phosphoinositide-dependent protein kinase 1 (PDPK1) at T308 and mammalian target of rapamycin (mTOR) or other kinases at S473 takes place. Activated Akt leads to metabolic changes and mediates cell survival, growth and proliferation. Reprinted with permission from Springer Nature and Copyright Clearance Center: Springer Nature, Nat Rev Cancer, The PI3K-AKT network at the interface of oncogenic signalling and cancer metabolism, Hoxhaj G and Manning BD, © 2019.[220]

Substrates of Akt contain a specific Akt consensus phosphorylation motif followed by a large hydrophobic residue.[221] More than 100 target proteins are known to date, of which some are activated and some are inactivated by Akt-dependent phosphorylation.[222] Many substrates are involved in cell survival and apoptosis, like Bcl-2-associated agonist of cell death (Bad), Bcl-2-associated X protein (Bax), FOXO and MDM2. Subsequently, cleavage of caspase-3, initiation of intrinsic apoptosis and activation of DNA damage-induced p53-depedent apoptosis

is prevented.[222] Furthermore, Akt plays a crucial role during angiogenesis through activating HIFs and endothelial nitric oxide synthase (eNOS) by phosphorylation at serine 1177.[223, 224] eNOS generates NO from L-arginine, which stimulates vasodilation, vascular remodeling, cell migration and growth.[225] In general, Akt recognizes and phosphorylates its substrates in a cell type- and context-dependent manner.[226]

Aberrant Akt activation is commonly observed in cancer, probably as mechanism to increase DNA repair, promote genotoxic resistance and enhance overall survival, and is often associated with dysregulated PTEN or PI3K activation. Abnormal Akt signaling contributes to tumor growth, metastasis and resistance to anticancer treatment.[227-229]

3.4.4 The Hippo signaling pathway

The Hippo signaling pathway is evolutionally conserved and plays a pivotal role in homeostasis through organ size control, tissue regeneration and self-renewal. Especially proliferation, migration and survival of endothelial cells is coordinated by Hippo signaling.[230] Hippo signaling negatively regulates the activation and activity of transcriptional coactivators like Yes associated protein 1 (YAP) and transcriptional coactivator with PDZ-binding motif (TAZ).[231-234] Transcriptional coactivators themselves do not possess a DNA-binding activity but interact with other transcription factors, including the TEA domain family (TEAD), SMAD, RUNT-related transcription factors (RUNX1/2), T-box transcription factor 5 (TBX5) and p73, thereby enhancing their activity.[235-240] Amongst the YAP/TAZ target genes, many encode for proteins essential for cell proliferation, apoptosis and cell fate, including CTGF and cysteine-rich angiogenic inducer 61 (Cyr61).[241] In early stages of development, endothelial progenitor cell differentiation and retinal blood vasculature, YAP/TAZ expression is elevated. In mature, quiescent and tightly connected adjacent endothelial cells, on the contrast, the transcriptional coactivators are inactivated.[242, 243] In VEGF-induced endothelial cell angiogenesis, phosphorylation and thus inhibition of YAP/TAZ is prevented. At the same time, downregulation of YAP/TAZ effectively reduces VEGF-induced angiogenesis. Hence, VEGF-signaling and YAP/TAZ work tightly together.[244-246]

In general, the Hippo signaling pathway strongly relies on the activity of serine/threonine kinases: In case of activated Hippo signaling, various upstream signals lead to the auto-phosphorylation of mammalian STE20-like protein kinases 1/2 (MST1/2), which then undergo homo- or heterodimerization. MST1/2 heterodimers form a complex with Salvador 1 (SAV1) and phosphorylate the downstream large tumour suppressor kinases 1/2 (LATS1/2).[247, 248] At the same time, MOB kinase activator 1A and 1B (MOB1A/1B) are also phosphorylated by MST1/2, which allows them to interact with LATS1/2.[249] Interaction of LATS1/2 with MOB1A/1B further initiates the auto-phosphorylation of LATS1/2, which is crucial for its kinase activity.[250] Key substrates of LATS1/2 are the transcriptional coactivators YAP and TAZ.[234,

[251] Phosphorylation of YAP/TAZ by LATS1/2 either primes the transcriptional coactivators for interaction with 14-3-3 proteins, which causes cytosolic retention, or for ubiquitin-dependent protein degradation. As soon as LATS1/2 is inactive, YAP/TAZ are not phosphorylated any longer and, thus, can translocate to the nucleus, where they enhance gene expression.[251] Key features of activated and inactivated Hippo signaling are depicted in Figure 14.

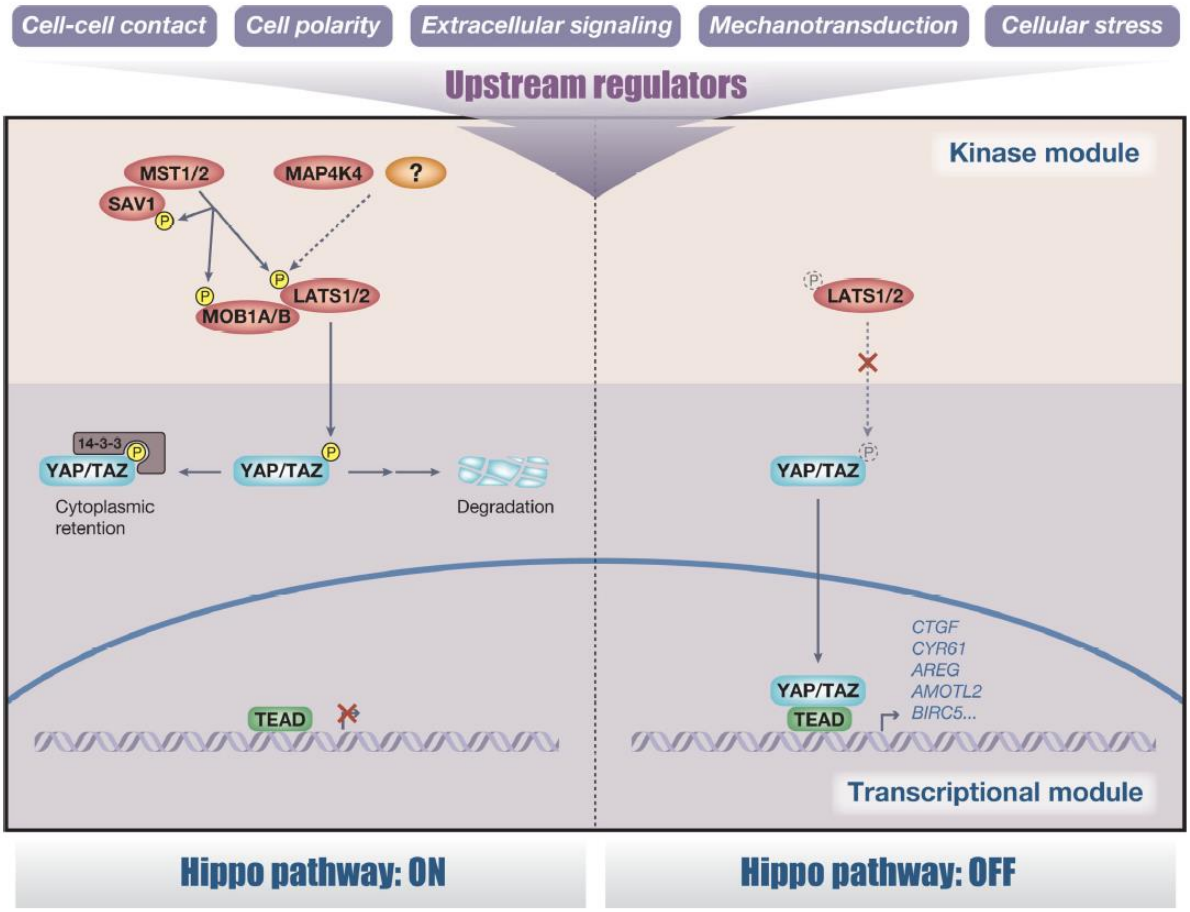

Figure 14: Regulation of the transcriptional coactivators YAP/TAZ. Hippo signaling is turned on by numerous upstream regulators, which initiate MST1/2 activation and interaction with SAV1. The MST1/2-SAV1-complex then phosphorylates LATS1/2 and MOB1, which form a second complex. This LATS1/2-MOB1-complex phosphorylates YAP/TAZ at several sites, thereby retaining the transcriptional coactivators in the cytosol or inducing ubiquitin-dependent degradation (left). When the Hippo signaling is inactivated, YAP/TAZ translocate to the nucleus where they interact with transcription factors like TEAD and initiate target gene expression (right). Reprinted with permission from Elsevier Inc. and Copyright Clearance Center: Elsevier, Trends in Cell Biology, YAP and TAZ: a nexus for Hippo signaling and beyond, Hansen CG *et al*., © 2015.[252]

The molecular guides as well as the underlying mechanisms commanding nuclear translocation and retention of YAP/TAZ are not fully understood. Also, mammalian YAP/TAZ proteins contain no functional NLS, as seen in other transcription factors like the NF-κB subunits p50 and p65. Nevertheless, it was recently shown that Mastermind-like 1 and 2 (MAML1/2) are involved in the translocation of the transcriptional coactivators to and their arrest in the nucleus. Furthermore, MAML1/2 regulate the transcriptional activity of YAP/TAZ. In this context, depletion of MAML1/2 can provoke the cytosolic retention of YAP and TAZ.[253]

To date, many regulatory mechanisms and factors that control YAP/TAZ activity have been identified. Regulating factors include transcriptional regulators like p53 and β-catenin, kinases like JNK1/2, Akt and MEK1, adaptor proteins including 14-3-3, epithelial cadherin (E-cadherin) or SMAD, Rho-GTPases, chromatin modulators, ubiquitin ligases and miRNAs.[254] Mechanisms regulating the Hippo signaling comprise cell polarity, cell adhesion, mechanical cues and signal transduction. Especially in apical-basal polarized cells, Hippo signaling is activated. Furthermore, mechanical forces such as stress, strain, cell density, stiffness and extracellular environment regulate the cellular localization of YAP/TAZ depending on changes in the actin cytoskeleton and Rho GTPase activity.[255] Cell contact-mediated adhesion potently restricts YAP/TAZ in the cytosol.[233]

3.5 Pathological angiogenesis

Pathological angiogenesis comprises both vascular insufficiencies and vascular overgrowth evoked through an unstable and dysfunctional endothelium. While under physiological conditions angiogenesis is a self-limiting process, pathological conditions, such as diabetes, neovascular age-related macular degeneration, tumor hypoxia and tumor-secreted factors, lead to a persistent and unresolved angiogenic cascade, irregular vascular networks and integrity and disturbed blood flow.[256, 257]

3.5.1 Tumor angiogenesis

Tumor growth heavily relies on the formation of new blood vessels since their growth rate exceeds the physiological formation of new vasculature. Thus, to satisfy the demand for oxygen and nutrients, which quickly surpasses the physiological supply, tumor cells induce hypoxic events that induce endothelial cell angiogenesis through HIFs and the subsequent release of pro-angiogenic factors (see III.3.2).[258] Importantly, not only tumor growth but also metastasis is mediated by angiogenesis, since spreading of malignant cells from the primary site is carried out via the blood stream. Therefore, single malignant cells detach from the primary tumor and invade the surrounding tissue. Upon migration towards nearby blood vessels, these cells can enter the blood stream by invasion through the endothelium. At distant organs, the malignant cells can adhere to and transmigrate through the endothelial monolayer into the underlying tissue, where they form a secondary tumor upon cell proliferation.[259] Key steps of tumor metastasis are shown in Figure 15.

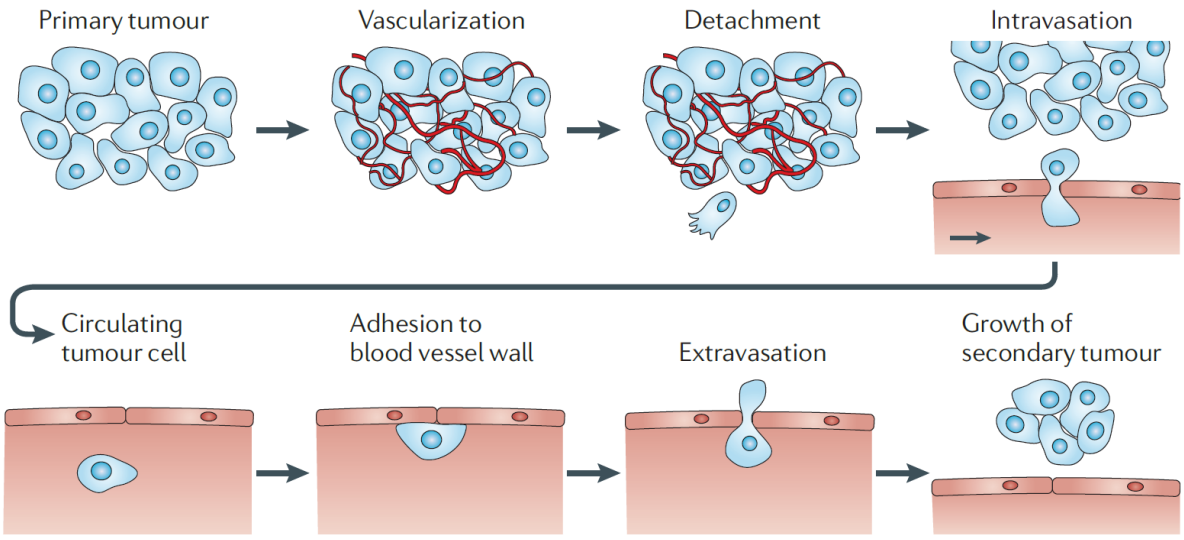

Figure 15: The metastatic process of tumors. Individual tumor cells detach from the primary, vascularized tumor and access the surrounding tissue. Upon physical proximity to blood vessels, the detached tumor cells can enter the blood stream by intravasation through the endothelium. At distant organs, tumor cells adhere to and transmigrate through the endothelium to the underlying tissue, where they proliferate and establish a secondary tumor. Reprinted with permission from Springer Nature and Copyright Clearance Center: Springer Nature, Nat Rev Cancer, The physics of cancer: the role of physical interactions and mechanical forces in metastasis, Wirtz D *et al*., © 2011.[259]

Interestingly, pathological vessels mainly derive from VEGF-A overexpression, which leads to several organizational abnormalities including excessive branching and sprouting, fragility, lack of stabilizing pericytes, bleeding and exudation. Moreover, cells of tumor blood vessels show altered gene expression and functionality. Structurally and functionally abnormal blood vessels decrease the efficiency of blood flow and oxygen supply but also affect delivery of anti-angiogenic and chemotherapeutic drugs to the tumor tissue. This secondary effect highlights a huge burden in the field of anti-cancer treatment.[260, 261]

3.5.2 Angiogenesis and inflammation

Angiogenesis and inflammation are two distinct mechanisms, which, however, show high frequency of crosstalk.[262] On the one hand, immune cells can secret pro-angiogenic factors, thus promoting inflammation-mediated angiogenesis. On the other hand, unresolved, sustained angiogenesis can amplify the chronic inflammatory response, thereby intensifying tissue damage. A schematic overview of the cross-talk between angiogenesis and inflammation is provided in Figure 16. Typical binary inducers of inflammation and angiogenesis comprise hypoxia, NO and immune cells. Hypoxia induces the accumulation of immune cells like macrophages at the site of hypoxia during inflammation, while at the same time, angiogenic sprouts penetrate towards the hypoxic tissue through secretion of HIFs and growth factors.[152, 263] Activation of the inducible NO synthase (iNOS) in immune cells like macrophages and T-cells evokes NO secretion. NO constitutes a pivotal pro-inflammatory agent through stimulating immune cell extravasation while also acting pro-angiogenic by

inducing endothelial cell migration and tube formation.[225, 264] Immune cells like T cells or neutrophils can produce growth factors like VEGF, hepatocyte growth factor (HGF) or MMPs. T cells express VEGFR2, thus they can react themselves to extracellular VEGF. This leads to pro-inflammatory T cell differentiation and accelerated VEGF production.[265-268] Increased VEGF concentrations at the site of inflammation again trigger site-specific angiogenesis. Importantly, chemotactic agents, which are released during angiogenesis, also mediate the migration of inflammatory cells towards the tissue, thereby sustaining inflammatory actions.[269]

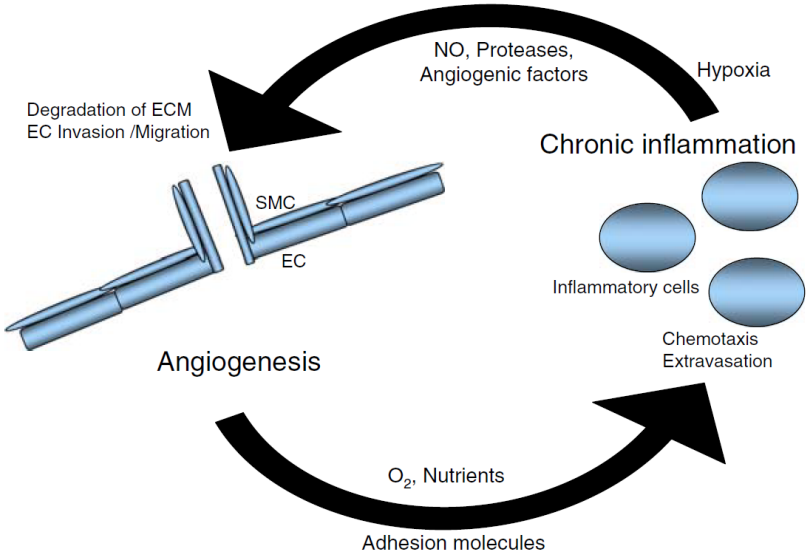

Figure 16: Crosstalk between chronic inflammation and angiogenesis. Inflammatory cells produce angiogenic factors, NO and proteases, which evoke degradation of the extracellular matrix (ECM) as well as endothelial cell (EC) growth, migration and invasion, which are key features of angiogenesis. Conversely, smooth muscle cells (SMCs) and ECs secrete pro-inflammatory cytokines. In combination with oxygen and nutrients, the chemotactic extravasation of inflammatory cells is enhanced. These two processes mutually reinforce each other. Reprinted with permission from Springer Nature and Copyright Clearance Center: Springer Nature, Angiogenesis, Angiogenesis and chronic inflammation: cause or consequence?, Costa C *et al*., © 2007.[262]

Rheumatoid arthritis (RA) and psoriasis are prominent examples of chronic autoimmune disease with both inflammatory and angiogenic features.[262] RA is mainly observed in the joints but can also include extra-articular manifestations, pulmonary features, vasculitis and systemic comorbidities. Typically, patient suffer from swelling, painful deformations, and immobility of the affected regions. These characteristics are evoked through persistent leukocyte and fibroblast infiltration and subsequent synovitis. Immune cells and fibroblasts in the inflamed synovial tissue release growth factors, thereby inducing angiogenesis. Through elevated angiogenesis, again, more inflammatory cells can enter the synovial tissue resulting in synovial hyperplasia and progressive bone destruction.[270]

Psoriasis is a skin disease, which typically affects the limbs, scalp and intergluteal cleft, and is characterized by erythematous lesion that are covered with white plaques. The disease is defined by extensive immune cell activation, which evokes proliferation and differentiation of dermal cells as well as an expansion and dilation of the dermal microvasculature. The

microvasculature is tortuous and leaky, thereby accelerating leukocyte recruitment to the injured tissue and production of pro-inflammatory cytokines.[271]

3.6 Angiogenesis as therapeutic target

Based on the observation that abnormal angiogenesis is associated with numerous pathological disorders, targeting angiogenesis is a promising and useful tool for disease treatment. While pro-angiogenic therapeutic approaches (so-called “therapeutic angiogenesis”), i.e. the treatment with angiogenesis-stimulating agents, are applied in disorders characterized by deficient angiogenesis like ischemia, anti-angiogenic therapy, i.e. the application of angiogenesis-inhibiting agents, is beneficially used to attenuate excessive angiogenesis in diseases like cancer or RA.[272, 273]

In general, two different approaches for therapeutic angiogenesis are used, comprising growth factor therapy and cell-based therapy. Growth factor therapy serves to deliver growth factors to the target tissue. This can either be achieved through direct application of the protein or through genes which encode the growth factor protein.[274-276] In 1977, the first recombinant platelet-derived growth factor, becaplermin, was approved as angiogenesis-stimulating drug for the treatment of lower extremity diabetic neuropathic ulcers.[277] Cell-based therapies are proposed to deliver progenitor or stem cells to the tissue to either secrete pro-angiogenic mediators or directly participate in blood vessel formation.[278]

For anti-angiogenic therapies, multiple approaches are available. In general, however, the most common treatment consists of an anti-VEGF therapy.[279] In this regard, either VEGF is directly targeted through specific neutralizing antibodies, or VEGF-signaling is antagonized through tyrosine kinase inhibitors (TKI). Bevacizumab is a humanized antibody against VEGF-A, which was approved for the treatment of various cancer types.[280-282] TKIs comprise the multi-kinase inhibitors sorafenib and pazopanib as well as the VEGFR3 inhibitor sunitinib. Sorafenib targets the cell surface kinase receptors VEGFR2, VEGFR3 and PDGFR as well as intracellular Raf kinases, while pazopanib inhibits VEGFR1, VEGFR2, VEGFR3, PDGFR and FGFR.[283] Especially in eye diseases, such as age-related macular degeneration, diabetic retinopathy or diabetic macular edema, anti-VEGF therapy is widely used. Here, anti-VEGF drugs, such as the humanized antibody fragment ranibizumab and the recombinant fusion protein aflibercept have been approved for application.[284-286]

Importantly, long-term administration of anti-VEGF therapy has been found to decrease treatment efficacy, evoke therapy resistance and cause side effects such as hypertension, proteinuria, thrombosis, renal dysfunction and many more.[287-291] For this reason, there is an ongoing demand for innovative, efficient and safe new anti-angiogenic compounds.

4. The natural product vioprolide A

4.1 Natural products as drugs and tools for disease treatment

Finding new drug candidates for the treatment of diseases is still an ongoing and huge challenge. In this regard, natural products represent exquisite lead structures and tools for the identification of innovative cellular targets and modes of actions. Natural products originate from bacterial, fungal, plant and marine animal sources and usually constitute secondary metabolites, i.e. molecules that are not initially needed for survival but provide a survival benefit. Up to 2013, approximately 40 % of all new chemical entities approved by the US Food and Drug Administration were natural products themselves, their semi-synthetic derivatives or synthetic compounds based on natural product structures.[292] Natural products and their derivatives are exceptionally well-established in the field of oncology and infections but also play a role in the treatment of cardiovascular and inflammatory diseases.[293-295] Especially through different screening approaches, such as phenotypic or target-based screening as well as the recent genomics-based approaches, ongoing discovery of new secondary metabolites is ensured.[296, 297]

Amongst the top producers of secondary metabolites are myxobacteria. Myxobacteria belong to the proteobacteria and are well-known for their collective swarms called fruiting bodies, which they form when resources are truncated.[298] The most common bioactivities of myxobacterial secondary metabolites comprise antifungal or antibacterial actions. However, a wide variety of myxobacterial metabolites also provides differing biological activities, including immunosuppressive, antiviral or antimalarial actions.[299, 300] Furthermore, various metabolites, including the tubulin-targeting agent tubulysin or the actin-targeting compound chondramide, exhibit cytostatic or cytotoxic effects towards mammalian cells.[301, 302] Considering that from many myxobacterial species not just one but multiple different biologically active secondary metabolites have been isolated, there is an ongoing demand for their systematic characterization, which in the future could also ensure a reliable source for promising leads regarding the discovery of new disease treatments.[303]

4.2 Discovery and chemistry of vioprolide A

Vioprolide A belongs to a group of four metabolites, vioprolide A-D, which have initially been isolated from the myxobacterium *Cystobacter violaceus* Cb vi35 by fermentation.[304] All vioprolides share the same basic molecular structure of a cyclic depsipeptide consisting of eight amino acids and one glyceric acid. Starting from the N-terminal site, the building blocks of vioprolide A can be identified as: L-Ala, D-Leu, L-Cys, (E)-dehydrobutyrine, L-Homopro, L-Thr, L-Me-Val, L-glyceric acid. In addition, vioprolide A and vioprolide C contain the rare

structural moiety of a trans-(2*S*, 4*R*)-4-methylazetidinecarboxylic acid (MAZ) between D-Leu and L-Cys.[304] The chemical structure of vioprolide A is provided in Figure 17. To date, MAZ has only been reported as MAZ methyl ester in the chemical structure of one further natural product called bonnevillamide A, a linear heptapeptide from *Streptomyces sp.* GSL-6B.[305] Targeted LC-MS screening has validated that of approximately 3,000 different myxobacteria included into the study, *C. violaceus* Cb vi35 is the sole natural producer of these unique metabolites.[306] Due to the structurally complex MAZ, which is particularly challenging to access, a chemical synthesis of vioprolide A has not been reported to date. Nevertheless, various approaches towards vioprolide precursors are available, amongst them the synthesis of an azetidinyl-thiazoline fragment and of macrocyclic precursors, which, however, involve high difficulties especially due to the sensitivity of the thiazoline fragment and delicate bond formation between E-dehydrobutyrine and L-Pro or L-Homopro.[307]

Besides approaches towards the chemical synthesis, more in-depth investigations regarding a heterologous expression of the natural product have been conducted. Through genome sequencing, gene clustering and gene cluster cloning, heterologous expression of vioprolides in *Myxococcus xanthus* DK1622 is possible and allows higher yields and less production time. Interestingly, heterologous production of the MAZ-containing vioprolide A and vioprolide C is only triggered when the growth cultures are supplemented with vitamin B12, an important co-factor for S-adenosylmethionine (SAM) biosynthesis.[308] Indeed, the SAM-dependent methyltransferase VioH, present in *C. violaceus* Cb vi35, catalyses an unusual SAM cyclization during vioprolide biosynthesis leading to the formation of azetidine-2-carboxylic acid, the proposed precursor of MAZ.[309]

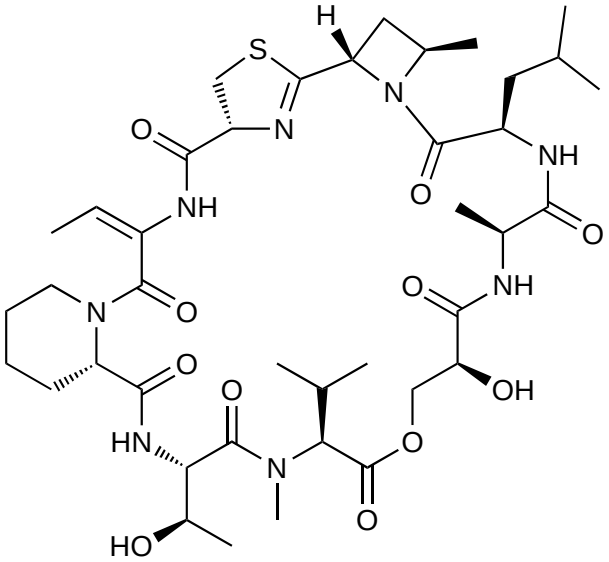

Figure 17: Chemical structure of vioprolide A. The building blocks of vioprolide A consist of: L-Ala, D-Leu, L-Cys, (E)-dehydrobutyrine, L-Homopro, L-Thr, L-Me-Val, L-glyceric acid. In addition, vioprolide A contains the rare structural moiety of a trans-(2*S*, 4*R*)-4-methylazetidinecarboxylic acid (MAZ) between D-Leu and L-Cys.

4.3 Biological properties of vioprolide A

Vioprolide A shows a strong cytotoxicity in the eukaryotic murine fibroblast cell line L929 with a median half maximal inhibitory concentration (IC_{50}) of only 2 µg/ml. Furthermore, strong antifungal properties but no antibacterial effect are observed.[304] Despite the high potency and uniqueness of the natural product, biological studies remain rare. Only recently, more in-depth investigations regarding the biological effects of vioprolide A have been conducted. In primary murine bone marrow-derived macrophages (BMDMs) and peripheral blood mononuclear cells (PBMC), vioprolide A at concentration of 0.1 to 20 µM exerts immunomodulatory actions by inducing IL-1β maturation and caspase-1 cleavage, while at the same time triggering lactate dehydrogenase release, a typical marker for cell death. Mechanistically, vioprolide A downregulates the pro-survival proteins Mcl-1 and Bcl-2, which induces intrinsic apoptosis a Bax- and Bak-dependent mechanism. This involves mitochondrial outer membrane permeabilization, the release of the pro-apoptotic factor cytochrome c and early proteolytic processing of caspase-3. Especially the loss of inhibitors of apoptosis proteins results in caspase-8 cleavage and subsequent IL-1β maturation.[310]

Besides exerting immunomodulatory actions, vioprolide A provides strong antiproliferative effects in different cell lines, including Jurkat cells with an IC_{50} ranging between 2.5 to 8 nM. At the same time, the apoptosis rate in cancer cells is strongly increased by vioprolide A with half maximal effective concentrations (EC_{50}) between 15 nM to 30 nM for the acute lymphoblastic leukemia (ALL) cell lines CEM and Jurkat.[311] Interestingly, the pro-apoptotic effect of vioprolide A on acute myeloid leukemia (AML) cell lines is lower with EC_{50} values between 90 nM (HL-60) and 135 nM (HeLa). The anticancer effects can be traced back to an induction of intrinsic apoptotic cell death comprising the activation of caspase-3 followed by PARP cleavage. While in ALL cell lines and ALL patient-derived xenografts strong cytotoxic effects are observed, the apoptosis rate of normal PBMCs is not influenced by concentrations of 5 nM to 50 nM of vioprolide A.[311]

4.4 The cellular target of vioprolide A

Chauhan *et al.* have been the first to report an inhibitory effect of vioprolide A on protein biosynthesis *in vitro* with an IC_{50} of 112 nM using a eukaryotic cell-free translational system.[310] Through thermal proteome profiling Kirsch *et al.* have later identified the nucleolar protein NOP14 as cellular target of vioprolide A in Jurkat cells.[311] The emergence of NOP14 has first been reported in the yeast *Saccharomyces cerevisiae*. Functional investigations in *Saccharomyces cerevisiae* indicate that NOP14 occurs in the nucleolus and coordinates the nuclear accumulation of EMG1, which is in non-interacting conditions spread throughout all cellular compartments. The study further underlines that the interaction of NOP14 with EMG1

is mandatory for the maturation of the 18S rRNA and 40S ribosome production, as depletion of NOP14 in yeast causes reduced levels of 20S pre-rRNA, mature 18S rRNA and 40S ribosomal subunits. Importantly, functional analysis of the mammalian orthologues of NOP14 and EMG1 suggests a functional conservation among all eukaryotes.[312] The expression of NOP14 is coordinated by the ribosomal biogenesis transcriptional program, which is activated by ribosomal protein S6 kinase.[313]

Especially in cancer cells, increased ribosome production and dysregulated protein biosynthesis are associated with excessive cell proliferation, angiogenesis, survival and altered energetics.[314, 315] Studies incorporating pancreatic, bladder and colorectal cancer cells have revealed an increased level of NOP14 compared to normal cells, which is connected to enhanced cancer cell motility. Mechanistically, NOP14 overexpression stabilizes mutant p53 mRNA, suppresses p21 expression and upregulates β-catenin signalling. Targeted knockdown of NOP14 lowers cell proliferation and cell migration and evokes a cell cycle arrest at the G_1 phase. Moreover, cell viability is decreased through activation of caspase - 3.[316-320] Surprisingly, studies conducted with divergent cancer cell types, including melanoma cells and breast cancer cells, have revealed opposing actions of NOP14. In these cancer cell types, NOP14 is poorly expressed compared to healthy control cells, and overexpression of NOP14 downregulates cell proliferation, migration and cell viability, while inducing the cell cycle in the G_1 phase mainly through inhibition of the Wnt/β-catenin pathway.[321, 322] Interestingly, besides being connected to cancer cell functions, NOP14 has also been shown to constitute a key gene in sepsis and may thus be associated with systemic inflammation.[323]

5. Eukaryotic protein biosynthesis

Protein synthesis represents the process of translating information, which is stored in the DNA and has been transcribed to messenger RNA (mRNA), into functional proteins. Translation of mRNA takes place at macromolecular complexes called ribosomes. Both ribosome biogenesis and mRNA translation are cellular process with high energy demands.[324]

5.1 The ribosomal biogenesis

Ribosomes constitute the cellular machines needed for the translation of mRNA into proteins.[324] In eukaryotes, ribosomes comprise a small 40S and large 60S ribosomal subunit, which both are composed of ribosomal RNA (rRNA) and ribosomal proteins.[325, 326] The formation of the ribosomal subunits takes place in small nuclear compartments called nucleoli and is divided into five major steps: (I) formation of pre-ribosomal RNA and assembly of ribosomal proteins, (II) pre-rRNA modification, (III) pre-RNA folding, (IV) connection of pre-

rRNA and ribosomal proteins and (V) deletion of spacer rRNAs from the pre-rRNA.[327, 328] A schematic overview of the ribosomal biogenesis is given in Figure 18.

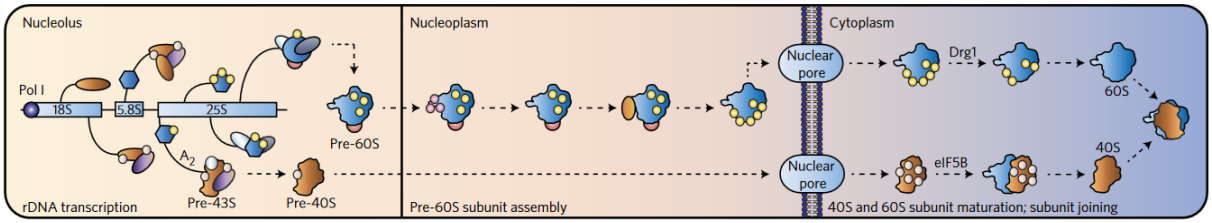

Figure 18: Simplified scheme of eukaryotic ribosome biogenesis. Ribosomal biogenesis is mainly conducted in the nucleolus, where pre-ribosomal RNA and ribosomal protein formation, pre-rRNA processing, assembly and modification takes place. For the final step of maturation, the pre-40S and -60S subunits are exported to the cytosol. The figure was reprinted with permission from Springer Nature and Copyright Clearance Center: Springer Nature, Nat Chem Biology, Chemical modulators of ribosome biogenesis as biological probes, Stokes JM *et al.,* © 2015.[329]

A tremendous number of ribosome assembly factors, including the family of nucleolar proteins (Nops) and small nucleolar RNAs (snoRNAs), participate in the process of ribosome biogenesis.[330, 331] In this context, the nucleus is supplied with ribosomal proteins and biogenesis factors by nuclear import factors of the importin family and chaperones.[332-336] To transport the 60S and 40S ribosomal subunits from the nucleus to the cytosol for final maturation, the subunits are coupled to an adaptor protein containing a nuclear export sequence (NES). Nuclear export is guided by nucleoporins, the Ran-GTPase system and nuclear export proteins including exportins and karyopherins.[337-341]

5.2 The translation of mRNA into protein

The translation of mRNA into proteins is sectioned into three major steps: initiation, elongation and termination. Translation initiation is the rate-limiting step of protein synthesis.[342] A schematic overview of the key processes of mRNA translation is depicted in Figure 19.

During translation initiation, the 40S small and 60S large ribosomal subunit are brought together with the mRNA that needs to be translated as well as the initiator methionyl-transfer RNA (Met-tRNA). The Met-tRNA is the initiator tRNA, which carries the first amino acid, methionine, of all new polypeptide chains. The structure and sequence of the Met-tRNA are unique and differ from other aminoacylated tRNAs (aa-tRNA) or deacylated tRNAs.[343] Initially, the eukaryotic initiation factor 2 (eIF2) establishes a complex with the Met-tRNA, called the ternary complex (TC).[344] Importantly, eIF2 exclusively binds to the Met-tRNA, thereby on the one hand excluding other aa-tRNAs from ternary complex formation and on the other hand excluding the Met-tRNA from participating in the translation elongation phase. In the presence of varying initiation factors, including eIF1, eIF1A and eIF3, the TC binds to the 40S small ribosomal subunit, thereby creating the larger 43S pre-initiation complex.[345] Simultaneously, the initiation factors eIF4A, eIF4E and eIF4G join each other and build an individual initiation

complex called eIF4F. The eIF4F complex interacts with the 7-methylguanosine 5’ cap of the mRNA and unwinds the secondary structure of the mRNA through its RNA helicase activity. Subsequently, the 43S pre-initiation complex connects with the untangled mRNA at or close to the 5’ cap. This connection is further stabilized by the initiation factors eIF3 and eIF4G. The 43S pre-initiation complex then scans the mRNA in an ATP-dependent mechanism until an initiation base codon, typically AUG, is detected on the mRNA.[346] The mRNA sequence between the 5’ cap and the initiation base codon is referred to as 5’ untranslated region (UTR). When the initiation codon is reached, the Met-tRNA of the 43S pre-initiation complex binds to the base sequence of the initiation codon. At last, the 60S large ribosomal subunit joins the 40S small ribosomal subunit in an eIF5B-dependent mechanism, creating the 80S ribosomal complex. Release of eIF5B and eIF1A marks the end of the initiation step.[344]

The large ribosomal subunit contains three sites, called the acceptor site (A-site), the peptidyl site (P-site) and the entry site (E-site).[347] In the step of translation elongation, aa-tRNAs are shuttled to the empty A-site of the 80S ribosome complex in an elongation factor (eEF1) complex- and GTP-dependent mechanism. The eEF1A subunit of the eEF1-complex thereby functions as classic G-protein and its activation state depends on whether GTP or GDP is bound. Only when the anticodon of the aa-tRNA matches the codon of the mRNA, GTP is hydrolysed to GDP, which inactivates eEF1A and causes its release from the ribosome. The peptidyl transferase center, which lies in the 60S large ribosomal subunit, then catalyzes the peptide bond formation of the new aminoacyl-residue of the tRNA in the A-site of the ribosome with the adjacent aminoacyl-residues of the tRNA, which is located in the P-site of the ribosome. In the following, the tRNAs bound to the aminoacyl-residue are translocated from the P- to the E-site and from the A- to the P-site in an eEF2-dependent mechanism. The tRNA located in the E-site now represents the deacylated tRNA, while the tRNA in the P-site contains the growing peptidyl chain. After successful peptide bond formation, the ribosome continues to the next base sequence and a new aa-tRNA can bind to the A-site. This process is pursued until a stop codon, such as UAA, UGA or UAG, reaches the A-site of the ribosome.[348]

At this point, translation termination takes over. Therefore, the eukaryotic release factors eRF1 and eRF3 form a complex with GTP. While eRF1 indentifies the stop codon at the mRNA, eRF3 catalyzes the hydrolysis of GTP to GDP, which leads to the release of the nascent polypeptide chain from the ribosome. Then, the 80S ribosomal complex is splitted back into the 40S small and 60S large ribosomal subunits and the mRNA and deacylated tRNA are released from the 40S small ribosomal subunit. The ribosomal subunits are then recycled to be available for the formation of a new translation complex.[349]

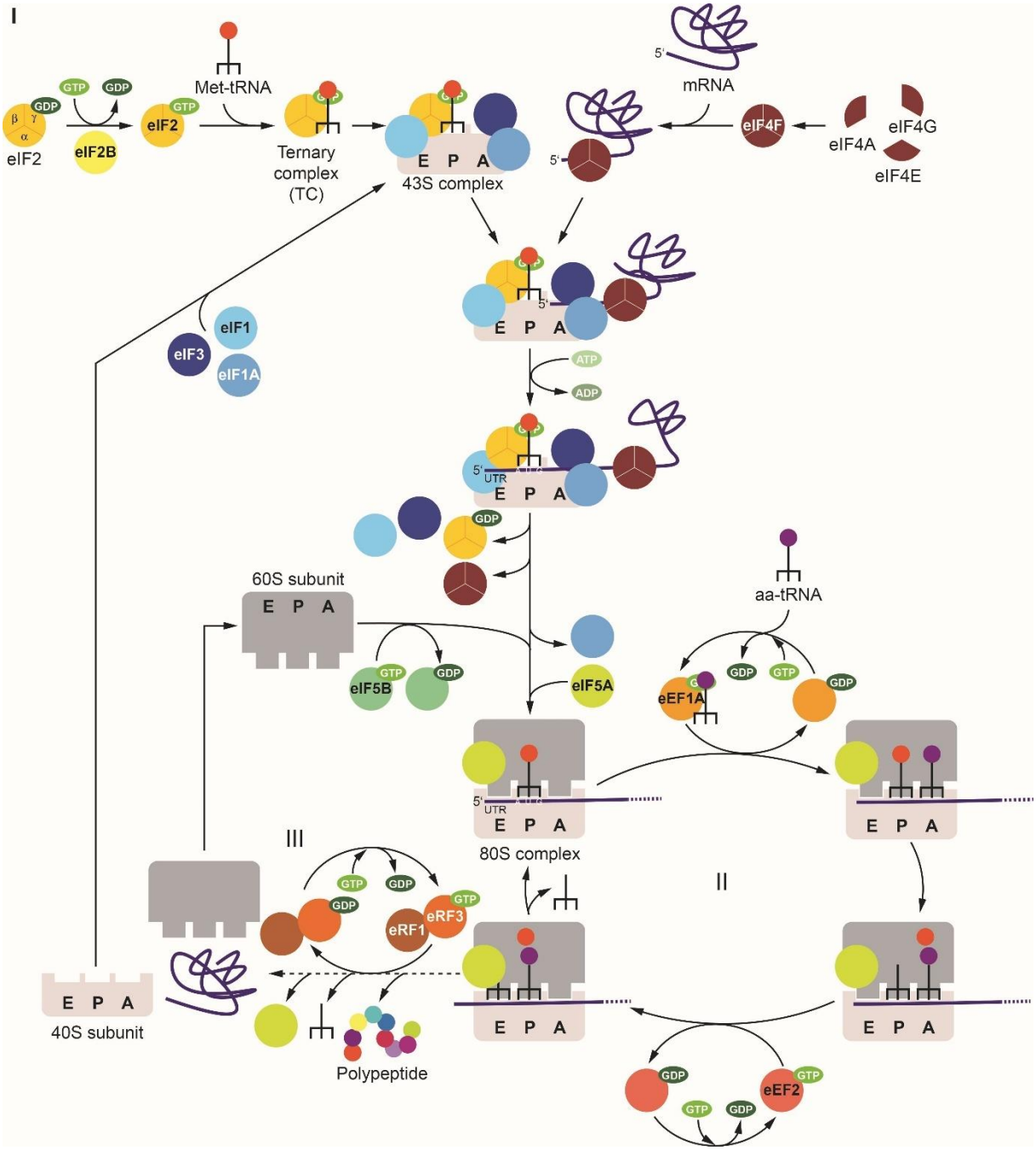

Figure 19: Schematic overview of eukaryotic mRNA translation, including translation initiation (I), elongation (II) and termination (III). I consists of TC formation, 43S and 48S complex assembly and screening of the mRNA for a start codon. It is completed by joining of the 60S ribosomal subunit to form a functional 80S ribosome. During **II**, binding of the aa-tRNA to the ribosome, peptide bond formation and translocation of the ribosome towards the 3' end of the mRNA take place. **III** evokes, when a stop codon on the mRNA is reached and causes the release of the finalized polypeptide chain from the ribosome. The ribosomal subunits separate from each other and are subsequently recycled for the next round of ribosomal assembly. Reprinted in accordance with the author rights and publishing agreements from Elsevier Inc., Pharmacol Res, Natural products as drugs and tools for influencing core processes of eukaryotic mRNA translation, Burgers LD and Fürst R, © 2021.[342]

5.3 Protein biosynthesis and diseases

Alterations in mRNA translation play a delicate role in the development and progression of diseases, including cancer, inflammatory diseases, neurodegenerative diseases, psychiatric disorders, diabetes and viral infections.[350-355] Translational alterations include an altered

occurrence or activity of ribosomal biogenesis, mRNA translation, initiation factors, elongation factors or tRNAs. In general, mutations in genes that encode proteins of the translational machinery can cause errors during mRNA translation and hence less functional proteins.[356]

5.3.1 Protein biosynthesis and cancer

Cancer cells rely on increased rates of protein synthesis to ensure fast cell proliferation and increased cell survival. Indeed, in many cancer cells, the control mechanisms of mRNA translation are degenerated, while at the same time the number of ribosomes is increased.[357] Importantly, besides altering global mRNA translation, cancer cells have also developed mechanisms to promote the translation of specific mRNAs involved in angiogenesis, survival and metastasis.[358-360] An overview of translational dysregulations in cancer is provided in Figure 20.

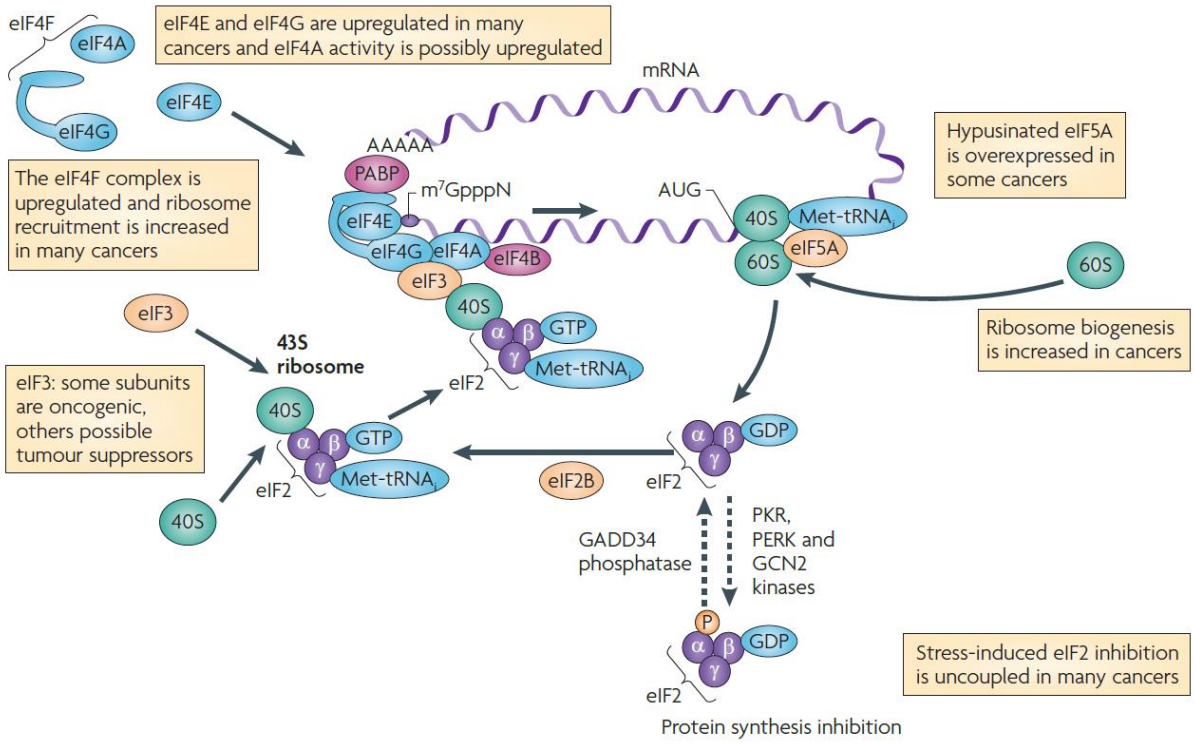

Figure 20: Translational dysregulations in cancer. Besides revealing an overall increase in protein biosynthesis, cancer cells frequently show overexpression or hyperactivation of initiation factors, including eIF3, eIF4F, eIF4E, eIF4G, eIF5 and eIF2. The figure was reprinted with permission from Springer Nature and Copyright Clearance Center: Springer Nature, Nat Rev Cancer, Translational control in cancer, Silvera D *et al.*, © 2010.[357]

Translation initiation represents the rate-limiting step of mRNA translation. It is, thus, not surprising that alterations in the expression and function of initiation factors is frequently observed in cancer. The initiation factor eIF3, which is involved in all subprocesses of mRNA translation from initiation to quality control and which regulates the translation of specific mRNAs important for cell growth, has been connected to cancer development. Intriguingly,

though, the expression of various eIF3 subunits is regulated differentially. While cancer cells show an overexpression of eIF3A, eIF3C and eIF3H, the level of eIF3F is decreased.[357] Furthermore, overexpression of eIF2α and eIF4E has been linked to aggressive cancer cell types as well as cancer progression.[361-364] Dysregulation of eIF4E is oncogenic through triggering the ongoing translation of a specific mRNA pool with highly structured 5' UTR, which encode proteins like VEGF or cyclins that are important for cell proliferation and survival.[365, 366] Increased levels in eIF5A1 and eIF5A2, which are under physiological conditions highly important for the stimulation of peptide bond formation, are associated with cancer progression, recurrence and an overall poor prognosis.[367-369]

Importantly, several factors involved in translation elongation have been implicated in diseases development as well.[370] The kinase eEF2K, which phosphorylates the elongation factor eEF2 and, thereby, reduces the elongation rate, evokes cancer cell type-specific beneficial or detrimental functions.[371] Deregulation of eEF1 complex proteins, including eEF1A1, eEF1D and eEF1G, correlates with the survival rate in various types of cancer.[372]

Besides affecting the process of mRNA translation, cancer cells also show alterations in the ribosome biogenesis through influencing the expression of eIF6, an important factor during the early biogenesis steps in the nucleolus.[373, 374]

5.3.2 Ribosomopathies – diseases involving ribosome dysfunctions

Alterations involving ribosomal assembly factors, ribosomal proteins and the ribosomal assembly are termed ribosomopathies. Ribosomopathies occur through a malfunctioning rRNA synthesis, rRNA maturation, pre-RNA assembly, an imbalanced level of ribosomal proteins as well as a deregulation of ribosomal factor import to the nucleus or ribosomal subunit export to the cytosol.[375] Ribosomal haploinsufficiency has been shown to cause anemia, defects in growth and development and congenital anomalies including craniofacial defects.[376] To date, several congenital syndromes have been linked to ribosomopathies.[370] Interestingly, the deregulated ribosome biogenesis and, in this context, the overexpression of ribosomal proteins has been linked to cancer.[376, 377] Moreover, patients with gene defects that lead to ribosomopathies have a high overall risk of developing cancer.[378-381] Besides being linked to cancer, especially alterations affecting ribosomal proteins have been connected to inflammation and cardiovascular diseases. While overexpression of ribosomal protein S3 and S19 exerts pro-inflammatory actions by increasing the DNA binding activity of the pro-inflammatory transcription factor NF-κB or by acting as leukocyte chemoattractant, the ribosomal protein L13a contains anti-inflammatory properties through regulating the expression of inflammatory cytokines.[382-386] Ribosomal protein S15a enhances the Wnt/β-catenin signaling pathway, thereby inducing tumor angiogenesis, and ribosomal protein L29 influences blood vessel density and VEGF-induced sprouting.[387, 388] In patients with psoriasis

or atopic dermatitis, the ribosomal protein S6 is abnormally phosphorylated, which is correlated with hyperproliferation of keratinocytes in the epidermis.[389] Furthermore, overexpression of the ribosomal protein S19 is involved in tumor migration and angiogenesis.[390]

5.4 Protein biosynthesis as druggable pathway

Due to the strong implication of deregulated protein biosynthesis with manifold disorders, targeting mRNA translation has become an emerging field in disease therapies.[391, 392] Nevertheless, protein synthesis is also needed in normal cells for a healthy and working environment, which constitutes a huge obstacle in the field of drug development.

Approaches towards the specific inhibition of deregulated mRNA translation include the targeting of protein synthesis regulating signaling pathways, like the mTOR signaling, or proteins involved in protein synthesis, including initiation factors, the application of antisense oligonucleotides or RNA interference.[393] Prominent inhibitors of the mTOR signaling are the natural metabolite rapamycin from *Streptomyces hygroscopicus* and its derivatives everolimus and temsirolimus. Interfering with the mTOR signaling pathway inhibits cancer metabolism and suppresses disease-like phenotypes of Parkinson's disease. Everolimus is approved for the treatment of different types of cancer.[394, 395]

The initiation factor eIF2α represents a popular target for the direct inhibition of the translational apparatus. Natural compounds as well as various small molecules have been found to influence eIF2α activity, either through increasing its phosphorylation or inhibiting its dephosphorylation.[396] Besides eIF2α, the initiation factors eIF4A and eIF4E represent potential targets of translation inhibition. For eIF4A, mainly natural inhibitors, like pateamine A, have been identified, whereas numerous small molecules have been synthesized to inhibit the eIF4E-cap interaction.[342] In particular, the nucleoside analog ribavirin is a prominent eIF4E inhibitor, which has been approved for the treatment of virus infections.[397, 398]

Besides translation initiation, the elongation step and direct interactions with the ribosome at the A-, P- or E-site have emerged as interesting target for anticancer and antiviral therapies as well as for the treatment of genetic disorders.[399]

Antisense oligonucleotides are short, single stranded DNA molecules with a complementary sequence to the target mRNA or non-coding RNA. The interaction of the antisense oligonucleotide with the mRNA inhibits the translation and, thus, expression of one specific protein. To date, antisense oligonucleotides have been approved for the treatment of nervous muscular or familial metabolic diseases. Clinical trials with regards to cancer treatment with the antisense oligonucleotides AP12009, which is directed against TGF-β2, and AZD4785, which targets the expression of the oncogene KRAS, are ongoing.[393]

Over the past decades, a broad range of other natural secondary metabolites have been identified to influence mRNA translation and to provide promising anti-cancer, anti-angiogenic,

anti-inflammatory and many more properties. In this regard, natural products reveal a broad range of potential druggable targets in the process of mRNA translation comprising not only the usual widely studied initiation factors or ribosomal interactions but also rare interacting partners, such as ribosomal assembly factors.[342]

6. Aim of the study

6.1 Characterization of the influence of vioprolide A on inflammatory processes in the endothelium

Inflammation is a multicellular physiological process, which protects the body against pathogens and altered cells. After successful elimination of the inflammatory stimulus, tissue homeostasis is reinstalled through resolution of inflammation and tissue restoration. In case of non-resolving or inadequate inflammation, chronic inflammation develops, which contributes to the pathology of severe diseases, for example rheumatoid arthritis. Chronic inflammation is defined by dysfunctional endothelial cells, which facilitates persistent leukocyte recruitment from the blood to the tissue. The search for novel drugs and trug targets in this field is an ongoing demand.

Vioprolide A is a cyclic peptide produced by the myxobacterium *Cystobacter violaceus* Cb vi35. Recently, vioprolide A was shown to target the nucleolar protein NOP14 in Jurkat cells. NOP14 is involved in the ribosomal biogenesis and was identified as potential key gene in sepsis. Hence, NOP14 may play an important role in inflammation. Besides, no data are available regarding the effects of NOP14 and vioprolide A on inflammation. In this context, our first aim of this part of the study was to elucidate the influence of vioprolide A on inflammatory processes and more specific on the leukocyte-endothelial cell interaction. For this purpose, vioprolide A-evoked effects on the infiltration of immune cells in the laser-induced choroidal neovascularization and rolling, adhesion and transmigration of leukocytes through postcapillary venules observed in the cremaster muscle in mice were examined *in vivo*. The leukocyte-endothelial cell interaction was further analysed *in vitro* using primary human endothelial cells, thereby focusing on the impact of vioprolide A on endothelial cells. Leukocytes were, thus, at no time point of the experimental procedure in contact with the compound. The second aim of this part of the study was to explore the underlying mechanism of the anti-inflammatory actions. Since NOP14 is involved in ribosomal biogenesis, we first focused on the general effect of vioprolide A on *de novo* protein synthesis. In this connection, the expression of endothelial cell adhesion molecules that participate in the leukocyte extravasation during the inflammatory response, was studied. Simultaneously, the influence of vioprolide A on the prominent pro-inflammatory NF-κB signalling pathway, including kinase activation, NF-κB subunit nuclear translocation, NF-κB promotor activity and expression of NF-

κB target genes, was determined. Finally, a potential involvement of the cellular target NOP14 in the observed anti-inflammatory actions of vioprolide A was analysed by using siRNA mediated knockdown of the nucleolar protein.

6.2 Characterization of the influence of vioprolide A on angiogenic processes in the endothelium

Angiogenesis, the formation of new blood vessels from preexisting ones, is a physiologically important process both in embryogenesis and adulthood. Angiogenesis strongly relies on the activation of the endothelium, the innermost lining of the blood vessels. Nevertheless, angiogenesis can also occur under pathological conditions, including cardiovascular diseases and angiopathies, like macular degeneration, which eventually leads to severe tissue damage. Moreover, tumor growth and metastasis heavily depend on the formation of new blood vessels. In general, deregulated angiogenesis is commonly associated with dysregulated functions of endothelial cells. Thus, inhibiting angiogenesis and targeting endothelial cells is of great benefit for shifting angiogenesis from a pathological situation back to the normal physiological status. As current anti-angiogenic pharmacotherapy is frequently unsatisfactory, the discovery of new antiangiogenic drug leads is of great demand.

Vioprolide A was recently shown to target the nucleolar protein NOP14. NOP14 is involved in the ribosomal biogenesis and was connected to tumor angiogenesis. Nevertheless, no data are available regarding the effects of NOP14 and vioprolide A on angiogenic processes in normal, non-cancerous cells. In this context, the first aim of this second part of the study was to characterize the impact of vioprolide A on angiogenic processes in the endothelium. Therefore, a choroidal neovascularization experiment was performed in mice. Furthermore, the influence of vioprolide A on key angiogenic features of primary human endothelial cells, including sprouting, migration and proliferation, was determined *in vitro*. The second aim was to obtain insights into the underlying mechanism of action provided by vioprolide A. Pro-angiogenic actions are initiated by multiple intracellular signalling cascades, which are activated by growth factors and their respective tyrosine kinase receptors. Thus, a potential effect of vioprolide A on the protein levels of relevant tyrosine kinase receptors, including VEGFR2, FGFR1 and EGFR, was examined. Important downstream signalling molecules investigated in the study comprise the mitogen activated protein kinases ERK1/2, p38 and JNK as well as the pro-survival kinase Akt. Since angiogenic processes are not exclusively mediated by receptor tyrosine kinase signalling, also the evolutionary conserved Hippo signalling pathway was considered as possible target of vioprolide A. At last, a potential involvement of the cellular target NOP14 in the observed anti-angiogenic actions of vioprolide A was analysed by using siRNA mediated knockdown of the nucleolar protein.

IV MATERIALS AND METHODS

1. Materials

1.1 Compounds

Vioprolide A (vioA) was kindly provided by the group of Prof. Dr. Rolf Müller (Helmholtz Institute for Pharmaceutical Research Saarland, Saarland University, Saarland, Germany), dissolved in dimethyl sulfoxide (DMSO) to 1 mM and stored at -80°C. Cycloheximide (CHX) was dissolved in DMSO to 100 mg/ml and stored at -20 °C. Doxorubicin was diluted in DMSO to a stock solution of 10 mM and stored at 4 °C in the dark. The PI3K inhibitor Ly294002 was dissolved in DMSO to a stock solution of 10 mM and stored at -80 °C. For cell culture purposes, the stock solutions were freshly diluted without exceeding a final DMSO concentration of 0.1 % (v/v). The used concentrations are described in the respective passages.

1.2 Biochemicals, dyes and cell culture reagents

The following tables (Table 2 and Table 3) display biochemicals, dyes and cell culture reagents used in this study.

Table 2: Biochemicals and dyes

Reagent	Supplier
1,4-Dithiothreitol (DTT)	Sigma-Aldrich Chemie GmbH, Taufkirchen, Germany
2-Mercoptoethanol	Sigma-Aldrich Chemie GmbH, Taufkirchen, Germany
5-Bromo-2'-deoxyuridine ≥ 99 %	Sigma-Aldrich Chemie GmbH, Taufkirchen, Germany
6-Aminocaproic acid ≥ 99 %	Sigma-Aldrich Chemie GmbH, Taufkirchen, Germany
Acetic acid	Sigma-Aldrich Chemie GmbH, Taufkirchen, Germany
Adenosine-5'-triphosphate (ATP) disodium hydrate	Sigma-Aldrich Chemie GmbH, Taufkirchen, Germany
Ammonium persulfate (APS)	Carl Roth GmbH, Karlsruhe, Germany
BlueStar Prestained Protein Marker	Nippon Genetics Europe GmbH, Düren, Germany
Bovine serum albumin (BSA)	Sigma-Aldrich Chemie GmbH, Taufkirchen, Germany
Bromophenol Blue sodium salt	Carl Roth GmbH, Karlsruhe, Germany

Reagent	Supplier
Calcium chloride dihydrate, $CaCl_2 \cdot H_2O$	Carl Roth GmbH, Karlsruhe, Germany
CAPS PUFFERAN® ≥ 99.3 %	Carl Roth GmbH, Karlsruhe, Germany
CellTracker™ Green CMFDA dye	Life Technologies GmbH, Darmstadt, Germany
Collagen I, rat tail (3.36 µg/ml)	Corning, New York, USA
cOmplete™ Mini, EDTA-free	Roche Diagnostics GmbH, Mannheim, Germany
Crystal violet	Sigma-Aldrich Chemie GmbH, Taufkirchen, Germany
Cycloheximide	Sigma-Aldrich Chemie GmbH, Taufkirchen, Germany
Dextran from *Leuconostoc spp.*	Sigma-Aldrich Chemie GmbH, Taufkirchen, Germany
Dimethyl sulfoxide (DMSO)	Sigma-Aldrich Chemie GmbH, Taufkirchen, Germany
DNase I (RNase free)	Jena Bioscience, Jena, Germany
Disodium ethylenediaminetetraacetic acid (EDTA)	Carl Roth GmbH, Karlsruhe, Germany
Disodium hydrogen phosphate dihydrate, $Na_2HPO_4 \cdot 2\ H_2O$	Carl Roth GmbH, Karlsruhe, Germany
Disodium tetraborate decahydrate, $Na_2B_4O_7 \cdot 10\ H_2O$	Carl Roth GmbH, Karlsruhe, Germany
Doxorubicin	Sigma-Aldrich Chemie GmbH, Taufkirchen, Germany
Ethanol absolute 99.8 %	Sigma-Aldrich Chemie GmbH, Taufkirchen, Germany
Ethyleneglycol-bis-(beta-aminoethylether)-N,N,N‘,N‘-tetraacetic acid (EGTA)	Carl Roth GmbH, Karlsruhe, Germany
FluorSave™ Reagent	Merck KGaA, Darmstadt, Germany
Glycerol	Carl Roth GmbH, Karlsruhe, Germany
Glycin PUFFERAN® ≥ 99 %	Carl Roth GmbH, Karlsruhe, Germany
HEPES PUFFERAN® ≥ 99.5 %	Carl Roth GmbH, Karlsruhe, Germany
HOECHST 33342	Sigma-Aldrich Chemie GmbH, Taufkirchen, Germany

Reagent	Supplier
Hydrogen peroxide (H_2O_2, 30 % solution)	Sigma-Aldrich Chemie GmbH, Taufkirchen, Germany
L-Glutamine 200 mM (100x)	Life Technologies GmbH, Darmstadt, Germany
Luminol	Sigma-Aldrich Chemie GmbH, Taufkirchen, Germany
Ly294002	PeproTech GmbH, Hamburg, Germany
Magnesium chloride hexahydrate, $MgCl_2 \cdot 6\ H_2O$	Merck KGaA, Darmstadt, Germany
Methanol AnalaR NORMAPUR® Reag. Ph.Eur.	VWR International GmbH, Darmstadt, Germany
Methyl cellulose	Sigma-Aldrich Chemie GmbH, Taufkirchen, Germany
Nonidet™ P40	Sigma-Aldrich Chemie GmbH, Taufkirchen, Germany
p-Coumaric acid ≥ 98.0 %	Sigma-Aldrich Chemie GmbH, Taufkirchen, Germany
peqGOLD dNTP-Set	VWR International GmbH, Darmstadt, Germany
Phenylmethylsulfonyl fluoride (PMSF)	Sigma-Aldrich Chemie GmbH, Taufkirchen, Germany
Potassium chloride, KCl	Merck KGaA, Darmstadt, Germany
Potassium dihydrogen phosphate, KH_2PO_4	Carl Roth GmbH, Karlsruhe, Germany
Powdered milk (low fat, blotting grade)	Carl Roth GmbH, Karlsruhe, Germany
Power SYBR® Green PCR Master Mix	Thermo Fisher Scientific GmbH, Dreieich, Germany
Propidium iodide	Sigma-Aldrich Chemie GmbH, Taufkirchen, Germany
ProtoScript® II Reverse Transkriptase	New England BioLabs GmbH, Frankfurt, Germany
Pyronin Y	Sigma-Aldrich Chemie GmbH, Taufkirchen, Germany
Random Primer 6	New England BioLabs GmbH, Frankfurt, Germany
Recombinant human tumor necrosis factor-α (TNF)	PeproTech GmbH, Hamburg, Germany
Recombinant human $VEGF_{165}$	PeproTech GmbH, Hamburg, Germany

Reagent	Supplier
Recombinant RNasin® Ribonuclease Inhibitor	Promega GmbH, Mannheim, Germany
RNase AWAY®	Molecular BioProducts Inc., San Diego, CA, USA
Rhodamin Phalloidin	Life Technologies, Darmstadt, Germany
Roti®-Histofix, 4 %	Carl Roth GmbH, Karlsruhe, Germany
Rotiphorese® Gel 30	Carl Roth GmbH, Karlsruhe, Germany
Sodium chloride, NaCl	Carl Roth GmbH, Karlsruhe, Germany
Sodium deoxycholate ≥ 97 %	Sigma-Aldrich Chemie GmbH, Taufkirchen, Germany
Sodium dodecyl sulfate (SDS)	Carl Roth GmbH, Karlsruhe, Germany
Sodium fluoride, NaF	Merck KGaA, Darmstadt, Germany
Sodium hydrogen carbonate ($NaHCO_3$)	Carl Roth GmbH, Karlsruhe, Germany
Sodium orthovanadate, Na_3VO_4	Sigma-Aldrich Chemie GmbH, Taufkirchen, Germany
Sodium pyrophosphate decahydrate, $Na_4P_2O_7 \cdot 10\ H_2O$	Sigma-Aldrich Chemie GmbH, Taufkirchen, Germany
Spectra™ Multicolor High Range Protein Ladder	Thermo Fisher Scientific GmbH, Dreieich, Germany
Staurosporine	Sigma-Aldrich Chemie GmbH, Taufkirchen, Germany
Stromal cell-derived factor 1 (SDF-1)	PeproTech GmbH, Hamburg, Germany
Tetramethylethylenediamine (TEMED)	Sigma-Aldrich Chemie GmbH, Taufkirchen, Germany
TRIS PUFFERAN® ≥ 99.3 %	Carl Roth GmbH, Karlsruhe, Germany
Trisodium citrate dihydrate	Carl Roth GmbH, Karlsruhe, Germany
Triton X®-100	Merck KGaA, Darmstadt, Germany
Tween® 20	Sigma-Aldrich Chemie GmbH, Taufkirchen, Germany
β-glycerophosphate disodium salt hydrate	Sigma-Aldrich Chemie GmbH, Taufkirchen, Germany

Table 3: Cell culture reagents

Reagent	Supplier
10x Trypsin/EDTA (T/E)	Pan-Biotech GmbH, Aidenbach, Germany
Accutase® Solution	Sigma-Aldrich Chemie GmbH, Taufkirchen, Germany
Amphotericin B (250 µg/ml)	PAN-Biotech GmbH, Aidenbach, Germany
Collagen G	Biochrom AG, Berlin, Germany
Collagenase A	Roche Diagnostics GmbH, Mannheim, Germany
EASY Endothelial cell growth medium (ECGM)	PELOBiotech GmbH, Planegg/Martinried, Germany
EASY Growth Supplements	PELOBiotech GmbH, Planegg/Martinried, Germany
Fetal Bovine Serum (FCS) Superior	Biochrom AG, Berlin, Germany
Medium 199	PAN-Biotech GmbH, Aidenbach, Germany
Penicillin-Streptomycin (P:10.000 U/ml, S: 10 mg/ml)	Pan-Biotech GmbH, Aidenbach, Germany
RPMI-1690	Pan-Biotech GmbH, Aidenbach, Germany
Lymphocyte seperation medium 1077 (LSM)	PromoCell GmbH, Heidelberg, Germany

1.3 Buffers, solutions and media

Compositions of buffers and solutions are depicted in Table 4. Media for cell cultivation are listed in Table 5.

Table 4: List of buffers, solutions and their compositions

Buffer or solution	Composition
1x SDS sample buffer	125 mM Tris-HCL (pH 6.8), 20 % glycerol, 4 % SDS, 0.8 % DTT, 0.01 % Pyronin Y, in ddH_2O
3x SDS sample buffer	188 mM Tris-HCl (pH 6.8), 30 % glycerol, 6 % SDS, 15 % Bromophenol Blue, in ddH_2O freshly added: 2-mercaptothenaol (1:9)
5x SDS sample buffer	312.5 mM Tris-HCl (pH 6.8), 50 % glycerol, 5 % SDS, 2 % DTT, 0.025 % Pyronin Y, in ddH_2O,

Buffer or solution	Composition
Anode buffer 1 (AP1; pH 10.4)	300 mM Tris, 20 % methanol, in ddH_2O
Anode buffer 2 (AP2; pH 10.4)	25 mM Tris, 20 % methanol, in ddH_2O
Blotto in TBS-T (5 %; Blotto-T)	5 % powdered milk, in TBS-T
BrdU staining solution	Anti-BrdU-FITC (1:27), 1 % BSA, 0.5 % Tween® 20, in PBS
BSA in TBS-T (1 %, 5 %; BSA-T)	1 %/5 % BSA, in TBS-T
Cathode buffer (pH 9.4)	25 mM Tris, 40 mM 6-aminocaproic acid, 20 % methanol, in ddH_2O
CellTracker™ Green solution	5 µM CellTracker™ Green CMFDA dye, in serum-free RPMI
Dextran-solution	5 % dextran, in PBS
DNase I solution	14 µl DNase I (2 units/µl), 7 µl 10x Reaction Buffer, 49 µl DNase/RNase free water per sample
Dissolving solution	20 % acetic acid, in ddH_2O
Electrophoresis buffer	192 mM glycine, 25 mM Tris, 0.1 % SDS, in ddH_2O
Enhanced chemiluminescence solution (ECL)	98.5 mM Tris-HCl (pH 8.5), 1 % luminol solution, 0.4 % p-coumaric acid solution, 0.02 % H_2O_2, in ddH_2O
Fractionation buffer A	10 mM Hepes (pH 7.9), 10 mM KCl, 0.1 mM EDTA, 0.1 mM EGTA, in ddH_2O
Fractionation buffer C	20 mM Hepes (pH 7.9), 0.4 M NaCl, 1 mM EDTA, 1 mM EGTA, in ddH_2O
HBSS	5.4 mM KCl, 0.4 mM KH_2PO_4, 136.9 mM NaCl, 4.2 mM $NaHCO_3$, 0.3 mM Na_2HPO_4 • 2 H_2O, 5 mM glucose, in ddH_2O
Hypotonic fluorochrome solution (HFS)	0.1 % Triton X-100, 0.1 % sodium citrate, 50 µg/ml propidium iodide, in PBS
Luminol solution	250 mM luminol, in DMSO
Matsudaira transfer buffer (pH 11)	10 mM CAPS, 15 % methanol, in ddH_2O
Methanol/ethanol-mixture	2 volumes methanol, 1 volume ethanol
Methanolic crystal violet solution	0.5 % crystal violet, 20 % methanol, in ddH_2O
Methyl cellulose solution	1.25 % methyl cellulose, 10 mM l-glutamine, in basal ECGM
Modified RIPA lysis buffer	4 mM cOmplete™ Mini, 1 mM NaF, 0.3 mM Na_3VO_4, 1 mM PMSF, 3 mM β-glycerophosphate, 10 mM sodium pyrophosphate, 0.12 % H_2O_2, freshly added to RIPA buffer

Buffer or solution	Composition
PBS (pH 7.4)	137 mM NaCl, 1.8 mM KH_2PO_4, 2.7 mM KCl, 10 mM Na_2HPO_4 • 2 H_2O, in ddH_2O
PBS (pH 7.4) + collagen G	10 µg/ml collagen G, in PBS
PBS containing Ca^{2+} and Mg^{2+} (PBS+; pH 7.4)	137 mM NaCl, 1.8 mM KH_2PO_4, 2.7 mM KCl, 10 mM Na_2HPO_4 • 2 H_2O, 1 mM $CaCl_2$ • 2 H_2O, 0.5 mM $MgCl_2$ • 6 H_2O, in ddH_2O
p-coumaric acid solution	90 mM p-coumaric acid, in DMSO
RIPA buffer	150 mM NaCl, 50 mM Tris-HCl (pH 7.5), 1 % Nonidet™ P40, 0.25 % sodium deoxycholate, 0.1 % SDS
RIPA lysis buffer	4 mM cOmplete™ Mini, 1 mM NaF, 0.3 mM Na_3VO_4, 1 mM PMSF, freshly added to RIPA buffer
Separation gel (7.5 %)	25 % Rotiphorese® Gel 30, 150 mM Tris-Base (pH 8.8), 0.1 % SDS, 0.2 % TEMED, 0.1 % APS, in ddH_2O
Separation gel (10 %)	33.3 % Rotiphorese® Gel 30, 150 mM Tris-Base (pH 8.8), 0.1 % SDS, 0.2 % TEMED, 0.1 % APS, in ddH_2O
Separation gel (12 %)	40 % Rotiphorese® Gel 30, 150 mM Tris-Base (pH 8.8), 0.1 % SDS, 0.2 % TEMED, 0.1 % APS, in ddH_2O
siRNA dilution buffer	60 mM KCl, 0.2 mM $MgCl_2$, 6 mM Hepes (pH 7.5), in ddH_2O
Stacking gel (4 %)	17 % Rotiphorese® Gel 30, 125 mM Tris-Base (pH 6.8), 0.1 % SDS, 0.2 % TEMED, 0.1 % APS, in ddH_2O
Stripping buffer (pH 2.2)	200 mM glycine, 1 % Tween® 20, 0.1 % SDS, in ddH_2O
Tank buffer	10 % methanol, 25 mM Tris (pH 7.4), 192 mM glycine, in ddH_2O
TBS (pH 7.4-7.5)	25 mM Tris, 150 mM NaCl, in ddH_2O
TBS-T (pH 7.4-7.5)	25 mM Tris, 150 mM NaCl, 0.05 % Tween® 20, in ddH_2O
1x Trypsin/EDTA (T/E)-solution	10 % 10x Trypsin/EDTA, in sterile ddH_2O

Table 5: Media for cell cultivation

Medium	Composition
Endothelial cell growth medium (ECGM)	10 % FCS Superior, 2.5 % EASY Growth Supplements, 100 U/ml penicillin, 100 µg/ml streptomycin, 2.5 µg/ml amphotericin B, in EASY ECGM
Basal endothelial cell growth medium (basal ECGM)	100 U/ml penicillin, 100 µg/ml streptomycin, in EASY ECGM
Freezing medium	10 % DMSO, in FCS Superior
Medium 199 (M199)	10 % FCS Superior, 100 U/ml penicillin, 100 µg/ml streptomycin, in Medium 199
RPMI-1690 (RPMI, basal for cell labeling)	100 U/ml penicillin, 100 µg/ml streptomycin, in RPMI-1690
RPMI-1690 (RPMI, full)	10 % FCS Superior, 100 U/ml penicillin, 100 µg/ml streptomycin, in RPMI-1690
Starvation medium	1 % FCS Superior, 100 U/ml penicillin, 100 µg/ml streptomycin, in Medium 199

1.4 Commercial kits

Kits used for this study are listed in the following table (Table 6).

Table 6: Kits

Product	Supplier
CellTiter-Blue® Cell Viability Assay	Promega GmbH, Mannheim, Germany
CellTiter-Glo® Luminescent Cell Viability Assay	Promega GmbH, Mannheim, Germany
Click-iT® Plus OPP Alexa Fluor® 488 Protein Synthesis Assay Kit	Thermo Fisher Scientific GmbH, Dreieich, Germany
CytoTox® 96 Non-Radioactive Cytotoxicity Assay	Promega GmbH, Mannheim, Germany
Dual-Luciferase® Reporter Assay System	Promega GmbH, Mannheim, Germany
HUVEC Nucleofector® Kit	Promega GmbH, Mannheim, Germany
MiraCLEAN® Endotoxin Removal Kit	Mirus Bio LLC, Madison, WI, USA
Pierce™ BCA Protein Assay Kit	Thermo Fisher Scientific GmbH, Dreieich, Germany

Product	Supplier
PureYield™ Plasmid Maxiprep System	Promega GmbH, Mannheim, Germany
RNeasy® Mini Kit	Quiagen GmbH, Hilden, Germany

1.5 Antibodies

Antibodies used for western blot experiments (Table 7 and Table 8), immunocytochemistry (Table 9 and Table 10) and flow cytometric analysis (Table 11) are listed in the following.

Table 7: Primary antibodies used for western blot experiments

Immunogen, Ref. number	Species	Dilution	Supplier
Anti-human Akt, 4691	Rabbit, monoclonal	1:4000 in 5 % BSA-T	Cell Signaling Technology, Frankfurt, Germany
Anti-human caspase-3, 9662	Rabbit, monoclonal	1:750 in 5 % Blotto-T	Cell Signaling Technology, Frankfurt, Germany
Anti-human EGFR, sc373746	Mouse, monoclonal	1:500 in 5 % Blotto-T	Santa Cruz Biotechnology, Heidelberg, Germany
Anti-human eNOS/NOS Type III, 610296	Mouse, monoclonal	1:500 in 5 % Blotto-T	BD Biosciences, Heidelberg, Germany
Anti-human ERK1/2, 9102	Rabbit, monoclonal	1:2000 in 5 % BSA-T	Cell Signaling Technology, Frankfurt, Germany
Anti-human E-selectin, sc137054	Mouse, monoclonal	1:1000 in 5 % Blotto-T	Santa Cruz Biotechnology, Heidelberg, Germany
Anti-human FGFR1, 9740	Rabbit, monoclonal	1:750 in 5 % Blotto-T	Cell Signaling Technology, Frankfurt, Germany
Anti-human ICAM1, 4915	Rabbit, monoclonal	1:4000 in 5 % BSA-T	Cell Signaling Technology, Frankfurt, Germany
Anti-human IκBα, 9242	Rabbit, monoclonal	1:4000 in 5 % BSA-T	Cell Signaling Technology, Frankfurt, Germany
Anti-human IKKβ, 8943	Rabbit, monoclonal	1:250 in 5 % BSA-T	Cell Signaling Technology, Frankfurt, Germany
Anti-human KPNA2, 14372	Rabbit, monoclonal	1:750 in 5 % Blotto-T	Cell Signaling Technology, Frankfurt, Germany
Anti-human KPNA4, sc390535	Mouse, monoclonal	1:1000 in 5 % Blotto-T	Santa Cruz Biotechnology, Heidelberg, Germany

Immunogen, Ref. number	Species	Dilution	Supplier
Anti-human KPNB1, 60769	Rabbit, monoclonal	1:2000 in 5 % BSA-T	Cell Signaling Technology, Frankfurt, Germany
Anti-human MAML1, 12166	Rabbit, monoclonal	1:500 in 5 % Blotto-T	Cell Signaling Technology, Frankfurt, Germany
Anti-human MDM2, sc5304	Mouse, monoclonal	1:750 in 5 % Blotto-T	Santa Cruz Biotechnology, Heidelberg, Germany
Anti-human NF-κB p65, sc-8008	Mouse, monoclonal	1:1000 in 5 % Blotto-T	Santa Cruz Biotechnology, Heidelberg, Germany
Anti-human NOP14, PA5-58851	Rabbit, polyclonal	1:2000 in 5 % BSA-T	Thermo Fisher Scientific GmbH, Dreieich, Germany
Anti-human p38, 9212	Rabbit, polyclonal	1:2000 in 5 % BSA-T	Cell Signaling Technology, Frankfurt, Germany
Anti-human p53, sc126	Mouse, monoclonal	1:1000 in 5 % Blotto-T	Santa Cruz Biotechnology, Heidelberg, Germany
Anti-human phospho-Akt, 4060	Rabbit, monoclonal	1:1000 in 5 % BSA-T	Cell Signaling Technology, Frankfurt, Germany
Anti-human phospho-eNOS (Ser1177), 612392	Mouse, monoclonal	1:500 in 5 % Blotto-T	BD Biosciences, Heidelberg, Germany
Anti-human phospho-ERK1/2, 9106	Mouse, monoclonal	1:2000 in 5 % Blotto-T	Cell Signaling Technology, Frankfurt, Germany
Anti-human phospho-IκBα (Ser32), 2859	Rabbit, monoclonal	1:1000 in 5 % BSA-T	Cell Signaling Technology, Frankfurt, Germany
Anti-human phospho-IKKα/β, 2697	Rabbit, monoclonal	1:250 in 5 % BSA-T	Cell Signaling Technology, Frankfurt, Germany
Anti-human phospho-p38 MAPK, 4511	Rabbit, monoclonal	1:1000 in 5 % BSA-T	Cell Signaling Technology, Frankfurt, Germany
Anti-human phospho-SAPK/JNK, 4668	Rabbit, monoclonal	1:1000 in 5 % BSA-T	Cell Signaling Technology, Frankfurt, Germany
Anti-human phospho-TAK1 (Thr184/187), 4508	Rabbit, monoclonal	1:250 in 5 % BSA-T	Cell Signaling Technology, Frankfurt, Germany
Anti-human phospho-VEGFR2, 3770	Rabbit, monoclonal	1:750 in 5 % BSA.T	Cell Signaling Technology, Frankfurt, Germany

Immunogen, Ref. number	Species	Dilution	Supplier
Anti-human PTEN, 9559	Rabbit, monoclonal	1:1000 in 5 % BSA-T	Cell Signaling Technology, Frankfurt, Germany
Anti-human SAPK/JNK, 9258	Rabbit, monoclonal	1:1000 in 5 % BSA-T	Cell Signaling Technology, Frankfurt, Germany
Anti-human TAK1, 4505	Rabbit, monoclonal	1:250 in 5 % BSA-T	Cell Signaling Technology, Frankfurt, Germany
Anti-human TAZ, 72804	Rabbit, monoclonal	1:2000 in 5 % BSA-T	Cell Signaling Technology, Frankfurt, Germany
Anti-human TNFR1, 3736	Rabbit, monoclonal	1:750 in 5 % BSA-T	Cell Signaling Technology, Frankfurt, Germany
Anti-human topoisomerase I, sc271285	Mouse, monoclonal	1:1000 in 5 % Blotto-T	Santa Cruz Biotechnology, Heidelberg, Germany
Anti-human VCAM-1, sc13160	Mouse, monoclonal	1:2000 in 5 % Blotto-T	Santa Cruz Biotechnology, Heidelberg, Germany
Anti-human VEGFR2, 9698	Rabbit, monoclonal	1:2000 in 5 % BSA-T	Cell Signaling Technology, Frankfurt, Germany
Anti-human β-actin peroxidase, A3854	Mouse, monoclonal	1:100.000 in 1 % BSA-T	Sigma-Aldrich Chemie GmbH, Taufkirchen, Germany
Anti-human β-tubulin, 2128	Rabbit, monoclonal	1:1000 in 5 % BSA-T	Cell Signaling Technology, Frankfurt, Germany

Table 8: Secondary antibodies used for western blot experiments

Immunogen, Ref. number	Label	Dilution	Supplier
Goat anti-mouse IgG 7076	HRP	1:3000 in 5 % Blotto-T	Cell Signaling Technology, Frankfurt, Germany
Goat anti-rabbit IgG, 7074	HRP	1:3000 in 5 % Blotto-T	Cell Signaling Technology, Frankfurt, Germany

Table 9: Primary antibodies used for immunocytochemistry

Immunogen, Ref. number	Species	Dilution	Supplier
Anti-human KPNA2, 14372	Rabbit, monoclonal	1:400 in PBS with 0.2 % BSA	Cell Signaling Technology, Frankfurt, Germany
Anti-human MAML1, 12166	Rabbit, monoclonal	1:400 in PBS with 0.2 % BSA	Cell Signaling Technology, Frankfurt, Germany
Anti-human NF-κB p65, sc-8008	Mouse, monoclonal	1:400 in PBS with 0.2 % BSA	Santa Cruz Biotechnology, Heidelberg, Germany
Anti-human TAZ, 72804	Rabbit, monoclonal	1:400 in PBS with 0.2 % BSA	Cell Signaling Technology, Frankfurt, Germany

Table 10: Secondary antibodies used for immunocytochemistry

Immunogen, Ref. number	Label	Dilution	Supplier
Goat anti-mouse IgG, A11001	Alexa Fluor® 488	1:400 in PBS with 0.2 % BSA	Thermo Fisher Scientific GmbH, Dreieich, Germany
Goat anti-rabbit IgG, A11008	Alexa Fluor® 488	1:400 in PBS with 0.2 % BSA	Thermo Fisher Scientific GmbH, Dreieich, Germany

Table 11: Antibodies used for flow cytometric analysis

Immunogen, Ref. number	Label	Species	Dilution	Supplier
Anti-BrdU, 347583	FITC	Mouse, monoclonal	1:27 in PBS with 1 % BSA, 0.5 % Tween® 20	BD Biosciences, Heidelberg, Germany
Anti-CD106 (VCAM-1), 555647	PE	Mouse, monoclonal	1:20 in PBS with 0.2 % BSA	BD Biosciences, Heidelberg, Germany
Anti-CD54 (ICAM-1) MCA1615F	FITC	Mouse, monoclonal	1:33 in PBS with 0.2 % BSA	Bio-Rad Laboratories GmbH, Munich, Germany
Anti-CD62E (E-selectin) 551145	PE	Mouse, monoclonal	1:10 in PBS with 0.2 % BSA	BD Biosciences, Heidelberg, Germany

1.6 Oligonucleotides for RT-qPCR

Primers used in this study were designed using the Primer-BLAST tool (NCBI, Bethesda, Maryland, USA) and purchased from Eurofins Scientific SE (Luxemburg). The primers used are listed in the following table (Table 12).

Table 12: Oligonucleotides for RT-qPCR

Gene name	Gene product	Direction	Sequence (5'-3')
APAF1	Apoptotic peptidase activating factor 1	Forward	GCCAAGCAGGAGGTCGATAATG
APAF1	Apoptotic peptidase activating factor 1	Reverse	GACCATCCTCAGAAAAGCAGGC
COL8A1	Collagen Type VIII, alpha 1	Forward	AGGAAGCCGTACCCAAGAAAGG
COL8A1	Collagen Type VIII, alpha 1	Reverse	GGTATCCCATGACCTGGCAAAC
CTGF	Connective tissue growth factor	Forward	CGAGGAGTGGGTGTGTGAC
CTGF	Connective tissue growth factor	Reverse	GACCAGGCAGTTGGCTCTAA
CYR61	Cystein-rich angiogenic inducer 61	Forward	AAGGGGCTGGAATGCAACTT
CYR61	Cystein-rich angiogenic inducer 61	Reverse	TTGGGGACACAGAGGAATGC
E2F1	E2F Transcription factor 1	Forward	GGACCTGGAAACTGACCATCAG
E2F1	E2F Transcription factor 1	Reverse	CAGTGAGGTCTCATAGCGTGAC
GAPDH	Glyceraldehyde-3-phosphate dehydrogenase (Gapdh)	Forward	CCACATCGCTCAGACACCAT
GAPDH	Glyceraldehyde-3-phosphate dehydrogenase (Gapdh)	Reverse	TGAAGGGGTCATTGATGGCAA
ICAM1	Intercellular adhesion molecule 1 (ICAM-1)	Forward	CTGCTCGGGGCTCTGTTC
ICAM1	Intercellular adhesion molecule 1 (ICAM-1)	Reverse	AACAACTTGGGCTGGTCACA
KDR	Vascular endothelial growth factor receptor 2 (VEGFR2)	Forward	GTGACCAACATGGAGTCGTGT
KDR	Vascular endothelial growth factor receptor 2 (VEGFR2)	Reverse	AGCTGATCATGTAGCTGGGAA

Gene name	Gene product	Direction	Sequence (5'-3')
KPNA2	Karyopherin subunit alpha 2, Importin subunit alpha-1	Forward	GCAGCAATGTGGAAAATCAGC
KPNA2	Karyopherin subunit alpha 2, Importin subunit alpha-1	Reverse	TTCGGAATCAAACCAGCCCG
KPNA4	Karyopherin subunit alpha 4, Importin subunit alpha-3	Forward	CATTTGGTTCCTCTGCTCAGCC
KPNA4	Karyopherin subunit alpha 4, Importin subunit alpha-3	Reverse	CTTGTGTTTGCTCATCAGTTCCAG
KPNB1	Karyopherin beta 1, Importin subunit beta-1	Forward	CTGCTTCCTGAAGCTGCCATCA
KPNB1	Karyopherin beta 1, Importin subunit beta-1	Reverse	CTTCAGCCAGACTGGAGAAAGC
PMAIP1/ NOXA	Phorbol-12-myristate-13-acetate-induced protein 1, NOXA	Forward	CTGGAAGTCGAGTGTGCTACTC
PMAIP1/ NOXA	Phorbol-12-myristate-13-acetate-induced protein 1, NOXA	Reverse	TGAAGGAGTCCCCTCATGCAAG
SELE	E-selectin	Forward	AGATGAGGACTGCGTGGAGA
SELE	E-selectin	Reverse	GTGGCCACTGCAGGATGTAT
TNFRSF1A	Tumour necrosis factor receptor 1 (TNFR1)	Forward	CAAGCCACAGAGCCTAGACA
TNFRSF1A	Tumour necrosis factor receptor 1 (TNFR1)	Reverse	GAATTCCTTCCAGCGCAACG
VCAM1	Vascular cell adhesion molecule 1 (VCAM-1)	Forward	CCACAGTAAGGCAGGCTGTAA
VCAM1	Vascular cell adhesion molecule 1 (VCAM-1)	Reverse	GCTGGAACAGGTCATGGTCA

1.7 Plasmids and siRNAs

Plasmids used in this study are depicted in Table 13, siRNAs used are listed in Table 14.

Table 13: Plasmids

Plasmid	Structure	Supplier
pGL4.32[*luc2P*/NF-κB-RE/Hygro]	NF-κB response element (5 copies), minimal promotor, *luc2p* reporter gene, SV40 late poly(A) signal, reporter vector primer 4 (RVprimer4)-binding region, *CO*/E1-derived plasmid replication origin, coding region for synthetic β-lactamase (Amp^r), synthetic poly(A) signal/transcriptional pause site, reporter primer 3 (RVprimer3)-binding region	Promega GmbH, Mannheim, Germany
pGL4.74[*hRluc*/TK]	HSV-TK promotor, *hRluc* reporter gene, SV40 late poly(A) signal, reporter vector primer 4 (RVprimer4)-binding region, *CO*/E1-derived plasmid replication origin, coding region for synthetic β-lactamase (Amp^r), synthetic poly(A) signal/transcriptional pause site, reporter primer 3 (RVprimer3)-binding region	Promega GmbH, Mannheim, Germany

Table 14: siRNAs

siRNA	Target sequences	Supplier
siGENOME Non-Targeting siRNA Pool #2, D-001206-14-05	UAAGGCUAUGAAGAGAUAC AUGUAUUGGCCUGUAUUAG AUGAACGUGAAUUGCUCAA UGGUUUACAUGUCGACUAA	Dharmacon, Lafayette, CO, USA
ON-TARGET plus Human NOP14 siRNA SMARTpool, L-024157-02-0005	GGUCAAAGUCCUCGAGUUU GCUGAGAGACUUCGAAGAA AAAGAUGAAUGUCGAGGAA CAUGAUGGUUCGCGAGCUU	Dharmacon, Lafayette, CO, USA

1.8 Primary cells and cell lines

Primary cells and cell lines used in this study are listed in Table 15.

Table 15: Primary cells and cell lines

Cell type	Supplier	Ref. number
CDC/EU.HMEC-1 (HMEC-1)	Centers for Disease Control and Prevention (CDC, Atlanta, GA, USA)	n.a.
HUVEC	Isolated from the veins of umbilical cords, provided by Bürgerhospital Frankfurt and Hochtaunusklinik Bad Homburg	n.a.
HUVEC	PELOBiotech GmbH, Planegg/Martinsried, Germany	PB-CH-190-8013
Jurkat	Leibniz Institute for German Collection of Microorganisms and Cell Culture (DSMZ), Braunschweig, Germany	ACC-282
PBMC	Isolated from buffy coats, provided by Deutsches Rotes Kreuz, Blutspendedienst Baden-Württemberg/Hessen, Institut für Transfusionsmedizin und Immunhämatologie, Frankfurt, Germany	n.a.
PL	Isolated from buffy coats, provided by Deutsches Rotes Kreuz, Blutspendedienst Baden-Württemberg/Hessen, Institut für Transfusionsmedizin und Immunhämatologie, Frankfurt, Germany	n.a.
THP-1	Leibniz Institute for German Collection of Microorganisms and Cell Culture (DSMZ), Braunschweig, Germany	ACC-16

1.9 Technical equipment

Technical equipment used in this study is listed in Table 16.

Table 16: Technical equipment

Device	Supplier
accu-jet® *pro* pipettor	VWR International GmbH, Darmstadt, Germany
ARPEGE 110 liquid nitrogen storage system	Air Liquide S.A., Paris, France
Astacus Reagent Ultra Pure Water System	MembraPure GmbH, Henningsdorf, Germany
CP1000 film processor	AGFA, Cologne, Germany

Device	Supplier
Criterion™ Blotter with Plate Electrodes	Bio-Rad Laboratories GmbH, Munich, Germany
DM IL LED (inverted) microscope	Leica Microsystems, Wetzlar, Germany
Eppendorf Multipette® plus pipette	Eppendorf AG, Hamburg, Germany
Eppendorf Research® plus pipettes	Eppendorf AG, Hamburg, Germany
F1-ClipTip™ multichannel pipette	Thermo Fisher Scientific GmbH, Dreieich, Germany
FACSVerse™ flow cytometer	BD Biosciences, Heidelberg, Germany
FE20 pH meter	Mettler-Toldeo GmbH, Gießen, Germany
DMI6000b fluorescence microscope	Leica Microsystems, Wetzlar, Germany
HERACell 150i CO2 incubator	Thermo Fisher Scientific GmbH, Dreieich, Germany
Heraeus™ Megafuge™ 16R centrifuge	Thermo Fisher Scientific GmbH, Dreieich, Germany
IKA® RH basic 2 magnetic stirrer	IKA-Werke GmbH & Co. KG, Staufen, Germany
infinite F200 Pro microplate reader	Tecan, Männedorf, Switzerland
Julabo ED water bath	Julabo GmbH, Seelbach, Germany
Mettler-Toledo (0.1 – 200 mg) scale	Mettler-Toldeo GmbH, Gießen, Germany
MICRO STAR 17R centrifuge	VWR International GmbH, Darmstadt, Germany
Mini-PROTEAN® 3 Multi-Casting Chamber	Bio-Rad Laboratories GmbH, Munich, Germany
Mini-PROTEAN® Tetra Cell Casting Module	Bio-Rad Laboratories GmbH, Munich, Germany
Mini-PROTEAN® Tetra Vertical Electrophoresis Cell	Bio-Rad Laboratories GmbH, Munich, Germany
MiniStar silverline centrifuge	VWR International GmbH, Darmstadt, Germany
Nanophotometer P330	Implen GmbH, Munich, Germany
Neubauer-improved hemocytometer	Paul Marienfeld GmbH & Co. KG,

Device	Supplier
Nucleofector™ 2b Device	Lonza Cologne GmbH, Cologne, Germany
peqSTAR thermocycler	PEQLAB Biotechnology, Erlangen, Germany
PIONEER™ (10 – 1000 g) scale	Ohaus Europe GmbH, Greifensee, Switzerland
Pipetus® pipettor	Hirschmann Laborgeräte GmbH & Co. KG, Eberstadt, Germany
PowerPac™ Basic Power Supply	Bio-Rad Laboratories GmbH, Munich, Germany
PowerPac™ Universal Power Supply	Bio-Rad Laboratories GmbH, Munich, Germany
SAFE 2020 steril bench	Thermo Fisher Scientific GmbH, Dreieich, Germany
Seastar™ Digital Orbital Shaker	Heathrow Scientific, Vernon Hills, IL, USA
StepOnePlus™ System	Applied Biosystems GmbH
Suart® SRT9D tube roller	VWR International GmbH, Darmstadt, Germany
Systec VX-95 Autoclave	Systec GmbH, Linden, Germany
Thermomixer basic heating block	CellMedia GmbH & Co. KG, Zeitz
Trans-Blot® Turbo™ Blotting Instrument	Bio-Rad Laboratories GmbH, Munich, Germany
USC300TH ultrasonic cleaner	VWR International GmbH, Darmstadt, Germany
Vacusafe™ extraction system	Integra Biosciences GmbH, Biebertal, Germany
VarioSkan® Flash microplate reader	Thermo Fisher Scientific GmbH, Dreieich, Germany
Vortex Genie® 2	Scientific Industries Inc., Bohemia, NY, USA
VWR Digital Heatblock	VWR International GmbH, Darmstadt, Germany

1.10 Consumable materials

Consumable materials used in this study are given in Table 17.

Table 17: Consumable materials

Product	Supplier
8-tube PCR strips + lids	Greiner Bio-One GmbH, Frickenhausen, Germany
Biosphere® plus filter tip 1000 µl XL	Sarstedt AG & Co., Nürnbrecht, Germany
Biosphere® plus filter tip 200 neutral	Sarstedt AG & Co., Nürnbrecht, Germany
Cable straps	Hornbach Baumarkt AG, Bornheim, Germany
Cell culture dish (10 cm)	Sarstedt AG & Co., Nürnbrecht, Germany
Cell culture flasks (25 cm^2, 75 cm^2)	Greiner Bio-One GmbH, Frickenhausen, Germany
Cell culture plates (6-, 12-, 24-, 48-, 96-well)	Greiner Bio-One GmbH, Frickenhausen, Germany
Cell scraper	Sarstedt AG & Co., Nürnbrecht, Germany
Centrifuge falcons (15 ml, 50 ml)	Greiner Bio-One GmbH, Frickenhausen, Germany
ClipTip 200, sterile low retention	Thermo Fisher Scientific GmbH, Dreieich, Germany
Corning® 96 well NBS™ Microplate for luminescence measurement	Sigma-Aldrich Chemie GmbH, Taufkirchen, Germany
Cover slips	Helmut Saur, Reutlingen, Germany
Cryo vials	Greiner Bio-One GmbH, Frickenhausen, Germany
Dnase/RNase free reaction tubes (1.5 ml)	VWR International GmbH, Darmstadt, Germany
FACS tubes	Ratiolab GmbH, Dreieich, Germany
Filter paper	Carl Roth GmbH, Karlsruhe, Germany
ibiTreat µ-Slide 8 well	Ibidi GmbH, Planegg/Martinsried, Germany
Immun-Blot® PVDF	Bio-Rad Laboratories GmbH, Munich, Germany
MicroAmp™ Fast Optical 96-Well Reaction Plate	Applied Biosystems GmbH, Frickenhausen, Germany

Product	Supplier
Microplate 96-well PS without lid	Greiner Bio-One GmbH, Frickenhausen, Germany
Mini-PROTEAN® Short Plates	Bio-Rad Laboratories GmbH, Munich, Germany
Mini-PROTEAN® Spacer Plates with 1.5 mm spacers	Bio-Rad Laboratories GmbH, Munich, Germany
Nunc™ MicroWell™ 96-Well Microplate for fluorescence measurement	Thermo Fisher Scientific GmbH, Dreieich, Germany
Pasteur pipettes for extraction system	VWR International GmbH, Darmstadt, Germany
Pipette tips (standard, 10 µl, 100 µl, 1000 µl)	Greiner Bio-One GmbH, Frickenhausen, Germany
Reaction tubes (0.2 ml, 1.5 ml, 2 ml)	Greiner Bio-One GmbH, Frickenhausen, Germany
Serological pipettes (5 ml, 10 ml, 25 ml)	Greiner Bio-One GmbH, Frickenhausen, Germany
Square petri dish 120x120x17 (hydrophobic)	Greiner Bio-One GmbH, Frickenhausen, Germany
StarSeal Sealing Tape Polyolefin Film for qRT-PCR	STARLAB INTERNATIONAL GmbH, Hamburg, Germany
Steril compresses	NOBAMED Paul Danz AG, Wetter, Germany
Super RX-N x-ray films	FUJIFILM Europe GmbH, Düsseldorf, Germany
Surgical clamp	Medi-King Medical Trading GmbH, Oyten, Germany
SurPhob® SafeSeal filter tip 10 µl	Biozym Scientific GmbH, Hessisch Oldendorf, Germany
Syringes	Carl Roth GmbH, Karlsruhe, Germany
Three-way valves	Medi-King Medical Trading GmbH, Oyten, Germany
Transwell® Insert (polycarbonate membrane, diameter 6.5 mm, pore size 5 µm, 8µm)	Corning, New York, USA

2. Cell culture

All primary cells and cell lines used were cultured under constant humidity at 37 °C and 5% CO_2. Growth and morphology were monitored regularly. Unless otherwise stated, buffers, solutions and cell culture media were pre-warmed at 37 °C before being added to the cells. Cell culture flasks and multi-well plates used for seeding of HUVECs and HMEC-1 cells were coated with collagen G (10 mg/l in PBS) for a minimum of 20 min at 37 °C before seeding cells.

2.1 Isolation of human umbilical vein endothelial cells (HUVECs)

The isolation of human umbilical vein endothelial cells (HUVECs) was performed as described previously with slight modifications.[400] In brief, a cannula was inserted into each end of the vein of an umbilical cord and tightly fixed with a cable strap. The vein was flushed twice with 25 ml PBS+ to remove excessive blood and contaminations. Cuts or leaks were closed with a surgical clamp. Next, three-way valves were positioned on both cannulas, and one of them was closed immediately. For detachment of the cells, collagenase A (0.1 g/l) was injected through the open three-way valve into the vein until tightly filled. The umbilical cord was incubated for 45 min at 37 °C. Subsequently, the HUVEC-containing collagenase A solution was transferred to a fresh tube. The vein was rinsed with 30 ml M199 and the rinsing solution was collected in the same tube. The cell suspension was centrifuged at 300 g for 5 min and the supernatant was discarded. The remaining, endothelial cells-containing pellet was resuspended in 5 ml ECGM and transferred to a T25 cell culture flask (25 cm^2 growth area). On the next day, non-adherent cells were washed away using 10 ml PBS+, and 5 ml fresh ECGM was added to the adhering endothelial cells. Passaging of HUVECs was performed as described in section IV.2.4.

2.2 Isolation of peripheral blood mononuclear cells (PBMCs)

Peripheral blood mononuclear cells (PBMCs) were isolated from buffy coats obtained from Deutsches Rotes Kreuz, Blutspendedienst Baden-Württemberg/Hessen, Institut für Transfusionsmedizin und Immunhämatologie, Frankfurt, Germany using density gradient centrifugation following the instructions of Bøyum.[401] Briefly, buffy coats were diluted 1:1 with PBS and up to 30 ml were stacked on 10 ml dextran-solution to separate red blood cells through sedimentation. After 30 min, the PBMCs-containing upper phase was removed, carefully stacked on 10 ml lymphocyte separation medium (LSM) and centrifuged at 800 g for 10 min without brake. The PBMCs-containing ring (middle phase, Figure 21) was carefully transferred to a pre-chilled falcon and filled up with cold HBSS. The cell suspension was centrifuged at 300 g and 4 °C for 10 min. The supernatant was removed, and the PBMCs-

containing pellet was washed once more with 30 ml cold HBSS and then with 30 ml cold serum-free RPMI. After each washing step, cells were centrifuged at 300 g and 4 °C for 5 min. The pellet was suspended in cold serum-free RPMI. PBMCs were instantly used for cell adhesion experiments. For the separation of primary lymphocytes (PLs) from total PBMCs, the cell suspension was seeded to plastic dishes and cells were allowed to adhere for 2.5 h. Subsequently, the lymphocyte-containing cell culture supernatant was collected, centrifuged at 300 g for 5 min, resuspended in 20 ml pre-warmed RMPI and transferred to a T75 cell culture flask (75 cm^2 growth area). Lymphocytes were allowed to rest for 24 h before performance of cell adhesion experiments.

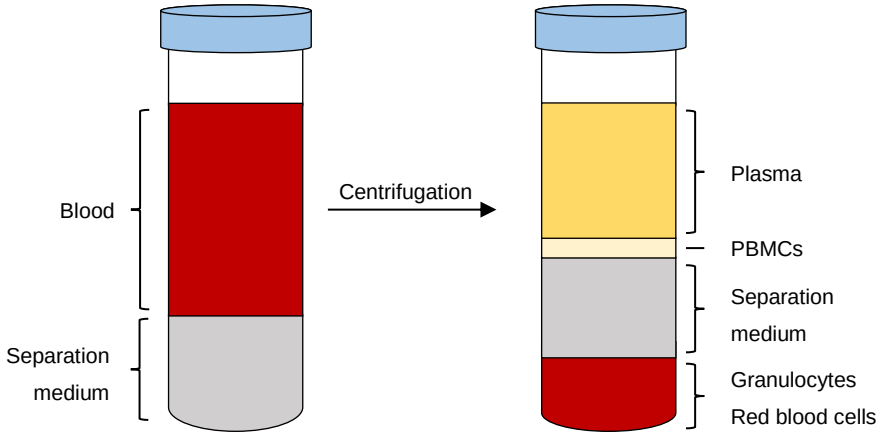

Figure 21: Isolation of peripheral blood mononuclear cells. The PBMC-containing fraction of the buffy coats is stacked on lymphocyte separation medium and centrifuged. Through density centrifugation, the samples are separated into an upper plasma phase, a middle ring containing peripheral blood mononuclear cells, a lower lymphocyte separation medium phase and a bottom phase containing granulocytes and red blood cells.

2.3 Cell lines

2.3.1 Human dermal microvascular endothelial cells (HMEC-1)

HMEC-1 cells are immortalized human microvascular endothelial cells created by transfection of human dermal microvascular endothelial cells with a PBR-322-based plasmid containing the codon region of large T antigen, an SV40 A gene product.[402] HMEC-1 cells were cultured in ECGM.

2.3.2 Human leukemia monocyte-like cell line (THP-1)

The human monocyte-like cell line THP-1 was established from the peripheral blood of a one-year-old boy suffering from acute monocytic leukemia (AML).[403] THP-1 cells were cultured in RPMI.

2.3.3 Human T lymphocyte cell line (Jurkat)

The human T lymphocyte cell line Jurkat was established from the peripheral blood of a 14 year-old boy with acute lymphoblastic leukemia (ALL).[404] Jurkat cells were cultured in RPMI.

2.4 Passaging of cells

Adherent cells (HUVECs, HMEC-1) were passaged upon building a confluent monolayer. The cell culture medium was removed and the cell layer was washed twice with 10 ml PBS. For detachment of the cells, 2 ml T/E-solution was added and cells were incubated for approximately 2 min at 37 °C, or until completely detachmented. The enzymatic reaction was stopped using 10 ml M199. Cells were harvested by centrifugation at 300 g for 5 min and the supernatant was discarded. The pellet was resuspended in fresh culture medium and either transferred to new cell culture flasks (75 cm^2) or seeded in cell culture dishes or plates for experimental purpose. Passaging was performed two to three times a week in a ratio of 1:3 regarding the growth area. HUVECs were cultivated up to passage 2 and were used for experimental purposes exclusively in passage 3. HMEC-1 were used for experimental purposes up to passage 25.

For passaging the suspension cell lines THP-1 and Jurkat, the number of cells was calculated using a hemocytometer (Neubauer cell chamber). The cell concentration was adjusted to 3 x 10^5 cells per ml in a total volume of 20 ml and transferred to a new cell culture flask (25 cm^2 or 75 cm^2). Suspension cell lines were split three times a week and were used for experimental purposes up to passage 25.

2.5 Freezing and thawing of cells

For freezing of adherent cells, the cell monolayer was washed twice with 10 ml PBS, and detachment was carried out using 2 ml T/E-solution. Detachment reaction was stopped by adding 10 ml M199. The cells were harvested by centrifugation at 300 g for 5 min, and the supernatant was discarded. The cell pellet was suspended in 2 ml freezing medium (confluent 75 cm^2 cell culture flask) and transferred to cryo vials.

For freezing of suspension cells, the cells were counted using a hemocytometer (Neubauer cell chamber), and 6 x 10^6 cells were centrifuged at 300 g for 5 min. The supernatant was discarded, the pellet was suspended in 2 ml freezing medium and transferred to cryo vials.

Cryo vials were frozen at -80 °C overnight and subsequently introduced to liquid nitrogen for long term storage.

For thawing of cells, cryo vials were rapidly warmed at 37 °C and immediately transferred to 10 ml ice-cold cell culture medium. The cell suspension was centrifuged at 300 g for 5 min, and the supernatant was discarded. The cell pellet was suspended in fresh culture medium and transferred to a cell culture flask (25 cm^2 or 75 cm^2 depending on the cell count).

3. Cytotoxicity assays

To ensure that observed effects on inflammation- and angiogenesis-related endothelial processes are independent of cytotoxic actions, the influence of vioA on cell viability was investigated.

3.1 Cell viability assay

The metabolic activity of HUVECs was determined by using the CellTiter-Blue® cell viability assay. The CellTiter-Blue® reagent contains the non-fluorescent redox dye resazurin, which can be converted into the fluorescent product resorufin by living cells. Non-viable cells lose their metabolic activity, thus they are not able to generate a fluorescent signal anymore.
The cell viability assay was performed according to the manufacturer's instructions. For investigating the viability of confluent cells, HUVECs were seeded to 96-well plates, grown to confluence and treated as indicated. For analysing the viability of subconfluent cells, 3 x 10^4 HUVECs were seeded to 96-well plates, grown for 24 h and treated with vioA as indicated. 4 h before the end of the incubation period, the CellTiter-Blue® reagent was added to the cells in a dilution of 1:10. Fluorescence intensity was measured using a microplate reader (Infinite F200 Pro; Tecan, Männedorf, Switzerland) at 535 nm (ex) and 590 nm (em).

3.2 Determination of late apoptosis

Measurement of late apoptotic cells was performed by propidium iodide (PI) staining according to Nicoletti *et al*.[405] Briefly, HUVECs were seeded to 24-well plates, grown to confluence and treated as indicated. For analysing subconfluent cells, 1.1 x 10^5 HUVECs were seeded to 24-well plates, grown for 24 h and treated with vioA as indicated. Treatment with staurosporine (1 µM) for 24 h served as positive control for the induction of apoptosis. Next, cell culture supernatants were collected, and the adherent cells were washed twice with 500 µl PBS. The wash fractions were added to the respective cell culture supernatants. For detachment, cells were incubated with 200 µl T/E-solution at 37 °C for approx. 2 min. The enzymatic reaction was stopped by adding 600 µl ice-cold M199. The cell suspensions were added to the respective cell culture supernatants and wash fractions and the total volume was centrifuged

at 300 g and 4 °C for 5 min to harvest the cells. The supernatant was discarded and the cell pellet was washed with 1 ml ice-cold PBS followed by centrifugation at 300 g and 4 °C for 5 min. The supernatant was discarded, and the cell pellet was incubated with a hypotonic fluorochrome solution (HFS) for a minimum of 2 h at 4 °C in the dark. The percentage of cells with subdiploidic DNA content was analysed by recording median values for 10.000 events per sample using a FACSVerse flow cytometer (BD Bioscience, San Jose, CA, USA).

3.3 Determination of membrane integrity

Cell death and subsequent cell lysis leads to the release of lactate dehydrogenase (LDH) into cell culture supernatants. The LDH release was measured by using the CytoTox 96® Non-Radioactive Cytotoxicity Assay, which is based on the enzymatic reaction. LDH catalyses the conversion of lactate to pyruvate, which in the following leads to the reduction of nicotinamide adenine dinucleotide (NAD^+) to NADH. The production of NADH results in the conversion of the tetrazolium salt iodonitrotetrazolium violet (INT) into a red formazan product. The generation of the red formazan product is proportional to the amount of released LDH.

The CytoTox 96® Non-Radioactive Cytotoxicity Assay was used according to the manufacturer's instructions. In brief, HUVECs were seeded to 96-well plates, grown to confluence and treated as indicated. As positive control, lysis buffer was added to non-treated HUVECs in a ratio of 1:10 for the last 45 min of the treatment period. Subsequently, 50 µl of the supernatant of each well was transferred to a new 96-well plate. 50 µl of CytoTox 96® reagent was added to the samples, and the plate was incubated for 30 min at room temperature in the dark. The enzymatic reaction was stopped by adding 50 µl of stop solution, and the absorbance of the red formazan product was measured at 490 nm using a Varioskan Flash microplate reader (Thermo Fisher Scientific, Dreieich, Germany).

3.4 Investigation of intracellular ATP levels

Adenosine triphosphate (ATP) is required for energy-consuming reactions and processes in living cells, including phosphorylation or protein transport. Thus, the intracellular ATP level is a solid indicator for living cells and their viability. Intracellular ATP levels were determined using the CellTiter-Glo® Luminescent Cell Viability Assay. The assay is based on an 'add-mix-measure' format, comprising cell lysis and detection of ATP through the mono-oxygenation of luciferin to oxyluciferin, which is catalyzed by luciferase in the presence of Mg^{2+}, ATP and molecular oxygen.[406]

HUVECs were seeded to 96-well plates, grown to confluence and treated as indicated. Then, the plate was equilibrated at room temperature for 30 min. An ATP standard curve was freshly prepared (0.01-100 µM) and integrated to the free wells of the sample plate. Immediately

thereafter, the CellTiter-Glo® Reagent was added in a ratio of 1:10. The plate was mixed for 2 min on an orbital shaker to induce cell lysis and incubated for 10 min at room temperature in the dark to stabilize the luminescent signal. 50 µl of the mixture were transferred to a fresh 96-well plate suitable for luminescence measurement. Medium without addition of CellTiter-Glo® Reagent served as background control. Luminescence was measured with a microplate reader (Infinite F200 Pro, Tecan) using an integration time of 1 s per sample. The ATP concentrations of the samples were determined based on nonlinear regression of the ATP standard curve.

4. Leukocyte adhesion assay

For investigating the influence of vioA on the leukocyte-endothelial cell interaction, cell adhesion experiments were performed. HUVECs were seeded to 24-well plates, grown to confluence and treated as indicated. If needed, HUVECs in 48-well plates were transfected with siRNA against NOP14 prior to vioA treatment. TNF treatment (10 ng/ml) alone, without vioA treatment, served as positive control for leukocyte adhesion. Non-treated HUVECs served as negative control. 1 h before the end of the TNF treatment period, leukocytes (THP-1, Jurkat, PBMC, PL) were counted using a hemocytometer (Neubauer cell chamber), and the desired number of leukocytes (1 x 10^5 per well; NOP14 knockdown: 5 x 10^4 per well) was centrifuged at 300 g for 5 min. The cell pellet was suspended in CellTracker™ Green solution (1 ml per 1 x 10^6 cells, Table 4) and incubated at 37 °C for 30 min in the dark. Subsequently, leukocytes were centrifuged at 300 g for 5 min, washed once with serum-free RPMI and centrifuged again under the same conditions. The cell pellet was resuspended in the appropriate volume of ECGM (500 µl per well). Next, the cell culture medium was removed from the HUVECs, and the CellTracker™ Green-stained leukocytes were added to the HUVEC monolayer. Leukocytes were allowed to adhere (THP-1, Jurkat: 5 min; PBMC, PL: 10 min) before non-adherent cells were removed by three washing steps using 500 µl PBS+ each. The amount of adhered fluorescence-labeled leukocytes was determined using a microplate reader (Infinite F200 Pro; Tecan) at 485 nm (ex) and 535 nm (em).

5. Transmigration assay

To investigate the influence of vioA on the transmigration of leukocytes through an endothelial monolayer, a transmigration assay was performed. 1 x 10^5 HUVECs in 100 µl ECGM were seeded to the upper compartment of Transwell insertes (growth area 0.33 cm^2, 5 µm pore size, polycarbonate; Corning, NY, USA). The lower compartment was filled with 600 µl ECGM. Cells were grown for 24 h and subsequently treated as indicated. THP-1 cells were counted using a hemocytometer, and the desired number of cells (2 x 10^4 cells per well) was centrifuged at

300 g for 5 min. The cell pellet was suspended in CellTracker™ Green solution (1 ml per 1 x 10^6 cells, Table 4) and incubated for 30 min at 37 °C. The stained leukocytes were centrifuged at 300 g for 5 min and suspended in Medium 199 containing 0.1 % BSA, 100 U/ml penicillin and 100 µg/ml streptomycin to a final concentration of 2 x 10^5 cells per ml. Next, the cell culture medium was removed from the upper and lower compartment of the Transwell system. 100 µl (2 x 10^4 cells) of the fluorescence-labeled THP-1 cells containing solution was added to the HUVEC monolayer on the upper compartment of the Transwell system. The lower compartment was filled with either 600 µl of Medium 199 supplemented with 0.1 % BSA, 100 U/ml penicillin and 100 µg/ml streptomycin in case of the negative control or with 600 µl Medium 199 containing 500 ng/ml SDF-1 as chemoattractant, 0.1 % BSA, 100 U/ml penicillin and 100 µg/ml streptomycin in case of all other experimental conditions. THP-1 cells were allowed to transmigrate through the HUVEC monolayer towards the SDF-1 gradient for 2 h. Subsequently, non-migrated THP-1 cells in the upper compartment were removed using a cotton swap and the Transwell inserts were cleaned from culture medium residues. The Transwell inserts with the transmigrated leukocytes sticking at the bottom side were transferred to new wells with 200 µl RIPA buffer, and cell lysis was performed with gentle agitation for 15 min. 60 µl of the lysates were transferred to a 96-well plate suitable for fluorescence measurement, and fluorescence intensity was determined using a microplate reader (Infinite F200 Pro, Tecan) at 485 nm (ex) and 535 nm (em).

6. Reporter gene assay

Reporter gene assays represent a well-established method to study cellular events associated with signal transduction and gene expression.[407] Here, a Dual-Luciferase® Reporter Assay was performed to analyse the influence of vioA on the NF-κB promotor activity.

6.1 Plasmid transfection and sample preparation

For reporter gene assays, HUVECs were transfected with the purified reporter plasmids using the HUVEC Nucleofactor® Kit (Lonza Cologne GmbH, Cologne, Germany), which is based on electroporation. Through an electric shock, electroporation leads to the formation of pores in the cell membrane, thereby enabling the cellular uptake of plasmid DNA.[408]

The HUVEC Nucleofactor® Kit was used according to the manufacturer's instructions. In brief, HUVECs were detached (see IV.2.4) and counted using a hemocytometer (Neubauer cell chamber). 1 x 10^6 cells were centrifuged at 300 g for 5 min, the supernatant was discarded, and the cell pellet was resuspended in 100 µl Nucleofector® Solution. 3.5 µg purified firefly reporter plasmid pGL4.32[*luc2P*/NF-κB-RE/Hygro] and 1.4 µg purified *Renilla* reporter plasmid

pGL4.74[*hRluc*/TK] (ratio of 10:4, Table 13) were added to the cells, and the cell suspension was immediately transferred to a Nucleofector® Cuvette. Cells were co-transfected with both plasmids using the Nucleofector® Program A-034 for HUVECs (Nucleofector 2b, Lonza Cologne GmbH). Immediately thereafter, 600 µl ECGM was added to the cuvettes and the cells were seeded to 48-well plates (1.25 x 10^5 cells per well). After 4-5 h, cells were carefully washed once with 500 µl PBS+ to remove dead cells and remaining Nucleofector® Solution and 500 µl fresh culture medium was added. 24 h post transfection, HUVECs were treated with vioA and TNF as indicated. TNF-treatment alone served as positive control, and non-treated HUVECs were used as negative control. After the end of the treatment period, cells were washed once with 500 µl PBS, lysed with 65 µl 1x passive lysis buffer (PLB, Promega GmbH) and frozen at -80 °C until further use.

6.2 Dual-Luciferase® Reporter Assay

In the Dual-Luciferase® Reporter Assay, the two distinct reporter enzymes (i) firefly (*Photinus pyralis*) luciferase and (ii) *Renilla* (*Renilla reniformis* or sea pansy) luciferase are simultaneously expressed and measured in the same sample. The firefly luciferase reporter gene contains five NF-κB response element copies and serves to measure the NF-κB promotor activity. It catalyzes the oxidation of beetle luciferin to oxyluciferin, which evokes a bioluminescent signal at 550-570 nm. The *Renilla* luciferase reporter gene is coupled to an unregulated promotor and acts as internal control. It catalyzes the oxidation of coelenterazine to coelenteramide, which leads to a bioluminescent signal at 480 nm.

The assay was performed according to the manufacturer's protocol. In brief, lysates prepared as described in section IV.6.1 were thawed for 30 min under constant agitation, transferred to tubes and cleared by centrifugation at 17.000 g for 1 min. Of each sample, 10 µl (triplicates) were transferred to a 96-well plate suitable for luminescence measurement. The luciferase substrates LARII and Stop & Glo® Reagent were freshly prepared and transferred to two independent injectors of a microplate reader (Infinite F200 Pro, Tecan). After priming both injectors, 50 µl LARII were injected to the wells and the activity of *Photinus* firefly luciferase was analysed by luminescence measurement. The *Photinus* firefly luciferase signal was quenched, and the *Renilla* luciferase activity was measured by injecting 50 µl Stop & Glo® Reagent. Measurements were performed with a delay of 2 s and a read time of 10 s. The signal detected for *Photinus* firefly luciferase was normalized to the signal of the *Renilla* luciferase.

7. Cell proliferation assay

To measure the influence of vioA on endothelial cell proliferation, crystal violet staining was performed. Crystal violet is a triarylmethane dye, which binds to proteins and DNA of cells attached to the cell culture plate. Dead cells lose their ability to adhere, thus they are removed during washing steps. The intensity of the crystal violet staining is directly proportional to the number of viable cells under stimulating conditions.

1.5 x 10^3 HUVECs or HMEC-1 cells were seeded to 96-well plates and grown for 24 h. Untreated control cells were washed once with 100 µl PBS+ and fixed for 10 min using 100 µl methanol/ethanol-mixture. Cells were washed twice with 100 µl PBS and stained for 10 min at room temperature using methanolic crystal violet solution (Table 4). Cells were washed with distilled water until all excessive crystal violet solution was removed and the cell monolayers were air-dried. Simultaneously, non-fixed cells were treated with vioA as indicated. After the end of the treatment period, cells were washed, fixed, stained and air-dried as described above. To solubilize crystal violet, 100 µl dissolving solution (Table 4) was added to the dried wells and incubated for 30 min under constant agitation. 60 µl of the resulting solution was transferred to a new 96-well plate and absorbance was measured at 540 nm using a microplate reader (Infinite F200 Pro, Tecan). To determine the proliferation rate, the absorbance of untreated control cells was subtracted from the absorbance of treated cells.

8. Sprouting assays

The influence of vioA on the sprouting of microvascular and macrovascular cells was analysed *in vitro* in endothelial cell spheroids and *ex vivo* in choroidal explant cultures.

8.1 Sprouting of endothelial cell spheroids

Endothelial cell spheroids represent an efficient and robust method to analyze the effect of pro- and anti-angiogenic compounds on the angiogenic sprouting in a 3-dimensional environment. The hanging drop method was used to create endothelial cell spheroids.

In brief, confluent HUVECs or HMEC-1 cells were detached from the cell culture flask (see IV.2.4) and counted using a hemocytometer (Neubauer cell chamber). 5 x 10^4 cells per condition were suspended in 3,125 µl ECGM supplemented with 20 % methyl cellulose solution (Table 4). In case of NOP14 knockdown experiments, vioA (10 nM) was additionally added to the cell culture medium. The cell suspension was brought onto a hydrophobic 10 cm dish in separate 25 µl droplets and the plates were incubated upside-down at 37 °C for approximately 24 h to induce spheroid formation. Subsequently, the spheroid-containing

droplets were washed from the plate using 5 ml PBS and centrifuged at 200 g for 4 min without break. The spheroids were resuspended in basal ECGM, split into 2 ml fractions and centrifuged again at 200 g for 4 min without break. The supernatant was discarded and each fraction was covered with 400 µl methyl cellulose solution (Table 4) supplemented with 10 % FCS. On ice, 500 µl collagen type I (3.36 mg/ml) was mixed with 62.5 µl 10x M199. The pH value was adjusted by adding dropwise 0.5 M sodium hydroxide until the pH indicator phenol red (present in 10x M199) indicated the pH change by turning from yellow to pink. Immediately thereafter, 400 µl of the collagenase typ I mix was added to one fraction of spheroids containing methyl cellulose solution and thoroughly mixed with a pipette tip. 600 µl of the resulting mixture was equally divided between two wells of a 48-well plate. The plate was incubated in a waterbath at 37 °C until the collagen matrix polymerized. In the following, the spheroids were treated with vioA and VEGF as indicated. VEGF-only treatment served as positive control for spheroid sprouting. After the end of the treatment period, spheroids were fixed using 450 µl Roti®-Histofix (4 % paraformaldehyde). Microscopical images were taken with a Leica DM IL LED inverted microscope (Leica Microsystems, Wetzlar, Germany). Total sprout length and number of sprouts per spheroid were analysed using ImageJ software (version 1.49k).

8.2 Sprouting of choroidal explant cultures

Investigation of the sprouting of choroidal explant cultures was kindly performed by Yanfen Li and Prof. Dr. Stylianos Michalakis (Department of Ophthalmology, University Hospital, Ludwig Maximilians University of Munich (LMU), Munich, Germany) as described previously with slight modifications.[409] In brief, the retinal pigment epithelium (RPE)/choroid/sclera complex of 22 to 25 days old BL6j mice was cut into small pieces (approx. 1 x 1 mm) and embedded in growth factor-reduced Matrigel. 1 ml EBM-2 Basal Medium supplemented with EGM-2 SingleQuots containing VEGFA and 1% penicillin/streptomycin and indicated concentrations of vioA or vehicle was added to the explant cultures. Medium was replaced every day for a total of 6 days. On day 6, images were taken with an EVOS M5000 microscope (Thermo Fisher Scientific). The sprouting areas were analysed using ImageJ software with SWIFT-choroid macros.

9. Migration assays

Endothelial cell migration crucially contributes to the process of angiogenesis. Cell migration comprises the undirected, thus random movement as well as the directed movement of cells towards a chemoattractant. To investigate the influence of vioA on the different subtypes of cell migration, the following experiments were performed.

9.1 Scratch assay

The scratch assay is a well-developed and established method for measuring undirected cell migration *in vitro*.[410]

HUVECs or HMEC-1 were seeded into 24-well plates, grown to confluence and treated as indicated for 16 h. Non-treated cells served as control. Subsequently, a scratch was inflicted to the cell monolayer using a pipette tip followed by two washing steps with 500 µl M199 to remove detached cells. Cells were covered with 500 µl fresh ECGM, the negative control (representing 0 % migration) was treated with 500 µl starvation medium. Only gaps with the same width were used to ensure comparable results. The scratches were observed over time until the gap of the positive control (representing 100 % migration) was fully closed. Microscopical images were taken using a Leica DM IL LED inverted microscope (Leica Microsystems), and the ImageJ software (version 1.49k) was used to determine the relative migration in relation to the starvation control.

9.2 Boyden chamber assay

The Boyden chamber assay is suitable for investigating the migratory response of cells towards a chemotactic gradient (directed migration).[411] The assay allows the examination of cell motility without the need to consider potential effects from cell proliferation, since the migration time is set much shorter than the time required for cells to proceed though the cell cycle.[412]

1×10^5 HUVECs in 100 µl ECGM were seeded to the upper compartment of Transwell inserts (growth area 0.33 cm^2, 8 µm pore size, polycarbonate; Corning, NY, USA). The lower compartment was filled with 600 µl ECGM. Cells were allowed to adhere for 4 h. Subsequently, cells were treated with vioA in starvation medium as indicated and a chemotactic gradient (20 % FCS in the lower compartment, 1 % FCS in the upper compartment) was applied. Cells without FCS gradient were used as negative control. HUVECs were allowed to migrate for 16 h and the migration process was terminated by fixing the cells for 10 min with Roti®-Histofix (4 % paraformaldehyde; 100 µl in the upper compartment, 600 µl in the lower compartment). The Transwell inserts were stained for 10 min with methanolic crystal violet solution (100 µl in the upper compartment, 600 µl in the lower compartment, Table 4) and subsequently washed with PBS to remove excessive solution. Non-migratory HUVECs in the upper part of the Transwell inserts were removed using a cotton swap and the inserts were dried overnight. The dried inserts were placed in 200 µl dissolving solution (Table 4) and incubated for 30 min at room temperature under constant agitation to solubilize the crystal violet. 100 µl of the stained solution was transferred to a new 96-well plate, and the absorbance was measured using a microplate reaser (Infinite F200 Pro, Tecan) at 540 nm. The amount of reconstituted crystal violet directly correlates with the number of migrated cells.

10. Western blot analysis

Western blot is an established technique for the qualitative and semi-quantitative detection of specific proteins out of a cell lysate through separation of the proteins by size and transferring them to a solid support. The proteins can then be visualized by incubating the solid support with appropriate antibodies.[413]

10.1 Sample preparation

HUVECs were seeded to 6-well plates and grown to confluence or seeded in low density and grown for 24 h. Subsequently, cells were treated as indicated, washed with ice-cold PBS and lysed with 70-100 µl RIPA lysis buffer (Table 4) or in the case of investigating phosphorylated proteins with modified RIPA lysis buffer (Table 4). Lysed cells were frozen at -80 °C for at least 1 h. Frozen cells were thawed on ice and collected in 1.5 ml tubes using a cell scraper. Cell lysates were centrifuged at 17.000 g and 4 °C for 15 min and the protein containing supernatants were transferred to a fresh tube. Subsequently, the protein concentration of each sample was determined (protein quantification, II.2.9.2), and 5x SDS sample buffer (ratio 1:4) was added to the samples. The protein concentration of each sample was adjusted to the sample with the lowest protein concentration using 1x SDS sample buffer. Samples were boiled at 95 °C for 5 min to denature the proteins, centrifuged at 17.000 g for 5 min and stored at -20 °C.

10.2 Protein quantification

The Pierce™ BCA Protein Assay Kit was used to determine the total amount of protein in the prepared cell lysates (see IV.10.1). The Bicinchoninic acid (BCA) assay is based on two reactions. First, peptide bonds of proteins reduce Cu^{2+} to Cu^{+} ions (biuret reaction). Second, two molecules of bicinchoninic acid build a violet-colored chelate complex with Cu+, which absorbs light at a wavelength of 562 nm.[414]

Cell lysates were diluted 1:10 in ddH_2O, and 10 µl (triplicates) were transferred to a new 96-well plate. The BCA Reagent was freshly prepared according to the manufacturer's instructions (Reagent A and B, 1:50). 190 µl of the BCA Reagent was added to each well and incubated at 37 °C for 30 min. Absorbance was measured at 562 nm using a microplate reader (Infinite F200 Pro, Tecan). The protein concentrations were determined based on linear regression using a bovine serum albumin (BSA) dilution series (0, 50, 100, 150, 200, 300, 400, 500 µg/ml).

10.3 Sodium dodecyl sulfate polyacrylamide gel electrophoresis (SDS-PAGE)

SDS-PAGE is used to separate proteins according to their electrophoretic mobility based on their molecular weight. In this study, discontinuous SDS-PAGE was performed (Mini-PROTEAN Tetra System, Bio-Rad Laboratories GmbH, Munich, Germany) as previously described by Laemmli.[415] The polyacrylamide (PAA; Rotiphorese Gel 30, Carl Roth GmbH, Karlsruhe, Germany) concentration was chosen based on the molecular weight of the target protein. For proteins larger than 120 kDa, a PAA concentration of 7.5 % was used. In case of proteins with a molecular weight ranging between 40 and 120 kDa, 10 % PAA was applied. Proteins smaller than 40 kDa were separated in gels with a PAA concentration of 12 %. As reference for specific protein weights, an individual gel pocket was filled with 5 µl of a pre-stained protein ladder. For gels with a PAA concentration of 7.5 %, the Spectra™ Multicolor High Range Protein Ladder (Table 2) was applied. For gels with 10 % and 12 % PAA, the BlueStar Protein Marker (Table 2) was employed. Equal volumes of each sample according to equal amounts of total protein were loaded to the pockets of the PAA gel and electrophoresis buffer (Table 4) was added to the electrophoresis chamber. The proteins were aligned at the front of the stacking gel for approximately 20 min at 80 V. Then, the voltage was increased to 120 V to achieve protein separation until the sample buffer started to leak out of the gel.

10.4 Immunoblotting

The separated proteins were transferred from the polyacrylamide gel onto a polyvinylidene difluoride membrane (PVDF; Immun-Blot® PVDF, Bio-Rad Laboratories GmbH). The PVDF membranes were activated in methanol before blotting. Immunoblotting of proteins smaller than 130 kDa was performed either by wet-tank blotting (Criterion™ Blotter, Bio-Rad Laboratories GmbH) with Tank buffer at 4 °C and a constant voltage of 100 V for 60 min or by semi-dry blotting (Trans-Blot® Turbo™ Transfer System, Bio-Rad Laboratories GmbH) using anode buffer 1 (AP1), anode buffer 2 (AP2) and cathode buffer at a constant voltage of 25 V for 30 min. Proteins with a molecular weight higher than 130 kDa were immunoblotted by wet-tank blotting at 4 °C and a constant voltage of 30 V for 16 h using Matsudaira transfer buffer (Table 4).

10.5 Protein detection

Proteins transferred onto PVDF membranes were detected based on the oxidation of luminol in the presence of hydrogen peroxide (H_2O_2), which is catalyzed by the horseradish peroxidase (HRP) and leads to a chemiluminescent signal.[416] The chemiluminescent signal is detected on radiographic films (Super RX-N, FUJIFILM Europe GmbH, Düsseldorf, Germany) developed with an Agfa CP 1000 X-ray film processor (AGFA, Cologne, Germany).

After immunoblotting, PVDF membranes were incubated with 5 % non-fat dry milk powder (Blotto) or 5 % BSA in Tris-buffered saline with 0.2 % Tween® 20 (TBS-T) for a minimum of 1 h to prevent unspecific antibody binding. The membranes were then incubated a with primary antibody solution (Table 7) at 4 °C overnight. Subsequently, membranes were washed four times (3 min each) with TBS-T to remove unbound antibody and incubated with the respective HRP-conjugated secondary antibody solution (Table 8) for 2 h at room temperature or at 4 °C overnight. The membranes were washed four times (3 min each) with TBS-T, and 1 ml homemade enhanced chemiluminescence solution (ECL, Table 4) was applied in the dark. The target protein was detected as described above. To verify equal amounts of protein in each sample, loading controls were used (β-actin, β-tubulin, topoisomerase I) depending on the protein size of the protein of interest. For detection of β-actin, membranes were incubated with the HRP-conjugated primary mouse monoclonal anti-β-actin antibody (Table 7) for 1 h and detection was performed as described above except for that no secondary antibody was needed. Densitometry measurements were performed using ImageJ software (version 1.49k).

10.6 Stripping of membranes

To investigate proteins with similar molecular weights on the same membrane, a stripping step was performed to remove the already bound antibody. For this, membranes were incubated twice for 10 min each with stripping buffer (Table 4) under constant agitation. Next, membranes were washed twice for 10 min with PBS and then twice for 5 min with TBS-T under constant agitation. Membranes were blocked again using 5 % Blotto or 5 % BSA in TBS-T for at least 1 h before membranes were incubated with the next primary antibody.

11. Cell fractionation

Cell fractionation was performed to investigate the influence of vioA on the subcellular localization of different proteins.

HUVECs were seeded onto 10 cm dishes, grown to confluence and treated as indicated. Subsequently, cells were washed with 10 ml and then covered with 1 ml ice-cold PBS. By using a cell scraper, cells were carefully removed from the dish and transferred to a 1.5 ml tube. The cell suspension was centrifuged at 17.000 g and 4 °C for 1 min and the supernatant was discarded. The pellet was resuspended (but not vortexted) in 200 µl ice-cold fractionation buffer A (Table 4) and incubated on ice for 15 min. Subsequently, 15 µl Nonidet P40 (10 % v/v in ddH_2O; final concentration of 0.75 %) was added, and the samples were vortexed for 10 sec and then centrifuged at 17.000 g and 4 °C for 1 min. The supernatant containing the cytosolic fraction was transferred to a fresh 1.5 ml tube, and the cell pellet was washed with 200 µl ice-

cold fractionation buffer A, centrifuged at 17.000 g and 4 °C for 1 min, and the supernatant was discarded. The pellet was resuspended in 50 µl fractionation buffer C (Table 4), vortexed for 15 sec and incubated on ice for 15 min. After centrifugation at 17.000 g and 4 °C for 5 min, the supernatant containing the nuclear fraction was transferred to a fresh 1.5 ml tube. The remaining pellet with the insoluble fraction was discarded. The total amount of protein in each sample was detected as described in section IV.10.2. The protein concentration of each sample was adjusted to the sample containing the lowest amount of protein and boiled at 95 °C for 10 min. For western blot analysis (section IV.10.3-10.5), 40 to 50 µg of protein was loaded to the pockets of the PAA gels. β-tubulin was used as marker for the cytosolic fraction and topoisomerase I was used as marker for the nuclear fraction. Both markers served for the detection of potential cross-contaminations in the subcellular fractions.

12. Reverse transcription quantitative polymerase chain reaction (RT-qPCR)

Quantitative (real-time) polymerase chain reaction (qPCR) is a fast and sensitive method for determining expression levels of messenger ribonucleic acid (mRNA) based on the $2^{-\Delta\Delta CT}$ method using the fluorescent reporter SYBR Green. SYBR Green binds to double-stranded DNA, thus all replicated transcripts after each PCR cycle. As soon as the fluorescent signal is stronger than the background signal, enough DNA is amplified to enable its detection, which is called the threshold cycle (C_T). The higher the amount of target gene mRNA and, therefore, of cDNA as template for the PCR, the lower is the number of cycles needed to reach the C_T. For normalization, the C_T value of the housekeeping gene GAPDH was determined in each reaction. The $2^{-\Delta\Delta CT}$ method is used for relative quantification of the normalized mRNA expression of the target gene in relation to an untreated control.[417] For all steps of the qPCR, nuclease and nucleic acid free equipment was used to avoid digestion and contamination with foreign DNA or RNA.

12.1 Sample preparation

HUVECs were seeded onto 6-well plates, grown to confluence and treated as indicated. Cells were washed with 2 ml ice-cold PBS and lysed with 350 µl Buffer RLT (RNeasy® Mini Kit, Quiagen GmbH, Hilden, Germany) containing freshly added 2-mercaptoethanol (1:100). The cell lysates were frozen at -80 °C for at least 1 h.

12.2 RNA isolation

Total cellular RNA was isolated using the RNeasy® Mini Kit (Quiagen) according to the manufacturer's protocol. Cell lysates were thawed on ice and collected in 1.5 ml tubes using a cell scraper. 70 % ethanol (1:1) was added to the lysates and properly mixed. The mixture was transferred to RNeasy® silica membranes placed in RNeasy® Mini spin columns and centrifuged at 17.000 g for 15 sec. The flow-though was discarded and the spin column membranes were washed with 350 µl Buffer RW1 and centrifuged at 17.000 g for 15 sec. The flow-through was discarded and the spin column membrane was incubated with 70 µl DNase I solution for 15 min at room temperature to initiate DNA digestion. 350 µl Buffer RW1 was added to the spin column membranes and centrifuged at 17.000 g for 15 sec. The flow-though was discarded, and the spin column membrane was washed with 500 µl Buffer RPE followed by centrifugation at 17.000 g for 15 sec. The step was repeated except that the centrifugation time was increased to 2 min. The flow-through was discarded and a centrifugation step at 17.000 g for 1 min served to fully dry the spin column membrane. RNA on the membrane was eluted with 30 µl DNase/RNase-free water and centrifuged at 17.000 g for 1 min. To determine the RNA concentration of each sample, absorbance was measured at 260 nm using a P330 nanophotometer (Implen GmbH). Isolated mRNA was stored at -80 °C until further use.

12.3 Complementary DNA (cDNA) synthesis

Isolated mRNA was transcribed into complementary DNA (cDNA) by reverse transcriptase. For this, 1 µg RNA was adjusted to a final volume of 7 µl using DNase/RNase-free water. 100 pmol random N6 primer and 2 mM deoxynucleoside triphosphates (dNTPs) were added, and the samples were incubated for 10 min at 65 °C. Samples were cooled down on ice for 2 min, and a reaction mixture containing 0.2 µl RNAsin/RNase out, 0.8 µl DNase/RNase-free water, 4 µl Protoscript Buffer, 2 µl 100 mM DTT and 1 µl Protoscript Reverse Transcriptase was added to each sample. The mixture was incubated for 5 min at room temperature followed by 1 h at 42 °C. 100 µl DNase/RNase-free water was added to each sample and the enzymatic reaction was stopped by incubation at 65 °C for 20 min. Samples were stored at -20 °C for experimental use.

12.4 Performance of qPCR

For the performance of a qPCR, the StepOnePlus™ System (Applied Biosystems GmbH) and the PowerSYBR® Green PCR Master Mix (Life Technologies GmbH, Darmstadt, Germany) were used. Forward and reverse primers for the gene of interest (Table 12) were diluted in DNase/RNase-free water in a ratio of 1:25 to a final concentration of 4 pmol, and 1.25 µl of the diluted primers were added to 5 µl PowerSYBR® Green PCR Master Mix. 4.15 ng cDNA

(calculated) was diluted to 2.5 µl with DNase/RNase-free water and was used as template. All components were mixed and applied as triplicates to a MicroAmp® Fast 96-well Reaction Plate. The plate was covered with a plate sealer for optical assays and centrifuged at 300 g for 30 sec. qRT-PCR was performed using a StepOnePlus™ System according to the following program (Table 18).

The results were analyzed using the StepOne® 2.3 Software and relative gene expressions were calculated using the $2^{-\Delta\Delta CT}$ method. For this, the mean C_T-value of the housekeeping gene GAPDH was subtracted from the C_T-value of the gene of interest resulting in ΔC_T-values. To investigate a potential up- or downregulation of the target gene in treated cells compared to untreated control cells, the mean ΔC_T-value of the untreated control was then subtracted from the ΔC_T-values of the treated samples, generating $\Delta\Delta C_T$-values. Then, the relative expression level $2^{-\Delta\Delta CT}$ was calculated, which corresponds to the x-fold gene expression.

Table 18: Program for qPCR

Reaction step	Temperature	Period	Number of cycles
Activation of DNA polymerase	95 °C	10 min	1
Denaturation Annealing/Elongation	95 °C 60 °C	15 s 60 s	40
Melt curve stage	95 °C 60 °C 95 °C	15 s 60 s 15 s	1
Hold	4 °C	∞	1

13. Flow cytometry

Flow cytometry is widely used in different research areas and is based on the principle that cells are transported in a liquid flow, which enables measurement of single cells. To ensure this, flow cytometric systems provide different lasers, which examine various cellular characteristics. In this study, all flow cytometric measurements were conducted using a FACSVerse™ (BD Bioscience).

13.1 Cell surface expression of adhesion molecules

Flow cytometric analysis of fluorescence-labeled cells was performed to investigate the influence of vioA on the cell surface expression of inflammatory adhesion molecules.

HUVECs were seeded onto 12-well dishes, grown to confluence and treated with vioA and TNF as indicated. Subsequently, cells were washed twice with 1 ml PBS and detached with

200 µl Accutase® solution (Sigma-Aldrich) at 37 °C. Detachment reaction was stopped by adding 800 µl ice-cold M199. The cell suspension was transferred to FACS tubes and cells were harvested by centrifugation at 300 g and 4 °C for 5 min. The supernatant was discarded and the cells were washed with 1 ml ice-cold PBS followed by centrifugation at 300 g and 4 °C for 5 min. Again, the supernatant was discarded, 1 ml ice-cold PBS containing 0.2 % BSA was added to the tubes and cells were harvested again by centrifugation at 300 g and 4 °C for 5 min. The supernatant was discarded and the cells were incubated with 100 µl antibody solution (Table 11) for 45 min at 4 °C in the dark. Next, the mixture was washed twice with 1 ml ice-cold PBS containing 0.2 % BSA followed by centrifugation at 300 g and 4 °C for 5 min. The supernatant was discarded and the cell pellet was suspended in 300 µl ice-cold PBS containing 0.2 % BSA. The protein surface expression of the adhesion molecules was quantified by recording median values for 10.000 events per sample using flow cytometry.

13.2 BrdU incorporation assay

5-Bromo-2'-deoxyuridine (BrdU) is a thymidine analog that is incorporated into nuclear DNA during cell replication, thereby enabling the detection of DNA synthesis *in vivo* and *in vitro* after labeling the incorporated BrdU with a fluorescent antibody.[418]

4.4×10^4 HUVECs were seeded to 6-well plates, grown for 16 h and subsequently serum-starved for 8 h using starvation medium. Subsequently, the starvation medium was exchanged with fresh ECGM and cells were treated with vioA as indicated for 24 h. Treatment with starvation medium instead of ECGM served as negative control for BrdU incorporation. 8 h before the end of the treatment period, 10 µM BrdU was added to the cells. Thereafter, cells were washed twice with 2 ml PBS and detached using 400 µl T/E-solution at 37 °C. The enzymatic reaction was stopped with 1 ml ice-cold M199. The cell suspension was transferred to FACS tubes and cells were harvested by centrifugation at 300 g and 4 °C for 10 min. The cells were washed with 1 ml ice-cold PBS followed by centrifugation at 300 g and 4 °C for 10 min. The supernatant was discarded, the cell pellet was resuspended in 100 µl ice-cold PBS and the cell suspension was carefully dropped into 3 ml ice-cold ethanol (99.8 %) while gently vortexing to allow cell fixation. Cells were fixed for 3 days at 4 °C.

The fixed cells were centrifuged at 300 g and 4 °C for 20 min. The supernatant was discarded, and 1 ml 2 M HCl containing 0.5 % Triton X-100 was added to the cell pellet for DNA denaturation. Cells were incubated for 30 min followed by centrifugation at 300 g and 4 °C for 20 min. The supernatant was discarded and 1 ml 0.1 M $Na_2B_4O_7$ (pH 8.5) was added to neutralize the samples. Cells were centrifuged again at 300 g and 4 °C for 20 min and then incubated with 75 µl BrdU staining solution (Table 11) at 4 °C overnight protected from light. Next, 3 ml ice-cold PBS was added to the tubes, and cells were harvested by centrifugation at

300 g and 4 °C for 20 min. BrdU incorporation was quantified by recording median values for 3.000 events per sample using flow cytometry.

13.3 Cell cycle analysis

The analysis of the cell cycle distribution using PI staining is based on the principle that the DNA content varies between the different cell cycle stages. While cell in the G_0/G_1 phase contain a haploidic DNA content, cells in the G_2/M phase have a diploidic DNA content. Cells with a DNA content between haploidic and diploidic are regarded as being in the S phase of the cell cycle. The amount of intercalating PI is directly proportional to the amount of DNA present in the cell.[419]

4.4 x 10^4 HUVECs were seeded into 6-well plates, grown for 24 h and subsequently treated with vioA as indicated. Thereafter, cells were washed twice with 1 ml PBS and detached using 400 µl T/E-solution at 37 °C. The enzymatic reaction was stopped with 1 ml ice-cold M199. The cell suspension was transferred to FACS tubes and cells were harvested by centrifugation at 300 g and 4 °C for 10 min. The supernatant was discarded and the cells were washed with 1 ml ice-cold PBS followed by centrifugation at 300 g and 4 °C for 10 min. The supernatant was discarded and the cell pellet was incubated with HFS (Table 4) for a minimum of 2 h at 4 °C in the dark. The percentage of cells in the different cell cycle stages was analysed by recording median values for 10.000 events per sample using flow cytometry.

14. Immunocytochemistry

Immunocytochemistry was performed to investigate the effect of vioA on the nuclear translocation and cellular accumulation of various proteins.

For obtaining a confluent monolayer of HUVECs, 5.5 x 10^4 HUVECs were seeded to 8-well µ-slides (ibidi GmbH) and grown for 48 h. For the analysis of subconfluent HUVECs, 4.5 x 10^3 cells were seeded to 8-well µ-slides (ibidi GmbH) and grown for 24 h. Subsequently, cells were treated as indicated. Thereafter, cells were washed with 300 µl PBS+ and fixed for a minimum of 10 min using 300 µl Roti®-Histofix (4 % paraformaldehyde). Cells were washed twice with 300 µl PBS before the cell membrane was permeabilized with 300 µl PBS containing 0.2 % Triton X-100 for 5 min. After two washing steps with 300 µl PBS, unspecific binding sites were blocked by adding 300 µl PBS containing 0.1 % BSA for 30 min at room temperature. Next, cells were incubated with 150 µl primary antibody solution (Table 9) for 2 h at room temperature under constant agitation. Subsequently, the cells were washed twice (5 min each) with 300 µl PBS and incubated with 150 µl secondary Alexa Fluor® 488-conjugated antibody (Table 10) for 1 h at room temperature in the dark under constant agitation. For visualizing F-

actin, cells were incubated with a fluorescent rhodamine phalloidin solution (1:400 in PBS with 0.2 % BSA) for 2 h at room temperature in the dark under constant agitation without secondary antibody application. If staining of the nuclei was desired, cells were subsequently incubated with 150 µl HOECHST 33342 solution (1:10.000 in PBS) for 10 min at room temperature protected from light and under constant agitation. Cells were washed twice (5 min each) with 300 µl PBS, embedded in FluorSave™ Reagent and sealed with coverslips. Microscopical images were taken using a Leica DMI6000b fluorescence microscope (Leica Microsystems).

15. *De novo* protein synthesis assay

To analyse the influence of vioA on the *de novo* protein synthesis, the Click-iT® Plus OPP Protein Synthesis Assay Kit (Thermo Fisher Scientific) was used. O-propargyl-puromycin (OPP), an alkyne analogue of puromycin, covalently conjugates with nascent polypeptide chains during active protein biosynthesis. Through copper(I)-catalyzed azide-alkyne cycloaddition, the alkyne group of OPP is linked to a fluorescence-labeled picolylazide dye. The resulting product can be visualized by fluorescence microscopy.[420]

The assay was performed according to the manufacturer's instructions. In brief, 5.5 x 10^4 HUVECs were seeded to 8-well µ-slides (ibidi GmbH), grown to confluence and treated as indicated. 30 min before the end of the incubation period, 20 µM Click-iT® OPP Reagent was added to the cells. Next, cells were washed with 300 µl PBS+ and fixed for 15 min using Roti®-Histofix (4 % paraformaldehyde). Cells were washed twice with 300 µl PBS and permeabilized for 15 min with 300 µl PBS containing 0.5 % Triton X-100. After two washing steps with 300 µl PBS, cells were incubated for 30 min with 150 µl Click-iT® Plus reaction cocktail in the dark. Cells were washed with 300 µl PBS and nuclei were stained with 150 µl HCS NulearMask™ Blue Stain (1:2.000 in PBS) for 30 min protected from light. After two washing steps with 300 µl PBS, cells were embedded in FluorSave™ Reagent and covered with coverslips. Microscopical images were taken using a Leica DMI6000b fluorescence microscope (Leica Microsystems). ImageJ software (version 1.49k) was used to normalize the intensity of the Click-iT® OPP signal to the intensity of the cell nuclei staining.

16. siRNA transfection

To investigate the involvement of NOP14 inhibition on the effects of vioA, knockdown of NOP14 was conducted by lipofection, a lipid-mediated DNA-transfection using the GeneTrans II transfection reagent (MoBiTec GmbH, Goettingen, Germany).

The transfection was performed according to the manufacturer's instructions. In brief, 2 x 10^4 HUVECs were seeded per cm^2 growth area and grown for 24 h until 70 to 80 % confluence

was reached. For transfection, two separate solutions were prepared. In solution one, 60 µl basal ECGM and 14 µl GeneTrans II Reagent (per 9.6 cm^2 growth area, equal to 1 well of a 6-well plate) were mixed. In solution two, 70 µl DNA Diluent B was mixed with the respective siRNA (Table 14) (per 9.6 cm^2 growth area, equal to 1 well of a 6-well plate). Non-targeting control siRNA (Table 14) was used as control. As required by the manufacturer's instructions, the DNA Diluent B was not vortexed at any time. The solutions were incubated for 5 min at room temperature. Then, solution one was added to solution two without excessively pipetting the solution up and down. The resulting mixture was incubated at room temperature for 20 min to allow the incorporation of siRNA into the lipids. Then, the medium was removed from the cells and basal ECGM was added (104 µl per 1 cm^2 growth area). The siRNA-containing solution was added drop by drop to the cells (144 µl per 9.6 cm^2 growth area, equal to 1 well of a 6-well plate) to achieve a final siRNA concentration of 80 nM and incubated for 4 h at 37 °C. Subsequently, the medium was refreshed with ECGM. 24 h after transfection, medium was changed once more. The effectiveness of the siRNA mediated knockdown was validated by western blot analysis (see IV.10). Concerning NOP14 knockdown experiments, all further investigations were performed 48 h after transfection.

17. Cellular thermal shift assay (CETSA)

In the cellular thermal shift assay (CETSA), thermal denaturation and thus protein stability are assessed by heating cells with increasing temperatures. After cell lysis, denatured and thus aggregated proteins can be removed from the samples by centrifugation, and the stable proteins in the supernatant can be analysed concerning their aggregation temperatures (T_{agg}) with and without compound treatment.[421]

CETSA was performed as described previously with slight modifications. In brief, HUVECs were seeded into 10 cm dishes, grown to confluence and treated as indicated for 1 h. After washing the cells with 10 ml PBS, detachment was performed with 2 ml T/E-solution at 37 °C. The enzymatic reaction was stopped by adding 8 ml ice-cold M199. Cell were harvested by centrifugation at 300 g and 4 °C for 5 min, washed twice with 10 ml ice-cold PBS, resuspended in PBS and counted using a hemocytometer (Neubauer cell chamber). The cell number was adjusted to 5.8 x 10^6 cells per ml. 100 µl of the cell suspension (equal to 5.8 x 10^5 cells), each, were transferred to 0.2 ml 8-tube PCR strips (Bio-Rad Laboratories GmbH). The PCR strips were heated with eight temperature endpoints between 42.3 °C and 57.8 °C using a peqSTAR thermocycler (PEQLAB Biotechnology, Erlangen, Germany). The thermocycler program is shown in Table 19. Immediately after the end of the program, the tubes were snap-frozen in liquid nitrogen. The cell suspension was thawed at 21 °C, briefly vortexed and frozen again in liquid nitrogen. This freeze-thaw cycle was performed three times to ensure complete cell lysis.

Denatured proteins were then separated through centrifugation at 20,000 g and 4 °C for 30 min. 70 µl of the native proteins-containing supernatant was transferred to a fresh 1.5 ml tube, and 3x SDS sample buffer (Table 4) was added to the samples in a ratio of 1:2. The samples were briefly vortexed, boiled at 95 °C for 5 min and centrifuged at 17.000 g for 5 min. Thermal aggregation curves of NOP14 were analysed by western blotting (see IV.10.3-10.5).

Table 19: Program for CETSA

Reaction step	Temperature	Period
Heat lid	110 °C	Until intended temperature is reached
Temperature gradient	52 °C ± 11 °C	3 min
Cool down	21 °C	3 min

18. Animal experiments

All experimental procedures were conducted in compliance with the German legislation for the protection of animals. Animal experiments were approved by the Government of Upper Bavaria under the reference numbers ROB-55.2-2532-Vet 02-15-50 (CNV model; 08-10-2015) and ROB-55.2Vet-2532.Vet_02-17-68 (intravital microscopy; 01-03-2018).
For the *in vivo* laser-induced choroidal neovascularization (CNV) experiment, 6-8-week-old female C57BL/6J WT mice (Charles River Laboratories, Wilmington, MA, USA) were used. For the *in vivo* intravital microscopy of the murine cremaster muscle 10–20 weeks old male C57BL/6 mice (Charles River Laboratories, Sulzfeld, Germany) were used. Animals were housed on a 12-h light/dark cycle with free access to water and food.

18.1 Intravital microscopy of the murine cremaster muscle

For monitoring the leukocyte trafficking on the vascular endothelium in microvessels of the murine cremaster muscle, intravital microscopy was performed by Dr. Matthias P. Fabritius and Prof. Dr. Christoph A. Reichel (Department of Otorhinolaryngology and Walter Brendel Centre of Experimental Medicine, Clinical Centre of LMU Munich, Munich, Germany). The surgical preparation was performed as described by Baez with minor modifications.[422] Mice were injected with vioA (0.1 mg/kg; i.v. via the tail vein) or drug vehicle, and local inflammation was induced by intrascrotal injection of TNF (500 ng/ml in PBS). DMSO in a concentration of 0.01 % (v/v) served as vehicle and was applied to the control group. 6 h post injection, the mice were anesthetized using a ketamine/xylazine mixture (100 mg/kg ketamine, 10 mg/kg xylazine). Subsequently, intravital microscopy of the post-capillary venules of the cremaster

muscle was performed with an Olympus BX 50 upright microscope (Olympus Microscopy, Hamburg, Germany). Neutrophils and classical monocytes were identified by *in vivo* immunostaining with an intravenously injected fluorescence-labeled anti-Gr-1 mAb (Biolegend, San Diego, CA, USA). The leukocyte trafficking was analysed using the AxioVision 4.6 software (Zeiss MicroImaging, Jena, Germany). Off-line analysis of parameters describing the sequential steps of leukocyte extravasation was performed with AxioVision 4.6 software (Zeiss MicroImaging GmbH). ImageJ software (National Institutes of Health, Bethesda, MD, USA) was used for further image processing and analysis. Rolling leukocytes were defined as those moving slower than the associated blood flow and quantified for 30 sec. Firmly adherent cells were determined as those resting in the associated blood flow for > 30 sec and related to the luminal surface per 100 µm vessel length. Transmigrated cells were counted in regions of interest, covering 75 µm on both sides of a vessel with > 100 µm length. By measuring the distance between several images of one fluorescent bead (administered *via* the femoral catheter) under stroboscopic illumination, centreline blood flow velocity was determined. From measured vessel diameters and centreline blood flow velocity, apparent wall shear rates were calculated, assuming a parabolic flow velocity profile over the vessel cross-section.

18.2 Laser-induced choroidal neovascularization

Murine laser-induced choroidal neovascularization (CNV) was performed by Yanfen Li and Prof. Dr. Stylianos Michalakis (Department of Ophthalmology, University Hospital, LMU Munich, Munich, Germany) as described previously.[423] In brief, mice were anesthetized by an intraperitoneal injection of a mixture of ketamine (40 mg/kg body weight) and xylazine (20 mg/kg body weight), and their pupils were dilated with tropicamide (Mydriadicum Stulln, Pharma Stulln GmbH). 1 µl of vioA was delivered intravitreally into the right eyes (final concentration of 30 nM), and 1 µl of vehicle was applied to the left eyes as control. Immediately after the intravitreal injection, CNV was induced by laser photocoagulation. Retinal fundus was visualized with Micron IV Retinal Imaging Microscope (Phoenix Research Laboratories), and four laser burns per eye were induced with an image-guided argon laser system (Phoenix Research Laboratories) using the following parameter: laser wavelength, 532 nm; energy, 230 mW; burn duration, 70 ms.

The angiographic analysis of the CNV leakage was conducted on day 7 and 14 after laser photocoagulation. For this, mice were anesthetized, and pupils were dilated as described above. Fluorescein sodium solution (7.5 mg/kg) was injected subcutaneously to visualize vessels. Fundus fluorescein angiography (FFA) was performed 5-10 min after using a retinal imaging microscope (Phoenix Research Laboratories). The leakage area was quantified with ImageJ64 software (National Institutes of Health, NIH).

Mice were euthanatized 14 days after CNV. Eyes were enucleated, and eyecups were isolated from the posterior area of the eye. They were flat-mounted and fixed in 4 % paraformaldehyde for immunohistochemistry studies. Flat-mounts were immunostained with rabbit anti-Iba1 (1:500, Wako) and Alexa Fluor 488-conjugated *Griffonia (Bandeiraea) simplicifolia* isolectin B4 (IB4; 1:25; I21411, Thermo Fisher Scientific) followed by the incubation in presence of a secondary Alexa Fluor 555 donkey anti-rabbit IgG antibody (1:500, Invitrogen).
The flat-mounts were viewed under Leica TCS SP8 spectral confocal laser scanning microscope (Leica Microsystems, Wetzlar, Germany). Images were captured with identical settings and analyzed with ImageJ64 software (NIH).

19. Statistical analysis

All experiments were conducted at least three times. For experiments with HUVECs, individual donors were utilized, experiments in HMEC-1 cells were performed with different passages. The actual number of independently performed experiments (n) is stated in the respective figure legend. Data are depicted in bar graphs and expressed as means ± standard error of the mean (SEM). In case of western blot experiments and immunocytochemistry, representative images are shown.
Statistical analysis was carried out using the GraphPad Prism software version 5.0 (San Diego, USA). One-way analysis of variance (ANOVA) followed by Tukey's post-hoc test or Mann-Whitney student's t-test were used to evaluate non-grouped experiments. Grouped experiments were analysed by two-way ANOVA followed by Bonferroni post-hoc test. P-values ≤ 0.05 were considered as statistically significant.

V RESULTS

1. The influence of vioprolide A on inflammatory and angiogenic processes *in vivo*

To study the *in vivo* effects of vioprolide A, two different experimental setups were used: The choroidal neovascularization (CNV) describes the growth of new blood vessels originating from the choroid through a break in the Bruch membrane. By using a laser-induced CNV mouse model, the influence of vioprolide A on the retinal vasculature and the cell infiltration around the laser lesion area was examined. This assay was kindly performed by Yanfen Li from the group of Prof. Dr. Stylianos Michalakis (Department of Ophthalmology, University Hospital, Ludwig Maximilians University of Munich (LMU), Munich, Germany). Chronic inflammation is characterized by a deregulated endothelial barrier function coupled to an ongoing leukocyte infiltration into the inflamed tissue. Therefore, the leukocyte-endothelial cell interaction was investigated *in vivo* by performing intravital microscopy of the TNF-activated cremaster muscle in mice. This assay was kindly performed by Dr. Matthias P. Fabritius and Prof. Dr. Christph A. Reichel (Department of Otorhinolaryngology and Walter Brendel Centre of Experimental Medicine, Clinical Centre of the LMU Munich, Munich, Germany).

1.1 VioA reduces the laser-induced CNV leakage area

To study CNV *in vivo*, vioprolide A was injected to murine eyes, and laser burns were applied to disrupt the Bruch membrane. On day 7 and 14 after laser treatment, the retinal vasculature was visualized by fundus fluorescein angiography (FFA). Vioprolide A treatment (30 nM) significantly decreased the fluorescence leakage area after both 7 and 14 days by approx. 70 % compared to vehicle control (Figure 22).

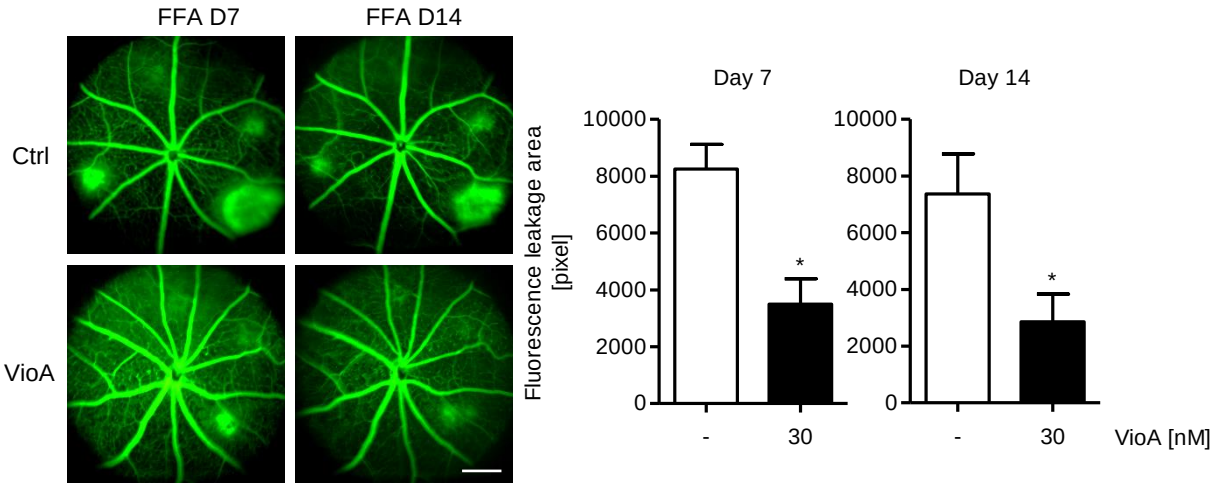

Figure 22: Vioprolide A reduces the laser-induced CNV leakage *in vivo*. VioA (30 nM) or vehicle (0.03 % DMSO in 0.9 % NaCl) was intravitreally injected to the eyes of mice. Laser photocoagulation was conducted immediately thereafter. Fundus fluorescein angiography (FFA) was performed on day 7 and day 14 after laser photocoagulation to evaluate CNV leakage. Representative images are shown. Scale bar, 300 µm. VioA, vioprolide A; FFA, fundus fluorescein angiography. Data are expressed as mean ± SEM. n=6. *p ≤ 0.05 vs. control.

1.2 The infiltration of endothelial cells and microcglia/macrophages to the laser lesion area is impaired by vioA

Laser-induced CNV is characterized by the infiltration of cells around the laser lesion area. On the one hand, laser-treatment of the eye leads to an inflammatory response that triggers the infiltration with immune cells such as microglia and macrophages. On the other hand, it has been shown that the number of endothelial cells around the laser lesions increases and creates a well-defined CNV network through cell proliferation and migration.[424] To investigate the influence of vioprolide A on the cell infiltration around the laser lesions, retinal pigment epithelium (RPE)/choroid flat mounts from laser-induced CNV-treated eyes were immunostained for Isolectin B4 (IB4), a marker for endothelial cells, and allograft inflammatory factor 1 (AIF1 or Iba1), a marker for microglia and macrophages.[425, 426] As shown in Figure 23A-B, vioprolide A (30 nM) significantly decreased (approx. 50 %) the IB4- and Iba1-positive area and, thus, the amount of infiltrating endothelial cells, microglia, and macrophages around the laser lesions.

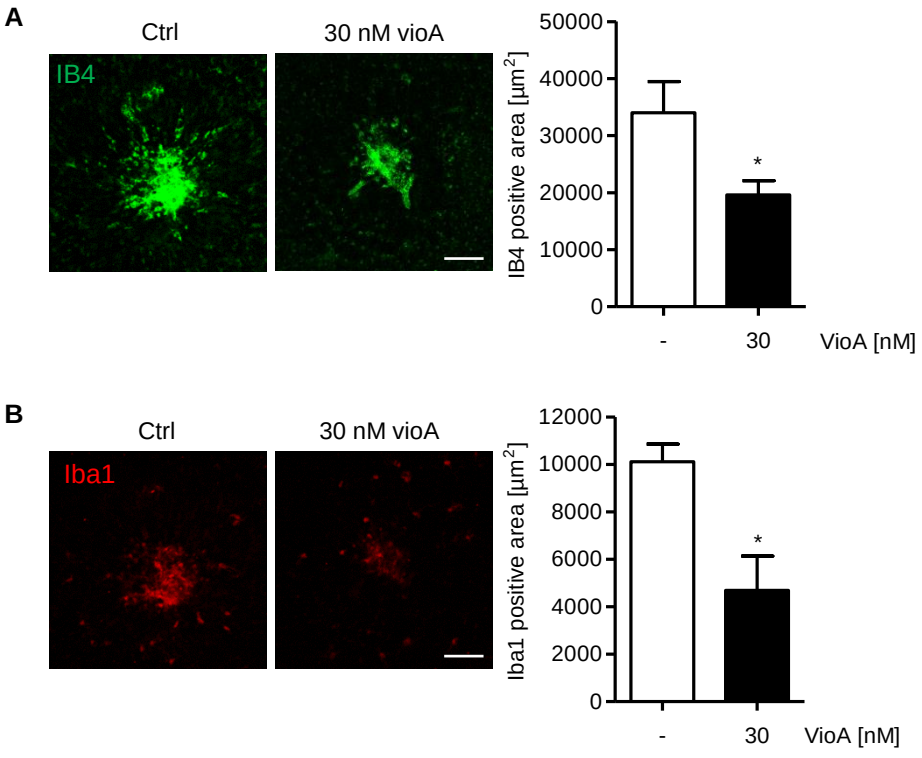

Figure 23: Vioprolide A attenuates the cell infiltration to CNV laser lesion areas *in vivo*. VioA (30 nM) or vehicle (0.03 % DMSO in 0.9 % NaCl) was intravitreally injected to eyes of mice, and laser photocoagulation was conducted. CNV lesions in eye cup flat mounts were immunostained with IB4 antibody (**A**) and Iba1 antibody (**B**) on day 14 after laser injury. Representative images are shown. Scale bar, 100 µm. VioA, vioprolide A; IB4, isolectin B4; Iba1, ionized calcium-binding adapter molecule 1. Data are expressed as mean ± SEM. n=6. *p ≤ 0.05 vs. control.

1.3 VioA attenuates the leukocyte-endothelial cell interaction in the TNF-activated cremaster muscle

The interaction of leukocytes with the endothelium is needed to promote the extravasation of leukocytes from the blood to the inflamed tissue.[48,49] For further in-depth *in vivo* analysis regarding this important aspect of inflammation, the rolling, adhesion and transmigration of Gr-1$^+$ neutrophils and classical monocytes were investigated using intravital microscopy of the TNF-activated murine cremaster muscle. The *in vivo* vioprolide A treatment (0.1 mg/kg) evoked a significant reduction (approx. 70 %) of the leukocyte adhesion to and transmigration through the vascular endothelium (Figure 24). The rolling motion of leukocytes on the endothelial surface, however, was slightly, but not significantly enhanced.

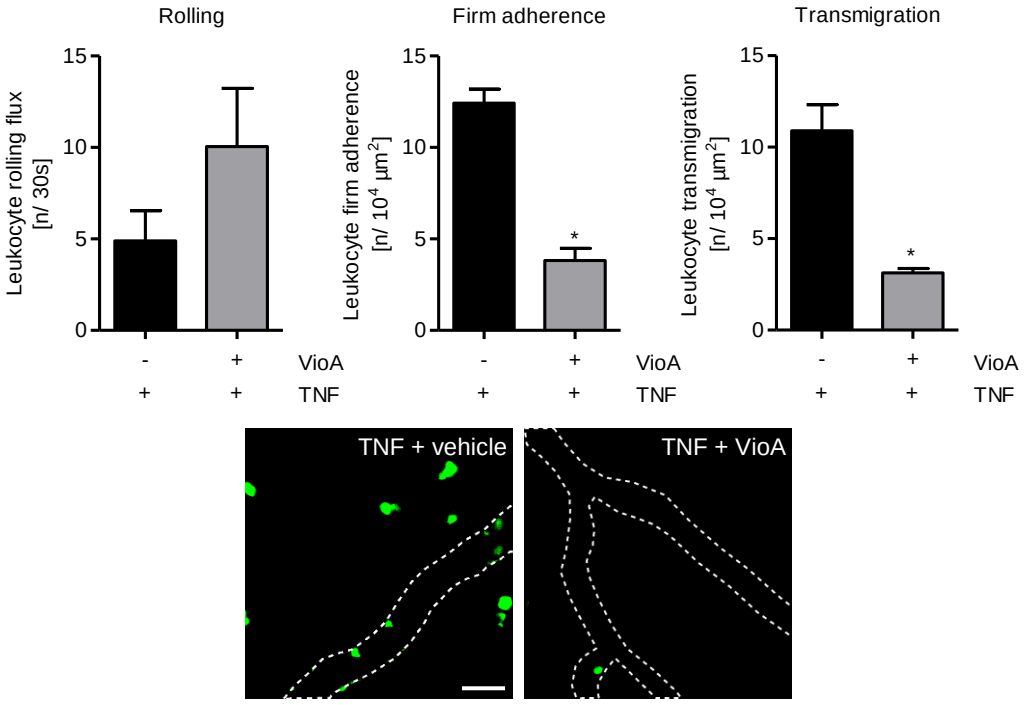

Figure 24: Vioprolide A lowers the leukocyte-endothelial cell interaction *in vivo*. Mice were injected with vioprolide A (0.1 mg/kg, i.a.) or vehicle (0.02 % DMSO). After 1 h, TNF (300 ng) was applied intrascrotally. After 4 h, TNF-elicited rolling, firm adhesion and transmigration of Gr-1$^+$ neutrophils and classical monocytes in postcapillary venules of the cremaster muscle were detected by intravital microscopy. One representative microscopic image is shown. Vessels are depicted as dotted lines. Scale bar, 100 µm. Data are expressed as mean ± SEM. n=6. *p ≤ 0.05 vs. TNF control.

2. The effects of vioprolide A on cell viability

To further investigate the effect of vioprolide A on inflammatory and angiogenic processes in endothelial cells *in vitro*, possible cytotoxic effects of the natural product had to be excluded first. Therefore, a set of cell viability experiments was performed.

2.1 Vioprolide A up to 10 nM has no impact on the metabolic activity of HUVECs

The CellTiter-Blue® Cell Viability Assay was used to investigate the effect of vioprolide A on the metabolic activity of HUVECs. Confluent cells were treated with increasing concentrations of vioprolide A for 24 h, 48 h and 72 h. For the investigation of certain angiogenic processes in endothelial cells, vioprolide A had to be added to subconfluent instead of confluent cells. Thus, the influence of vioprolide A on the metabolic activity of subconfluent cells was examined, too. As shown in Figure 25A-B, up to 10 nM of vioprolide A had no impact on the metabolic activity of confluent HUVECs after 24–72 h and of subconfluent HUVECs after 24 h. Treatment of HUVECs with 30 nM vioprolide A, on the contrary, slightly but significantly reduced the metabolic activity of HUVECs after a treatment period of 72 h.

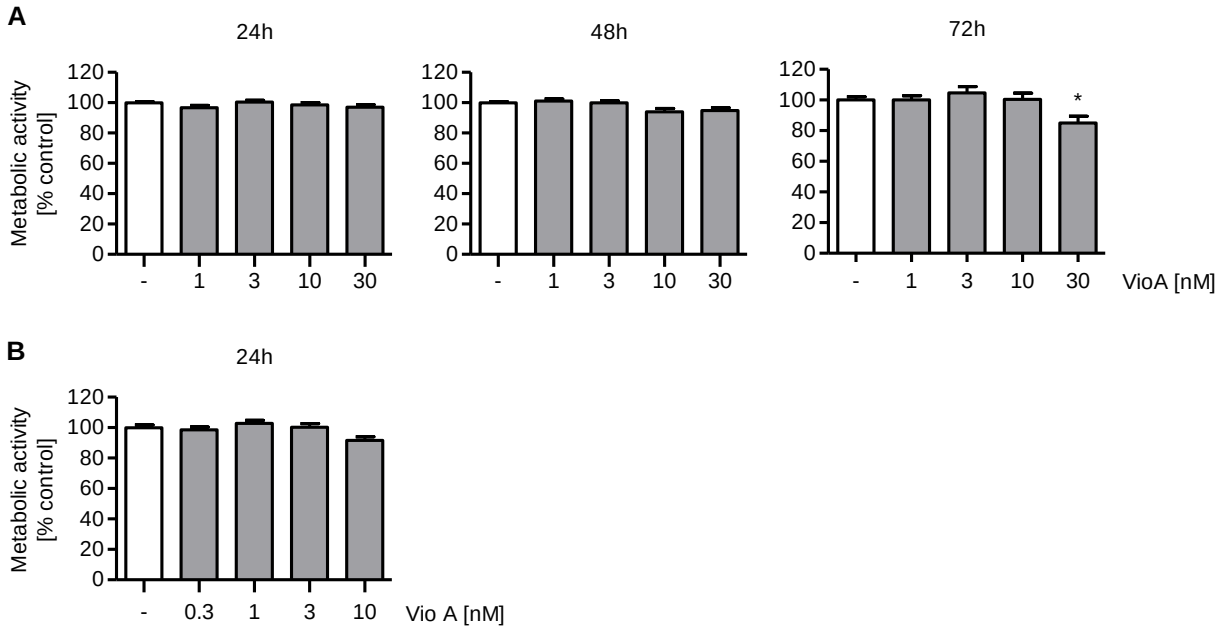

Figure 25: Treatment of HUVECs with up to 10 nM of vioprolide A has no impact on cell viability. A Confluent HUVECs were treated with vioA (1, 3, 10, 30 nM) for 24 h, 48 h and 72 h. **B** 3 x 10^4 HUVECs were grown for 24 h and treated with vioprolide A (0.3, 1, 3, 10 nM) for 24 h. **A**-**B** Metabolic activity was determined using the CellTiter-Blue® Cell Viability Assay. Fluorescence was measured at 590 nm. VioA, vioprolide A. Data are expressed as mean ± SEM. n=3. *p ≤ 0.05 vs. control.

2.2 Vioprolide A up to 10 nM does not exhibit late apoptotic cell death in HUVECs

Late apoptotic cell death, which is characterized by DNA fragmentation resulting in subdiploidic DNA content of the cell, was investigated according to Nicoletti *et al*.[405] For this, confluent or subconfluent HUVECs were treated with vioprolide A as indicated for up to 72 h and subsequently stained with propidium iodide, which binds to double stranded DNA and allows

the differentiation of subdiploidic from haploidic and diploidic cells. Confluent HUVECs showed no increase in the number of apoptotic cells after they were treated with concentrations of up to 10 nM of vioprolide A over a total period of 72 h (Figure 26A). Accordingly, late apoptotic cell death of subconfluent cells after 24 h was not altered by vioprolide A up to 10 nM (Figure 26B). In contrast, 30 nM vioprolide A slightly but significantly increased the percentage of subdiploidic cells after 24 h. In both experimental setups, staurosporine (1 µM) served as positive control for the induction of late apoptosis.

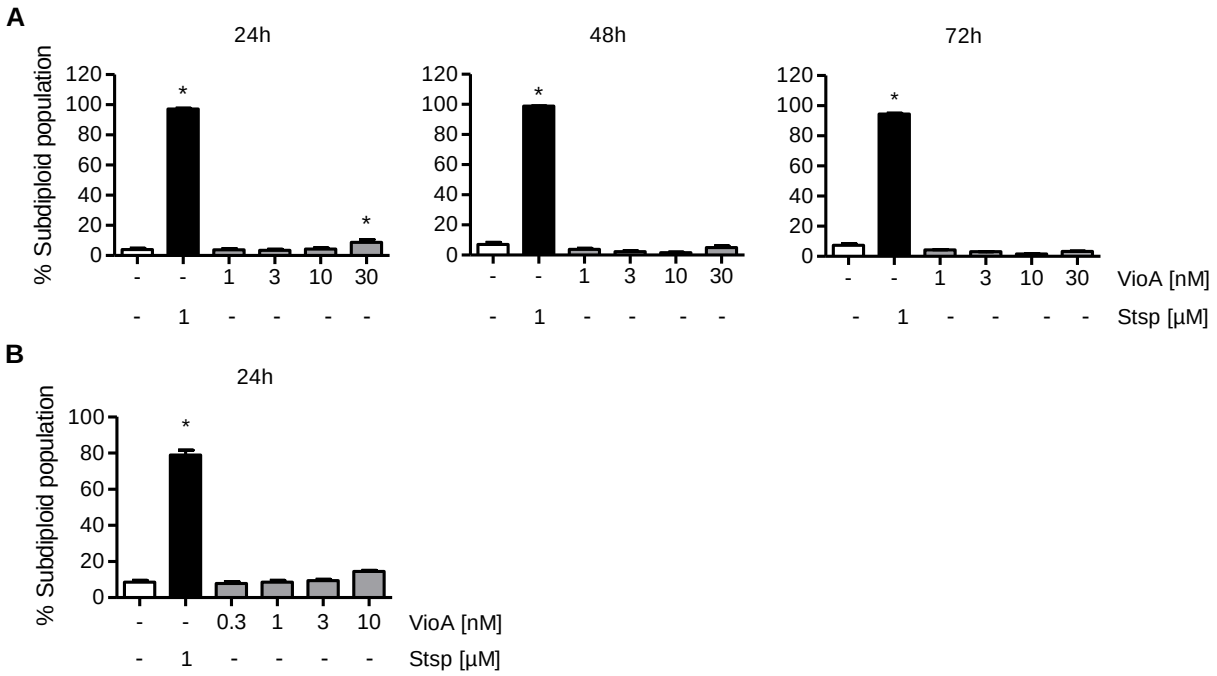

Figure 26: Apoptotic cell death of HUVECs is not increased by vioprolide A up to 10 nM. A Confluent HUVECs were treated with vioA (1, 3, 10, 30 nM) for 24 h, 48 h and 72 h. **B** 1.1 x 10^5 HUVECs were grown for 24 h and treated with vioprolide A (0.3, 1, 3, 10 nM) for 24 h. **A**-**B** Staursporine (1 µM) served as positive control for inducing apoptosis. HUVECs were stained with propidium iodide (PI) and late apoptosis was measured by analysing the percentage of sub-diploid events via flow cytometry. VioA, vioprolide A; Stsp, staurosporine. Data are expressed as mean ± SEM. n=3. *p ≤ 0.05 vs. control.

2.3 The membrane integrity of HUVECs is not influenced by vioprolide A up to 10 nM

The release of lactate dehydrogenase (LDH) indicates a defective cell membrane, which is often connected to cell death. To investigate the influence on the membrane integrity, LDH in the culture supernatant was measured using the CytoTox® 96 Non-Radioactive Cytotoxicity Assay. Therefore, confluent HUVECs were treated with vioprolide A for 24 h, 48 h and 72 h. As shown in Figure 27, treatment with concentrations of maximum 10 nM of vioprolide A did not affect the LDH release of HUVECs up to 72 h compared to the treatment with lysis buffer, which served as positive control to damage cell membrane integrity. Only after 24 h, treatment with 30 nM of vioprolide A evoked a very slight but significant increase in the LDH release.

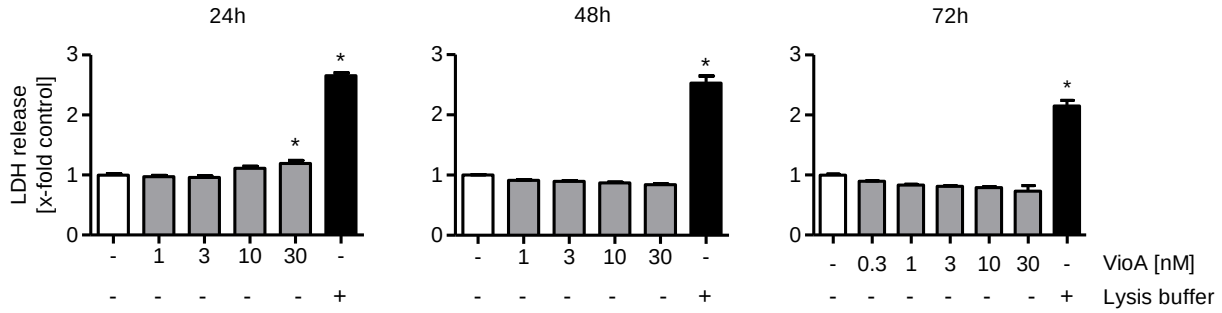

Figure 27: Concentrations below 30 nM of vioprolide A do not impair the membrane integrity of HUVECs. Confluent HUVECs were treated with vioprolide A (0.3, 1, 3, 10, 30 nM) for 24 h, 48 h and 72 h. Lysis buffer was used as positive control to damage cell membrane integrity. Lactate dehydrogenase (LDH) release was determined using the CytoTox® 96 Non-Radioactive Cytotoxicity Assay and absorbance was measured at 490 nm. VioA, vioprolide A; LDH, lactate dehydrogenase. Data are expressed as mean ± SEM. n=3. *p ≤ 0.05 vs. control.

2.4 Intracellular ATP levels of HUVECs are increased by vioprolide A up to 10 nM

Adenosine triphosphate (ATP) constitutes the energy source of living cells and is involved in crucial cellular biochemical reactions. Upon cell death, cells are not able to synthesize new ATP and the existing ATP is quickly degraded. Thus, intracellular ATP serves as marker for viable cells. To investigate the influence of vioprolide A on intracellular ATP levels, the CellTiter-Glo® Cell Viability Assay was used. Confluent HUVECs were treated with vioprolide A for 24 h and 48 h. Surprisingly, increasing concentrations of vioprolide A augmented the intracellular amount of ATP in HUVECs (Figure 28).

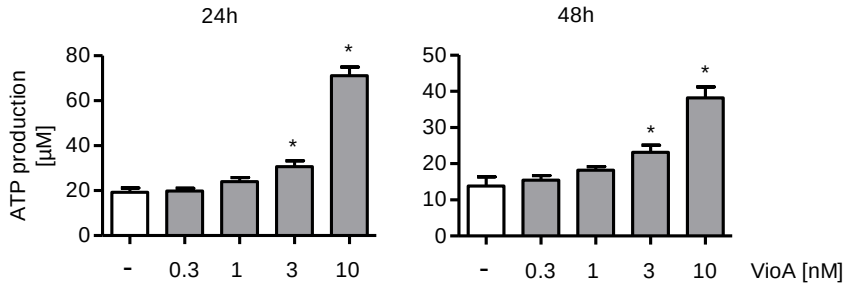

Figure 28: Vioprolide A concentration-dependently increases the amount of intracellular ATP in HUVECs. Confluent HUVECs were treated with vioprolide A (0.3, 1, 3, 10 nM) for 24 h and 48 h. The amount of intracellular ATP was determined by using the CellTiter-Glo® Cell Viability Assay. Luminescence measurement was performed with an integration time of 1 s per sample. The ATP concentrations of the samples were determined based on nonlinear regression of the ATP standard curve. VioA, vioprolide A; ATP, adenosine triphosphate. Data are expressed as mean ± SEM. n=3. *p ≤ 0.05 vs. control.

In summary, concentrations up to 10 nM of vioprolide A did not impair the cell viability of HUVECs up to 72 h. Therefore, all following *in vitro* experiments in endothelial cells were performed with 10 nM of vioprolide A being the highest applied concentration.

3. Investigations on the cellular target of vioprolide A

3.1 Vioprolide A targets the nucleolar protein NOP14 in HUVECs

To verify the interaction between vioprolide A and NOP14 in HUVECs, a cellular thermal shift assay (CETSA) was performed. In this assay, cells are exposed to increasing temperatures followed by the assessment of thermal denaturation and, thus, stability of the protein of interest (NOP14). After cell lysis, the denatured and, thus, aggregated protein fraction is removed from the samples and the stable, native protein fraction in the supernatant is examined.[427] The aggregation temperature (T_{agg}) curves of untreated and vioprolide A (300 nM, 1 h)-treated HUVECs revealed a shift of the NOP14 protein stability upon vioprolide A treatment from 46.1 °C to 48.2 °C, thus underlining an interaction between the natural product and NOP14 in HUVECs (Figure 29A). Interestingly, although NOP14 physiologically constitutes a nucleolar protein, treatment with vioprolide A led to a time-dependent increase of the NOP14 protein level both in the cytosolic and nuclear fraction of HUVECs over a total period of 48 h (Figure **29**B). Especially in the cytosolic fraction, which only contained a low basal amount of NOP14, the vioprolide A-induced increase of NOP14 was strongly observable.

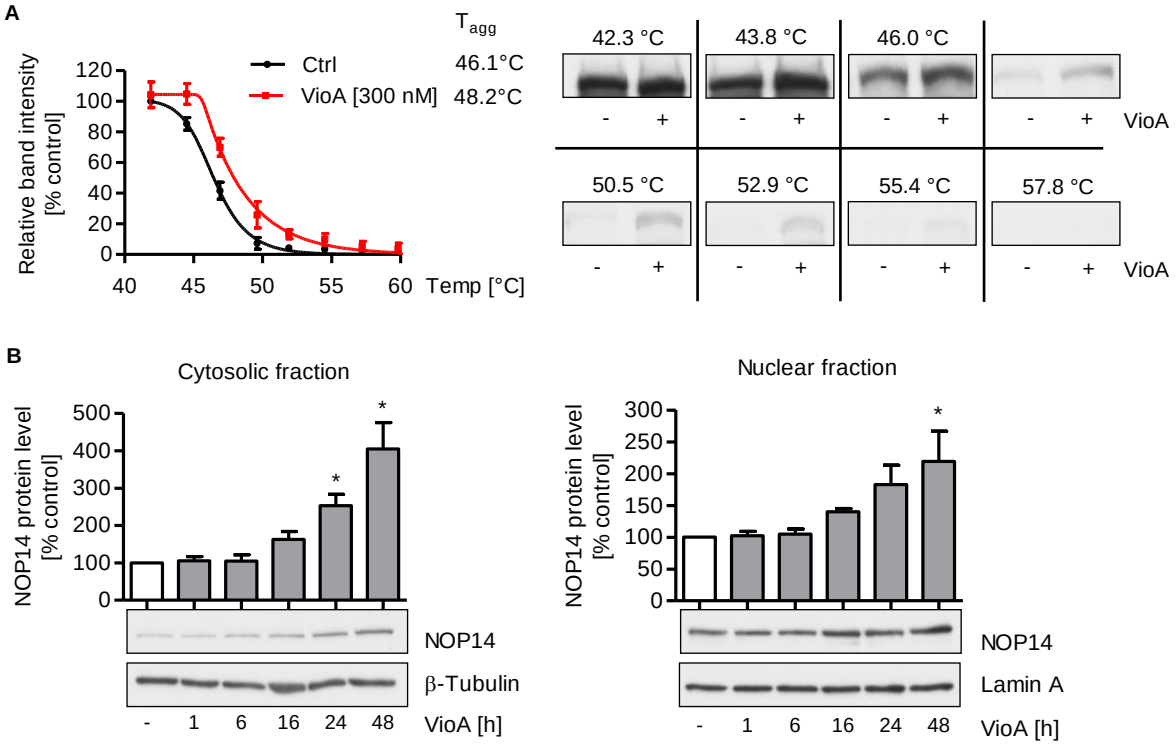

Figure 29: Vioprolide A interacts with NOP14 in HUVECs. A Confluent HUVECs were treated with 300 nM vioprolide A for 1 h or left untreated. Cells were treated with increasing temperatures between 42.3-57.8 °C and lysed by repeated freeze-thaw cycles in liquid nitrogen. Thermal aggregation curves of NOP14 were analysed by western blotting. One representative blot is shown. **B** Confluent HUVECs were treated with 10 nM of vioprolide A for the indicated time points. Cell fractionation was performed, and the NOP14 protein level in the cytosolic and nuclear fraction was determined by western blot. One representative blot is shown. VioA, vioprolide A, Ctrl, control; T_{agg}, aggregation temperature. Data are expressed as mean ± SEM. n=4. *p ≤ 0.05 vs. control.

3.2 The *de novo* protein synthesis in HUVECs is lower upon vioprolide A treatment

Since NOP14, the cellular target of NOP14, is involved in ribosome biogenesis, which is connected to cellular protein biosynthesis, we hypothesized that vioprolide A might impair *de novo* protein synthesis in HUVECs. Hence, the formation of newly synthesized polypeptide chains in HUVECs upon vioprolide A treatment was analysed using a protein synthesis assay. Therefore, confluent cells were either treated with increasing concentrations of vioprolide A for 16 h or with 10 nM of vioprolide A for a total of 48 h. The protein synthesis inhibitor cycloheximide served as positive control. As shown in Figure 30A-B, vioprolide A concentration- and time-dependently decreased the de novo protein synthesis in HUVECs. A maximum inhibitory effect was observed after vioprolide A treatment (10 nM) for 16 h, which was equally strong compared to the treatment with cycloheximide (10 µg/ml) for 24 h. After 24 h, a slight increase in protein synthesis was observed compared to 16 h vioprolide A treatment. To determine if this increase represented a recovery of the cells from the protein synthesis inhibition, HUVECs were treated repetitively each 12 h with vioprolide A for a total period of 48 h. While only a slight reduction of the protein synthesis (to approx. 85 %) was detectable with single treatment for 48 h, repetitive treatment with vioprolide A each 12 h for 48 h significantly lowered the de novo protein synthesis to approx. 50 % (Figure 30C). Concentration-response curves further indicated equally potent inhibitory effects of 10 nM of vioprolide A and 3 µg/ml CHX after 16 h on protein biosynthesis in HUVECs (Figure 30D). In summary, vioprolide A inhibited protein biosynthesis in HUVECs, which is most likely attributed to the interaction with the nucleolar protein NOP14.

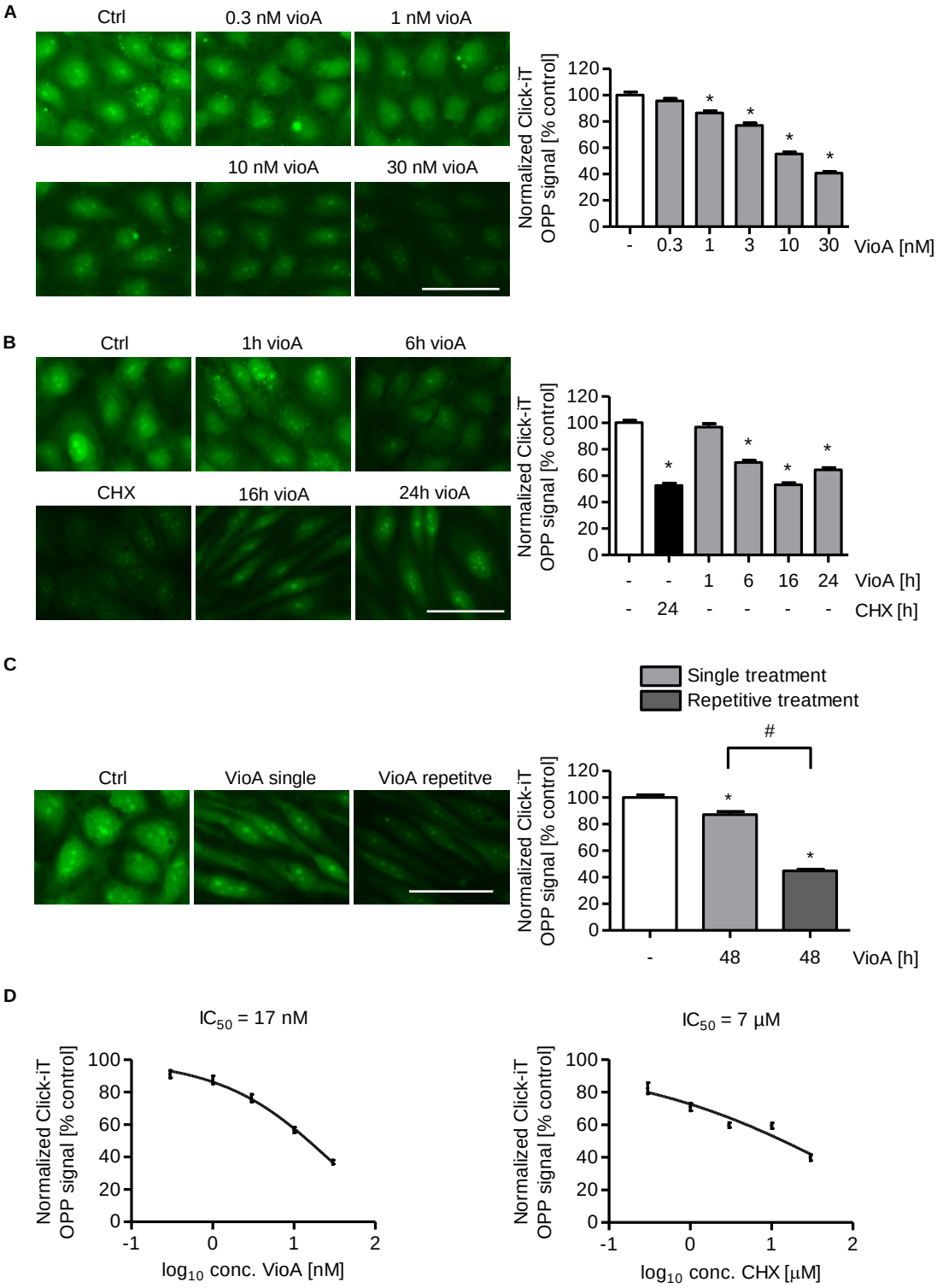

Figure 30: Vioprolide A inhibits *de novo* protein synthesis in HUVECs. A Confluent HUVECs were treated with vioprolide A (0.3, 1, 3, 10, 30 nM) for 16 h. **B** Confluent HUVECs were treated with vioprolide A (10 nM) for 1 h, 6 h, 16 h and 24 h. Cycloheximide treatment (10 µg/ml) for 24 h served as positive control. **C** Confluent HUVECs were treated with 10 nM of vioprolide A for a total of 48 h either as single treatment or repetitive treatment each 12 h. **A-C** Nascent polypeptide chains were visualized by immunocytochemistry using Click-iT® Plus OPP Alexa Fluor 488 and fluorescence microscopy. Representative images are shown. Scale bar, 50 µm. **D** Confluent HUVECs were treated with vioprolide A (0.3, 1, 3, 10, 30 nM) or cycloheximide (0.3, 1, 3, 10, 30 nM) for 16 h. The IC_{50} was determined by analysing nascent polypeptide chains by immunocytochemistry using Click-iT® Plus OPP Alexa Fluor 488 and fluorescence microscopy. Three independent experiments were used to calculate the respective IC_{50} of protein synthesis inhibition of vioprolide A and cycloheximide in HUVECs. VioA, vioprolide A; CHX, cycloheximide. Data are expressed as mean ± SEM. n=3. *p ≤ 0.05 vs. control.

4. The influence of vioprolide A on inflammatory processes in endothelial cells *in vitro*

4.1 The effect of vioprolide A on the leukocyte-endothelial cell interaction

The leukocyte-endothelial cell interaction was examined *in vitro* by focusing on the leukocyte adhesion to and transmigration through a TNF-activated monolayer of HUVECs. Importantly, only endothelial cells but not leukocytes were treated with vioprolide A to focus exclusively on the actions of the natural product on endothelial cells.

4.1.1 Vioprolide A lowers the leukocyte adhesion to an endothelial monolayer

Cell adhesion assays with different types of leukocytes were used to investigate a general of specific effect of vioprolide A on the adhesion of leukocytes to an endothelial monlayer. Therefore, HUVECs were treated with increasing concentrations of vioprolide A (0.3–10 nM) for 16 h and subsequently activated with the cytokine TNF for 6 h. Vioprolide A pretreatment significantly reduced the adhesion of all leukocyte cell types compared to TNF treatment alone (Figure 31A-D). The observed inhibition of leukocyte cell adhesion was concentration-dependent with the highest effect observed for 10 nM of vioprolide A.

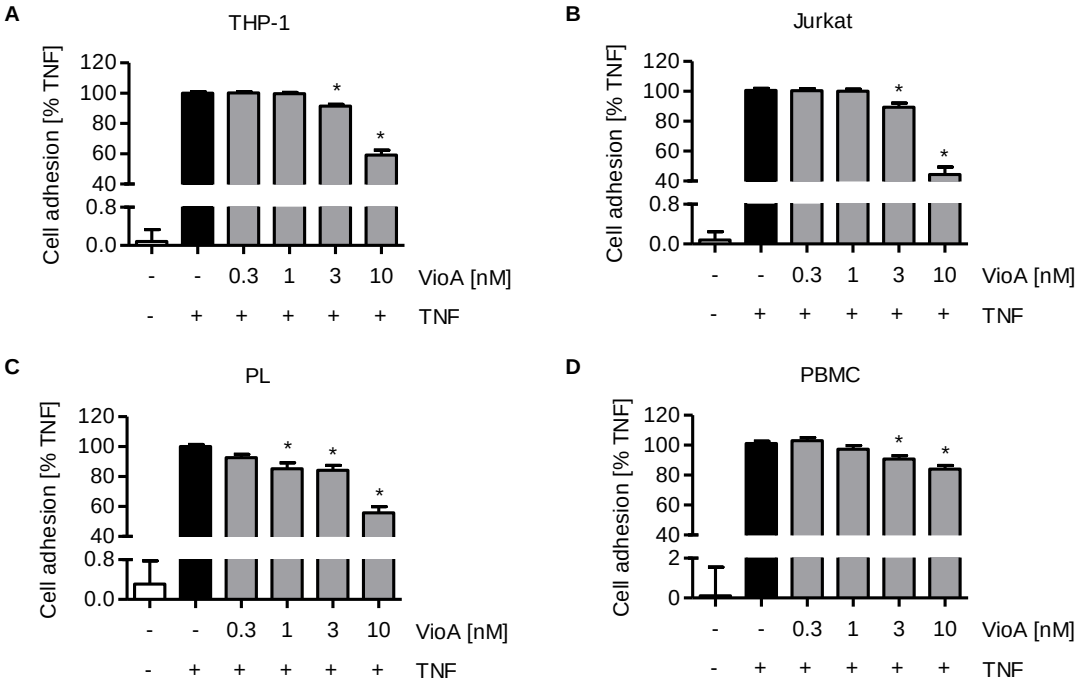

Figure 31: Vioprolide A lowers the leukocyte cell adhesion to a HUVEC monolayer. A-D Confluent HUVECs were treated with vioprolide A (0.3, 1, 3, 10 nM) for 16 h followed by activation with 10 ng/ml TNF for 6 h. Fluorescently labeled THP-1 cells (**A**), Jurkat cells (**B**), primary lymphocytes (PL, **C**) and primary blood mononuclear cells (PBMC, **D**) were allowed to adhere for 5 min (**A**, **B**) or 10 min (**C**, **D**). The relative amount of adhered leukocytes was analysed by fluorescence measurement. VioA, Vioprolide A; PL, primary lymphocyte; PBMC, primary blood mononuclear cell. Data are expressed as mean ± SEM. n=5 (**A**, **C**, **D**), n=6 (**B**). *p ≤ 0.05 vs. TNF control.

4.1.2 The transmigration of leukocytes through an endothelial monolayer is decreased by vioprolide A

To investigate the influence of vioprolide A on the transmigration of leukocytes through the endothelial monolayer, transmigration assays with SDF-1 as chemoattractant were performed. Consistent with the reduction of leukocyte cell adhesion, pretreatment with 10 nM of vioprolide A for 16 h significantly decreased the leukocyte transmigration through a TNF-activated endothelial monolayer towards an SDF-1 gradient (Figure 32).

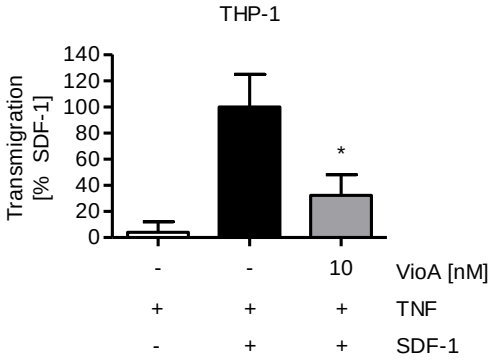

Figure 32: Vioprolide A decreases the leukocyte transmigration through a HUVEC monolayer. HUVECs were grown on a porous membrane of a Transwell insert (pore size 5 µm), treated with 10 nM of vioprolide A for 16 h and activated with 10 ng/ml TNF for 6 h. 500 ng/ml SDF-1 (CXCL12) was added to the lower compartment of the Transwell system as chemoattractant. Fluorescence-labeled THP-1 cells were added to the upper compartment of the Transwell system and allowed to transmigrate through the HUVEC monolayer for 2 h. The relative amount of transmigrated THP-1 cells was determined by fluorescence measurement. VioA, vioprolide A. Data are expressed as mean ± SEM. n=3. *p ≤ 0.05 vs. SDF-1 control.

Taken together, we showed that the treatment of endothelial cells with vioprolide A caused a significant reduction of TNF-induced leukocyte-endothelial cell interactions, including the leukocyte adhesion to and transmigration through an endothelial monolayer *in vitro*.

4.2 The effect of vioprolide A on endothelial cell adhesion molecules

Cell adhesion molecules (CAMs) play a crucial role in mediating leukocyte-endothelial cell interactions. While E-selectin is involved in the rolling motion of leukocytes on the endothelial surface, ICAM-1 and VCAM-1 mediate the firm adhesion of the leukocytes to the endothelium.[49,58,61] Based on the observed reduction of leukocyte adhesion to and transmigration through TNF-activated HUVECs, the influence of vioprolide A on the expression level of the endothelial CAMs was analysed in a next step.

4.2.1 Vioprolide A reduces the TNF-induced cell surface expression of endothelial cell adhesion molecules

The cell surface protein levels of ICAM-1, VCAM-1 and E-selectin on TNF-activated HUVECs with or without vioprolide A pretreatment for 16 h was monitored via flow cytometry. The cell surface protein levels were significantly downregulated, when HUVECs were pretreated with vioprolide A for 16 h prior to activation with TNF for 4 h (E-selectin) or 6 h (ICAM-1, VCAM-1) (Figure 33). The observed reduction was concentration-dependent, and the cell surface expression of all CAMs was almost completely inhibited at the highest vioprolide A concentration applied (10 nM).

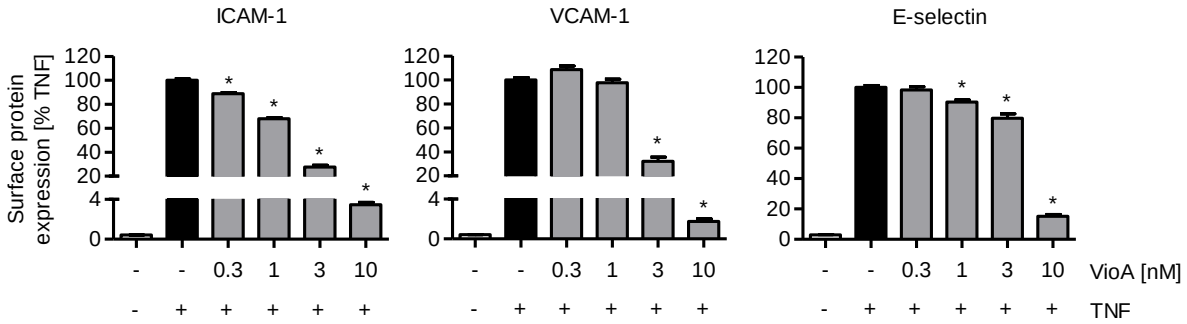

Figure 33: Vioprolide A reduces ICAM-1, VCAM-1 and E-selectin cell surface expression on HUVECs. Confluent HUVECs were treated with vioprolide A (0.3, 1, 3, 10 nM) for 16 h followed by activation with 10 ng/ml TNF for 4 h (E-selectin) or 6 h (ICAM-1, VCAM-1). Cell surface protein expression was measured by flow cytometry. VioA, vioprolide A. Data are expressed as mean ± SEM. n=3. *p ≤ 0.05 vs. TNF control.

4.2.2 The TNF-induced total protein expression of cell adhesion molecules is inhibited by vioprolide A

To further differentiate if vioprolide A specifically impairs the trafficking of CAMs to the cell surface or rather exerts a general effect on the overall protein expression of CAMs, the total protein level of ICAM-1, VCAM-1 and E-selectin was analyzed. For this purpose, confluent cells were pretreated with vioprolide A (0.3–10 nM) for 16 h and activated with TNF for 4 h (E-selectin) or 6 h (ICAM-1, VCAM-1). The total protein level of all three CAMs was determined by western blot experiments. In accordance with the results obtained for the cell surface expression of CAMs, the total protein levels of ICAM-1, VCAM-1 and E-selectin were significantly reduced when HUVECs were pretreated with vioprolide A (Figure 34). Again, the observed effects were concentration-dependent, and a complete inhibition of the protein expression was observed at the highest concentration of vioprolide A (10 nM).

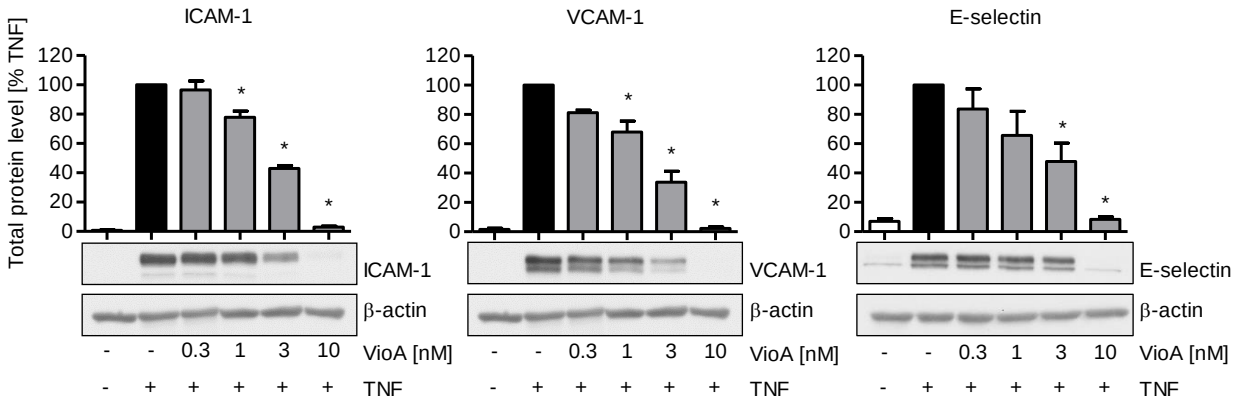

Figure 34: Vioprolide A reduces ICAM-1, VCAM-1 and E-selectin total protein levels in HUVECs. Confluent HUVECs were treated with vioprolide A (0.3, 1, 3, 10 nM) for 16 h followed by activation with 10 ng/ml TNF for 4 h (E-selectin) or 6 h (ICAM-1, VCAM-1). Total protein expressions of ICAM-1 (left), VCAM-1 (middle) and E-selectin (right) were detected by western blotting. One representative blot is shown. VioA, vioprolide A. Data are expressed as mean ± SEM. n=3. *p ≤ 0.05 vs. TNF control.

4.2.3 Vioprolide A decreases the TNF-induced mRNA expression of cell adhesion molecules

Vioprolide A impairs *de novo* protein synthesis. To further understand if vioprolide A reduces CAM protein levels only by inhibiting the translation of respective mRNAs into protein or rather by influencing their TNF-dependent gene expression, CAM mRNA expression was analysed by quantitative PCR. Considering, that it takes time to translate mRNA into protein, TNF activation periods were set shorter for analysing the mRNA expressions compared to the total protein levels. As shown in Figure 35A, pretreatment with vioprolide A (0.3, 1, 3, 10 nM) for 16 h decreased the TNF-induced mRNA expression of *ICAM1* and *VCAM1* after 4 h and of *SELE* after 2 h in HUVECs compared to TNF treatment alone. However, in contrast to the complete inhibition of the total protein expression by 10 nM of vioprolide A, no complete downregulation of the CAM mRNA expressions was observed. Similar effects on the mRNA expression of CAMs in HUVECs was also observed after 16 h of vioprolide A pretreatment followed by 4 h (*SELE*) and 6 h (*ICAM1*, *VCAM1*) of TNF activation (Figure 35B). Interestingly, unlike vioprolide A, pretreatment with the known protein synthesis inhibitor cycloheximide (3 µg/ml, 16 h) evoked an increase rather than decrease of *ICAM1* and *SELE* mRNA levels (Figure 35C). Solely the mRNA expression of *VCAM1* was significantly reduced upon cycloheximide pretreatment. In total, it could be demonstrated that the action of vioprolide A observed on the leukocyte-endothelial cell interaction is likely to be caused through impairment of CAMs in HUVECs. The reduced protein expression of CAMs, however, can only in part be attributed to a reduced TNF-induced mRNA expression.

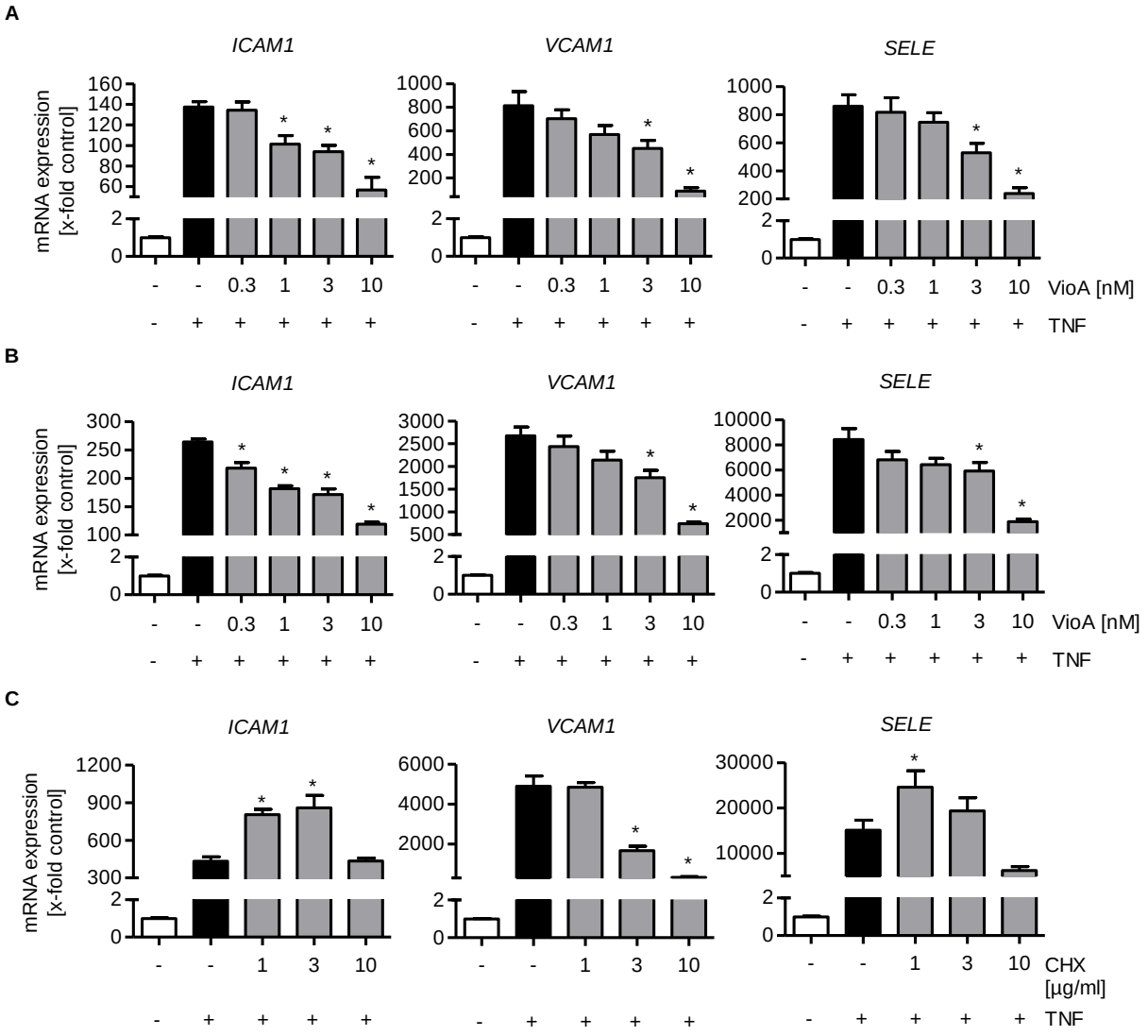

Figure 35: Vioprolide A decreases the *ICAM1*, *VCAM1* and *SELE* mRNA expression in HUVECs. Confluent HUVECs were treated with vioprolide A (0.3, 1, 3, 10 nM) for 16 h. **A** Cells were activated with 10 ng/ml TNF for 2 h (*SELE*) or 4 h (*ICAM1*, *VCAM1*). **B** Cells were activated with 10ng/ml TNF for 4 h (*SELE*) or 6 h (*ICAM1*, *VCAM1*). **C** Confluent HUVECs were treated with cycloheximide (1, 3, 10 µg/ml) for 16 h followed by activation with 10 ng/ml TNF for 2 h (*SELE*) or 4 h (*ICAM1*, *VCAM1*). A-C The mRNA expression of ICAM1, VCAM1 and SELE was analysed by quantitative PCR. VioA, vioprolide A; CHX, cycloheximide. Data are expressed as mean ± SEM. n=3 (**A**, **B** *SELE*, **C**), n=4 (**B** *ICAM1*, **B** *VCAM1*). *p ≤ 0.05 vs. TNF control.

5. The mechanism underlying the effects of vioprolide A on inflammatory processes in endothelial cells

The results shown in section V.1-4 clearly demonstrate that vioprolide A inhibits inflammatory processes *in vivo* and in endothelial cells *in vitro*. Consequently, the next aim was to elucidate the underlying anti-inflammatory cellular mode of action of vioprolide A.

5.1 Vioprolide A influences the TNF receptor 1 protein expression

Different natural inhibitors of mRNA translation, including the plant alkaloid narciclasine and the bacteria-derived cytotrienin A, exert their anti-inflammatory actions through influencing the TNF receptor 1 (TNFR1).[428, 429] The TNFR1 is the most important receptor in TNF-mediated inflammatory signaling in endothelial cells, and its activation causes the induction of the downstream NF-κB signaling cascade. Since vioprolide A was already shown to reduce the general *de novo* protein synthesis (see V.3.2) as well as the total protein level of cell adhesion molecules (see V.4.2.2), also the total protein level of the TNFR1 was investigated upon vioprolide A treatment over a period of 48 h. As demonstrated in Figure 36A, vioprolide A (10 nM) evoked a strong, time-dependent influence on the TNFR1 protein level with a maximum inhibitory effect after 16 h. After 24 h to 48 h, the protein level of the TNFR1 recovered again. These results are in line with the effect on general *de novo* protein synthesis. At the same time, the *TNFRSF1A* mRNA expression in HUVECs was upregulated by vioprolide A (Figure 36B), underlining that the effect on the TNFR1 protein level is attributed to an influence on mRNA translation rather than mRNA expression. To obtain more detailed information regarding the turnover and recovery of the TNFR1, the well-known protein synthesis inhibitor cycloheximide was used. Western blot analysis revealed a short half-live of the protein of approximately 30 min and cycloheximide treatment of up to 72 h completely inhibited the TNFR1 protein expression (Figure 36C). By contrast, the TNFR1 protein level recovered after vioprolide A treatment for 24 h or longer. Importantly, however, the TNFR1 protein level did not recover after repetitive treatment with vioprolide A each 12 h for a total period of 48 h (Figure 36D). These observations indicate that the TNFR1 has, on the one hand, a short half-live and is, on the other hand, quickly resynthesized when protein synthesis inhibition is relieved.

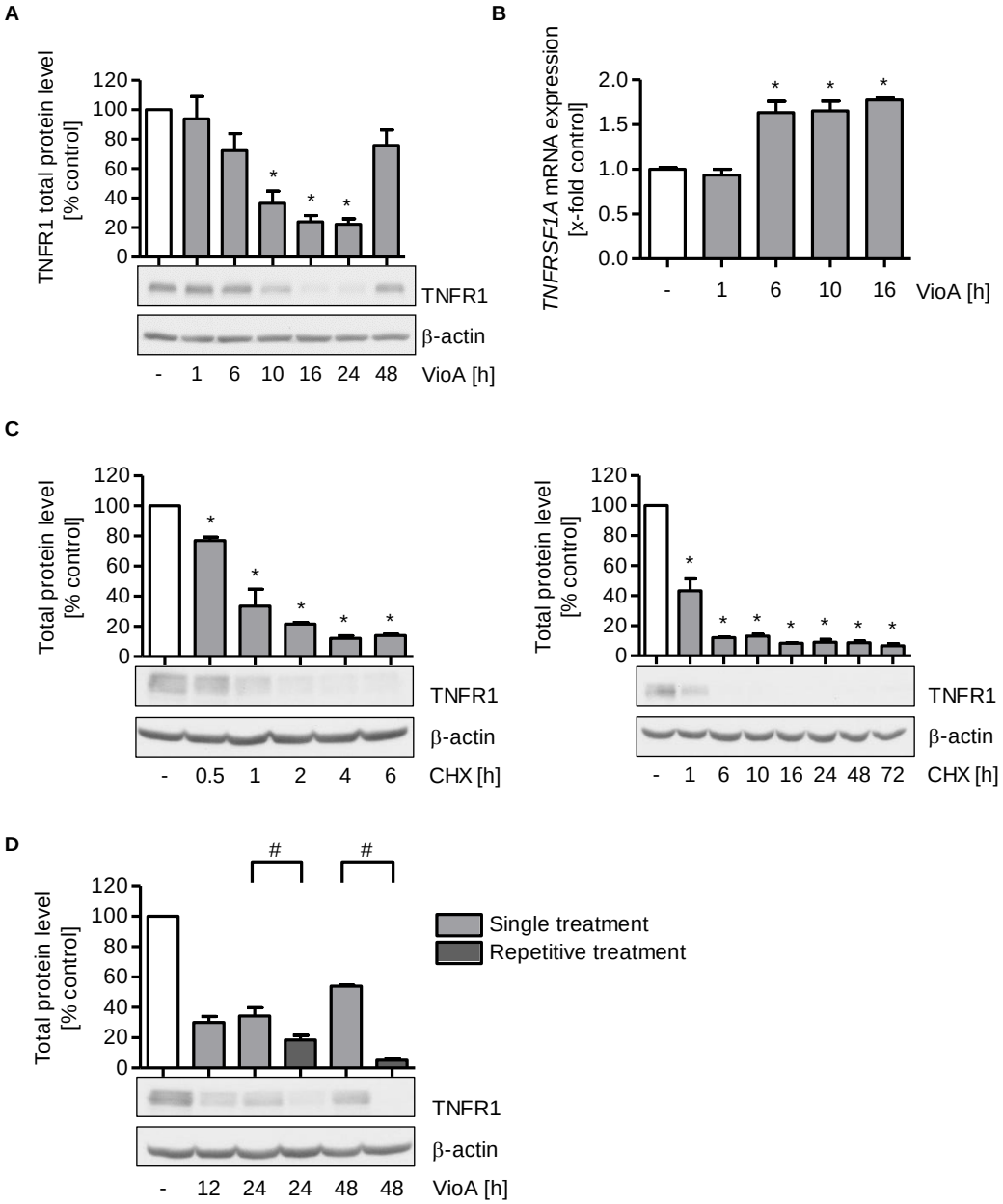

Figure 36: Vioprolide A downregulates the TNFR1 protein expression in HUVECs. A-**B** Confluent HUVECs were treated with 10 nM of vioprolide A as indicated. **A** Total protein level of the TNFR1 was determined by western blot analysis. One representative blot is shown. **B** Total mRNA expression of TNFRSF1A was detected by quantitative PCR. **C** Confluent HUVECs were treated with 3 µg/ml of cycloheximide for 0.5 h to 6 h (left) or 1 h to 72 h (right). Total protein level of the TNFR1 was analysed by western blotting. One representative blot is shown. **D** Confluent HUVECs were treated with 10 nM of vioprolide A either as single treatment or repetitive treatment each 12 h. Total protein level of the TNFR1 was detected by western blot analysis. One representative blot is shown. VioA, vioprolide A; CHX, cycloheximide. Data are expressed as mean ± SEM. n=3. *p ≤ 0.05 vs. control, #p ≤ 0.05 vs single treatment.

5.2 The effect of vioprolide A on important proteins of the NF-κB signaling pathway

Activation of the TNFR1 by TNF initiates the NF-κB signaling pathway and ultimately liberates the NF-κB subunits from their cytosolic retention. Hence, NF-κB subunits translocate to the nucleus, where they regulate the expression of important inflammatory genes, including the

cell adhesion molecules.[94] To further assess the role of the reduced TNFR1 protein level in the actions of vioprolide A, the NF-κB signaling pathway was analysed.

5.2.1 Vioprolide A lowers the activation of the kinases TAK1 and IKK

TAK1 and IKK are indispensable signaling intermediates in the NF-κB pathway. Their successive activation results in the phosphorylation and subsequent degradation of the inhibitory protein IκBα, which retains the NF-κB subunits in the cytosol.[90-92] To investigate the influence of vioprolide A on both kinases, their TNF-induced phosphorylation was analysed by western blot analysis. As shown in Figure 37A-B, pretreatment with 10 nM of vioprolide A for 16 h resulted in a significant decrease of the TNF-induced (5–60 min) phosphorylation of TAK1 and IKK. Interestingly, while vioprolide A strongly decreased the activation of IKK after only 5 min of TNF treatment, no effect on the phosphorylation of TAK1 after 5 min of TNF treatment was observable, yet, although TAK1 lies upstream of IKK.

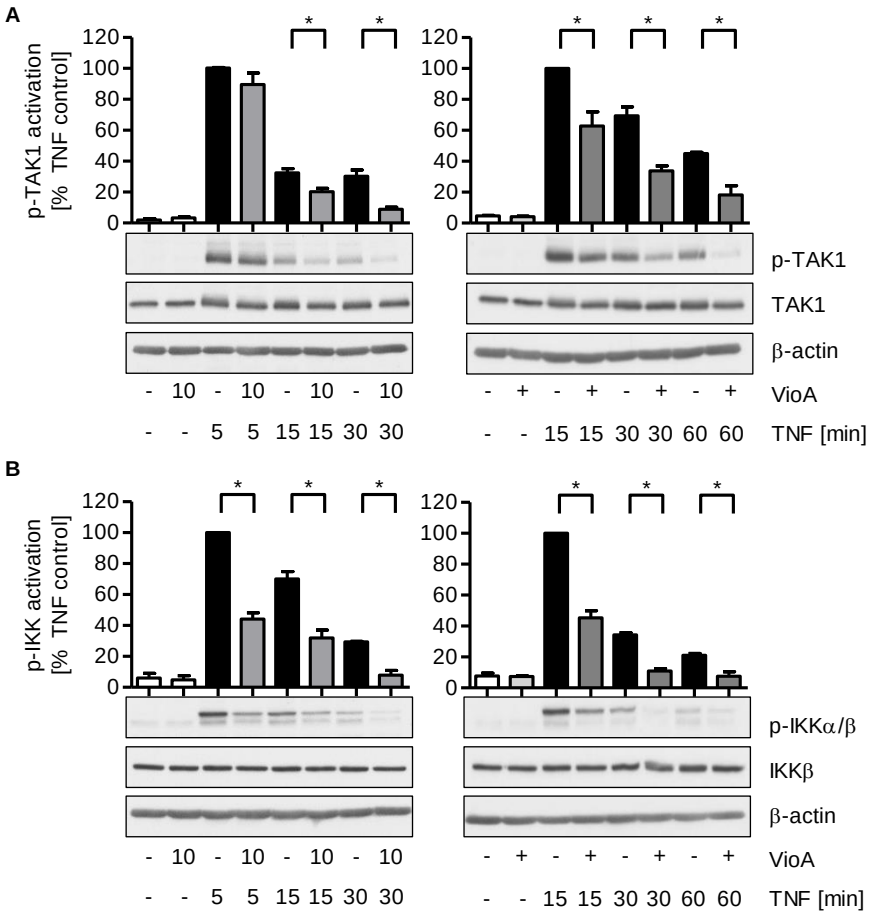

Figure 37: Vioprolide A reduces the activation of the kinases TAK1 and IKK. A-B Confluent HUVECs were treated with 10 nM of vioprolide A for 16 h followed by activation with 10 ng/ml TNF for 5 min, 15 min and 30 min (left) or 15 min, 30 min and 60 min (right). Total protein expression of phospho-TAK1 (p-TAK1, A) and phospho-IKKα/β (p-IKKα/β, B) was analysed by western blotting. One representative blot is shown. VioA, vioprolide A. Data are expressed as mean ± SEM. n=3. *p ≤ 0.05 vs. TNF control.

5.2.2 Vioprolide A does not resuce IκBα from phosphorylation and degradation

Based on the effects observed on the activation of TAK1 and IKK, further investigations on the activation and general protein level of IκBα were performed. IκBα is important for masking the NLS of NF-κB subunits and retaining them in the cytosol.[91,92] Western blot experiments revealed that pretreatment with 10 nM of vioprolide A for 16 h enhanced the reduction of the IκBα protein levels, which was triggered by TNF treatment for 15 min, 30 min and 60 min (Figure 38A). In addition, the relative amount of IκBα phosphoprotein in TNF-activated HUVECs was decreased upon vioprolide A pretreatment (10 nM) for 16 h (Figure 38B).

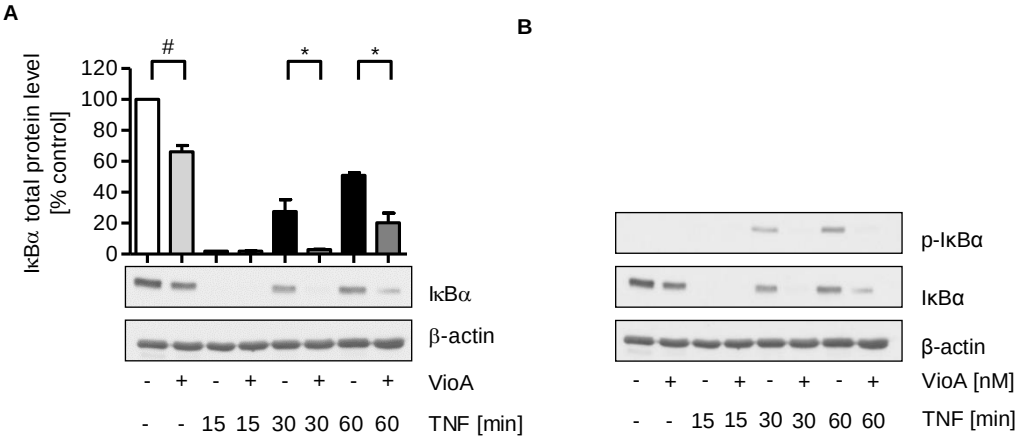

Figure 38: Vioprolide A does not rescue IκBα from TNF-induced degradation. A-**B** Confluent HUVECs were treated with 10 nM of vioprolide A for 16 h followed by activation with 10 ng/ml TNF for 15 min, 30 min and 60 min. The total protein level of IκBα (**A**) and phospho-IκBα (p-IκBα, **B**) was determined by western blotting. One representative blot is shown. VioA, vioprolide A. Data are expressed as mean ± SEM. n=3. *p ≤ 0.05 vs. TNF control.

5.2.3 Vioprolide A decreases the total protein level of IκBα in the absence of TNF

Based on these findings, the influence of vioprolide A alone (without TNF treatment) on the IκBα total protein level in HUVECs was assessed. As depicted in Figure 39A, the total protein level of IκBα was time-dependently lowered upon vioprolide A (10 nM) treatment. Compared to the rapid decrease of the TNFR1 protein level (see V.5.1), however, the IκBα protein level was reduced more slowly and showed no recovery up to 48 h. At the same time, the *NFKBIA* mRNA expression was time-dependently upregulated by 10 nM of vioprolide A (Figure 39B). Investigations on the protein half-life and recovery using cycloheximide (3 µg/ml) showed a similar time-dependent influence on the IκBα protein level in HUVECs compared to vioprolide A (Figure 39C). Importantly, cycloheximide treatment up to 6 h only evoked ~ 40 % reduction of the IκBα total protein level, which underlines that the protein has a longer half-life compared to the TNFR1. Similar to the results obtained for the TNFR1, repetitive treatment with vioprolide A every 12 h for a total of 48 h decreased the IκBα protein level even stronger compared to the single treatment for 48 h (Figure 39D).

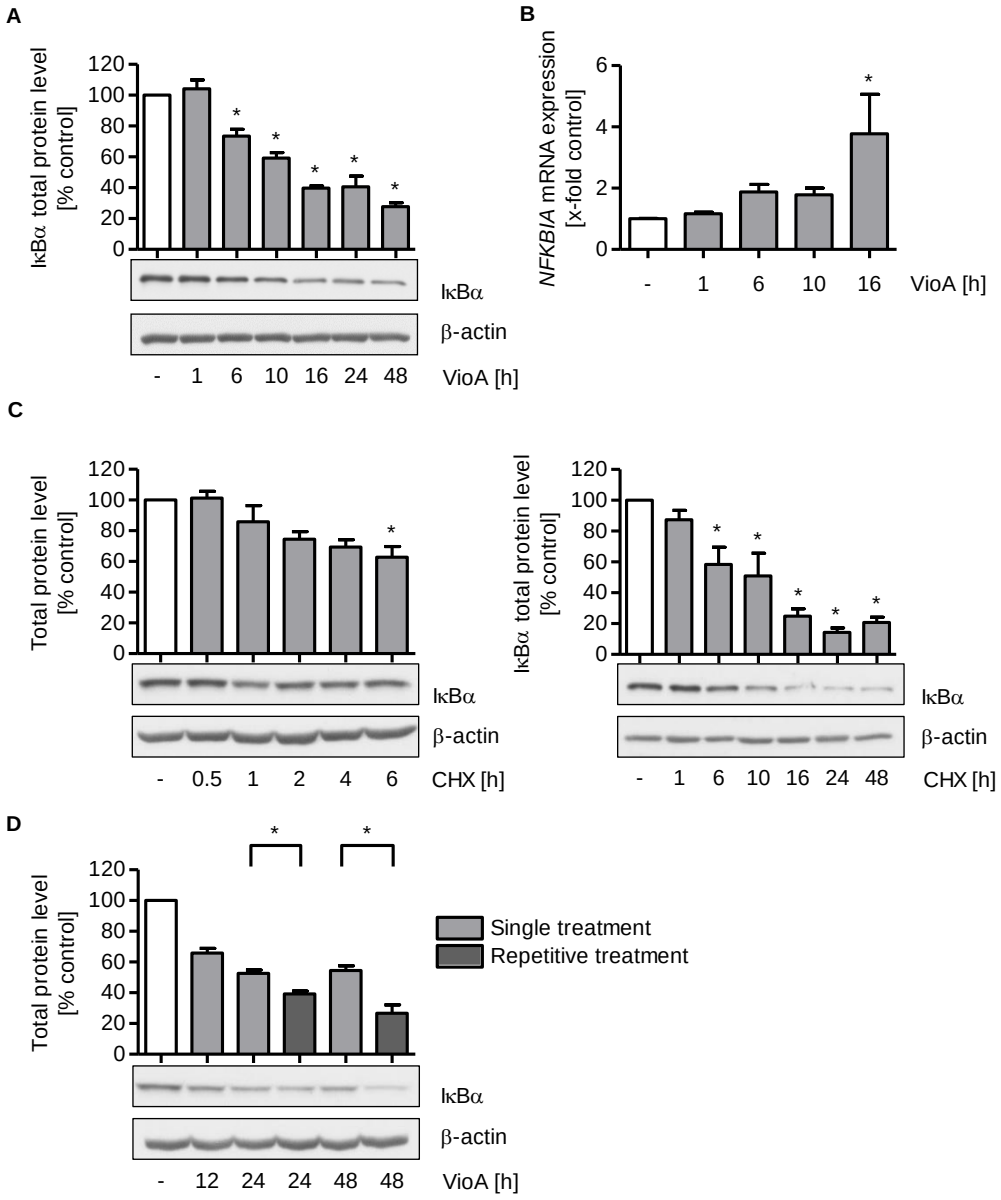

Figure 39: Vioprolide A reduces the IκBα total protein level in the absence of TNF. A Confluent HUVECs were treated with 10 nM of vioprolide A for the indicated time points. Total protein level of IκBα was determined by western blotting. One representative image is shown. **B** Confluent HUVECs were treated with 10 nM of vioprolide A for 1 h, 6 h, 10 h and 16 h. Total mRNA expression of *NFKBIA* was analysed by quantitative PCR. **C** Confluent HUVECs were treated with 3 µg/ml cycloheximide for 0.5 h - 6 h (left) or 1 h - 48 h (right). Total protein level of IκBα was determined by western blot analysis. One representative image is shown. **D** Confluent HUVECs were treated with 10 nM of vioprolide A either as single treatment or repetitive treatment each 12 h. Total protein level of IκBα was detected by western blot experiments. One representative blot is shown. VioA, vioprolide A; CHX, cycloheximide. Data are expressed as mean ± SEM. n=3. *p ≤ 0.05 vs. control (A-**C**) or single treatment (**D**).

Taken together, vioprolide A reduced the TNFR1 protein level and decreased the TNF-evoked activation of important kinases of the NF-κB signaling cascade, such as TAK1 and IKK. Still, the natural product did not rescue IκBα protein levels. In contrast, vioprolide A is likely to reduce the IκBα protein levels without TNF-activation due to its inhibitory effect on general *de novo* protein synthesis.

5.2.4 Vioprolide A does not influence the basal protein level and cellular distribution of NF-κB p65

Since vioprolide A reduced the basal IκBα protein level in HUVECs, potential effects on the NF-κB subunit p65 were examined next. For this, the total protein level and cellular distribution of p65 was determined by western blot and cell fractionation, respectively. The purity of the subcellular fractions was ensured in each individual experiment by analysis of β-tubulin and topoisomerase 1 as cytosolic and nuclear marker, respectively (Figure 40A). 10 nM of vioprolide A had no effect on the p65 total protein level in HUVECs up to 48 h, indicating a long protein half-life (Figure 40B). Despite reduced IκBα protein levels, the cellular distribution of p65 in HUVECs was not altered by vioprolide A alone without TNF activation (Figure 40C).

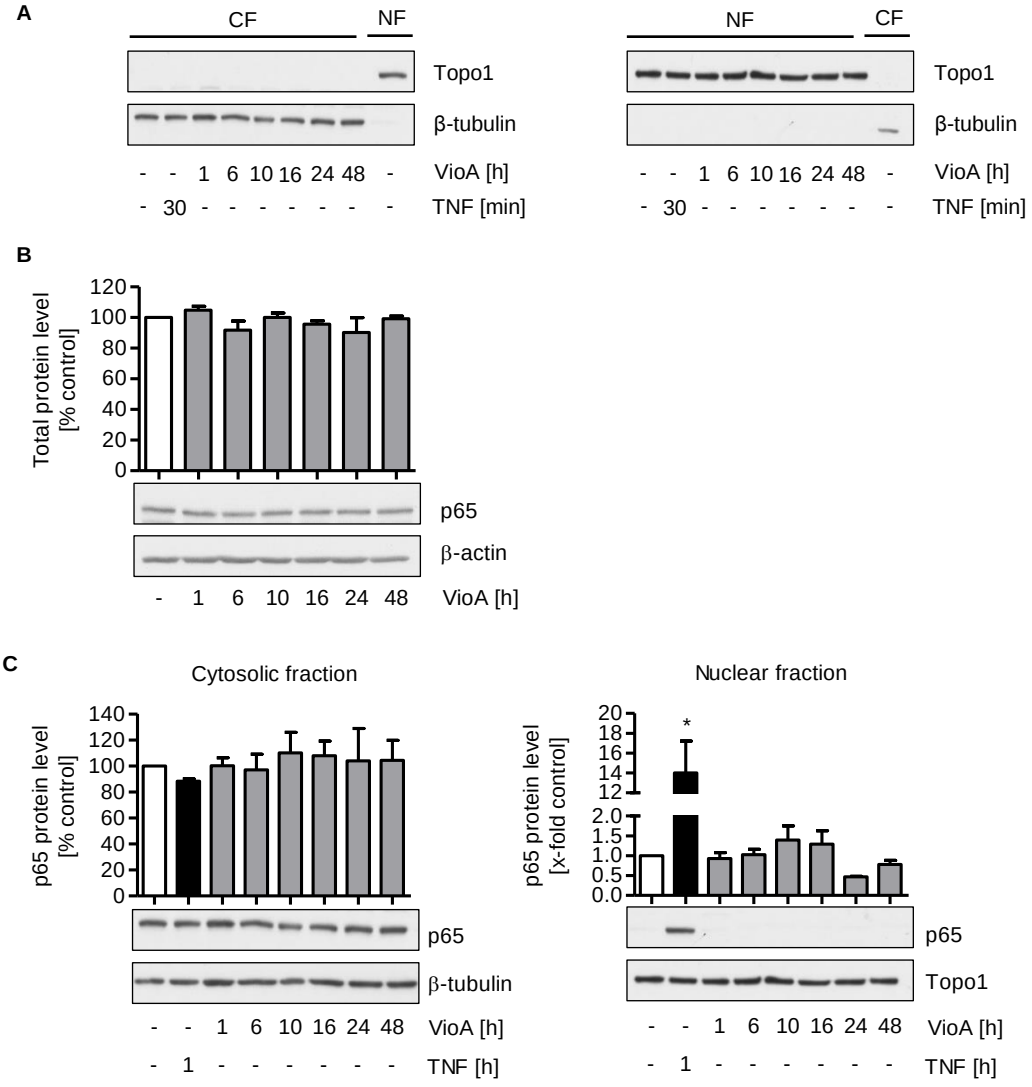

Figure 40: Vioprolide A neither influences the basal p65 protein level nor cellular distribution. A, C Confluent HUVECs were treated with vioprolide A (10 nM) or TNF (10 ng/ml) as indicated and subcellular fractions were separated. **A** Purity of the subcellular fractions was verified by β-tubulin and topoisomerase 1. One representative blot is shown. **B** Confluent HUVECs were treated with vioprolide A (10 nM) as indicated. Total protein level of p65 was determined by western blotting. One representative blot is shown. **C** Relative amounts of cytosolic (left) and nuclear (right) p65 was detected by western blotting. One representative blot is shown. VioA, vioprolide A; Topo1, topoisomerase 1; CF, cytosolic fraction; NF, nuclear fraction. Data are expressed as mean ± SEM. n=3. *p ≤ 0.05 vs. control.

5.2.5 The TNF-induced nuclear translocation of p65 is prevented by vioprolide A

Despite reduction of the IκBα total protein level, vioprolide A did not affect the basal cellular distribution of p65. Upon TNF treatment, IκBα is degraded, which leads to the exposure of the NLS of p65 and enables the translocation of the NF-κB subunit to the nucleus, where it binds to the promotor region of inflammation-related genes. [90-92,94] Hence, in the next step, the influence of vioprolide A on the TNF-induced nuclear translocation of p65 was determined using immunocytochemistry. Even after significant reduction of the IκBα total protein level, pretreatment for 16 h with 10 nM of vioprolide A still inhibited the p65 nuclear translocation upon TNF treatment for 15 min to 60 min (Figure 41A). Like vioprolide A, cyloheximide pretreatment (3 µg/ml for 16 h) significantly decreased the TNF-induced p65 nuclear translocation after 30 min despite downregulation of the IκBα total protein level (Figure 41B).

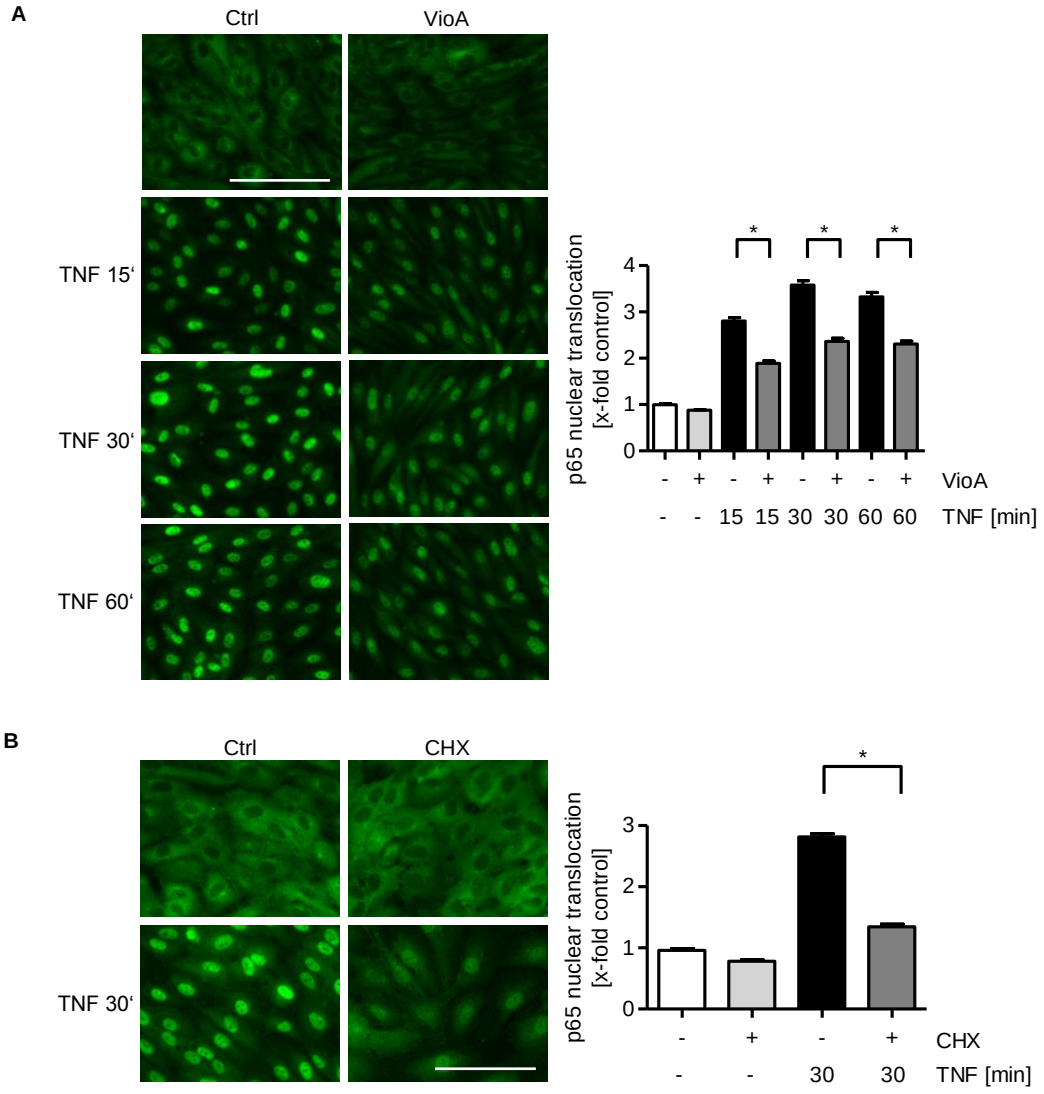

Figure 41: Vioprolide A and cycloheximide prevent p65 from TNF-induced nuclear translocation. A Confluent HUVECs were treated with 10 nM of vioprolide A for 16 h followed by activation with 10 ng/ml TNF for 15 min, 30 min and 60 min. **B** Confluent HUVECs were treated with 3 µg/ml cycloheximide for 16 h followed by activation with 10 ng/ml TNF for 30 min. **A**-**B** p65 was visualized by immunocytochemistry and fluorescence microscopy. Representative images are shown. Scale bar, 200 µm. VioA, vioprolide A; CHX, cycloheximide. Data are expressed as mean ± SEM. n=3. *p ≤ 0.05 vs. TNF control.

5.2.6 The promotor activity of NF-κB is concentration-dependently inhibited by vioprolide A

Since vioprolide A reduced the TNF-induced nuclear translocation of p65, potential effects on the promotor activity of NF-κB were examined next using a Dual-Luciferase® Reporter Assay (see IV.6.1-6.2). In accordance with the effects on the p65 nuclear translocation, the TNF-induced NF-κB promotor activity was concentration-dependently reduced upon pretreatment of HUVECs with vioprolide A for 16 h (Figure 42A). Although vioprolide A was assessed as protein synthesis inhibitor (see V.3.2), the expression of the *Renilla* control plasmid remained stable, which strengthens the results of the reporter gene assay (Figure 42B).

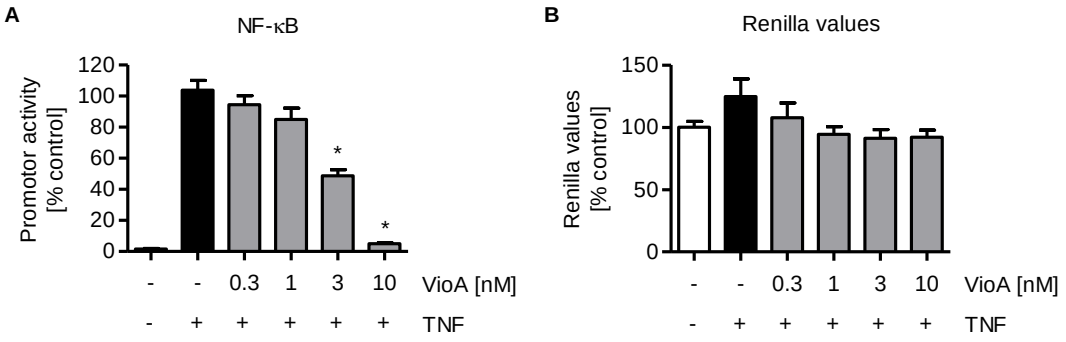

Figure 42: Vioprolide A reduces the NF-κB promotor activity. A-B HUVECs were co-transfected with a vector coding for the NF-κB response element and firefly luciferase and a control vector coding for *Renilla* luciferase. 24 h after transfection, HUVECs were treated with vioprolide A (0.3, 1, 3, 10 nM) for 16 h followed by activation with 10 ng/ml TNF for 6 h. NF-κB-dependent luciferase activity was measured by a dual-luciferase reporter gene assay. VioA, vioprolide A. Data are expressed as mean ± SEM. n=4. *p ≤ 0.05 vs. TNF control.

In summary, the results depicted in section V.5.1-5.2 indicate that the anti-inflammatory actions of vioprolide A can be attributed to an inhibition of the NF-κB p65 nuclear translocation and promotor activity.

5.3 The effect of vioprolide A on importin family members involved in the classical nuclear import pathway

Important for the successful nuclear translocation of NF-κB subunits is, on the one hand, the exposure of their NLS through degradation of IκBα and, on the other hand, the interaction with carrier proteins that ensure the shuttling of the protein through the nuclear pore complex.[90-92,99,100] Amongst the members of the importin family, KPNA2 and KPNA4 have been shown to interact with the NLS of p65 and to form a heterodimer with KPNB1, thereby mediating the p65 nuclear translocation.[115-119] To further elucidate how vioprolide A reduced the p65 nuclear translocation, the influence of the natural product on the importin family members was determined.

5.3.1 Vioprolide A reduces the total protein level of KPNA2 but not of KPNA4 and KPNB1

For more in-depth investigations regarding a potential effect on importin family members, the total protein levels of KPNA2, KPNA4 and KPNB1 was analysed upon vioprolide A treatment. For this, HUVECs were treated with 10 nM of vioprolide A for different time points up to 48 h, and the the protein levels were detected by western blot analysis. 10 nM of vioprolide A time-dependently decreased the total protein level of KPNA2 (Figure 43left) but did influence the levels of KPNA4 (Figure 43A middle) and KPNB1 (Figure 43A right). In accordance with the effects on the *de novo* protein synthesis and the TNFR1 total protein level, the maximum effect on the KPNA2 protein level was observed after 16 h of vioprolide A treatment. Again, a recovery of the KPNA2 protein level was observed after a longer treatment period of 48 h. Importantly, cycloheximide (3 µg/ml) showed similar time-dependent effects on the total protein level of KPNA2, KPNA4 and KPNB1 compared with vioprolide A (Figure 43B).

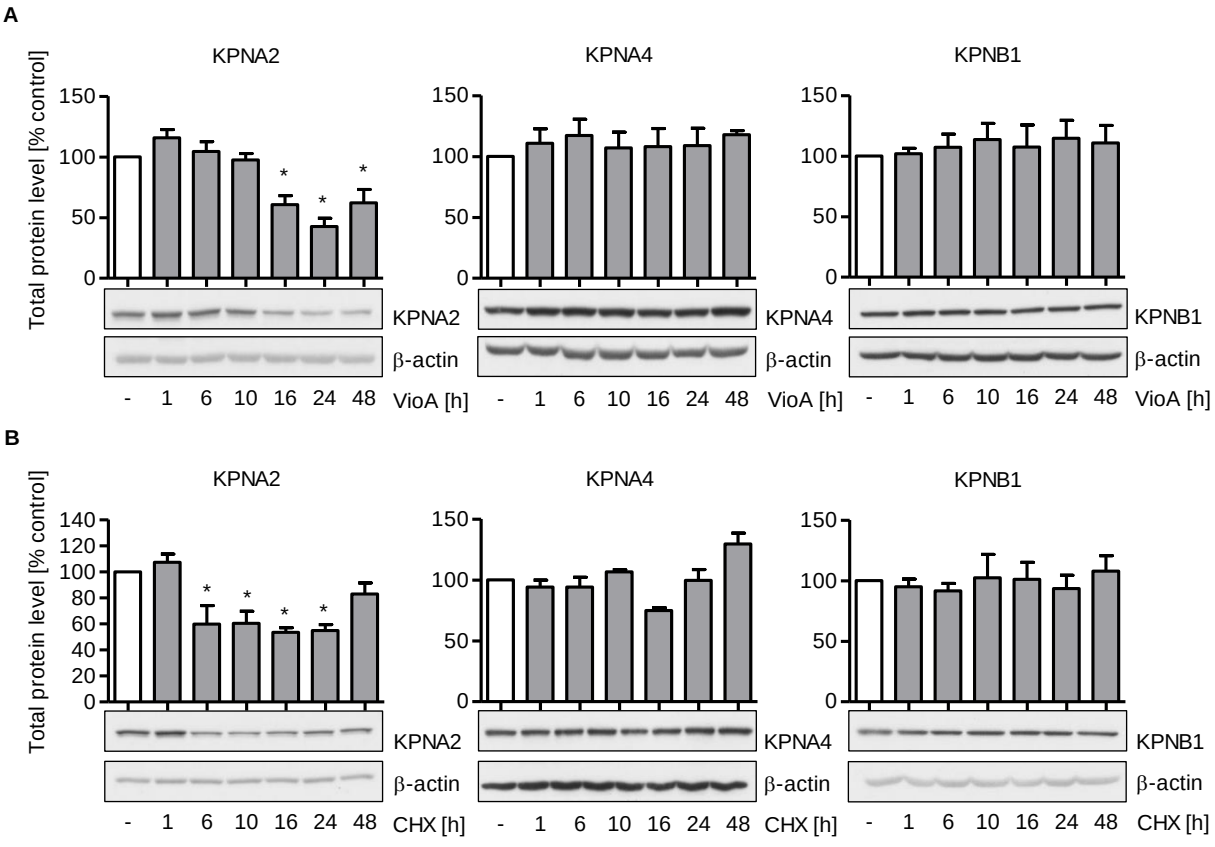

Figure 43: Vioprolide A reduces the total protein level of KPNA2 but not the levels of KPNA4 and KPNB1. A Confluent HUVECs were treated with 10 nM of vioprolide A for the indicated time periods. **B** Confluent HUVECs were treated with 3 µg/ml cycloheximide for the indicated time periods. **A**-**B** Total protein level of KPNA2 (left), KPNA4 (middle) and KPNB1 (right) was analysed by western blotting. One representative blot is shown. VioA, vioprolide A; CHX, cycloheximide. Data are expressed as mean ± SEM. n=3. *p ≤ 0.05 vs. control.

5.3.2 Vioprolide A differentially influences the mRNA expression of KPNA2, KPNA4 and KPNB1

The next step was to investigate whether the effect of vioprolide A on total protein levels of the importin family members was caused by inhibition of *de novo* protein synthesis or by a distinct, independent mechanism influencing the gene expression of *KPNA2*, *KPNA4* and *KPNB1*. For this, HUVECs were treated with 10 nM of vioprolide A up to 16 h, and the total mRNA level of the importin family members was determined by quantitative PCR. As demonstrated in Figure 44, 10 nM of vioprolide A time-dependently increased the mRNA expression of *KPNA4* and *KPNB1*. At the same time, the mRNA expression of *KPNA2* was not significantly influenced by vioprolide A treatment up to 16 h. Hence, the reduction in the KPNA2 protein level is likely to be caused by inhibition of mRNA translation into protein and not by lowering the mRNA expression itself.

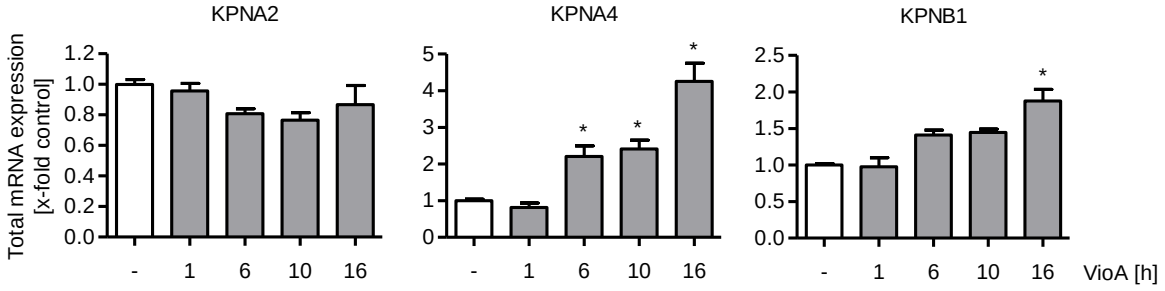

Figure 44: Vioprolide A differentially influences the mRNA expression of *KPNA2*, *KPNA4* and *KPNB1*. Confluent HUVECs were treated with 10 nM of vioprolide A for the indicated time periods. Total mRNA expression of *KPNA2* (left), *KPNA4* (middle) and *KPNB1* (right) was determined by quantitative PCR. VioA, vioprolide A. Data are expressed as mean ± SEM. n=3. *p ≤ 0.05 vs. control.

5.3.3 The nuclear localization of KPNA2 and KPNB1, but not of KPNA4, is altered by vioprolide A

For the classical nuclear import, importin alpha family members (KPNA2, KPNA4) bind to the NLS of NF-κB p65 on the one hand and to KPNB1 on the other hand. The interaction with the nuclear pore complex is mediated by KPNB1 and allows the importin-cargo-complex to enter the nucleus. Thus, in the last step it was analysed if vioprolide A, besides partially influencing the total protein level, also impairs the nucleus translocation of importins. Therefore, HUVECs were pretreated with 10 nM of vioprolide A for 16 h followed by activation with TNF for 5 min to 60 min. Consistent with the effect on the total protein level, vioprolide A pretreatment significantly reduced the TNF-triggered nuclear localization of KPNA2 (Figure 45A). An influence on the nuclear accumulation of KPNA4 was neither observed for TNF activation nor vioprolide A treatment (Figure 45B). Although the total protein level of KPNB1 was not influenced, pretreatment with vioprolide A for 16 h significantly downregulated the TNF-

dependent nuclear localization of KPNB1 after 15 min to 30 min (Figure 45C). This effect is most likely caused by the reduced presence of KPNA2 and thus lower interaction of the cargo-importin alpha-complex with KPNB1.

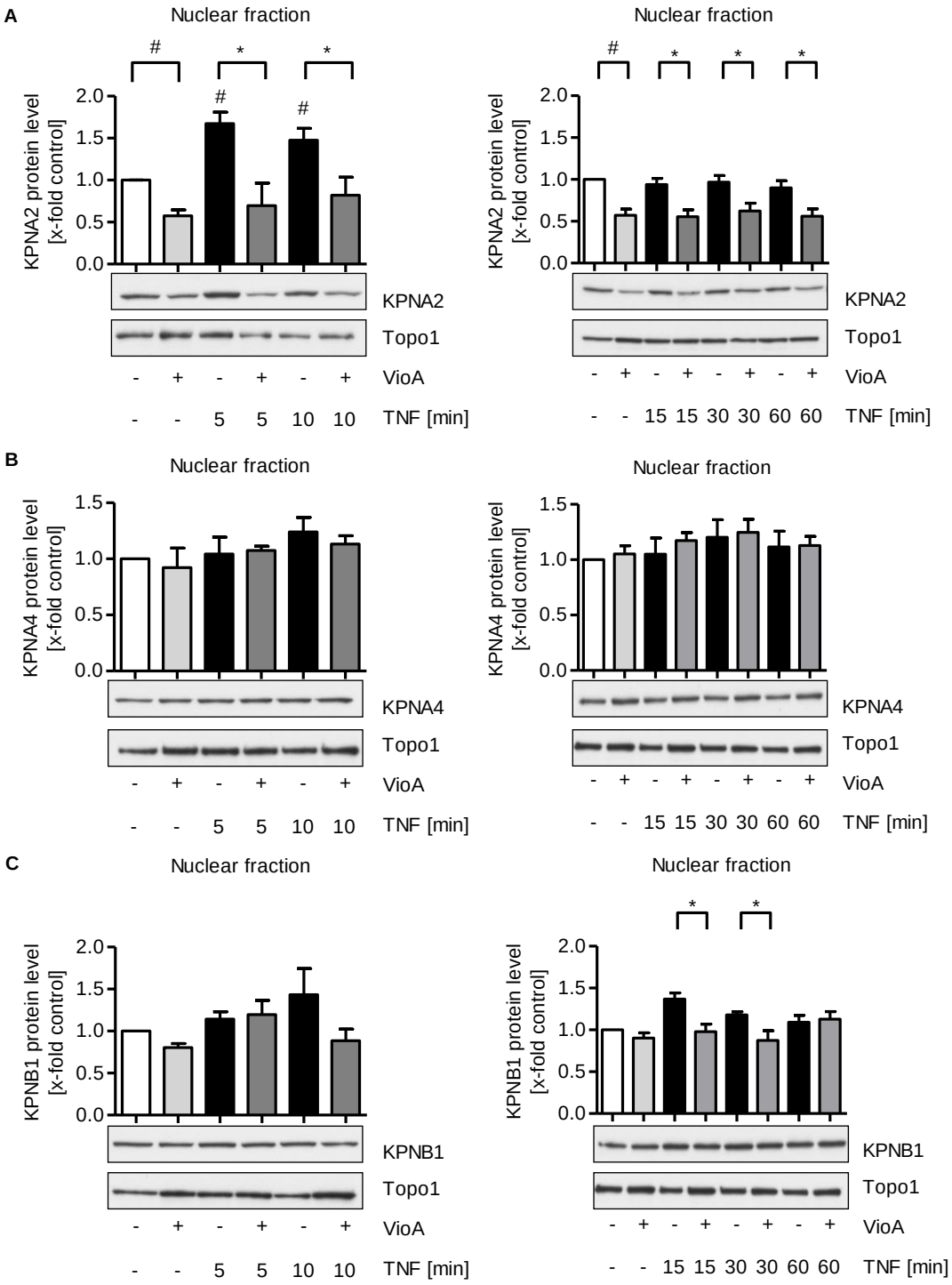

Figure 45: Vioprolide A lowers the nuclear translocation of KPNA2 and KPNB1 but not KPNA4. A-C Confluent HUVECs were treated with 10 nM of vioprolide A for 16 h followed by activation with 10 ng/ml TNF for 5 min and 10 min (left) or 15 min, 30 min and 60 min (right). Cytosolic and nuclear fractions were separated. The relative amount of nuclear KPNA2 (**A**), KPNA4 (**B**) and KPNB1 (**C**) was determined by western blotting. One representative blot is shown. VioA, vioprolide A; Topo1, topoisomerase 1. Data are expressed as mean ± SEM. n=3. *p ≤ 0.05 vs. TNF control, #p ≤ 0.05 vs. control.

5.4 Involvement of the cellular target NOP14 in the anti-inflammatory actions of vioprolide A

NOP14 has previously been studied regarding its involvement in tumor angiogenesis. Interestingly, though, nothing is known about a general participation of NOP14 in inflammatory processes. To determine whether the anti-inflammatory actions of vioprolide A are caused by the interaction and thus inhibition of NOP14, siRNA-mediated knockdown of NOP14 was performed, and its protein levels were determined by western blot analysis at 24 h, 48 h and 72 h after siRNA transfection to ensure a successful knockdown (Figure 46).

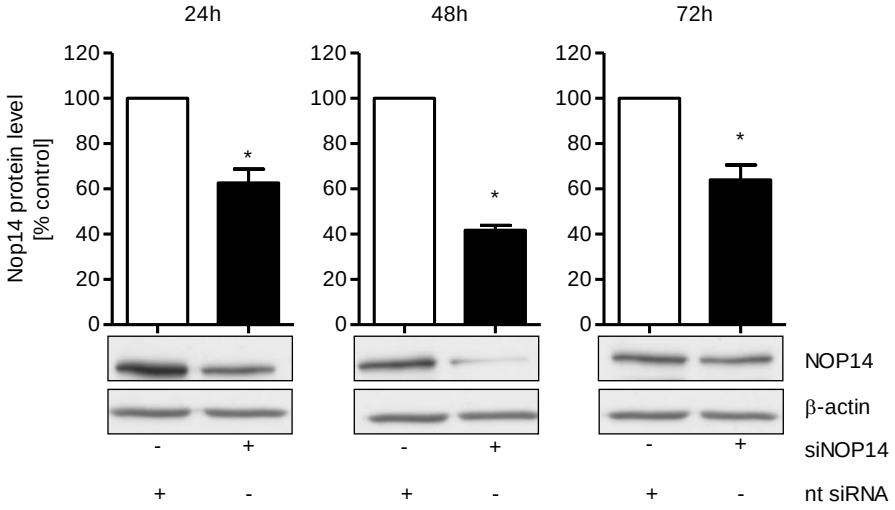

Figure 46: Knockdown of NOP14 in HUVECs. Subconfluent cells were transfected with siRNA against NOP14 (siNOP14, 60 nM) or non-targeting control siRNA (nt siRNA, 60 nM) using GeneTrans II Transfection Reagent. 24 h, 48 h and 72 h after transfection, total protein levels of NOP14 were analysed using western blotting. One representative blot is shown. Data are expressed as mean ± SEM. n=3. *p ≤ 0.05 vs. control.

5.4.1 NOP14 knockdown reduces the leukocyte adhesion to TNF-activated endothelial cells

To examine the effect of NOP14 knockdown on the leukocyte-endothelial cell interaction, cell adhesion assays were conducted. For this, 32 h post transfection, 10 nM of vioprolide A was added to the HUVECs for 16 h followed by activation with TNF for 6 h. Fluorescently labeled THP-1 cells were added to the HUVEC monolayer and allowed to adhere for 5 min. The amount of adhered cells was determined by fluorescence measurement. As demonstrated in Figure 47, knockdown of NOP14 significantly reduced the TNF-induced leukocyte cell adhesion, while the basal THP-1 cell adhesion to non-activated HUVECs remained unaffected. Importantly, the effect of vioprolide A on the TNF-induced leukocyte adhesion was not altered by NOP14 knockdown.

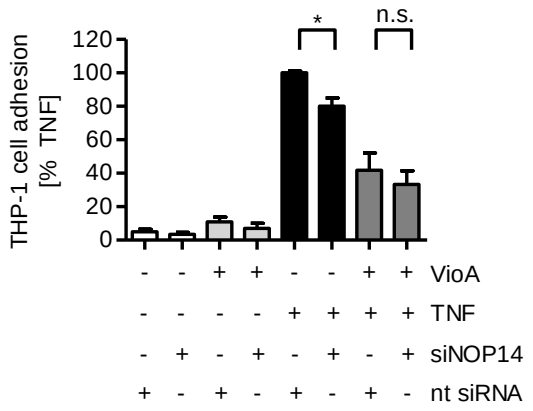

Figure 47: NOP14 knockdown reduces the TNF-induced THP-1 cell adhesion to HUVECs. Subconfluent HUVECs were transfected with siRNA against NOP14 (siNOP14, 60 nM) or non-targeting siRNA (nt siRNA, 60 nM) as control using the GeneTrans II Transfection Reagent. 32 h after transfection, HUVECs were treated with 10 nM of vioprolide A for 16 h and activated with TNF (10 ng/ml) for 6 h. Fluorescence-labeled THP-1 cells were allowed to adhere to the HUVEC monolayer for 5 min. The amount of adhered THP-1 was detected by fluorescence measurement. VioA, vioprolide A. Data are expressed as mean ± SEM. n=5. *p ≤ 0.05 vs. TNF control.

5.4.2 The mRNA expression of *ICAM1* is downregulated upon NOP14 knockdown

In a next step, we investigated whether the reduced leukocyte cell adhesion upon NOP14 knockdown, similar to vioprolide A treatment, is caused by downregulation of the TNF-induced mRNA expression of cell adhesion molecules. Therefore, 32 h post transfection, 10 nM of vioprolide A was added to the HUVECs for 16 h followed by activation with TNF for 4 h, and the total mRNA expression of *ICAM1* was analysed by quantitative PCR. Knockdown of NOP14 significantly reduced the TNF-induced *ICAM1* mRNA expression, while the basal *ICAM1* mRNA expression was not influenced (Figure 48). Again, the inhibitory effect of vioprolide A on the *ICAM1* mRNA expression was not altered by NOP14 knockdown.

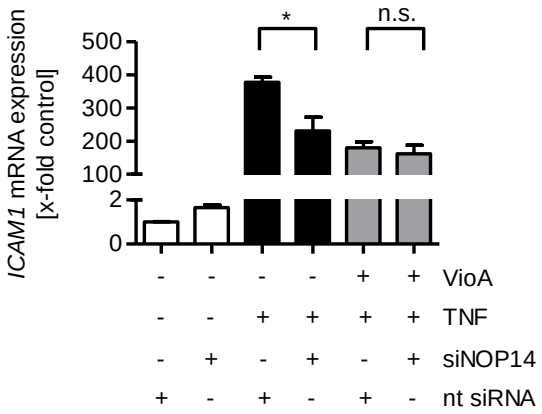

Figure 48: NOP14 knockdown reduces the TNF-induced *ICAM1* mRNA expression in HUVECs. Subconfluent HUVECs were transfected with siRNA against NOP14 (siNOP14, 60 nM) or non-targeting siRNA (nt siRNA, 60 nM) as control using the GeneTrans II Transfection Reagent. 32 h after transfection, HUVECs were treated with 10 nM of vioprolide A for 16 h and activated with TNF (10 ng/ml) for 4 h. Total mRNA expression of *ICAM1* was determined by quantitative PCR. VioA, vioprolide A. Data are expressed as mean ± SEM. n=3. *p ≤ 0.05 vs. TNF control.

5.4.3 NOP14 knockdown prevents the nuclear translocation of p65 in HUVECs

In a final step, it was assessed whether the reduced *ICAM1* mRNA expression upon NOP14 knockdown was caused by a reduced TNF-induced nuclear translocation of p65. Hence, 32 h post transfection, 10 nM of vioprolide A was added to the HUVECs for 16 h followed by activation with TNF for 30 min. The p65 nuclear translocation was determined by immunocytochemistry. Knockdown of NOP14 significantly reduced the TNF-induced p65 nuclear translocation, while the basal cellular distribution of p65 remained unchanged (Figure 49A). Moreover, the inhibitory effect of vioprolide A on the p65 nuclear translocation was neither increased nor decreased by NOP14 knockdown. Immunofluorescence staining of KPNA2 revealed that NOP14 knockdown decreased the fluorescence intensity, and thus cellular KPNA2 levels, equally compared with 16 h of vioprolide A (10 nM) treatment (Figure 49B).

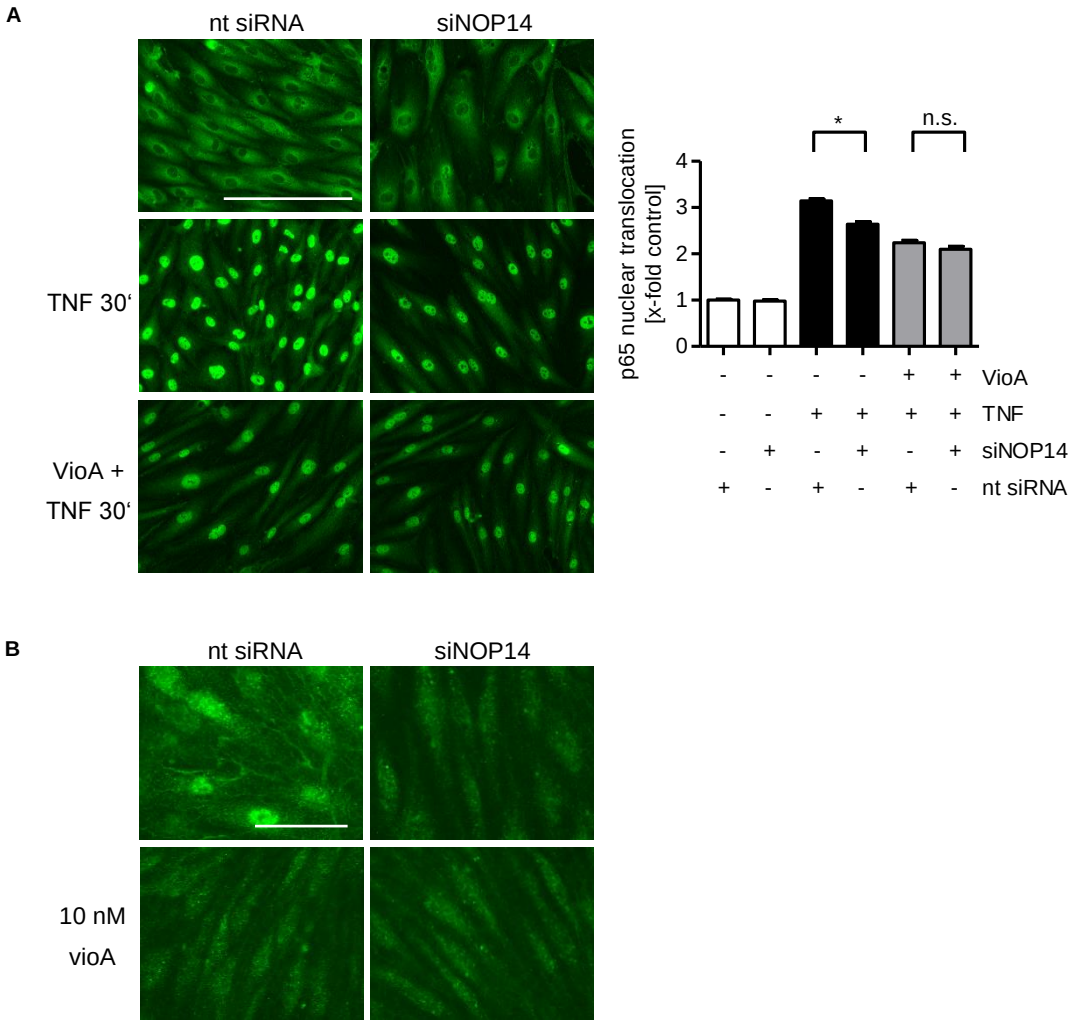

Figure 49: NOP14 knockdown prevents p65 nuclear translocation and reduces KPNA2 total protein levels. **A**-**B** Sparse cells were transfected with siRNA against NOP14 (siNOP14, 60 nM) or non-targeting siRNA (nt siRNA, 60 nM) as control using GeneTrans II Transfection Reagent. 32 h after transfection, HUVECs were treated with vioprolide A (10 nM) for 16 h. **A** HUVECs were activated with TNF (10 ng/ml) for 30 min. p65 was visualized by immunocytochemistry. One representative experiment is shown. Scale bar, 200 µm. **B** KPNA2 was visualized by immunocytochemistry. One representative experiment is shown. Scale bar, 50 µm. VioA, vioprolide A; Ctrl, control. Data are expressed as mean ± SEM. n=3. *p ≤ 0.05 vs. TNF control.

In summary, the results from the NOP14 knockdown experiments clearly highlight the involvement of NOP14 in inflammatory processes in the endothelium and demonstrate that the anti-inflammatory actions of vioprolide A are evoked, at least in part, by inhibition of NOP14.

6. The influence of vioprolide A on angiogenic key features of endothelial cells *in vitro*

Endothelial cells execute important angiogenic key features, including cell sprouting, cell migration and cell proliferation to ensure, on the one hand, a proper formation of new vessels and, on the other hand, to specifically address the origin of the angiogenic stimulus.[165] Since vioprolide A provided strong anti-angiogenic effects *in vivo*, the influence on the angiogenic features of endothelial cells was investigated more closely *in vitro*.

6.1 Effects of vioprolide A on cell sprouting

Cell sprouting represents the initial step in the process of forming new blood vessels.[165] The effect of vioprolide A on sprouting angiogenesis was determined by using macro- and microvascular cell spheroids *in vitro* and choroidal explant cultures *ex vivo*.

6.1.1 Vioprolide A downregulates the sprouting of endothelial cells *in vitro*

To investigate the influence of vioprolide A on macro- and microvascular cell sprouting *in vitro*, three-dimensional cell spheroids were generated from HUVECs and HMEC-1 cells using the hanging drop method. The spheroids were then embedded into a collagen gel, pretreated with vioprolide A for 16 h and sprouting was induced by VEGF treatment for 20 h. Vioprolide A concentration-dependently decreased the VEGF-induced total sprout length and number of sprouts per spheroid both in macrovascular HUVECs (Figure 50A) and microvascular HMEC-1 cells (Figure 50B). In general, the effect of vioprolide A on the total sprout length was slightly stronger compared to the influence on the number of sprouts per spheroid.

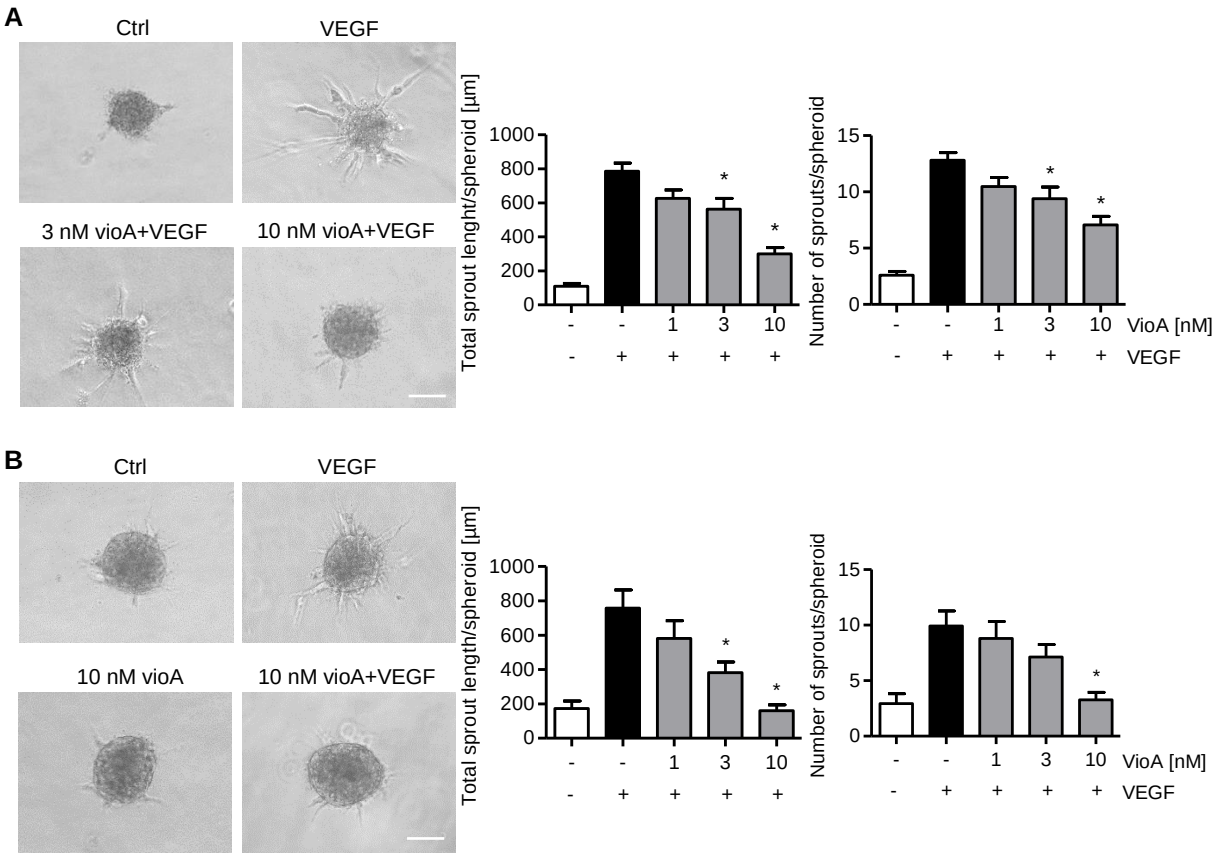

Figure 50: Vioprolide A decreases the VEGF-induced sprouting of endothelial cells. A HUVEC-derived spheroids were seeded in collagen gel, pretreated with vioprolide A (1, 3, 10 nM) for 16 h followed by treatment with VEGF (10 ng/ml) for 20 h. **B** HMEC-1 cell-derived spheroids were seeded in collagen gel, pretreated with vioprolide A (1, 3, 10 nM) for 16 h followed by treatment with VEGF (10 ng/ml) for 20 h. **A**-**B** Microscopical pictures were taken and the total sprout length and number of sprouts per spheroid were analysed using ImageJ software. Representative images are shown. Scale bar, 100 µm. VioA, vioprolide A; Ctrl, control. Data are expressed as mean ± SEM. n=3. *p ≤ 0.05 vs. VEGF.

6.2 The microvascular sprouting of choroidal explant cultures is reduced by vioprolide A ex vivo

For more in-depth and physiological analysis, the microvascular sprouting from choroidal explant cultures was observed *ex vivo*. Therefore, retinal tissue was dissected from the peripheral region of murine eyes, embedded in Matrigel, cultured in medium and treated with vioprolide A (3, 10, 30 nM). This assay was kindly performed by Yanfen Li from the group of Prof. Dr. Stylianos Michalakis (Department of Ophthalmology, University Hospital, Ludwig Maximilians University of Munich (LMU), Munich, Germany). Similar to the *in vitro* spheroid sprouting, vioprolide A concentration-dependently reduced the *ex vivo* choroidal sprouting area compared to control treatment (Figure 51). However, in contrast to the in vitro sprouting, 3 nM of vioprolide A did not show a significant decrease of the sprouting area of the choroidal explant cultures.

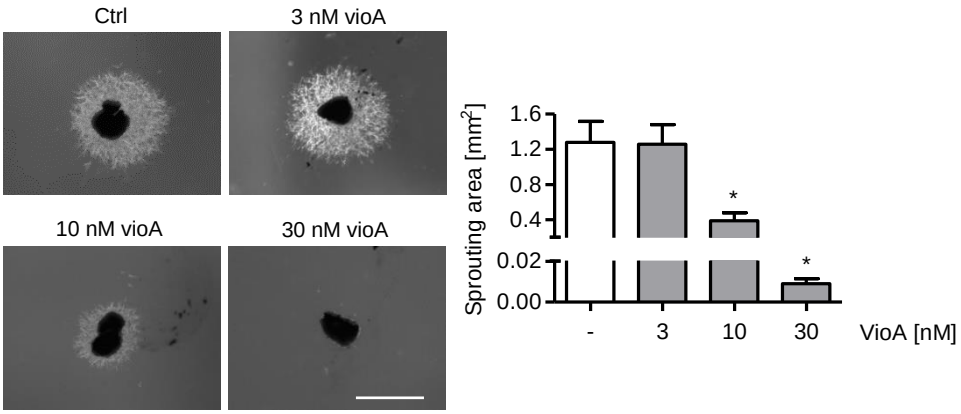

Figure 51: Vioprolide A reduces the sprouting area of chroidal explant cultures. Biopsies from retinal tissue were embedded in Matrigel, treated with vioprolide A (3, 10, 30 nM) and cultured in medium for 6 days. Microscopic images of microvascular sprouts were taken and analysed using the SWIFT-Choroid macro in the ImageJ software. Representative images are shown. Scale bar, 500 µm. VioA, vioprolide A; Ctrl, control. Data are expressed as mean ± SEM. n=6. *p ≤ 0.05 vs. control.

6.3 Effects of vioprolide A on endothelial cell migration

Directed and undirected cell migration are needed to ensure that the growing sprout reaches the origin of the angiogenic stimulus.[165] The random, undirected cell migration was investigated by a scratch assay, and the directed cell migration was analysed by a Boyden chamber experiment using FCS as chemoattractant for the induction of an active movement.

6.3.1 The undirected endothelial cell migration is impaired by vioprolide A

To investigate the effect of vioprolide A on the undirected endothelial cell migration, HUVECs or HMEC-1 cells were grown to confluence and pretreated with vioprolide A (1, 3, 10 nM) for 16 h. Subsequently, a scratch was inflicted to the monolayer using a pipette tip. The cells were then allowed to migrate until the control cells had closed the gap (100 % migration). Vioprolide A concentration-dependently decreased the undirected migration of both macrovascular HUVECs (Figure 52A) and microvascular HMEC-1 cells (Figure 52B). For both cell types, the maximum effect was observed for the highest applied concentration (i.e. 10 nM) of vioprolide A. This concentration showed a stronger anti-migratory action in HMEC-1 cells (90 % reduction) compared to HUVECs (60 % reduction).

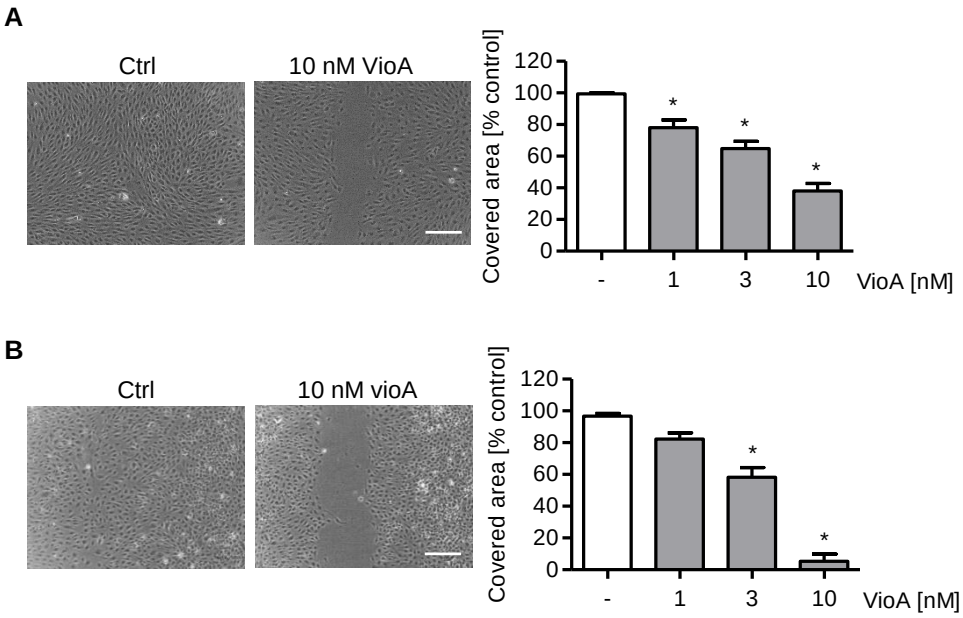

Figure 52: Vioprolide A reduces the undirected migration of endothelial cells. A Confluent HUVECs were treated with vioprolide A (1, 3, 10 nM) for 16 h. Subsequently, a scratch was inflicted to the HUVEC monolayer. **B** Confluent HMEC-1 cells were treated with vioprolide A (1, 3, 10 nM) for 16 h. Subsequently, a scratch was inflicted to the HMEC-1 monolayer. **A**-**B** The cells were allowed to migrate for 12 h either in starvation medium (1 % FCS; 0 % migration) or growth medium (10 % FCS; 100 % migration) until the untreated control cells closed the scratch. Microscopical images were taken, and the covered area was analysed using the ImageJ software. Scale bar, 200 µm. VioA, vioprolide A; Ctrl, control. Data are expressed as mean ± SEM. n=3. *p ≤ 0.05 vs. control.

6.3.2 Vioprolide A reduces the chemotactic migration of endothelial cells

In the next step, a Boyden chamber experiment was conducted to examine the influence of vioprolide A on the directed migration of endothelial cells towards a chemotactic gradient. Therefore, adherent HUVECs were treated with vioprolide A (3, 10 nM) and allowed to migrate towards FCS as chemoattractant for 16 h. As shown in Figure 53, treatment with vioprolide A significantly reduced the serum-induced directed migration of HUVECs to approximately 50 % of the control level.

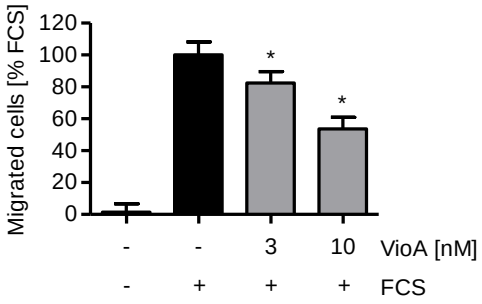

Figure 53: Vioprolide A decreases the directed serum-induced migration of HUVECs. HUVECs were seeded to the porous membrane of Transwell inserts (pore size 8 µm) and allowed to adhere for 4 h. Cells were then treated with vioprolide A (3, 10 nM) and allowed to migrate towards a chemotactic gradient (20 % FCS) for 16 h. Migrated cells were stained with crystal violet solution, and absorbance measurement was performed at 540 nm. VioA, vioprolide A; FCS, fetal calf serum. Data are expressed as mean ± SEM. n=5. *p ≤ 0.05 vs. FCS.

6.4 The influence of vioprolide A on endothelial cell proliferation

Cell proliferation is needed to ensure that the angiogenic sprout is elongated and can reach the origin of the angiogenic stimulus. Cell proliferation relies on the proper progression of the cells through the cell cycle, which results in cell division and includes the synthesis of new DNA during the S-phase of the cell cycle.[419]

6.4.1 The cell proliferation and DNA synthesis of endothelial cells is inhibited by vioprolide A

To investigate the general proliferation of endothelial cells, macrovascular HUVECs and microvascular HMEC-1 were treated with vioprolide A (0.3–10 nM) and grown for 72 h followed by a wash step to remove dead, detached cells. Crystal violet staining was used to detect the relative amount of attached viable cells in the treated and non-treated wells. The intensitiy of the crystal violet staining is proportional the number of cells in the well. Vioprolide A concentration-dependently lowered the proliferation of both HUVECs (Figure 54A) and HMEC-1 cells (Figure 54B). At the highest concentration of vioprolide A (10 nM), the cell proliferation of both endothelial cell types was completely inhibited.

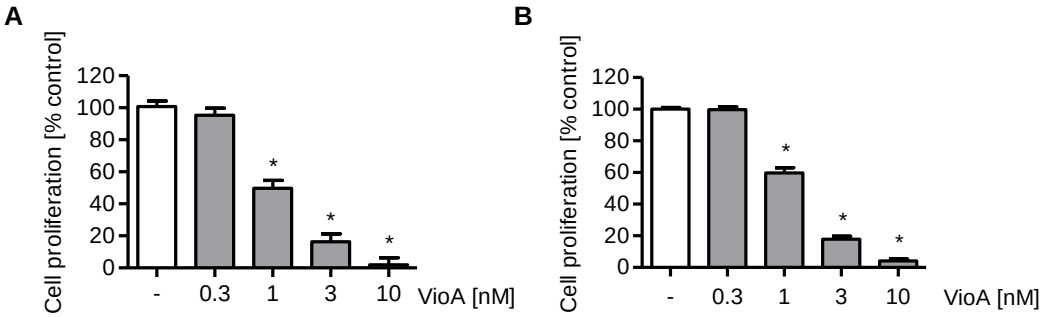

Figure 54: The proliferation of endothelial cells is inhibited by vioprolide A. A HUVECs were grown in low density for 24 h followed by treatment with vioprolide A (0.3, 1, 3, 10 nM) for 72 h. **B** HMEC-1 cells were grown in low density for 24 h followed by treatment with vioprolide A (0.3, 1, 3, 10 nM) for 72 h. **A**-**B** Cells were stained with crystal violet solution, and absorbance measurement was performed at 540 nm. VioA, vioprolide A. Data are expressed as mean ± SEM. n=3. *p ≤ 0.05 vs. control.

6.4.2 Vioprolide A shifts the cells to the G_0/G_1 phase of the cell cycle and reduces the formation of newly synthesized DNA

Cell proliferation relies on the proper progression of the cells through the cell cycle. The cell cycle consists of the G_0/G_1, S and G_2/M phase.[577] To analyse the influence of vioprolide A on the cell cycle distribution of HUVECs, cells were treated for 24 h or 48 h with vioprolide A (1, 3, 10 nM) and stained with propidium iodide. With the proceeding of the cell cycle, the DNA content of the cell increases, thus, the cells in the later cell cycle stages can proportionally take up more of the dye than cells in the early stages of the cell cycle. The propidium iodide staining

and cell cycle distribution was then measured by flow cytometry. After 24 h, a significant increase of cells in the G_0/G_1 phase and a significant decrease of cells in the S and G_2/M phase was observed (Figure 55A). After 48 h, the percentage of cells in the S phase was lowered even stronger compared to 24 h of vioprolide A treatment, while the amount of cells in the G_2/M phase recovered to control level (Figure 55A).

During the S phase of the cell cycle, cells synthesize new DNA to duplicate their genome. To investigate whether the reducing effect of vioprolide A on the percentage of cells in the S phase would also impair the cellular DNA synthesis, a BrdU incorporation assay was performed. For this, HUVECs were serum-starved to achieve a cell cycle synchronization in the G_0/G_1 phase and, subsequently, treated with vioprolide A for 24 h in full growth medium. During the last 8 h of the incubation period, BrdU was added and allowed to incorporate into the DNA. As shown in Figure 55B, 3 nM and 10 nM of vioprolide A drastically decreased the BrdU incorporation and thus synthesis of new DNA in HUVECs. 0.3 nM and 1 nM of vioprolide A showed no effect on the BrdU incorporation, consistent with the effects observed for the cell cycle distribution.

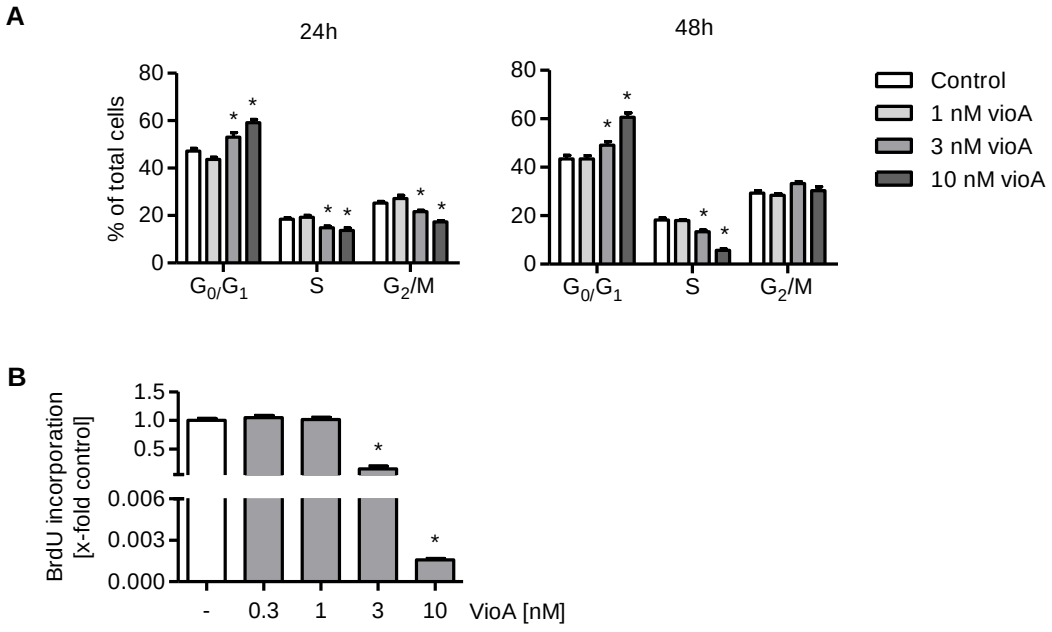

Figure 55: Vioprolide A impairs the cell cycle distribution and DNA synthesis of HUVECs. A HUVECs were grown in low density for 24 h and treated with vioprolide A (1, 3, 10 nM) for 24 h or 48 h. Cells were stained with propidium iodide solution, and cell cycle distribution was analysed using flow cytometry. **B** HUVECs were grown in low density for 24 h, serum-starved for 8 h and subsequently treated with vioprolide A (0.3, 1, 3, 10 nM) for 24 h in growth medium. 8 h before the treatment endpoint, BrdU (10 µM) was added to the cells. The relative amount of incorporated BrdU was determined using flow cytometry. VioA, vioprolide A; Ctrl, control. Data are expressed as mean ± SEM. n=4. *p ≤ 0.05 vs. control.

In total, it could be shown that vioprolide A strongly downregulates all angiogenic key features, including the VEGF-induced sprouting, undirected and directed migration and proilferation of endothelial cells *in vitro*. Furthermore, the inhibition of cell proliferation is most likely caused by arresting the progression of endothelial cells through the cell cycle and shifting the cells into

the G_0/G_1 phase of the cell cycle. This suggestion is furthermore underlined by the observation, that the reduced amount of cells in the S phase correlated with a decrease in DNA synthesis, which is needed by the cells to proceed to the G_2/M phase.

7. The mechanism underlying the effects of vioprolide A on angiogenic processes in endothelial cells

The results shown in section V.1 and V.6 clearly demonstrate that vioprolide A inhibits angiogenic processes *in vivo* and in endothelial cells *in vitro*. Consequently, the next aim was to elucidate the underlying anti-angiogenic cellular mode of action of vioprolide A.

7.1 The effect of vioprolide A on the VEGF receptor 2 signaling cascade in endothelial cells

The VEGF/VEGFR2 signaling cascade is a major regulator of endothelial cell proliferation, migration and survival. Through binding of VEGF to the VEGFR2, the receptor is auto-phosphorylated and induces downstream angiogenic kinases including JNK, ERK and p38.[187,194] Thus, it was investigated if an impairment of the VEGFR2 signaling pathway is involved in the anti-angiogenic actions of vioprolide A.

7.1.1 Vioprolide A reduces the activation and total protein level of the VEGFR2

Since vioprolide A was shown to inhibit protein biosynthesis (section V.3.2) and to reduce the total protein level of important pro-inflammatory proteins, a potential influence on VEGFR2 was investigated at first. Therefore, HUVECs were treated with vioprolide A up to 72 h, and the total protein level of VEGFR2 was analysed by western blotting. As shown in Figure 56A, vioprolide A time-dependently lowered the VEGFR2 protein expression. Consistent with the actions on protein biosynthesis and TNFR1, the maximum effect on the VEGFR2 protein level was observed after 16 h. A recovery of the protein level occurred after longer treatment times of 48 h to 72 h. Importantly, at the same time, the *KDR* (kinase insert domain receptor; *VEGFR2*) mRNA expression was time-dependently increased (Figure 56B). Thus, the influence on the total protein levels of VEGFR2 is likely to be caused by the inhibition of mRNA translation and not gene transcription. Next, the phosphorylation of the VEGFR2 was examined by western blot analysis to determine whether the VEGFR2 activation was impaired by vioprolide A in addition to the total protein level. Therefore, HUVECs were treated with vioprolide A for 16 h and activated with VEGF for 5 min. As shown in Figure 56C, vioprolide A significantly decreased the VEGF-induced phosphorylation of the VEGFR2.

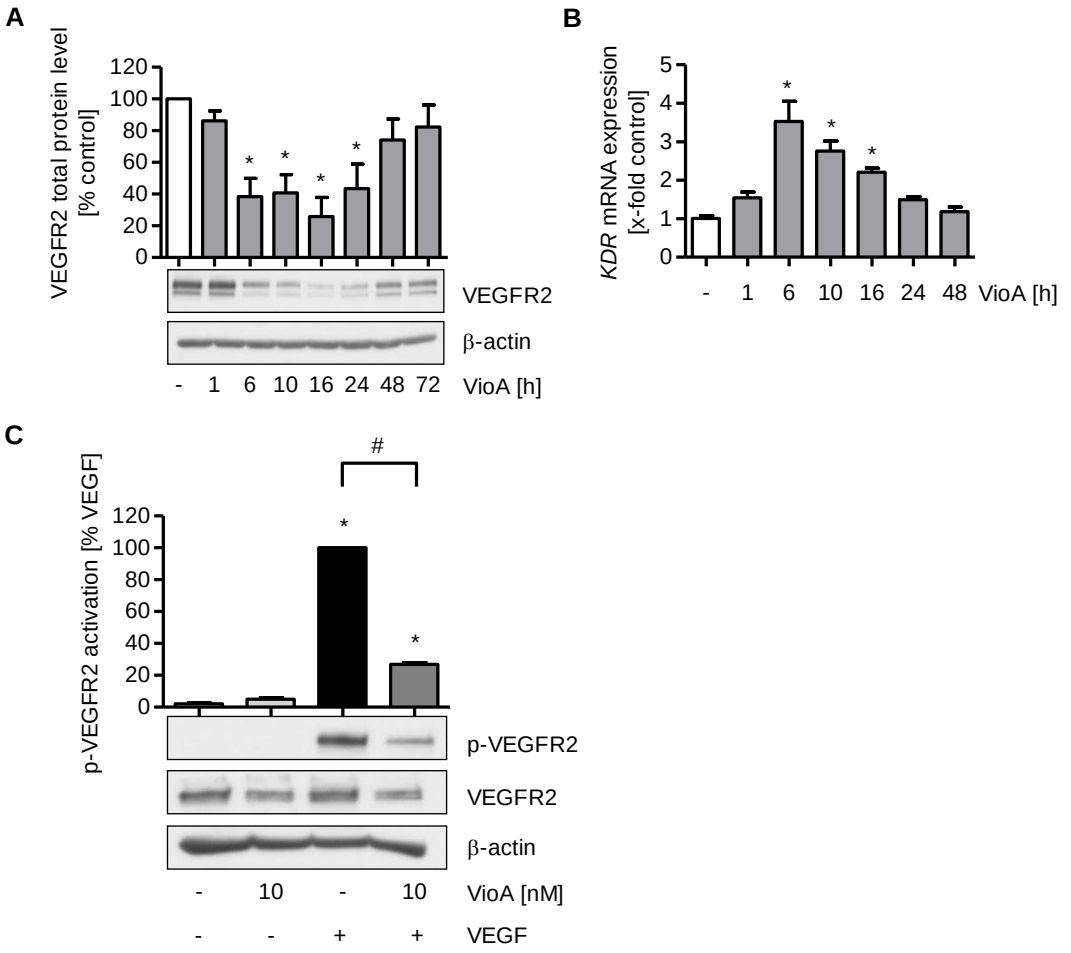

Figure 56: Vioprolide A reduces the total protein level and activation of the VEGFR2. A Confluent HUVECs were treated with 10 nM of vioprolide A for the indicated time points. Total protein levels of VEGFR2 were determined by western blotting. One representative blot is shown. **B** Confluent HUVECs were treated with 10 nM of vioprolide A for the indicated time points. Total *KDR* mRNA expression was analysed by quantitative PCR. **C** Confluent HUVECs were starved overnight, treated with 10 nM of vioprolide A for 16 h and activated with 10 ng/ml VEGF for 5 min. Total phospho-VEGFR2 (p-VEGFR2) was examined by western blot analysis. One representative blot is shown. VioA, vioprolide A; *KDR*; kinase insert domain receptor. Data are expressed as mean ± SEM. n=3. *p ≤ 0.05 vs control, #p ≤ 0.05 vs. VEGF.

7.1.2 Vioprolide A decreases the total protein level of the FGFR1 and EGFR but increases the VEGFR1 total protein level

Besides the VEGFR2, other growth factor receptors including the VEGFR1, FGFR1 and EGFR are involved in angiogenic processes in the endothelium as well.[180,181,189,190] To investigate whether – besides VEGFR2 – vioprolide A also reduces the protein level of other growth factor receptors, their total protein levels were determined by western blotting. Therefore, HUVECs were treated with vioprolide A for different time periods ranging from 1 h to 72 h. As shown in Figure 57A, vioprolide A time-dependently reduced the protein level of the FGFR1 with a maximum effect after 16 h of treatment and a recovery between 48 h to 72 h. The total protein level of the EGFR was influenced, too (Figure 57B). However, vioprolide A only reduced the EGFR protein expression significantly after longer treatment periods (24 h to 72 h). For the

EGFR, no recovery of the protein level was observed up to 72 h. Surprisingly, in contrast to FGFR1 and EGFR, vioprolide A time-dependently increased the total protein level of VEGFR1, showing a maximum effect after 16 h to 24 h of treatment (Figure 57C). However, treatment with cycloheximide significantly downregulated the VEGFR1 protein level, indicating that the effect of vioprolide A on the VEGFR1 protein level is not based on a cellular feedback mechanism towards the inhibition of protein biosynthesis (Figure 57D).

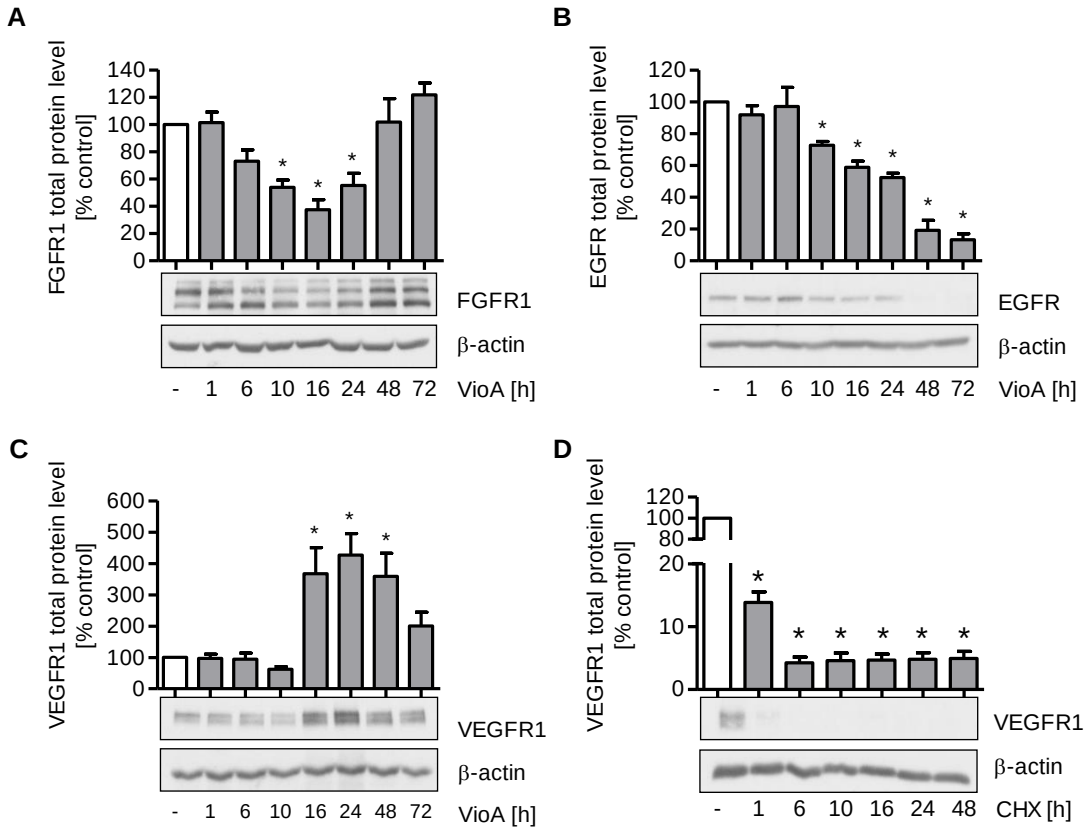

Figure 57: Vioprolide A influences the total protein level of different growth factor receptors. A-**C** Confluent HUVECs were treated with 10 nM of vioprolide A for the indicated time points. **D** Confluent HUVECs were treated with 3 µg/ml cycloheximide for the indicated time points. **A**-**D** Total protein levels of the FGFR1 (**A**), EGFR (**B**) and VEGFR1 (**C**, **D**) were analysed by western blotting. One representative blot is shown. VioA, vioprolide A; CHX, cycloheximide. Data are expressed as mean ± SEM. n=3. *p ≤ 0.05 vs control.

7.1.3 Vioprolide A reduces the activation of JNK, ERK1/2 and p38 downstream of the VEGFR2

Upon auto-phosphorylation of the VEGFR2, several downstream pro-angiogenic kinases including JNK, ERK1/2 and p38 are activated, which represent important signaling molecules that are involved in the regulation of angiogenic processes.[194] To assess if the reduced activation of the VEGFR2 upon vioprolide A treatment also impairs the activation of downstream kinases, the phosphorylation of ERK1/2, JNK and p38 was determined by western blot analysis. For this, confluent HUVECs were starved overnight, treated with vioprolide A for

16 h and activated with VEGF for 5 min (ERK1/2) or 15 min (JNK, p38). As shown in Figure 58A-C, vioprolide A significantly reduced the VEGF-induced activation of JNK, ERK1/2 and p38.

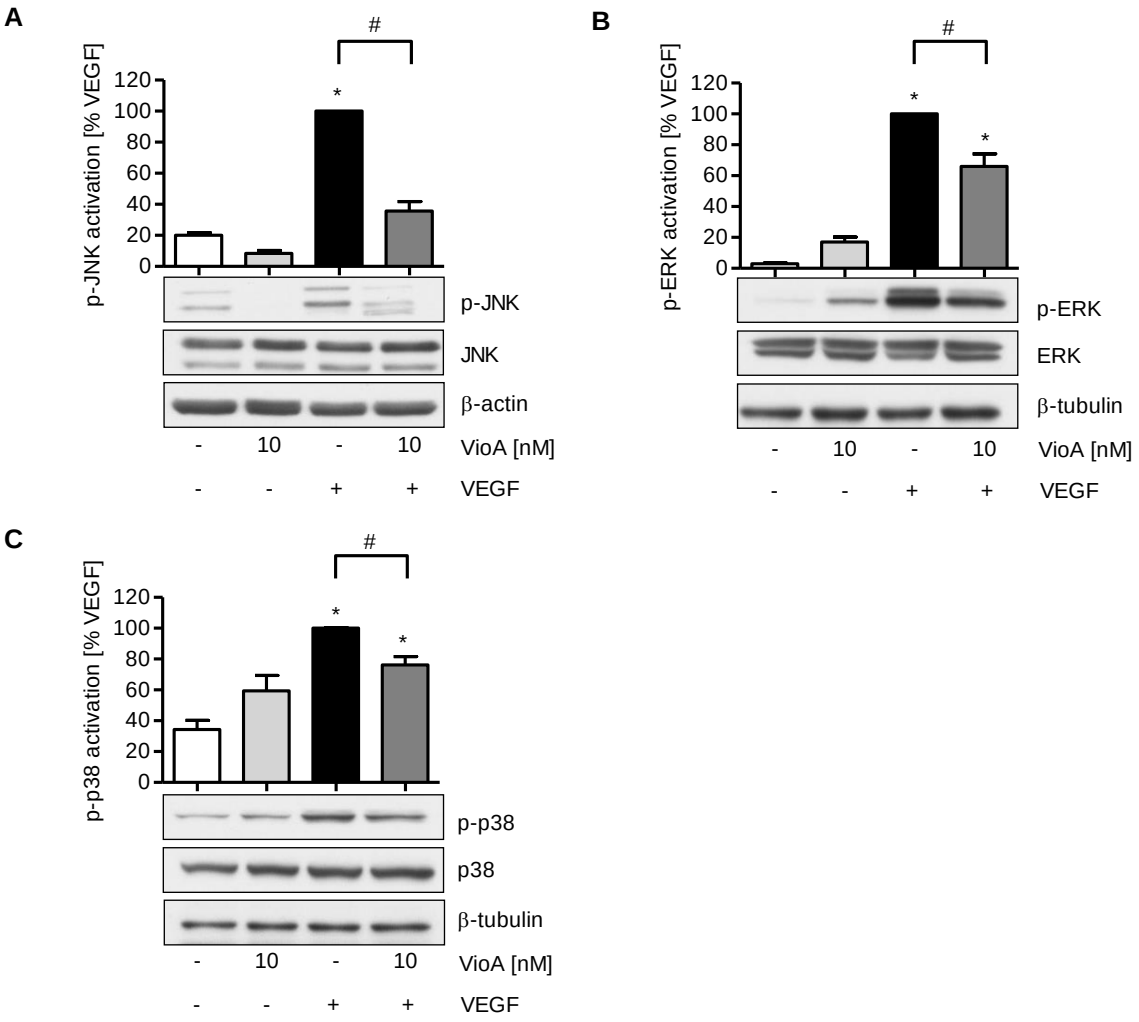

Figure 58: Vioprolide A downregulates the VEGF-induced activation of JNK, ERK and p38. A-C Confluent HUVECs were starved overnight, treated with 10 nM of vioprolide A for 16 h and activated with 10 ng/ml VEGF for 5 min (**B**) or 15 min (**A**, **C**). Protein levels of phospho-JNK (pJNK, **A**), phospho-ERK (p-ERK, **B**) and phospho-p38 (p-p38, **C**) were determined by western blotting. One representative blot is shown. VioA, vioprolide A. Data are expressed as mean ± SEM. n=3 (**A**, **B**), n=4 (**C**). *p ≤ 0.05 vs control, #p ≤ 0.05 vs VEGF.

7.1.4 The activation of Akt and eNOS downstream of VEGFR2 is increased by vioprolide A

Besides the mentioned pro-angiogenic kinases in section V.7.1.3, the signaling molecules Akt and eNOS are important proteins downstream of VEGFR2. Akt is involved in angiogenic and pro-survival signaling, and eNOS is responsible for the synthesis of nitric oxide.[208-211,225] While vioprolide A treatment significantly reduced the activation of the VEGFR2 as well as the pro-angiogenic MAPKs, western blot analysis revealed that the activation of Akt and eNOS was increased by the natural product (Figure 59A-B). Vioprolide A enhanced the VEGF-induced

Akt activation as well as the basal Akt and eNOS phosphorylation in HUVECs. VEGF-induced activation of eNOS, however, was in contrast to Akt not influenced.

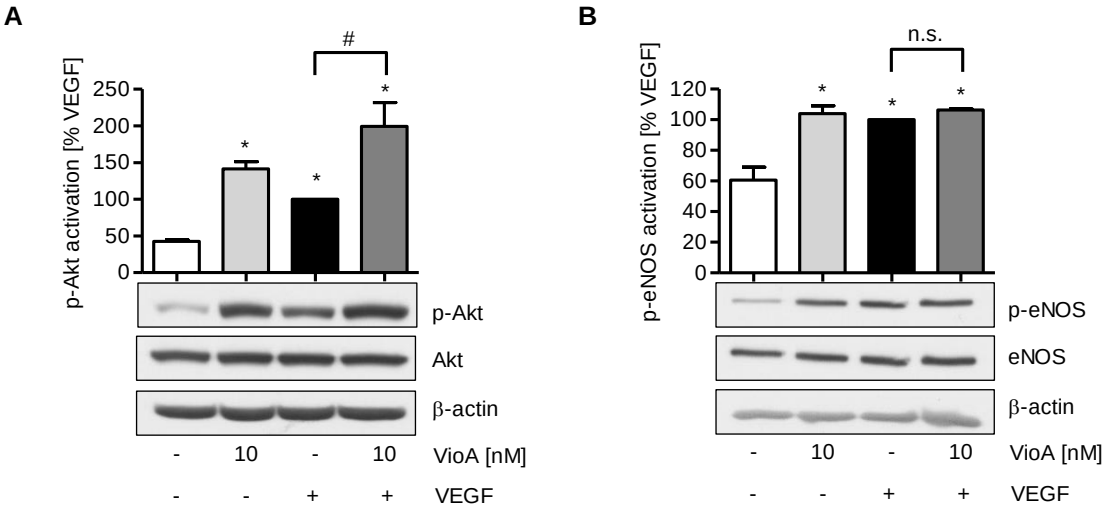

Figure 59: Vioprolide A enhances the activation of Akt and eNOS. A-**B** Confluent HUVECs were starved overnight, treated with 10 nM of vioprolide A for 16 h and activated with 10 ng/ml VEGF for 15 min. Protein levels of phospho-Akt (p-Akt, **A**) and phospho-eNOS (p-eNOS, **B**) were determined by western blotting. One representative blot is shown. VioA, vioprolide A. Data are expressed as mean ± SEM. n=3. *p ≤ 0.05 vs control, #p ≤ 0.05 vs VEGF.

7.1.5 The increased activation of Akt by vioprolide A is PI3K-dependent but only in part relies on a reduced PTEN protein level

The activation of the protein kinase Akt is mediated by PI3K and the second messenger PIP_3.[212,213] Under normal conditions, the activation of PI3K again is controlled by the suppressor PTEN, which prevents hyperactivation of Akt.[218] Hence, in the next step an influence of vioprolide A on PI3K and PTEN as root cause for the increased Akt phosphorylation in HUVECs was examined. For this, HUVECs were pretreated for 30 min with the PI3K-inhibitor Ly294002 before they were treated with vioprolide A for 16 h and activated with VEGF. Ly294002 significantly reduced the vioprolide A-induced basal and VEGF-evoked Akt activation (Figure 60A). Next, the total protein level of PTEN was assessed by western blotting. Indeed, treatment with vioprolide A time-dependently reduced the total protein level of PTEN (Figure 60B). For more in-depth analysis regarding the involvement of PTEN in vioprolide A-provoked Akt activation, control experiments with cycloheximide were performed. As shown in Figure 60C, treatment with cycloheximide caused a time-dependent reduction of the PTEN protein level after 16 h to 48 h. Interestingly, however, only a short cycloheximide treatment period (1 h) induced Akt activation, while a longer treatment period (24 h) showed no influence (Figure 60D). These effects stand in contrast to the observed influence on the PTEN protein level: After 1 h of cycloheximide treatment no reduction of the PTEN protein level was observed, yet.

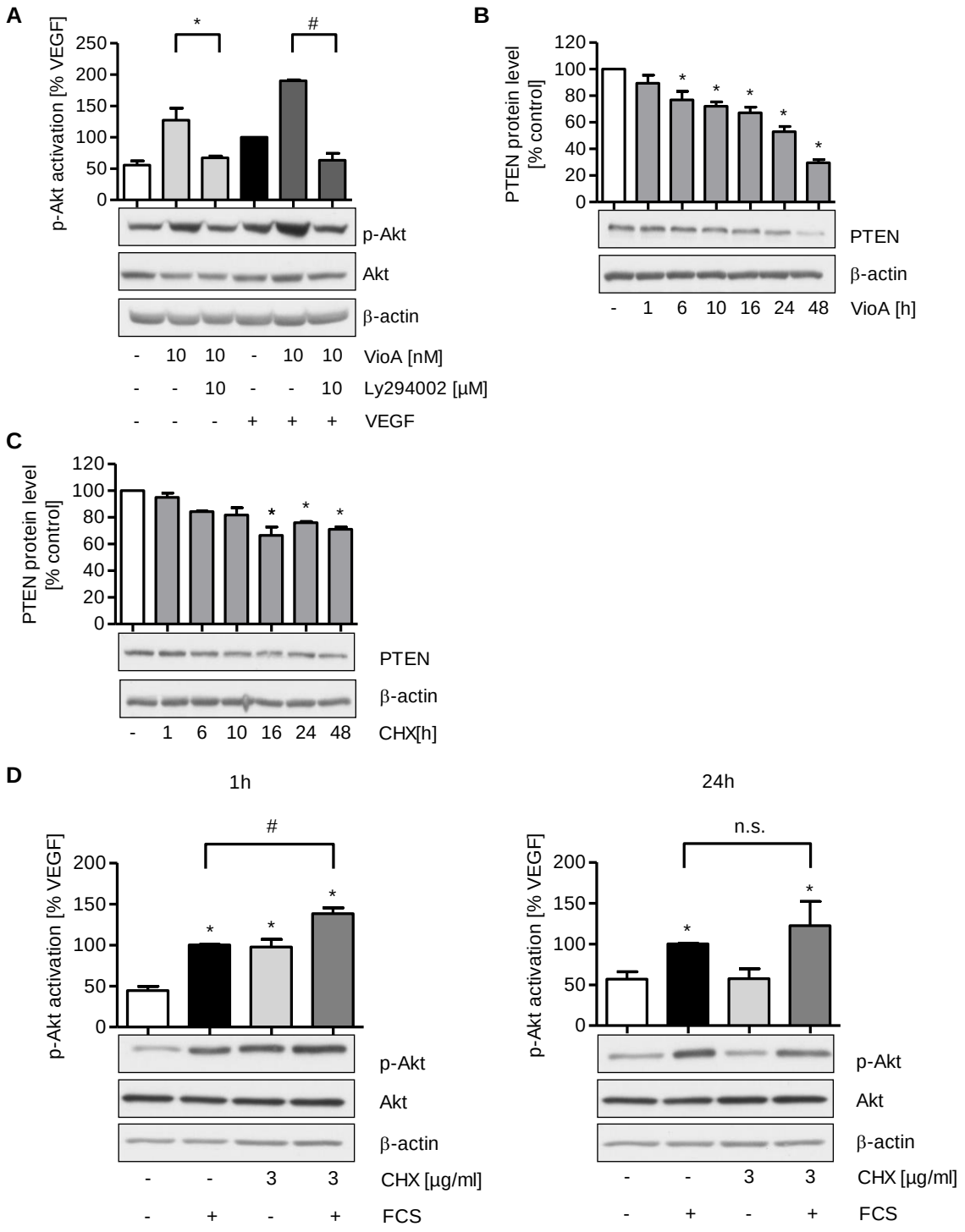

Figure 60: Vioprolide A induces Akt in a PI3K-dependent mechanism. A Confluent HUVECs were pretreated with 10 µM Ly294002 for 30 min, treated with vioprolide A (10 nM) for 16 h and activated with 10 ng/ml VEGF for 15 min. Phospho-Akt (p-Akt) protein level was determined by western blotting. One representative blot is shown. **B** Confluent HUVECs were treated with 10 nM of vioprolide A as indicated. **C** Confluent HUVECs were treated with 3 µg/ml of cycloheximide as indicated. **B**-**C** Total protein level of PTEN was examined by western blotting. One representative blot is shown. **D** Confluent HUVECs were starved overnight, treated with 3 µg/ml of cycloheximide for 1 h (left) or 24 h (right) and activated with FCS (10 % v/v) for 15 min. Total protein level of phospho-Akt (p-Akt) was determined by western blotting. One representative blot is shown. VioA, vioprolide A; CHX, cycloheximide. Data are expressed as mean ± SEM. n=3. *P ≤ 0.05 vs VioA (**A**) or control (**B**-**D**), #p ≤ 0.05 vs VEGF (**A**) or FCS (**D**).

In summary, vioprolide A reduced the protein level and phosphorylation of the cardinal angiogenesis-regulating VEGFR2. In concert with this, the VEGF-induced activation of the MAPKs ERK1/2, JNK and p38 were significantly reduced. In contrast, both the VEGF-dependent and -independent activation of the downstream signaling intermediate Akt as well as the VEGF-independent activation of eNOS were enhanced. Vioprolide A increased the activation of Akt in a PI3K-dependent mechanism, which, however, can only in part be explained by a decreased protein expression of the suppressor PTEN.

7.2 The effect of vioprolide A on the Hippo signaling pathway in HUVECs

The Hippo signaling pathway is an evolutionary conserved signaling pathway that plays a crucial role in the process of angiogenesis. In an active state, Hippo signaling prevents the nuclear translocation of transcriptional coactivators including the transcriptional coactivator TAZ. When the Hippo signaling pathway is inactivated, these transcriptional coactivators can translocate to the nucleus, where they bind to transcription factors including TEAD, thereby enhancing the expression of pro-angiogenic genes.[231-240] Thus, in the following, it was evaluated whether vioprolide A influences the Hippo signaling pathway in addition to the VEGFR2 signaling axis.

7.2.1 Vioprolide A inhibits the nuclear localization of the transcriptional co-activator TAZ in subconfluent HUVECs

In proliferating cell, the Hippo signaling pathway is inactivated, which allows TAZ nuclear translocation. In resting cells the Hippo signaling is activated leading to a retention of TAZ in the cytosol.[232,234] To investigate a potential effect of vioprolide A on the nuclear localization of TAZ, both subconfluent and confluent cells were treated with the natural product, and TAZ was visualized by immunocytochemistry. As shown in Figure 61, treatment with vioprolide A significantly reduced the nuclear accumulation of TAZ in subconfluent cells, while the basal nuclear localization of TAZ in confluent cells was not influenced by vioprolide A.

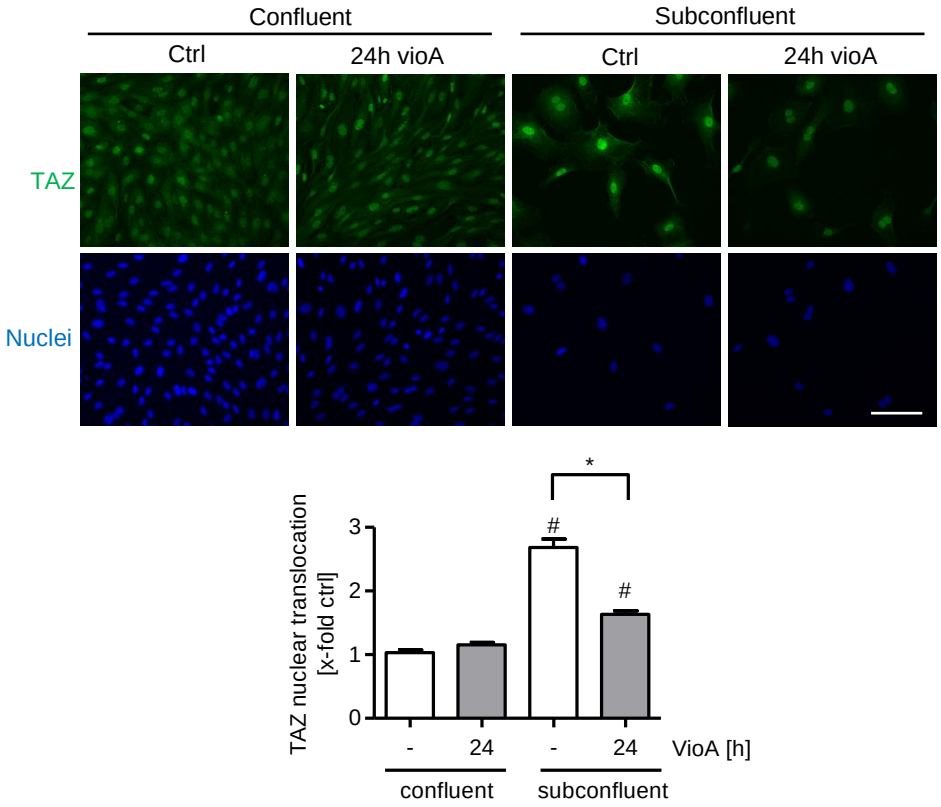

Figure 61: Vioprolide A inhibits the nuclear translocation of TAZ. HUVECs were seeded in low density or grown to confluence and treated with 10 nM of vioprolide A for 24 h. TAZ was visualized by immunocytochemistry and fluorescence microscopy. Representative images are shown. Scale bar, 100 µm. VioA, vioprolide A. Data are expressed as mean ± SEM. n=3. *p ≤ 0.05 vs subconfluent control, #p ≤ 0.05 vs confluent control.

7.2.2 The expression of angiogenic target genes of TAZ is reduced by vioprolide A

Since vioprolide A reduced the nuclear localization of TAZ in subconfluent cells, it was further examined whether also the expression of TAZ-related target genes, including *CYR61*, *CTGF*, *COL8A1* and *E2F1,* was influenced. For this purpose, subconfluent HUVECs were treated with vioprolide A for 24 h, and the mRNA expression of target genes was determined by quantitative PCR. Confluent untreated cells served as negative control. As shown in Figure 62A-D, vioprolide A treatment significantly lowered the mRNA expression of all selected pro-angiogenic TAZ target genes in subconfluent endothelial cells.

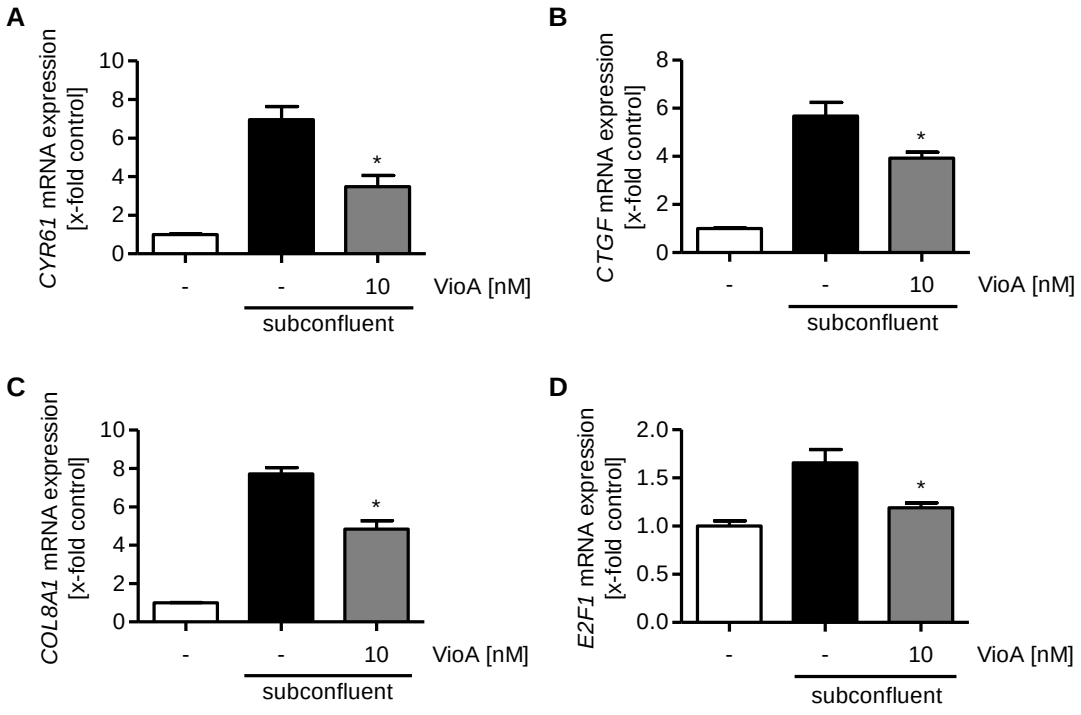

Figure 62: Vioprolide A reduces the mRNA expression of TAZ target genes. Cells were seeded in low density and treated with 10 nM of vioprolide A for 24 h. Untreated confluent cells served as negative control. The mRNA expression of *CYR61* (**A**), *CTGF* (**B**), *COL8A1* (**C**) and *E2F1* (**D**) was determined by quantitative PCR. VioA, vioprolide A. Data are expressed as mean ± SEM. n=3. *p ≤ 0.05 vs subconfluent control.

7.2.3 The total protein level of TAZ remains unchanged upon vioprolide A treatment

Due to the influence of vioprolide A on *de novo* protein synthesis and based on the observation that inhibition of mRNA translation evokes varying impacts on different proteins, it was investigated whether the reduced nuclear localization of TAZ is caused by a decrease of the TAZ total protein level or by an inhibition of the process of nuclear translocation. HUVECs were treated with vioprolide A for time periods between 1 h and 72 h, and the total protein level of TAZ was determined by western blot analysis. As shown in Figure 63A, the TAZ total protein expression remained unchanged upon vioprolide A treatment. To further evaluate if vioprolide A might specifically influence the increased TAZ protein level in subconfluent cells, HUVECs were seeded in low density and treated with vioprolide A for 24 h. Confluent cells served as negative control. In concert with the effect shown in Figure 61A, vioprolide A had no influence on the TAZ protein levels in subconfluent cells (Figure 63B).

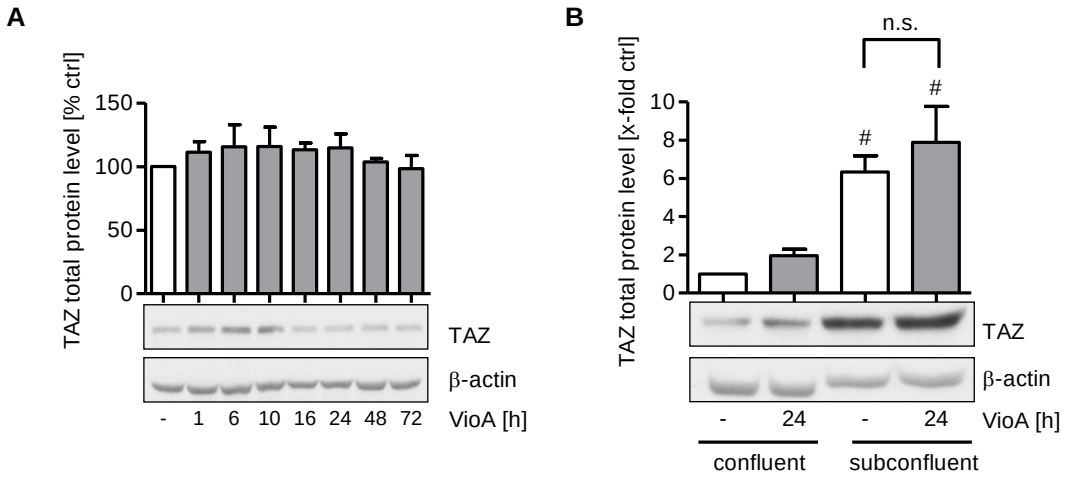

Figure 63: The protein level of TAZ remains unchanged upon vioprolide A treatment. A Confluent cells were treated with 10 nM of vioprolide A for the indicated time points. The total protein level of TAZ was determined by western blotting. One representative blot is shown. **B** Cells were seeded in low density or grown to confluence and treated with 10 nM of vioprolide A for 24 h. The protein level of TAZ was analysed by western blot experiments. One representative blot is shown. VioA, vioprolide A. Data are expressed as mean ± SEM. n=3. *p ≤ 0.05 vs subconfluent control.

7.2.4 Vioprolide A reduces the nuclear accumulation of MAML1

The release of TAZ from its cytosolic retention is an important aspect of its nuclear translocation. Nevertheless, molecular guides as well as the underlying mechanisms carrying out nuclear translocation and retention of TAZ remain unknown. Intriguingly, a functional NLS, which is available in other transcription factors like the NF-κB subunits p50 and p65, has not been reported for TAZ in mammals. However, MAML1/2 has been shown to be essential for TAZ nuclear maintenance and transcriptional activity. MAML1/2 depletion furthermore has been observed to cause cytosolic restraint of the transcriptional coactivator.[253] Considering that vioprolide A solely influenced the nuclear translocation but not the total protein expression of TAZ, a potential effect of the natural product on MAML1 was examined. HUVECs were seeded in low density or grown to confluence and treated with vioprolide A for 24 h. MAML1 was then examined by immunocytochemistry and fluorescence microscopy. Treatment of HUVECs with vioprolide A strongly reduced the nuclear localization of MAML1 both in confluent and subconfluent cells (Figure 64).

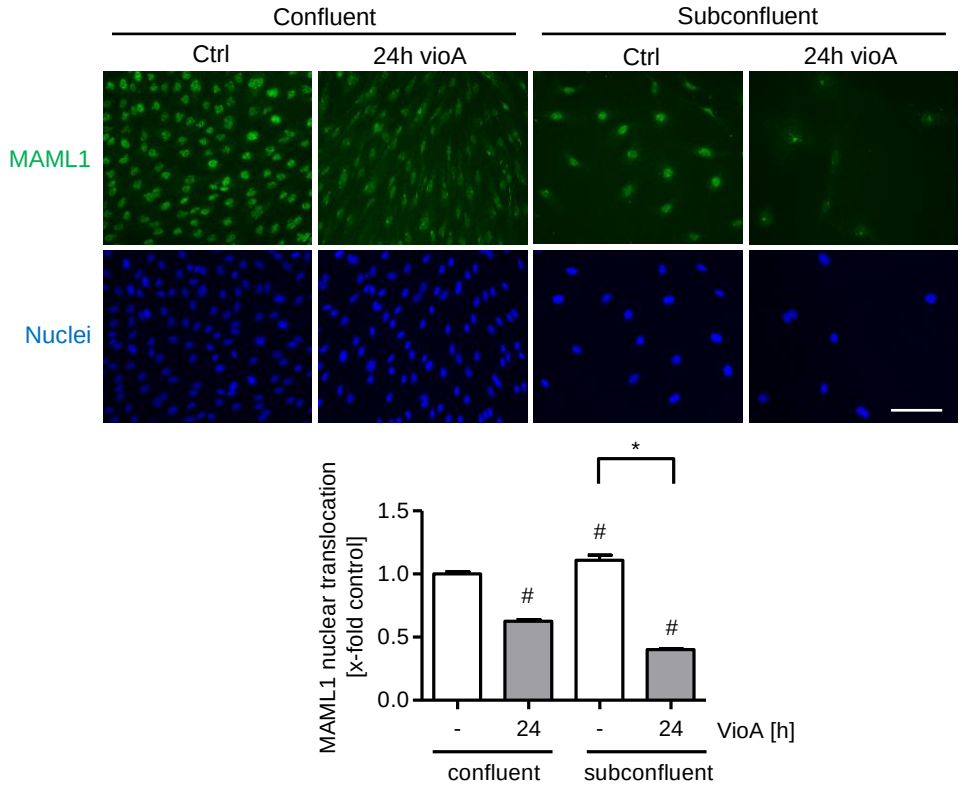

Figure 64: Vioprolide A inhibits the nuclear translocation of MAML1. HUVECs were seeded in low density or grown to confluence and treated with 10 nM of vioprolide A for 24 h. MAML1 was visualized by immunocytochemistry and fluorescence microscopy. Representative images are shown. Scale bar, 100 µm. VioA, vioprolide A. Data are expressed as mean ± SEM. n=3. *p ≤ 0.05 vs subconfluent control, #P ≤ 0.05 vs confluent control.

7.2.5 The total protein level of MAML1 in subconfluent endothelial cells is lowered by vioprolide A

Like for TAZ, we next evaluated whether the reduced nuclear localization of MAML1 was caused by a general inhibition of protein synthesis or rather by specifically impairing the nuclear accumulation of MAML1. HUVECs were treated with vioprolide A for time periods between 1 h and 72 h. While vioA had no effect on the total protein level of TAZ in confluent and subconfluent HUVECs, a time-dependent decrease of the MAML1 total protein level was observed in western blot experiments (Figure 65A). Next, the effect of vioprolide A on the increased MAML1 protein level in subconfluent cells was assessed. Thus, HUVECs were seeded in low density and treated with vioprolide A for 24 h. Confluent cells served as negative control. As shown in Figure 65B, the increased MAML1 protein expression in subconfluent HUVECs was effectively downregulated by the natural product. Notably, the inhibitory effect of vioprolide A on the MAML1 protein expression was stronger in subconfluent compared to confluent HUVECs. In summary, the downregulation of TAZ-mediated pro-angiogenic gene expression is most likely caused by a reduced nuclear retention of TAZ through decreasing the MAML1 total protein level.

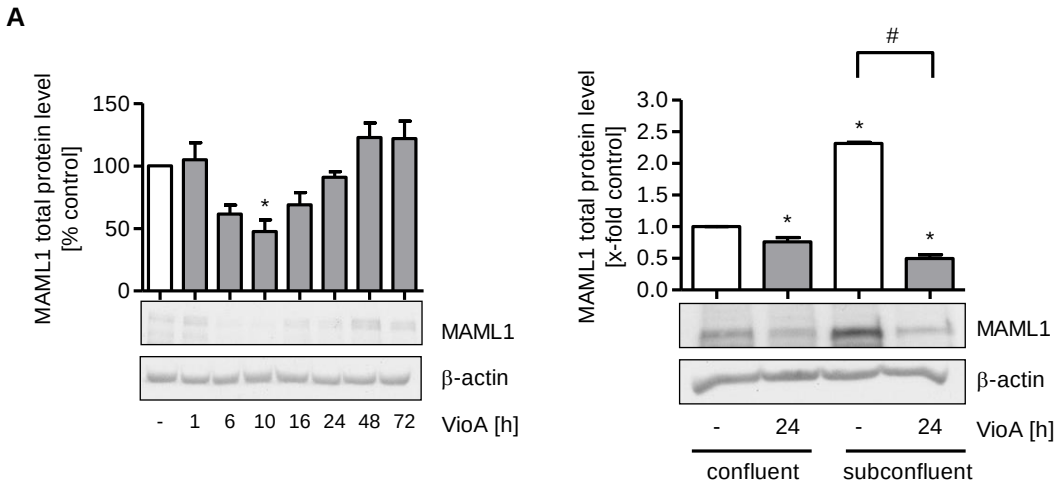

Figure 65: Vioprolide A decreased the MAML1 protein expression in HUVECs. A Confluent HUVECs were treated with 10 nM of vioprolide A for the indicated time points. The total protein level of MAML1 was determined by western blotting. One representative blot is shown. **B** Cells were seeded in low density or grown to confluence and treated with 10 nM of vioprolide A for 24 h. The protein level of MAML1 was analysed by western blot experiments. One representative blot is shown. VioA, vioprolide A. Data are expressed as mean ± SEM. n=3. *p ≤ 0.05 vs control (**A**) or confluent control (**B**), #p ≤ 0.05 vs. subconfluent control.

7.3 Pro-survival actions of vioprolide A in endothelial cells

Despite strong effects on endothelial cells including anti-angiogenic and anti-inflammatory ones, it was shown in section V.2 that up to 10 nM of vioprolide A do not impair the viability of endothelial cells. In addition, analysis of intracellular signaling events showed a strong induction of Akt by vioprolide A. Enhanced Akt signaling is an important pro-survival response. Interestingly, however, in patient-derived acute lymphoblastic leukemia cells, 10 nM of vioprolide A already induces an apoptosis rate of 10–30 %.[311] Thus, we next evaluated whether vioprolide A induces pro-survival signaling in endothelial cells.

7.3.1 Vioprolide A reduces the starvation-induced late apoptosis of endothelial cells

In different studies, serum starvation has been shown to induce cell apoptosis by downregulating pro-survival signaling molecules, such as Bcl-2, and by increasing the expression of pro-apoptotic proteins, such as p53, and via cleavage of caspases.[430-432] To investigate the influence of vioprolide A on apoptosis induced by serum starvation in endothelial cells, HUVECs were deprived of serum and treated with the natural product for 24 h and 48 h. Staurosporine served as positive control for the induction of apoptosis. The percentage of late apoptotic cells was then determined using propidium iodide staining. Vioprolide A concentration-dependently and significantly reduced the number of cells in late apoptosis after both 24 h and 48 h compared to the control treatment (Figure 66). After 48 h the anti-apoptotic effect of vioprolide A was even stronger compared to 24 h of treatment.

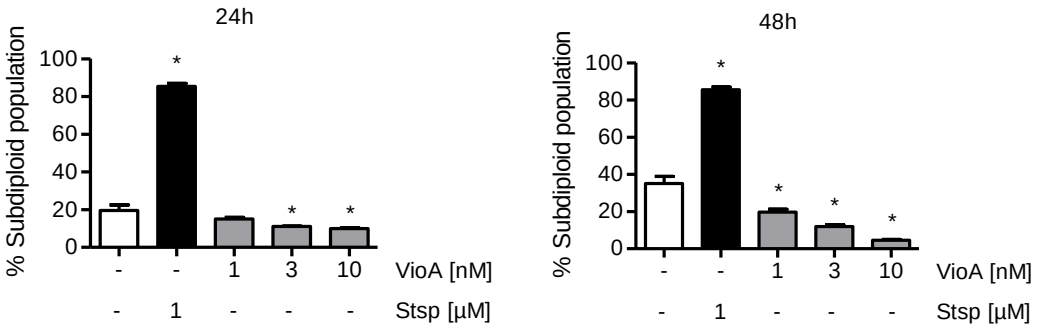

Figure 66: Vioprolide A reduces the serum starvation induced late apoptosis in HUVECs. Confluent HUVECs were treated with vioprolide A (1, 3, 10 nM) for 24 h (left) or 48 h (right) in starvation medium. Staursporine (1 µM) served as positive control for inducing apoptosis. HUVECs were stained with propidium iodide (PI), and late apoptosis was measured by analysing the percentage of sub-diploid events via flow cytometry. VioA, vioprolide A; Stsp, staurosporine. Data are expressed as mean ± SEM. n=3. *p ≤ 0.05 vs. control.

7.3.2 The cleavage of procaspase-3 is inhibited by vioprolide A

As shown in section V.7.1.4-7.1.5, vioprolide A induced the activation of Akt. Akt is an important pro-survival kinase that prevents the cleavage of procaspases into their active forms, which are involved in programmed cell death.[433] Cleavage of procaspase-3 can be induced via DNA damaging agents, such as the chemotherapeutic drug doxorubicin.[434] Hence, to examine whether vioprolide A evokes its pro-survival effects through inhibition of caspase-3 signaling, the total protein level and cleavage of procaspase-3 were observed. The total protein level of procaspase-3 was determined by western blot analysis after treatment of HUVECs with vioprolide A for time periods between 1 h and 48 h. As depicted in Figure 67A, vioprolide A treatment had no effect on the total protein level of procaspase-3. Next, the cleavage of procaspase-3 was investigated by western blotting, and doxorubicin served as positive control for the induction of procaspase cleavage. Treatment with doxorubicin for 24 h caused a significant increase of cleaved caspase-3 compared to untreated control cells. When cells were pretreated for 24 h with vioprolide A prior to the addition of doxorubicin for further 24 h, the level of cleaved caspase-3 was not detectable anymore (Figure 67B). This indicates a strong inhibitory action of vioprolide A on caspase cleavage. To further assess whether the vioprolide A induced Akt activation is involved in the inhibition of caspase cleavage, the PI3K-inhibitor Ly294002 was used. As demonstrated in Figure 67C, pretreatment with Ly294002 prior to vioprolide A treatment offset the vioprolide A evoked cleavage inhibition. Hence, vioprolide A increased the endothelial pro-survival signaling through Akt-mediated reduction of procaspase-3 cleavage.

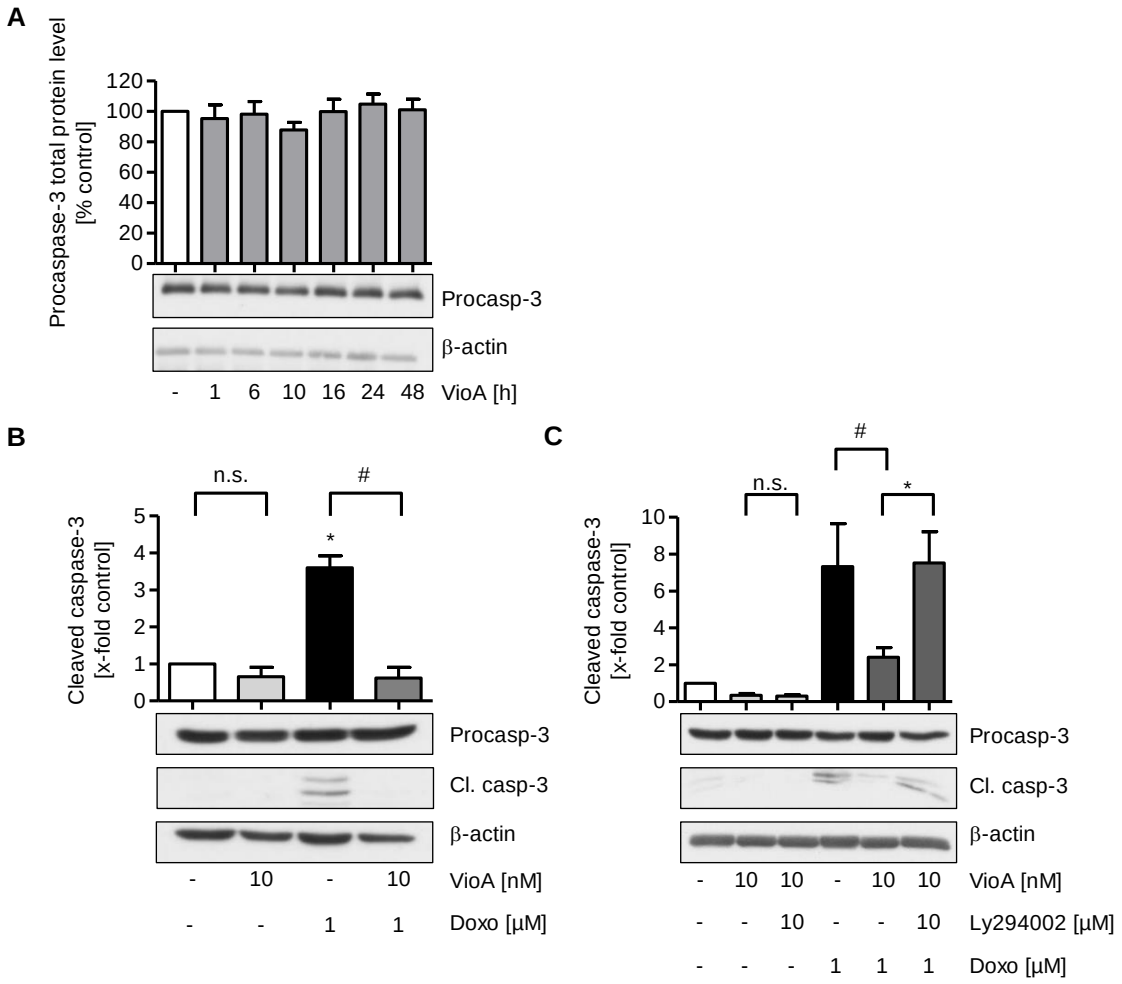

Figure 67: Vioprolide A decreases the cleavage of procaspase-3 via an Akt-dependent mechanism. A Confluent HUVECs were treated with 10 nM of vioprolide A for the indicated time points. Total protein level of procaspase-3 was determined by western blotting. One representative blot is shown. **B** Confluent HUVECs were pretreated with 10 nM of vioprolide A for 24 h followed by activation with 1 µM doxorubicin for 24 h. The total protein levels of procaspase-3 (Procasp-3) and cleaved caspase-3 (Cl. casp-3) were analysed by western blot experiments. One representative blot is shown. **C** Confluent HUVECs were pretreated with 10 µM Ly294002 for 30 min, treated with 10 nM of vioprolide A for 24 h and activated with 1 µM of doxorubicin for 24 h. Total protein levels of procaspase-3 and cleaved caspase-3 were examined by western blot analysis. One representative blot is shown. VioA, vioprolide A; Doxo, doxorubicin; Procasp-3, procaspase-3; Cl. casp-3, cleaved caspase-3. Data are expressed as mean ± SEM. n=3. *p ≤ 0.05 vs. control (**B**) or VioA+Doxo (**C**), #p ≤ 0.05 vs. Doxo.

7.3.3 Vioprolide A downregulates the expression of pro-apoptotic genes

Doxorubicin has been shown to reduce cell survival by activation of p53-dependent apoptosis.[435] Upon cellular stress, including DNA damage, p53 is upregulated and iniates the transcription of pro-apoptotic genes such as *NOXA* and *APAF1*, which then cleave procaspases.[436] Thus, it was investigated whether vioprolide A reduced the doxorubicin-induced expression of p53 target genes. For this, HUVECs were treated with vioprolide A for 24 h followed by activation with doxorubicin for 24 h. The expression *NOXA* and *APAF1* was then determined by quantitative PCR. Pretreatment with vioprolide A for 24 h strongly downregulated the doxorubicin induced mRNA expression of *NOXA* and *APAF1* (Figure 68).

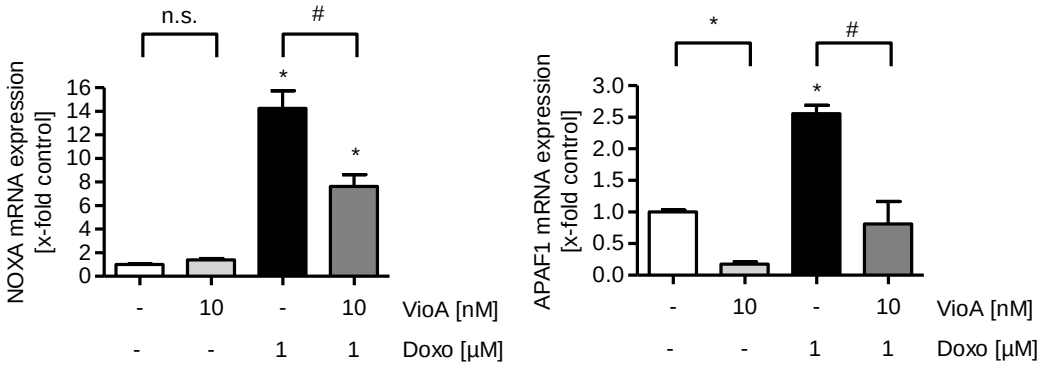

Figure 68: Vioprolide A inhibits the doxorubicin-induced expression of pro-apoptotic genes. Confluent HUVECs were treated with 10 nM of vioprolide A for 24 h and activated with 1 µM doxorubicin for 24 h. The mRNA expression of *NOXA* (left) and *APAF1* (right) was determined by quantitative PCR. VioA, vioprolide A; Doxo, doxorubicin. Data are expressed as mean ± SEM. n=3. *p ≤ 0.05 vs. control, #p ≤ 0.05 vs. Doxo.

7.3.4 The DNA damage-induced increase in the nuclear accumulation of p53 is lowered by vioprolide A

In a normal state, the cellular p53 protein level is low, as the protein is constantly ubiquitinated and degraded. Upregulation of the p53 protein level is caused by a DNA damage-induced increase of p53 mRNA expression and a prevention of p53 degradation through protein stabilization. Besides the increase of the total p53 protein level, nuclear translocation of p53 is highly important for the induction of p53-dependent gene expression.[435,436] To examine if the reduced mRNA expression of *NOXA* and *APAF1* is linked to an impairment of p53 by vioprolide A, its total as well as nuclear protein level was analysed by cell fractionation and western blotting. Doxorubicin treatment served as positive control for p53 nuclear accumulation. As shown in Figure 69A, vioprolide A time-dependently lowered the basal p53 total protein levels in HUVECs. A significant decrease was observed already after 6 h and lasted up to 48 h of treatment. Besides influencing the basal p53 protein level, pretreatment with vioprolide A for 24 h strongly reduced the doxorubicin-evoked nuclear accumulation of p53 (Figure 69B).

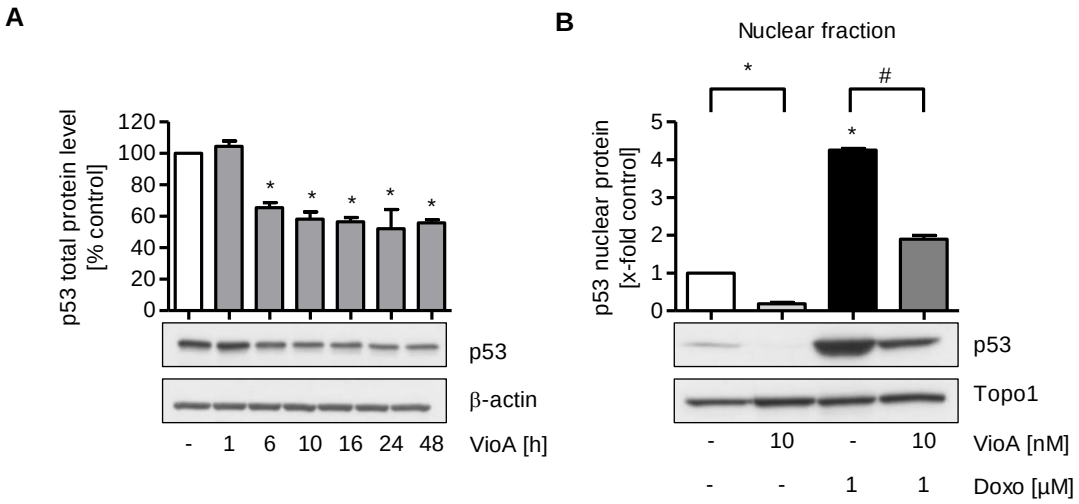

Figure 69: Vioprolide A reduces the p53 protein level and nuclear accumulation. A Confluent HUVECs were treated with 10 nM of vioprolide A for the indicated time points. Total protein level of p53 was determined by western blotting. One representative blot is shown. **B** Confluent HUVECs were treated with 10 nM of vioprolide A for 24 h and activated with 1 µM doxorubicin for 16 h. The nuclear cell fraction was separated, and the nuclear p53 protein level was investigated by western blot analysis. One representative blot is shown. VioA, vioprolide A; Doxo, doxorubicin; Topo1, topoisomerase 1. Data are expressed as mean ± SEM. n=3. *p ≤ 0.05 vs. control, #p ≤ 0.05 vs. Doxo.

7.3.5 Vioprolide A prevents the cleavage of the E3 ubiquitin-protein ligase MDM2

The E3 ubiquitin-protein ligase murine double minute 2-protein (MDM2) is responsible for the ubiquitination and, thus, degradation of p53, which keeps basal p53 at a low level. Cleavage of full-length MDM2 between residues 361 and 362 by activated caspases removes the C-terminal RING finger domain and builds a 60 kDa isoform. Interestingly, cleaved MDM2 takes part in a positive feedback loop for p53 activation, as it stabilizes rather than degrades the pro-apoptotic protein.[437] To investigate if the inhibitory actions observed on p53 by vioprolide A are related to an effect on MDM2, its total protein level and doxorubicin-induced cleavage were analysed. Treatment of HUVECs with vioprolide A for time periods between 1 h and 72 h showed no change in the total protein level of MDM2, indicating that the full-length protein is highly stable in viable cells (Figure 70A). While doxorubicin strongly upregulated the cleavage of MDM2 into its 60 kDa isoform, pretreatment with vioprolide A for 24 h completely abolished the presence of doxorubicin-induced 60 kDa MDM2 (Figure 70B).

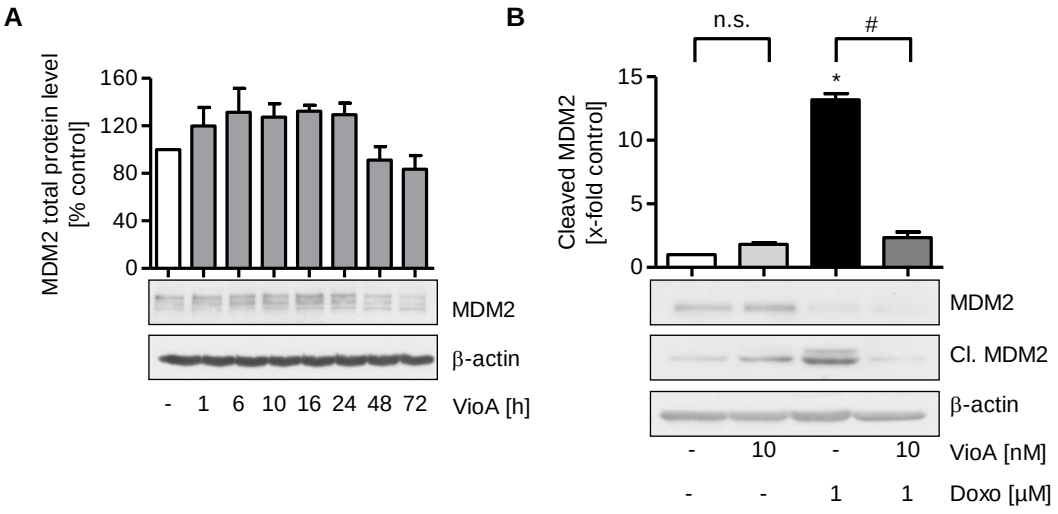

Figure 70: Vioprolide A prevents the doxorubicin-induced cleavage of MDM2. A Confluent HUVECs were treated with 10 nM of vioprolide A for the indicated time points. Total protein level of full-length MDM2 was determined by western blotting. One representative blot is shown. **B** Confluent HUVECs were treated with 10 nM of vioprolide A for 24 h and activated with 1 µM doxorubicin for 16 h. Total protein levels of MDM2 and cleaved MDM2 (Cl. MDM2) were determined by western blot analysis. One representative blot is shown. VioA, vioprolide A; Doxo, doxorubicin; Cl. MDM2, cleaved MDM2. Data are expressed as mean ± SEM. n=3. *p ≤ 0.05 vs. control, #p ≤ 0.05 vs. Doxo.

7.3.6 The inhibition of MDM2 cleavage but not of p53 protein upregulation relies on vioprolide A-induced Akt activation

To investigate whether the inhibition of p53-dependent apoptosis by vioprolide A, including reduced MDM2 cleavage and p53 nuclear accumulation, depend on the increased activation of Akt in HUVECs, the PI3K inhibitor Ly294002 was used. HUVECs were pretreated with Ly294002 for 30 min followed by treatment with vioprolide A for 24 h and activation with doxorubicin for 16 h. As shown in Figure 71A, pretreatment with Ly294002 led to a recovery of the MDM2 cleavage compared to vioprolide A treatment alone. Surprisingly, however, pretreatment with Ly294002 was not able to reverse the vioprolide A-evoked reduction of doxorubicin-induced p53 protein expression (Figure 71B).

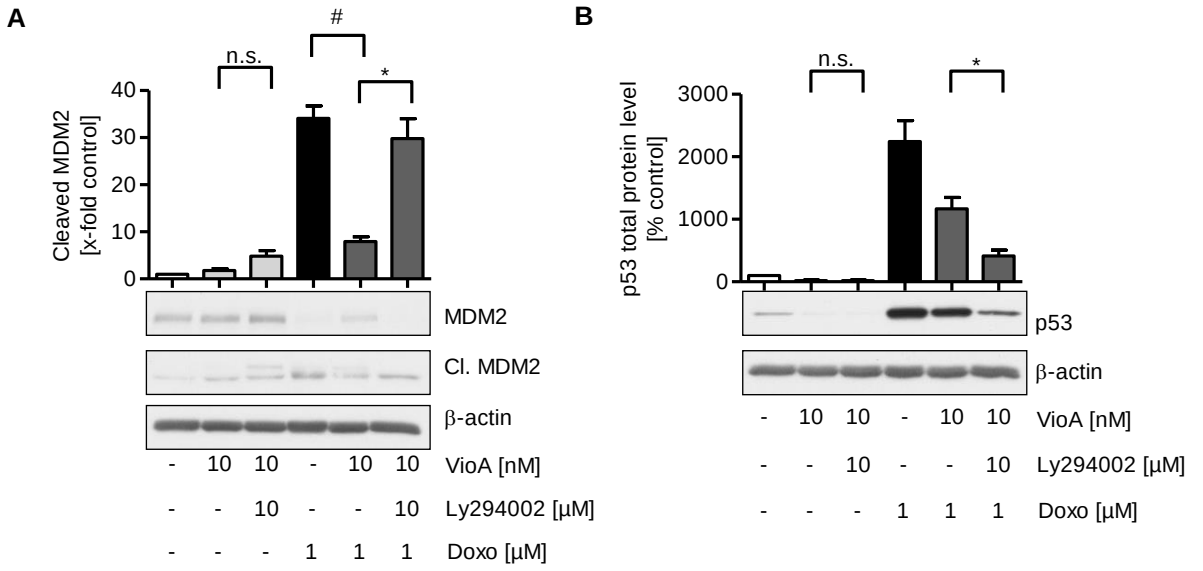

Figure 71: Vioprolide A-evoked effects on MDM2 cleavage, but not on p53 protein levels, is Akt-dependent. **A**-**B** Confluent HUVECs were pretreated with 10 µM Ly294002 for 30 min followed by treatment with 10 nM of vioprolide A for 24 h and activation with 1 µM doxorubicin for 16 h. Total protein levels of MDM2 (**A**), cleaved MDM2 (Cl. MDM2, **A**) and p53 (**B**) were determined by western blot analysis. One representative blot is shown. VioA, vioprolide A; Doxo, doxorubicin. Data are expressed as mean ± SEM. n=3. *p ≤ 0.05 vs. VioA+Doxo, #p ≤ 0.05 vs. Doxo.

In summary, vioprolide A activated pro-survival signaling in endothelial cells through an Akt-dependent inhibition of procaspase-3 cleavage and an, at least partially, Akt-independent suppression of the increase in p53 protein levels and expression of its pro-apoptotic target genes *NOXA* and *APAF1*.

7.4 Involvement of the cellular target NOP14 in the anti-angiogenic actions of vioprolide A

NOP14 is a ribosomal protein, which participates in the ribosome biogenesis, an upstream regulator of mRNA translation.[312] Considering, that mRNA translation is frequently upregulated in cancer cells, NOP14 has previously been studied regarding its involvement in tumor angiogenesis. Interestingly, the downregulation of NOP14 shows contradictory effects in different tumor cell types. Hence, NOP14 seems to evoke a cell-type specific effect on angiogenic processes.[314,315,321,322] To evaluate whether the anti-angiogenic actions of vioprolide A in HUVECs are caused by the interaction with and, thus, inhibition of NOP14, key angiogenic events were investigated upon siRNA-mediated knockdown of the nucleolar protein. The successful knockdown of NOP14 has already been demonstrated in Figure 46.

7.4.1 NOP14 knockdown reduces the undirected and chemotactic migration of endothelial cells

To investigate the effect of NOP14 knockdown on the undirected cell migration, a scratch assay was performed 48 h after siRNA transfection. As shown in Figure 72A, knockdown of NOP14 significantly reduced the covered area and, thus, undirected migration of HUVECs compared to non-targeting control siRNA treatment. To assess if NOP14 knockdown has a general effect on cell migration, also the directed migration was examined. A Boyden chamber experiment was performed with FCS as a chemoattractant. The serum-induced active migration of HUVECs was significantly lowered upon NOP14 knockdown (Figure 72B). In summary, inhibition of NOP14 impaired the cell migration of endothelial cells.

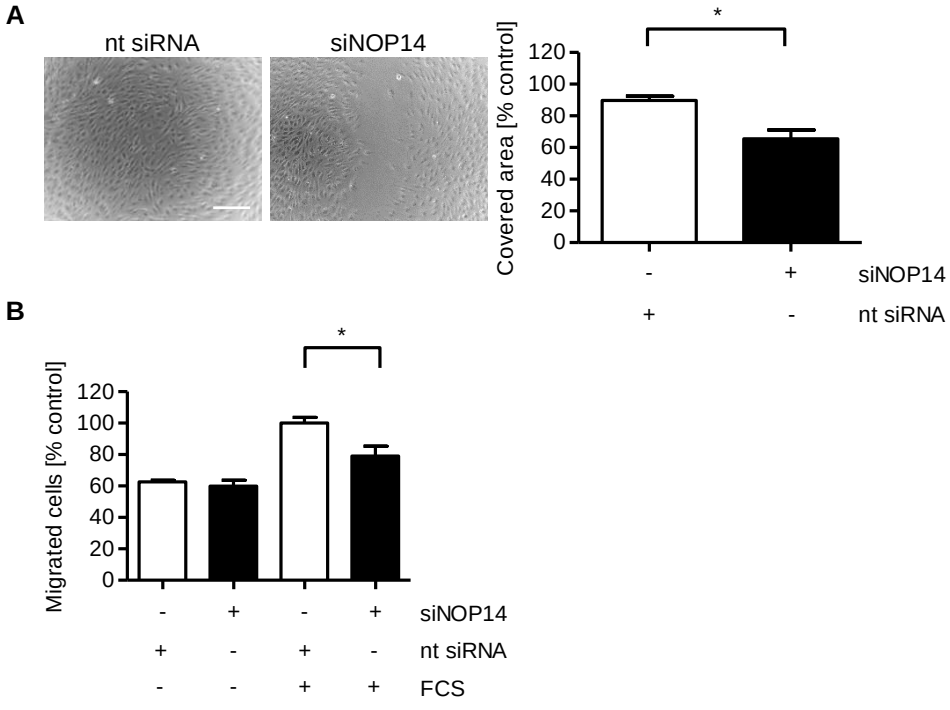

Figure 72: Knockdown of NOP14 impairs endothelial cell migration. Subconfluent cells were transfected with siRNA against NOP14 (siNOP14, 80 nM) or non-targeting siRNA (nt siRNA, 80 nM) using the GeneTrans II Transfection Reagent. **A** 48 h after transfection, a scratch was inflicted to the HUVEC monolayer, and the cells were allowed to migrate for 12 h either in starvation medium (1 % FCS; 0 % migration) or in growth medium (10 % FCS; 100 % migration) until the control siRNA treated-cells had closed the scratch. Microscopical images were taken, and the covered area was analysed using the ImageJ software. Scale bar, 200 µm. **B** 48 h after transfection, HUVECs were seeded to the porous filter membrane of Transwell inserts (pore size 8 µm) and allowed to adhere for 4 h. Cells were then allowed to migrate towards a chemotactic gradient (20 % FCS) for 16 h. Migrated cells were stained with crystal violet solution, and absorbance measurement was performed at 540 nm. Data are expressed as mean ± SEM. n=3. *p ≤ 0.05 vs. nt siRNA.

7.4.2 Knockdown of NOP14 reduces the DNA synthesis in endothelial cells

In the next step, a potential role of NOP14 in the process of DNA synthesis, which is a solid indicator for cell proliferation, was examined. For this, the relative amount of incorporated BrdU into newly synthesized DNA was examined upon NOP14 knockdown. As shown in Figure 73, knockdown of NOP14 signifiifantly reduced the BrdU incorporation into the DNA of HUVECs to approximately 80 % of non-targeting control siRNA-treated cells.

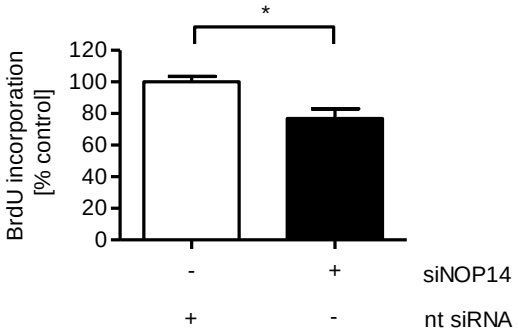

Figure 73: Knockdown of NOP14 impairs the BrdU incorporation into proliferating endothelial cells. Subconfluent cells were transfected with siRNA against NOP14 (siNOP14, 80 nM) or non-targeting siRNA (nt siRNA, 80 nM) using the GeneTrans II Transfection Reagent. 24 h after transfection, HUVECs were seeded in low density and grown for 16 h followed by serum-starvation for 8 h. The medium was refreshed with new full growth medium for a total period of 24 h. 8 h before the treatment endpoint, BrdU (10 µM) was added to the cells. The relative amount of incorporated BrdU was determined using flow cytometry. Data are expressed as mean ± SEM. n=5. *p ≤ 0.05 vs. nt siRNA.

7.4.3 The VEGF-induced sprouting of endothelial cells is increased by NOP14 knockdown

Besides endothelial cell migration and proliferation, we investigated how NOP14 knockdown would influence the VEGF-induced endothelial cell sprouting. Therefore, siRNA-mediated knockdown of NOP14 was conducted followed by spheroid formation using the hanging drop method. After embedding the spheroids into a collagen gel, cell sprouting was induced by VEGF. Surprisingly and in contrast to vioprolide A treatment, NOP14 knockdown caused no inhibitory effect on the VEGF-induced sprouting of endothelial cell spheroids but rather increased the stimulus-induced total sprout length and number of sprouts per spheroid compared to the non-targeting control siRNA treated spheroids. Moreover, NOP14 knockdown significantly enhanced the basal, VEGF-independent total sprout length and number of sprouts per spheroid (Figure 74).

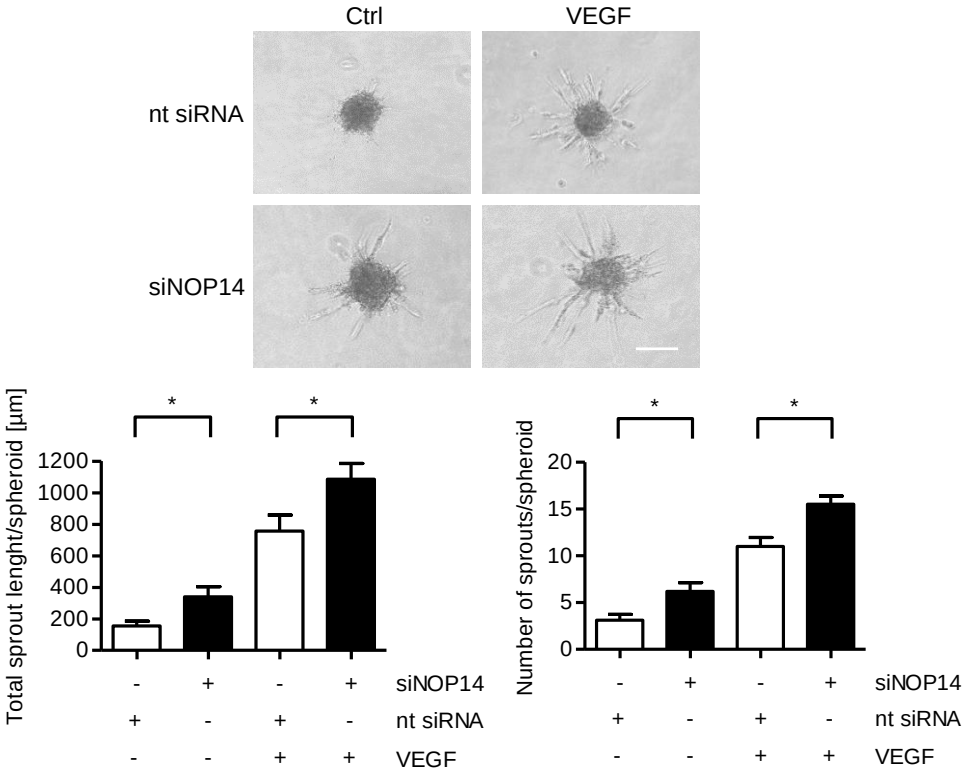

Figure 74: NOP14 knockdown increased the VEGF-dependent and -independent endothelial cell sprouting. 24 h after transfection, HUVEC spheroids were built using the hanging drop method. After embedding the spheroids into a collagen gel, VEGF (10 ng/ml) was added for 20 h. Microscopical pictures were taken, and the total sprout length and number of sprouts per spheroid were analysed using the ImageJ software. Scale bar, 100 µm. Ctrl, control A. Data are expressed as mean ± SEM. n=3. *p ≤ 0.05 vs. nt siRNA.

In summary, the results observed for NOP14 knockdown experiments only partially corresponded to the effects of vioprolide A on angiogenic processes in HUVECs. While NOP14 knockdown reduced the undirected and directed migration and proliferation of endothelial cells like vioprolide A, the effect of the nucleolar protein and vioprolide A on the process of cell sprouting considerably differed from each other. These results indicate that the inhibition of NOP14 by vioprolide A is only in part involved in the anti-angiogenic actions of vioprolide A.

7.4.4 NOP14 knockdown decreases the VEGF-induced activation of JNK and ERK

Besides evaluating the actions of NOP14 knockdown on functional aspects of angiogenesis in endothelial cells, it is equally important to assess whether inhibition of NOP14 knockdown is involved in the cellular mode of action of vioprolide A. For this, HUVECs were transfected with siRNA against NOP14 or non-targeting siRNA as control, and the phosphorylation of the kinases ERK, JNK and Akt was evaluated 48 h after transfection using western blotting. NOP14 knockdown significantly reduced the VEGF-induced activation of both ERK1/2 (Figure **75**A) and JNK (Figure 75B) without influencing the basal phosphorylation of both kinases. At the same time, both the VEGF-dependent and -independent phosphorylation of Akt was significantly increased by NOP14 knockdown (Figure 75C). Hence, the effects of NOP14

knockdown on the activation of MAPKs and Akt corresponds to the actions observed for vioprolide A treatment.

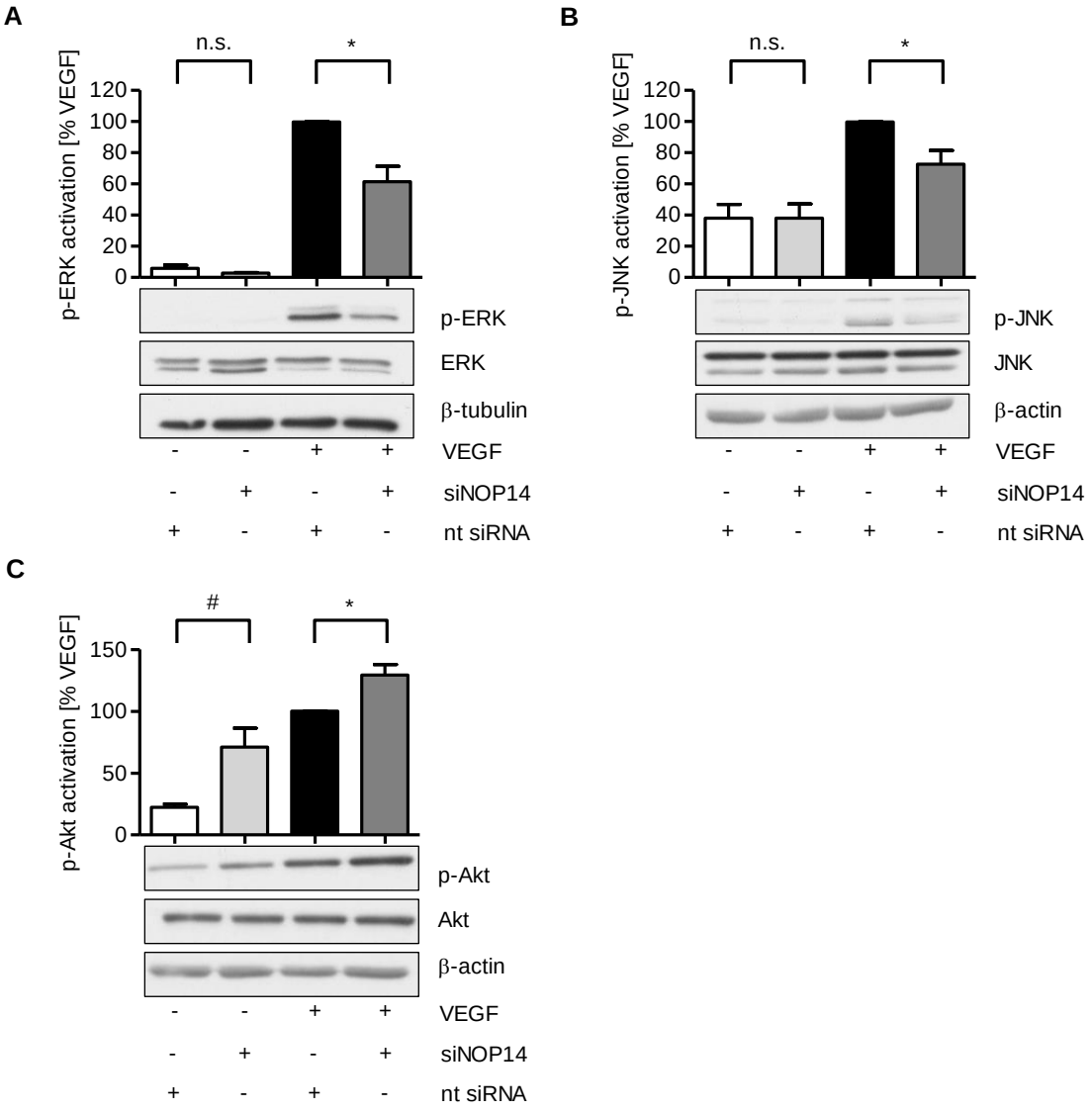

Figure 75: NOP14 knockdown decreases the VEGF-induced phosphorylation of ERK1/2 and JNK and increases the activation of Akt. Subconfluent cells were transfected with siRNA against NOP14 (siNOP14, 80 nM) or non-targeting siRNA (nt siRNA, 80 nM) using the GeneTrans II Transfection Reagent. 36 h after transfection, cells were serum-starved overnight, and 10 ng/ml VEGF was added for 5 min (**A**) or 15 min (**B, C**). Total protein levels of phospho-ERK (p-ERK, **A**), phospho-JNK (p-JNK, **B**) and phospho-Akt (p-Akt, **C**) were determined by western blotting. One representative blot is shown. Data are expressed as mean ± SEM. n=3 (**B**), n=4 (**A**, **C**). #p ≤ 0.05 vs. nt siRNA, *p ≤ 0.05 vs. nt siRNA+VEGF.

7.4.5 The nuclear translocation of TAZ is impaired by knockdown of NOP14

Considering that the effects of NOP14 knockdown on the angiogenic key features of HUVECs partially differed from the actions observed for vioprolide A and NOP14 knockdown still provided similar reducing effects on the VEGF-induced activation of the MAPKs ERK and JNK and Akt, we were interested how NOP14 deletion would affect the Hippo signaling pathway. Hence, siRNA-mediated knockdown was performed and TAZ was immunostained in dense

and sparse HUVECs 48 h later. NOP14 knockdown significantly reduced the nuclear translocation of TAZ in subconfluent cells, while the relative amount of TAZ in confluent HUVECs was not altered. These data are consistent with the effects observed for vioprolide A treatment (Figure 76).

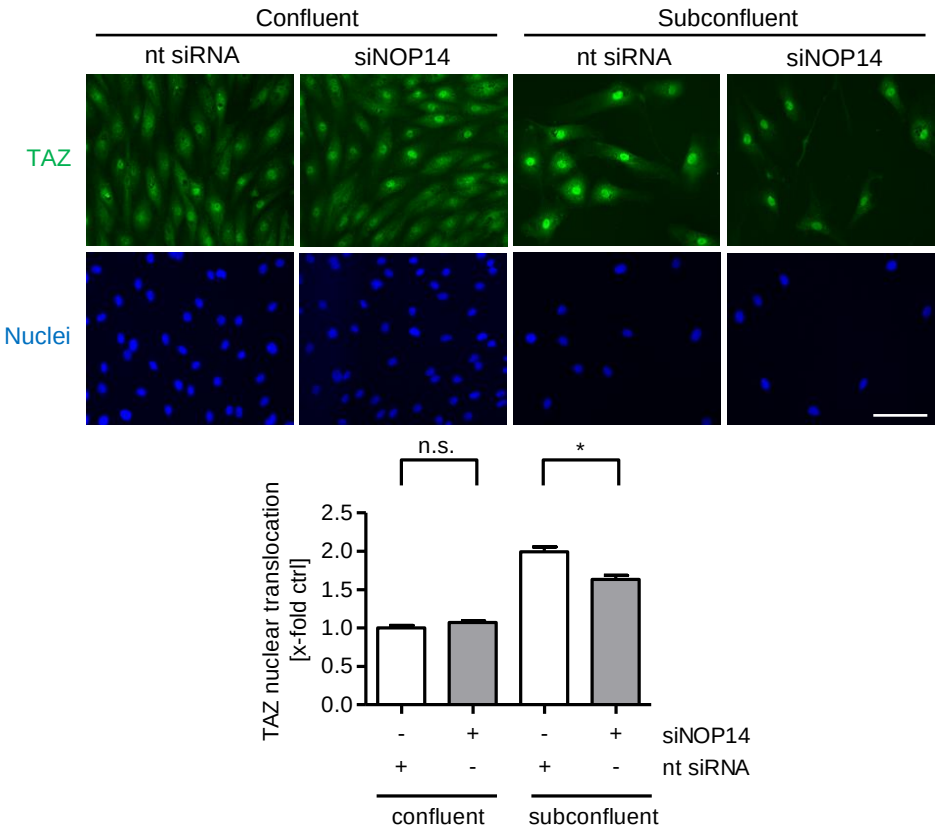

Figure 76: NOP14 knockdown loweres the nuclear translocation of TAZ in subconfluent HUVECs. Subconfluent cells were transfected with siRNA against NOP14 (siNOP14, 80 nM) or non-targeting siRNA (nt siRNA, 80 nM) using the GeneTrans II Transfection Reagent. 24 h after transfection, 4 x 10^3 cells or 5 x 10^4 cells were reseeded into new wells for monitoring TAZ cellular distribution in a subconfluent and confluent cell density, respectively. After 24 h, TAZ was visualized by immunocytochemistry and fluorescence microscopy. Representative images are shown. Scale bar, 100 µm. Data are expressed as mean ± SEM. n=4. *p ≤ 0.05 vs subconfluent nt siRNA.

In summary, NOP14 knockdown and vioprolide A treatment showed the same tendency regarding the activation of the VEGFR2 downstream signaling intermediates ERK1/2, JNK and Akt and the nuclear translocation of the transcriptional coactivator TAZ. These observations lead to the conclusion, the the differing effects of viopolide A and NOP14 on VEGF-induced endothelial cell sprouting rely on the differential influence of both on another, distinct cellular event.

VI DISCUSSION

1. The role of vioprolide A as inhibitor of eukaryotic protein biosynthesis

In a recent study, NOP14 has been identified by thermal proteome profiling as direct interaction partner of vioprolide A in Jurkat cells.[311] To ensure that vioprolide A interacts with NOP14 also in HUVECs, a cellular thermal shift assay (CETSA) was performed. Treatment with high concentrations (300 nM) of vioprolide A for short time periods shifted the aggregation temperature of NOP14 from 46.1 °C to 48.2 °C. Thus, in HUVECs, NOP14 is a direct target of vioprolide A. Interestingly, the molecular structure of the natural product contains a rare trans-(2*S*, 4*R*)-4-methylazetidinecarboxylic acid (MAZ) moiety, which has only been reported for two other natural products, namely vioprolide C and bonnevillamide A.[304, 305] In contrast to the vioprolides, which are cyclic peptides, bonnevillamide A is a linear peptide. It would be beneficial to investigate if the MAZ moiety is essential for the binding to NOP14 or if other additional factors, including the cyclic structure, are needed. Interestingly, the cytotoxicity of vioprolide B on L929 cells has been reported to be slightly stronger (LD_{50} of 20 ng/ml) compared to vioprolide C (LD_{50} of 30 ng/ml). Thus, although vioprolide B does not contain the MAZ moiety, its potency is comparably high compared to the MAZ-containing vioprolide C. On the contrary, vioprolide A has been demonstrated to evoke a 10-fold higher cytotoxicity in L929 cells (LD_{50} of 2 ng/ml) compared to vioprolide B and C.[304] Comparative studies should be performed regarding the cellular targets and biological activities of diverging vioprolides to shed more light on their specific mechanisms of action.

NOP14 is involved in the formation of an early 40S subunit precursor, called small subunit processome, during ribosome biogenesis.[312] Ribosome biogenesis is needed to provide the translational machinery with functional small and large ribosomal subunits. This process is mainly conducted in nucleoli, small nuclear inclusions which provide genes encoding for rRNAs that establish the backbone of the ribosomes.[325-328] Thus, through disturbing NOP14 functions and rRNA production, vioprolide A could evoke a reduction in the translational rate. Indeed, first *in vitro* investigations in a eukaryotic cell-free translation system have demonstrated an inhibitory effect of vioprolide A on mRNA translation with an IC_{50} of 112 nM.[310] In our study, we used a protein synthesis assay, which consists of a puromycin alkyne analogue that interacts with nascent polypeptide chains and can be visualized by coupling the alkyne group with a fluorophore followed by fluorescence microscopy. Vioprolide A evoked a concentration- and time-dependent effect on the *de novo* synthesis of polypeptide chains. Importantly, HUVECs recovered from the inhibition of mRNA translation after vioprolide A treatment periods of 24 h or longer. Hence, the downregulation of *de novo* protein synthesis by vioprolide A is reversible. Cell-free translation systems, as used for initial investigations regarding the effect of vioprolide A on *in vitro* protein synthesis, provide all basic components, including fully mature

80S ribosomes, to translate a specific input mRNA.[438] Hence, for cell-free translation systems, ribosomal assembly proteins, like NOP14, are dispensable. These observations raise the question, whether the interaction between NOP14 and vioprolide A is indeed responsible for the downregulation of *de novo* protein biosynthesis. In this regard, it should be emphasized that the IC_{50} value of vioprolide A in cell-free translation systems is approximately 7-fold higher (112 nM) compared with the IC_{50} value observed on protein synthesis in intact HUVECs (17 nM). Moreover, cell-free translation systems have been incubated with vioprolide A for only 40 min, whereas in HUVECs only longer treatment periods between 10 h and 24 h revealed an inhibitory effect of vioprolide A on mRNA translation. Thus, high concentrations of vioprolide A might affect more or differential aspects of mRNA translation compared to the concentrations we used in cellular systems.

Important interaction partners of NOP14 are NOC4L and EMG1.[311] NOC4L guides the nucleolar localization of NOP14, while EMG1 participates in the maturation of the 18S rRNA and biogenesis of the 40S ribosomal subunit.[439, 440] In Jurkat cells, vioprolide A has been shown to influence the interaction with EMG1 but not with NOC4L. The disturbed interaction with EMG1 has been shown to redistribute EMG1 from its basal location in the nucleus to the entire cell, which probably hampers 40S ribosomal subunit formation in Jurkat cells. In concert with the flawless interaction between NOP14 and NOC4L upon vioprolide A treatment, the nucleoli and NOP14 localization have been shown to remain intact in Jurkat cells.[311] Interestingly, cell fractionation of vioprolide A-treated HUVECs revealed an increase of NOP14 both in the cytosolic as well as nuclear fraction. Thus, interaction of vioprolide A with NOP14 in HUVECs stabilizes NOP14 and leads to a cellular redistribution. In contrast to the actions in Jurkat cells, vioprolide A might thus disrupt the interaction of NOP14 with both NOC4L and EMG1 in HUVECs. Further investigations are needed to understand the redistribution of NOP14 upon vioprolide A treatment in HUVECs. Interestingly, since NOP14 is described as nucleolar protein, studies regarding a potential off-label effect and potential interaction partners in the cytosol are not available. It would be of great importance to characterize the cytosolic interactome of NOP14 to fully understand its functions in the cellular context.

2. Vioprolide A in the treatment of inflammation and angiogenesis *in vivo* and *ex vivo*

In vivo models provide important information regarding the efficacy, safety and toxicity of a drug candidate. Moreover, most physiological processes, including inflammation and angiogenesis, are highly complex mechanisms that involve many different cell types. Hence, through performing *in vivo* studies, a general effect of drugs or genetic alterations on physiological and pathological conditions can be evaluated. The laser-induced choroidal

neovascularization (CNV) is a convenient animal model to simultaneously study inflammatory and angiogenic processes *in vivo*.[441] Animal models for specifically studying angiogenesis *in vivo* comprise zebrafish angiogenesis assays, the chick chorioallantoic membrane assay, the Matrigel plug assay or unilateral ischemia assays.[442-444] Cytokine- or phlogistic agent-induced paw or ear oedema, pleurisy, Freund's complete adjuvant (CFA)-induced arthritis, subcutaneous air pouch, zymosan-induced peritonitis and intravital microscopy of the cremaster muscle represent suitable animal models for distinctly examining acute and chronic inflammation *in vivo*.[445-447] In this study, the laser-induced CNV model was chosen to evaluate general anti-inflammatory and anti-angiogenic actions of vioprolide A, while the *in vivo* intravital microscopy of the cremaster muscle served to address the actions of vioprolide A on the leukocyte-endothelial cell interaction during inflammation.

In the CNV model, the eyes of mice are treated with a laser to evoke a rupture of the Bruch's membrane. This leads to a local inflammatory response and angiogenesis.[423] In this study, vioprolide A was injected to the murine eyes as single administration just before laser treatment. The experimental results showed that vioprolide A reduced the CNV leakage and, thus, retinal vasculature around the laser lesion as well as the infiltration of both immune and endothelial cells.

While endothelial cells recovered from vioprolide A treatment already after approximately 24 h *in vitro*, the effect of vioprolide A in the laser-induced CNV was long-lasting, since 14 days after laser treatment significant inhibitory effects on the vascularization were still observable. Importantly, detailed information regarding the pharmacokinetic properties of vioprolide A is not available. However, vioprolide A has been shown to induce toxicity at 2 µg/ml in the brine shrimp lethality test (BSLT) conducted with *Artemia salina*, a marine invertebrate.[304] The BSLT is a general bioassay that is performed to preliminarily assess the cytotoxicity of newly discovered natural products.[448] In the CNV model, we only used concentrations of vioprolide A up to 30 nM, corresponding to 26 ng/ml, which have been evaluated to influence cell viability *in vitro* only negligibly. For the total experimental period, no side effects were observed in the treated mice. Considering that the vioprolide A application was performed intraocularly, concerns regarding plasma concentration, bioavailability and terminal elimination can furthermore be neglected.

Based on the finding that vioprolide A reduced inflammatory processes in the CNV model, more in-depth investigations regarding a specific effect on the leukocyte-endothelial cell interaction were conducted *in vivo* by performing intravital microscopy of the TNF-activated murine cremaster muscle. To identify neutrophils and classical monocytes, these cells are stained for Gr-1 *in vivo*.[422] In our experimental setup, 0.1 mg/kg vioprolide A was injected to the tail vein of the mice and local inflammation was induced by intrascrotal injection of TNF. No adverse events in vioprolide A-treated mice were observed during the experimental period.

Vioprolide A strongly reduced the adhesion and transmigration of Gr-1$^+$ cells, indicating that an impairment of the leukocyte-endothelial cell interaction is a crucial part of the anti-inflammatory action of vioprolide A. CAMs like ICAM-1, VCAM-1 and E-selectin, which mediate the tight adhesion of leukocytes to the endothelium, are only expressed upon stimulus-induced *de novo* synthesis.[49, 60, 449] Considering that vioprolide A reduced *de novo* protein synthesis *in vitro*, similar effects might be evoked *in vivo*, thus preventing protein synthesis of CAMs involved in leukocyte adhesion and transmigration.

Interestingly, the rolling motion of leukocytes on the endothelium was not impaired. In contrast to above mentioned CAMs, the integrin P-selectin, which engages in the rolling motion of leukocytes on the endothelium, does not need to be synthesized *de novo* but is stored in intracellular granules called Weibel-Palade bodies. P-selectin is immediately released upon inflammatory activation of endothelial cells.[59] This might explain why vioprolide A hampered the adhesion and transmigration but not rolling of leukocytes *in vivo*.

3. *In vitro* anti-inflammatory potential of vioprolide A

3.1 Vioprolide A interferes with the leukocyte-endothelial cell interaction

The recruitment of leukocytes from the blood to the inflamed tissue is a multistep cascade, which involves the rolling on, adhesion to and transmigration through the vascular endothelium. Based on the *in vivo* results of the intravital microscopy of the murine cremaster muscle, we hypothesized that a direct influence of vioprolide A on endothelial cells might mediate the anti-inflammatory actions of the natural product.

Thus, the TNF-induced leukocyte-endothelial cell interaction with a special focus on the adhesion and transmigration of leukocytes was examined *in vitro*. To specifically focus on the effect of vioprolide A on endothelial cells, leukocytes were at no point of the experiment in contact with the natural product. Different leukocyte cell types were used to detect a potential specific effect of vioprolide A on a defined leukocyte cell type. Vioprolide A concentration-dependently reduced the cell adhesion of all leukocyte cell types investigated. While the inhibitory effect of vioprolide A on the adhesion of THP-1 cells, Jurkat cells and PLs was comparable, the effect on the adhesion of PBMCs was less pronounced. In contrast to the other leukocyte cell types investigated, PBMCs consist of a larger pool of different cell types, including T cells, B cells, natural killer (NK) cells, monocytes and dendritic cells. Since the composition of PBMCs varies between different donors depending on their physiological state, increased variations between differing biological replicates are not unexpected.[450] It has been demonstrated that freshly isolated NK cells express a two- to three-fold higher level of integrins like LFA-1 on their cell surface than resting lymphocytes.[451] Due to the experimental setup, PBMCs were used for cell adhesion assays directly after isolation, while PLs were allowed to

rest for one day before cell adhesion assays were performed. The discrepancy in adhesion molecules on the leukocyte cell surface may play a significant role in the results obtained, since in our study only endothelial cells were actively treated with TNF as inflammatory stimulus. In general, however, the tendency of the action that vioprolide A exerted on the adhesion of different leukocyte cell types was the same, indicating a general rather than a cell type specific effect.

CAMs expressed on the cell surface of endothelial cells, including ICAM-1, VCAM-1 and E-selectin are crucially involved in the tight adhesion of leukocytes through interacting with integrins, such as LFA-1 and VLA-4, on the leukocyte cell surface.[49, 60, 449] Importantly, in quiescent endothelial cells, the protein levels of these cell adhesion molecules are negligibly low. Only after endothelial cell activation by an inflammatory stimulus, their *de novo* expression is induced.[49,60] Vioprolide A significantly downregulated the TNF-induced cell surface, total protein and mRNA expression of all three adhesion molecules. Nevertheless, the effect of vioprolide A on the *ICAM1*, *VCAM1* and *SELE* gene expression was less pronounced compared to the decrease in their total protein level. These data suggest that vioprolide A impairs the leukocyte-endothelial cell interaction via a dual mechanism, consisting of the inhibition of pro-inflammatory gene expression and the reduction of *de novo* protein synthesis. Hence, although a small amount of cell adhesion molecule mRNA is still transcribed, vioprolide A impedes translation of the mRNA into protein. This hypothesis is further underlined by the observation that the strongest effect on leukocyte cell adhesion and on the expression of CAMs occurred after 16 h of vioprolide A pretreatment prior to the TNF-induced inflammatory activation. Considering that the maximum effect of vioprolide A on the *de novo* protein synthesis also occurred after 16 h, both properties of vioprolide A are likely to be connected.

In concert with the reduce leukocyte adhesion, vioprolide A further reduced the transmigration of THP-1 cells through the endothelial monolayer. In particular, the proteins PECAM-1 and CD99 participate in the extravasation of leukocytes.[62, 63] Hence, it would be of importance to investigate if vioprolide A directly affects these transmigration-mediating molecules or decreases the transmigration as secondary effect due to the reduction in leukocyte adhesion. However, since the effect of vioprolide A on the transmigration of THP-1 cells through HUVECs was stronger compared to their adhesion to HUVECs, it is likely that the process of transmigration is directly impaired. In contrast to inducible pro-inflammatory proteins like ICAM-1 and VCAM-1, PECAM-1 is constitutively expressed in endothelial cells and is crucially involved in the formation of intercellular junctions.[452] Since our study provided evidence that vioprolide A acts as general inhibitor of *de novo* protein synthesis, the protein expression of PECAM-1 and CD99 could be decreased provided that their half-lives are not overly long.

3.2 The mechanism underlying the anti-inflammatory actions of vioprolide A

3.2.1 The impact of vioprolide A on the pro-inflammatory NF-κB signaling pathway

During inflammation, endothelial cells are activated by cytokines, which bind to cell surface receptors and induce subsequent intracellular signaling pathways. The most prominent signaling pathway in the field of inflammation is the NF-κB signaling cascade.[453] A pivotal activating mechanism of the NF-κB signaling cascade consists of the binding of the cytokine TNF to its membrane-bound TNFR1.[454]

Several inhibitors of protein synthesis have been characterized as anti-inflammatory compounds in different studies. In most cases, the anti-inflammatory action has been linked to an impairment of the TNF/TNFR1 activation process. The triene-ansamycines mycotrienen II and cytotrienen A, the trichothecene mycotoxin deoxynivalenol, the pederin-type natural product irciniastatin A and the cyclohexene chalcone isopanduratin A have been shown to lower the TNF- but not IL-1α-induced ICAM-1 expression in human lung carcinoma cells.[429, 455-458] In the same cell type, the glutarimide antibiotics cycloheximide and acetoxycycloheximide have been reported to prevent TNF-induced expression of NF-κB target genes, like c-Flip, Cox-2 and ICAM-1.[459] These protein synthesis inhibitors have furthermore been demonstrated to induce the so called ribotoxic stress response, which activates the MAPKs ERK and p38.[456-458, 460] Activated MAPKs promote TNFα-converting enzyme (TACE)-dependent ectodomain shedding of the TNFR1, a proteolytic process that cleaves the receptor from the cell surface and, thus, downregulates the activation of downstream pro-inflammatory signaling pathways.[461] The isocarbostyril alkaloid narcilasine, an inhibitor of the elongation phase of protein synthesis, has been shown by our group to exert anti-inflammatory actions in HUVECs through downregulating the TNFR1 expression and the subsequent p65 nuclear translocation.[428] Whether the reduction of TNFR1 protein level is due to a general effect of narciclasine on protein synthesis or caused by the ribotoxic stress response and receptor ectodomain shedding has not been revealed, yet. Importantly, not all inhibitors of mRNA translation induce the ribotoxic stress response. Our working group has recently identified C81, a carbazole derivative of annamontine, as protein synthesis inhibitor with anti-inflammatory actions that rely on the impairment of the TNFR1 protein expression and recovery of the inhibitory IκBα protein. Since C81 has been shown to significantly lower the TNF-induced phosphorylation of MAPKs like p38 and JNK and to not alter their basal activation, the effect on the TNFR1 is most likely not linked to a ribotoxic stress response.[462] Besides, derivatives of the *Aglaia* flavagline rocaglamide have been shown to influence NF-κB activity in T cells by preventing phosphorylation- and ubiquitin-dependent degradation of IκBα.[463]

Based on these findings, we focused our interest in elucidating the anti-inflammatory mechanism of action of vioprolide A on its influence on the TNFR1 and the TNF-induced NF-κB signaling. Vioprolide A time-dependently reduced the protein level of TNFR1 while

increasing its mRNA expression. The vioprolide A treatment period, which showed the strongest decreasing effect on the TNFR1 protein level (16 h), corresponded with the time point after which general *de novo* protein synthesis was maximally impaired. For vioprolide A, the activation of MAPKs was solely investigated with regards to angiogenic signaling in endothelial cells. However, induction of MAPKs by an angiogenic stimulus was significantly downregulated. At the same time, vioprolide A only showed neglectable effects on the basal activation of ERK, p38 and JNK. It would be of importance to additionally investigate the activation of MAPKs in an inflammatory setup to safely exclude an inducible effect of vioprolide A. Nevertheless, considering that vioprolide A upregulated the *TNFRSF1A* mRNA level and that it did not significantly increase the basal phosphorylation level of MAPKs, the effect on the TNFR1 protein level is most likely due to the inhibition of mRNA translation but not due to a ribotoxic stress response induced TNFR1 ectodomain shedding. Interestingly, cycloheximide evoked a more sustained and complete inhibition of the TNFR1 protein level. Thus, compared to cycloheximide, vioprolide A has a rather short duration of action. This, however, could be of benefit in translational and clinical studies since sustained inhibition of protein synthesis might evoke more adverse events.

Upon binding of TNF to the TNFR1, an intracellular signaling cascade is initiated, which ultimately liberates the NF-κB subunits from their cytosolic retention. Therefore, the IKK complex needs to be activated, which then phosphorylates IκBα and induces its ubiquitin-dependent degradation. The IKK complex is either activated through auto-phosphorylation or through upstream kinases like TAK1.[464] Since our study revealed a downregulation of the TNFR1 protein level by vioprolide A, the activation of the downstream kinases TAK1 and IKK was evaluated. 16 h of pretreatment with vioprolide A significantly decreased the phosphorylation of IKK after 5–60 min of TNF-activation. While the phosphorylation of TAK1 between 15 min and 60 min of TNF induction was strongly lowered, too, vioprolide A showed no impairment of the phosphorylation level after a short TNF treatment period of 5 min. These results are highly interesting, since IKK, which is influenced by vioprolide A after earlier TNF treatment periods than TAK1, lies downstream of TAK1 and partially relies on its kinase activity. Besides TAK1, MEKK3 and Akt have also been shown to phosphorylate the IKK complex.[465, 466] Thus, vioprolide A might inhibit IKK activation through impairing various upstream kinases. Considering that vioprolide A induced rather than reduced the basal activation of Akt, inhibition of IKK activation by the compound is in all likelihood not connected to Akt signaling. MEKK3 is a MAPKKK that lies downstream of receptor tyrosine kinases and upstream of MAPKs like ERK, JNK and p38. Besides, MEKK3 lies downstream of the receptor-interacting protein (RIP) and the TNFR-associated factor 2.[465] Hence, through decreasing the TNFR1 protein level, vioprolide A might prohibit MEKK3 activation, thereby reducing TAK1- and MEKK3-dependent IKK phosphorylation.

The IKK complex is majorly involved in the phosphorylation- and ubiquitin-dependent degradation of IκB proteins, which hamper the nuclear translocation of NF-κB subunits.[91] Surprisingly, although vioprolide A significantly reduced the phosphorylation of the IKK complex, TNF-induced degradation of IκBα was not prevented. On the contrary, treatment with vioprolide A alone (without TNF induction) significantly reduced the IκBα total protein level, and the TNF-induced degradation was more sustained upon vioprolide A treatment. This observation has not been made in studies regarding the translation inhibitor narciclasine: In concert with a reduction in IKK activation, narciclasine has been shown to effectively prohibit the TNF-induced phosphorylation and degradation of IκBα while not impairing the TNF-independent IκBα total protein level.[428] Similar effects have also been observed for C81, which strongly downregulates IκBα phosphorylation and promotes IκBα recovery.[462] For more in-depth analysis, the influence of vioprolide A on the basal IκBα protein level over a total period of 48 h was examined using cycloheximide as control for protein synthesis inhibition. Both vioprolide A and cycloheximide time-dependently downregulated the IκBα protein level independent of TNF activation, while the respective mRNA expression was enhanced upon vioprolide A treatment. Thus, the observed effect on the protein level is most likely attributed to the influence of vioprolide A on *de novo* mRNA translation and not on a differing mechanism, which regulates IκBα at the transcriptional level.

In contrast to the TNFR1, the maximum effect of vioprolide A on IκBα occurred after later treatment periods of 24 h to 48 h, and the protein level showed no recovery. In quiescent, non-activated endothelial cells, IκBα interacts with the NF-κB subunits, which increases the stability of both proteins.[467] This could explain why the IκBα protein level was less quickly reduced by both vioprolide A and cycloheximide than the TNFR1 protein level. Furthermore, it has previously been reported that IκBα can be degraded independent of IKK activity through a PI3K- and proteasome-dependent mechanism.[468] PI3K is an upstream mediator of Akt, which has been linked to the proteasome both in an inhibiting and stimulating manner. While phosphorylation of cytosolic target proteins by Akt can prime them for ubiquitin-dependent degradation, interaction with and phosphorylation of deubiquitinating enzymes by Akt induces their activity and consequently hampers proteasomal degradation of ubiquitinated molecules.[469-471] Considering that vioprolide A increased Akt phosphorylation, IκBα could be a direct downstream target of Akt and be primed for TNF-independent degradation through Akt-dependent phosphorylation. This hypothesis is further underlined by the observation that cycloheximide enhanced basal Akt activation, too, while narciclasine has been shown to only provide a neglectable effect on the basal phosphorylation of Akt.[469, 472]

Both IKK-dependent and -independent degradation of IκBα can lead to NF-κB promotor activity and target gene expression.[468] Although vioprolide A time-dependently reduced the IκBα total protein level, the basal cellular distribution of the NF-κB subunit p65 remained unaffected.

Moreover, vioprolide A strongly decreased the TNF-induced nuclear translocation of p65. Interestingly, the hampered nuclear translocation of p65 was not evoked by an overall reduction of the p65 protein level based on the inhibitory effect of vioprolide A on *de novo* protein synthesis. On the contrary, the p65 total protein level remained unaffected over a total vioprolide A treatment period of 48 h, indicating that the NF-κB subunit is highly stable.

While 10 nM of vioprolide A reduced the TNF-induced nuclear translocation of p65 to approximately 50 %, the NF-κB promotor activity was almost completely inhibited. Thus, further mechanisms of vioprolide A besides the nuclear translocation of p65 are supposed to be involved in the inhibition of the NF-κB promotor activity. Upon liberation from the inhibitory IκB proteins, the NF-κB subunits are further posttranslationally modified. Such modifications include phosphorylation, methylation and acetylation and play a crucial role in the regulation of the DNA-binding activity of NF-κB.[473] The NF-κB subunit p65 contains seven serine and three threonine residues that serve as phosphorylation sites and alter the transcription efficiency either in a stimulatory or in an inhibitory way.[474] Interestingly, phosphorylation at one residue within the transactivation domain, for example serine 536, can lead to different functional consequences depending on the kinase that mediates the phosphorylation. Serine 536 can be phosphorylated by IKK, ribosomal subunit kinase-1 (RSK1) or TANK binding kinase (TBK). While IKK-dependent phosphorylation enhances the transcriptional activity, RSK1- and TBK-dependent phosphorylation lower the affinity of p65 for IκBα in the nucleus, thereby delaying its export back to the cytosol.[475-477] Considering that vioprolide A strongly downregulated the phosphorylation and thus activation of the IKK complex, it is likely that the IKK-dependent phosphorylation and thus transcriptional activity of NF-κB is impaired by vioprolide A, too. This would explain the discrepancy between the amount of p65 in the nucleus and the NF-κB promotor activity in vioprolide A-treated HUVECs.

3.2.2 The role of the classical nuclear import pathway in the anti-inflammatory actions of vioprolide A

Proteins with a molecular weight higher than approximately 40 kDa cannot diffuse through the NPC into the nucleus but rely on an active importin-dependent transport pathway. Various studies have reported a connection between deregulation of importins and chronic inflammatory diseases like atherosclerosis and cancer.[478, 479] In endothelial cells, KPNA3 and KPNA4 have been shown to mediate inflammatory signaling and barrier disruption.[480] KPNA2 has been evaluated as poor prognostic marker in multiple human cancers and has been linked to inflammatory processes in patients with rheumatoid arthritis.[481, 482] Hence, targeting deregulated importins represents a promising treatment possibility.[478]

The NF-κB subunit p65 has been shown to interact with a variety of importin alpha proteins, including KPNA2, KPNA4 and KPNA3.[115-119] Besides, KPNB1, which normally binds to

importin alpha and guides the trimeric complex through the NPC to the nucleus, can also directly bind to p65.[483, 484] Considering that vioprolide A on the one hand reduced the IκBα protein level and on the other hand still prevented p65 nuclear translocation, we hypothesized that the natural product would interfere with the nuclear transport of p65. Interestingly, while vioprolide A time-dependently reduced the protein level of KPNA2, the levels of KPNA4 and KPNB1 remained unaffected. Control experiments with the known translation inhibitor cycloheximide revealed comparable results regarding the influence on the total protein level of the importins. It has been shown that the overall expression levels of importin proteins vary widely between diverging cell types.[485] Our results indicate that importins are not only regulated differentially in deviating cell types but also intracellularly through unequal stabilities and half-lives. Although a subset of importin alpha isoforms has been identified to interact with p65, only nuclear accumulation of KPNA2 and to a small degree of KPNB1 was inducible in HUVECs by TNF activation. The cellular distribution of KPNA4 was not altered by TNF treatment. These findings are underlined by a recent study, which has shown that KPNA3 and KPNA4 are involved in thrombin-mediated NF-κB activation but are refractory to TNF-induced cell activation.[480] While the total protein level of KPNB1 was not altered, its TNF-induced nuclear localization was significantly lowered by vioprolide A. As mentioned before, KPNB1 mainly interacts with the importin alpha isoforms bound to the cargo. Considering that less KPNA2 was present in vioprolide A-treated cells, it can be concluded that the KPNB1 nuclear accumulation was impaired, since less cargo-KPNA2-complexes were available as interaction partners in the cytosol. In summary, our results indicate that in HUVECs, KPNA2 and KPNB1 but not KPNA4 are, at least in part, involved in the TNF-induced nuclear translocation of p65 and that downregulation of the KPNA2 protein level through inhibition of mRNA translation by vioprolide A is involved in the inhibition of the p65 nuclear translocation. This hypothesis is further underlined by the observation that cycloheximide exerted similar actions on importin alpha and beta protein levels and p65 nuclear translocation compared to vioprolide A. Interestingly, different importin alpha isoforms have been demonstrated to exhibit varying affinities for p65 and loss of one importin alpha protein could be substituted by another importin alpha isoform.[116] Hence, impairing KPNA2 might not be the sole reason for the vioprolide A evoked reduction of p65 nuclear translocation.

Microtubules and actin filaments are main components of the cellular cytoskeleton, which is essential for intracellular protein transport by motor proteins like kinesins, dyneins and myosins.[486] TNF has been reported to not only activate cellular signaling pathways but also to evoke actin remodelling.[487, 488] Interestingly, the initial shape of the cell plays a crucial role in its response towards TNF, too. In cells with an isotropic shape and low degree of actin polymerization and contractility, TNF treatment has been shown to induce a quicker and more efficient nuclear translocation of p65 compared to cells with a rectangular geometry and a high

degree of actin polymerization and myosin contractility. In the canonical NF-B signaling pathway, TNF treatment has been demonstrated to actively downregulate Rho/ROCK signaling, leading to a depolymerization of F-actin fibres and generation of actin nodes, which serve as scaffolds for IκB protein binding and are required for nuclear shuttling of p65.[489] Hence, besides influencing the carrier proteins responsible for p65 nuclear import, vioprolide A might additionally affect cell morphology and F-actin formation, thereby counteracting TNF-induced actin depolymerization. Narciclasine, an inhibitor of the elongation step of mRNA translation, as well as the eukaryotic elongation factor eEF1A have previously been reported to induce stress fibre formation in a Rho/ROCK-dependent manner.[490, 491] Furthermore, is has been assumed that cell morphology and the cytoskeleton exert important actions in the transport of mRNA from the nucleus to the cytosolic ribosomes and that protein biosynthesis relies on an intact F-actin filament system.[492, 493] These studies clearly show that stress fibre formation and cell morphology are tightly connected to cellular protein biosynthesis. Further investigations should therefore clarify if vioprolide A induces stress fibre formation. If the compound does so, it should be examined to what extend stress fibres are involved in the intracellular actions of the natural product.

4. *In vitro* anti-angiogenic potential of vioprolide A

4.1 Vioprolide A reduces key angiogenic features of endothelial cells

Endothelial cells are key players both in the physiological as well as pathological process of angiogenesis. Hence, we aimed to evaluate to what extend anti-angiogenic actions of vioprolide A in endothelial cells could mimic the strong effects observed *in vivo* and *ex vivo*. The first steps in the angiogenic process are the degradation of the basement membrane and the subsequent sprouting of endothelial tip cells towards the angiogenic stimulus.[165] By creating three-dimensional spheroids from HUVECs and HMEC-1 cells and treating them with VEGF as angiogenic stimulus, we found that vioprolide A concentration-dependently reduced the total sprout length and number of sprouts per spheroid. Both sprouting characteristics were equally strong impaired, indicating that the natural product leads to a general downregulation of sprout formation. Physiologically, the differentiation of quiescent endothelial cells into tip cells is mediated by the VEGFR2 and Notch signaling pathway: VEGF binds to the VEGFR2 on tip cells and leads to the expression of Dll4. Dll4 interacts with Notch receptors on neighbouring endothelial cells, thereby initiating an intracellular signaling cascade that ultimately causes reduced VEGFR2 expression on the cell surface of these cells.[494] Thus, the sensitivity of neighbouring cells towards VEGF is diminished, turning them into stalk cells that sprout and migrate less but proliferate more. Vioprolide A decreased the *de novo* protein biosynthesis and led to a significant reduction of proteins with a short to intermediate half-life

with an overall maximum effect after 16 h of treatment. Considering that the endothelial cell-derived spheroids were pretreated with vioprolide A for 16 h prior to addition of VEGF, it can be concluded that the total VEGFR2 expression on the spheroid building cells was decreased. Hence, not only stalk cells but all cells of the spheroids were less sensitive to VEGF. Consequently, less VEGF was able to bind to VEGFR2 and to initiate cell sprouting.

In vitro three-dimensional models to investigate cell sprouting are robust but fail to mimic the physiological environment due to a lack of interactions with other cell types involved in angiogenesis, like pericytes and macrophages. *Ex vivo* explant cultures are a useful tool to study angiogenic processes in response to specific stimuli in a controlled manner, thereby mimicking *in vivo* processes without the need to excessively use *in vivo* animal studies.[495] While aortic ring assays are helpful for studying the sprouting of large vessels, choroidal explant cultures more appropriately mimic angiogenesis of the microvasculature, which is stronger involved in the formation of new blood vessels than the macrovasculature. Furthermore, the microvasculature is more central to many diseases like retinopathy, age-related macular degeneration and cancer than macrovascular vessels.[409] Treatment of choroidal explant cultures with vioprolide A led to a concentration-dependent reduction of the sprouting area. Hence, the effects of vioprolide A observed *in vitro* can be translated to more physiological setups, too.

Following cell sprouting, migration is the next important step during the angiogenic cascade, which enables the sprout to grow towards the origin of the angiogenic stimulus. In general, migration can occur as undirected migration, a random movement in an environment where the migratory stimulus is distributed uniformly, or as directed migration, an active movement towards a chemoattractant that is presented in the form of a gradient.[496] Vioprolide A concentration-dependently lowered the undirected migration of HUVECs and HMEC-1 cells and the serum-induced directed migration of HUVECs. Interestingly, the directed migration was affected by vioprolide A without pretreatment. This indicates that besides the inhibition of mRNA translation and decrease of cellular proteins, other mechanisms might be involved in the anti-migratory actions of vioprolide A, too. For the directed migration of cells, several features are of high relevance: (I) the expression of chemokine and tyrosine kinase receptors, (II) flexibility and contractility to ensure pulling and squeezing motions, (III) cell polarization and cytoskeletal rearrangement (III) detachment or dismantling of interactions with the substrate.[497] The molecular structure of vioprolide A resembles actin-specific reagents, like macrocyclic peptide jasplakinolide.[498] Moreover, vioprolide A contains an α,β-unsaturated carbonyl moiety, which can act as Michael acceptor. Michael acceptors have been shown to form covalent bonds with cysteine residues of actin and induce actin polymerization.[499] In conclusion, vioprolide A might, besides indirectly influencing cell migration through inhibition

of protein synthesis, directly affect the formation of protrusive structures at the leading edge of the migrating cell, which emerge from actin polymerization.

While sprouting and migration is guided by tip cells, stalk cells mediate sprout elongation through proliferation. Vioprolide A concentration-dependently reduced the proliferation of both HUVECs and HMEC-1 cells over a total period of 72 h. While 10 nM vioprolide A caused a half-maximal reduction of both cell sprouting and cell migration, cell proliferation was completely inhibited. In this regard, it is important to take a closer look at the experimental setup. The spheroid outgrowth and migratory capability of endothelial cells were investigated in tightly connected cells, which mimics the physiological monolayer. However, endothelial cells in continuous monolayers are mostly quiescent rather than in an active, proliferative state.[500] Hence, to investigate the effects of vioprolide A on cell proliferation, cells had to be in a sparse state. Sparse cells, however, might be more sensitive to treatments due to the non-physiological conditions and vioprolide A might, thus, have had a greater impact on the cellular functions. Note that up to 10 nM vioprolide A did not impair the cell viability and percentage of apoptotic cells of subconfluent HUVECs. To proliferate, cells must properly pass the cell cycle including the S phase, where synthesis of new DNA takes place, and the G_2/M phase, where the separation of the mother cell into two daughter cells is performed.[577] Vioprolide A evoked a shift of the cells into the G0/G1 phase of the cell cycle with a strong reduction of cell in the S phase. It has been shown that proper ribosome biogenesis is pivotal for cell cycle progression and that only a sufficient amount of ribosomes generated in the G_1 phase of the cell cycle allows the cells to overcome the G_1/S restriction point.[501] Hence, the vioprolide A evoked cell cycle arrest in the G_0/G_1 phase can be attributed to its interaction with and inhibition of NOP14, which is involved in ribosome biogenesis.

In general, the effect of vioprolide A was more pronounced on all angiogenic key features investigated in microvascular HMEC-1 cells compared to macrovascular HUVECs. Importantly, HUVECs are primary endothelial cells and are due to their biological variation less homogenous than HMEC-1 cells. This might have played a role in the response of the biological replicates towards vioprolide A treatment.

4.2 The mechanism underlying the anti-angiogenic actions of vioprolide A

4.2.1 The impact of vioprolide A on the VEGF/VEGFR2-signaling cascade

The VEGF/VEGFR2 signaling cascade is the major regulator of angiogenic processes in endothelial cells.[502] VEGFR2 has been reported to belong to a subgroup of proteins that are selectively controlled: considering that both gene transcription and mRNA translation take time, cells produce mRNA of certain genes in beforehand and store them for future use, which allows

rapid mobilization for mRNA translation. Hence, VEGFR2 protein expression strongly relies on *de novo* protein synthesis.[503, 504]

Since in endothelial cells vioprolide A affected the *de novo* protein synthesis and potently downregulated all angiogenic key features, we hypothesized that the natural product might interfere with the VEGFR2 signaling cascade. Indeed, vioprolide A time-dependently reduced the total protein level and VEGF-induced phosphorylation of the VEGFR2, while its mRNA expression was at the same time increased. Importantly, the relation between phosphorylated and total protein level of the VEGFR2 in VEGF- versus vioprolide A-treated cell was the same. These observations indicate that the phosphorylation level of VEGFR2 is decreased, because there is less overall VEGFR2 protein available for phosphorylation and not because of less binding of VEGF to the available VEGFR2 proteins.

Although VEGFR2 represents a cardinal angiogenesis regulating receptor in endothelial cells, other VEGF receptors and tyrosine kinase receptors, such as FGFR1 and EGFR, have been shown to contribute to angiogenic actions as well. [180,181,189,190] Since VEGFR3 is mainly involved in lymphangiogensis and less important for angiogenic processes in endothelial cells, it was excluded from this study.[188] Vioprolide A downregulated the protein level of the FGFR1 and EGFR in a time-dependent manner. However, the period, after which the strongest inhibitory effect was evoked, varied. While FGFR1 and VEGFR2 were maximally influenced after 16 h of vioprolide A treatment, the EGFR protein level was influenced the strongest after longer vioprolide A treatment periods of 48 h to 72 h. These observations are in line with previous investigations regarding the half-lives of growth factor receptors, which have demonstrated that the VEGFR2 has a shorter half-life than the EGFR.[490]

In contrast to the other growth factor receptors, the protein level of the VEGFR1 was time-dependently increased with a maximum effect between 16h and 48 h. Considering that the strongest effect of vioprolide A on general protein synthesis was observed after 16 h to 24 h a feedback mechanism of the cell and an enhancement of VEGFR1 protein synthesis can be excluded. This conclusion is supported by the finding that the protein synthesis inhibitor cycloheximide completely inhibited the VEGFR1 protein level. The kinase Akt can both prime proteins for proteasomal degradation and inhibit it. Deactivation of Akt has been shown to enhance ubiquitin-dependent degradation of membrane-bound VEGFR1.[505] Vice versa, activation of Akt by vioprolide A might rescue VEGFR1 from proteasomal degradation. This hypothesis is underlined by the observation that 16 h of vioprolide A treatment strongly enhanced Akt activation.

It has been demonstrated that in stalk cells VEGFR1 mRNA expression is increased in response to DLL4/Notch signaling, while VEGFR2 mRNA expression is reduced.[506] Hence, through decreasing the protein level of the VEGFR2, vioprolide A could induce a stalk cell phenotype that enhances VEGFR1 expression. In comparison to VEGFR2, VEGR1 has a

higher binding affinity for VEGF but a 10-fold lower kinase activity.[507, 508] In this context, a previous study has shown that in NIH3T3 cells overexpressing VEGFR1, VEGF is not able to induce proliferation. Moreover, it has been reported that specific VEGFR1 ligands like PLGF and VEGF-B are not able to induce proliferation in endothelial cells.[509, 510] Like VEGFR2, downstream signaling pathways can only be activated when VEGFR1 is autophosphorylated at several residues. Phosphorylation of the VEGFR1 tyrosine residue 1175, which activates PKC-Raf-MEK-MAPK signaling, however, has been reported to be weak.[511] Hence, upregulation of VEGFR1 in vioprolide A-treated HUVECs does most likely not exert any biological function. Nevertheless, further studies should investigate if vioprolide A only upregulates the protein level of VEGFR1 without functional consequence or also induces its kinase activity by autophosphorylation.

Autophosphorylation of the VEGFR2 initiates pro-angiogenic signaling molecules, including the MAPKs ERK, JNK and p38 as well as the pro-survival kinase Akt and the NO-producing enzyme eNOS.[187] In concert with the reduced VEGFR2 activation, vioprolide A significantly decreased the VEGF-induced phosphorylation of all three MAPKs. While the overall influence on all three MAPKs was similar, the effect size apparently varied between ERK, JNK and p38 with JNK being most impaired. In this regard, it has been found that MAPKs do not respond equivalently to exogenous stimuli and, thus, show different activation profiles.[512] The specific MAPK response has been demonstrated to be mediated by incorporation of the MAPK into complexes or scaffolds. The scaffold proteins islet-brain 1 (IB1) and JNK-interacting protein 1 (JIP-1) have been identified to regulate JNK activity, while kinase suppressor of ras 1 (KSR-1) and MEK partner 1 (MP1) have been demonstrated to control ERK activation.[513-516] Thus, vioprolide A might influence these scaffolding proteins differentially, thereby evoking different inhibitory effect sizes on the VEGF-induced activation of the MAPKs.

In contrast to the MAPKs, both VEGF-dependent and -independent Akt phosphorylation was strongly enhanced by vioprolide A, while in case of eNOS only the VEGF-independent activation was significantly increased. Akt is recruited to the cell membrane in a PIP3-dependent mechanism and subsequently phosphorylated at two distinct residues, which leads to its activation.[219] Indeed, inhibition of PI3K with Ly294003 reduced the excessive phosphorylation of Akt upon vioprolide A treatment, indicating that the natural product affects the PI3K/PIP3-mediated activation of Akt. It has been shown that the activity of Akt rapidly returns to the basal level upon dissociation of PIP3.[517] Thus, vioprolide A might strengthen the interaction between Akt and PIP3, thereby extending the activation period.

While PIP3 mediates the activation of Akt, the phosphatase PTEN counteracts Akt activation through retransforming PIP3 to PIP2.[518] Comparative studies with cycloheximide, however, suggest only a minor role of the reduced PTEN protein level in the vioprolide A-evoked Akt

activation: Although CHX significantly reduced the PTEN protein level after periods between 16 h to 48 h, Akt was only overactivated after short CHX treatment periods.

Studies imply a pivotal role of the cell membrane composition, and in this regard cholesterol-rich plasma membrane domains named lipid rafts, in the activation of Akt. Although disruption of these lipid rafts neither changes PI3K activity nor PIP3 emergence, phosphorylation of Akt is hampered through inhibiting its PH-domain dependent interaction with the cell membrane.[519, 520] Conversely, vioprolide A might alter the membrane composition, including lipid rafts, in a favourable way for Akt binding, thereby enhancing Akt recruitment to and interaction with the cell membrane.

In general, induction of the kinase Akt is connected to an induction rather than an inhibition of angiogenic processes. Akt-deficient endothelial cells, for example, have been shown to sprout, proliferate and migrate to a lesser extent than cells expressing normal levels of Akt.[521] Moreover, an *in vivo* murine ischemia model has outlined that Akt depletion impairs VEGF-induced angiogenesis.[211] Surprisingly, however, differing *in vivo* studies in Akt-deficient mice, including Matrigel plus assay, have reported a pro-angiogenic effect of Akt depletion, indicating that Akt can also express anti-angiogenic functions.[521] In general, these studies outline that the tendency of Akt to act in a pro- or anti-angiogenic way is determined by its temporal regulation.[522] Hence, the vioprolide A-evoked activation of Akt does not necessarily contradict the anti-angiogenic actions of the natural product.

eNOS plays an essential role in the regulation of endothelial functions and various stimuli induce Akt-dependent phosphorylation of the synthase.[223, 224] However, other kinases, including adenosine-monophosphate-activated kinase (AMPK), calmodulin (CaM) kinase II and protein kinase A (PKA) can induce eNOS activity, too.[523-525] AMPK is activated upon metabolic stress or growth factor signaling and inhibited by the pro-survival kinase Akt. In quiescent cells, AMPK is usually inactivated.[526] Vioprolide A strongly upregulated the basal activation of Akt in endothelial cells. Hence, basal eNOS activation could be increased in vioprolide A-treated cells through Akt-mediated phosphorylation independent of AMPK. In VEGF-induced HUVECs, Akt could counteract the physiological AMPK activation and, therefore, prevent overactivation of eNOS. Importantly, environmental and cellular conditions have been shown to determine not only whether eNOS is phosphorylated but also at which residue: in the presence of Ca^{2+}-CaM, AMPK has been shown to phosphorylate serine 1177, which induces eNOS activation. In the absence of Ca^{2+}-CaM, AMPK favours threonine 495 phosphorylation, which inhibits eNOS.[527, 528] Akt on the contrary specifically phosphorylates serine 1177. Hence, through regulating the intracellular Ca^{2+}-CaM availability, vioprolide A could induce site-specific phosphorylation by Akt and AMPK. Further investigations should be performed concerning the effect of vioprolide A on other kinases that are involved in eNOS activation and on its influence on intracellular conditions, including Ca^{2+}-CaM levels.

4.2.2 The influence of vioprolide A on the Hippo signaling pathway

The Hippo signaling pathway is evolutionary conserved amongst mammalian species and is strongly involved in angiogenic processes in endothelial cells.[230] Since vioprolide A provided highly potent inhibitory effects on angiogenic key features of endothelial cells but only moderately impaired VEGFR2 downstream signaling, the Hippo signaling pathway was considered as potential additional target of the natural product. Vioprolide A significantly downregulated the nuclear translocation and subsequent target gene expression of the transcriptional coactivator TAZ, while not altering the total protein level in both dense and sparse endothelial cell layers. These data suggest that not only transcription factors like p65 but also transcriptional coactivators are highly stable proteins with a long half-life. TAZ can only translocate to the nucleus in a dephosphorylated state. In case of phosphorylation by upstream kinases like LATS1/2, TAZ is retained in the cytosol and eventually primed for ubiquitin-dependent degradation.[234, 251] Since vioprolide A evoked no alteration of the TAZ total protein level, it is unlikely that an increase in TAZ degradation is the cause for the reduction in nuclear translocation.

In contrast to the NF-κB subunits, which contain a NLS that enables their participation in the importin-mediated classical nuclear import pathway, mammalian TAZ proteins lack a NLS and the exact cellular events involved in the nuclear translocation of TAZ remain elusive.[529] Nevertheless, besides cellular events that mediate the nuclear translocation, other mechanisms are responsible for capturing TAZ in the nucleus and for preventing its export back to the cytosol. One important effector protein in this regard is MAML1/2, an essential coactivator of Notch-dependent transcription.[253] MAML1/2 contains a PPxY-interacting motif that can physically interact with the WW domain of TAZ, thereby withholding TAZ from nuclear export.[253] Indeed, vioprolide A completely downregulated the nuclear accumulation of MAML1 and reduced the total protein level in both dense and sparse HUVEC layers. The inhibitory effect of vioprolide A, however, was stronger in sparse cells compared to dense cells. This effect is most probably caused by the sensitivity of MAML1 protein expression towards cell density and the effect of vioprolide A on *de novo* protein synthesis. It has been shown that low abundance of MAML1 in the nucleus substantially decreases the nuclear accumulation of TAZ.[253] Hence, through impairing MAML1 protein expression, vioprolide A could lower the nuclear translocation of TAZ. Nevertheless, the effect of vioprolide A on MAML1 was stronger than the action on TAZ nuclear translocation. These observations suggest that downregulation of MAML1 might influence the nuclear translocation of TAZ but is not the key mediator of the observed reduction of translocation.

Besides phosphorylation, other cytosolic events further participate in the retention of TAZ. It has been demonstrated that merlin, kibra and angiomotin can directly bind to TAZ, thereby excluding the transcriptional coactivator from nuclear translocation.[530-532] Like VEGFR1,

vioprolide A could prevent these proteins from proteasomal degradation in an Akt-dependent manner, thereby increasing their protein levels.

Furthermore, TAZ activation is not only guided by biochemical signals but also by cell shape, cell-cell contacts, cell-matrix interactions and other mechanical forces.[533] In this regard, it has been reported that cells with a spread morphology and F-actin enrichment have higher TAZ nuclear levels compared to round and compact cells.[534] Moreover, junctional proteins have been demonstrated to regulate TAZ activity through binding and retaining the transcriptional coactivator in the cytosol.[535] In contrast, E-cadherin has been shown to activate transcriptional coactivators in response to mechanical forces.[536] Hence, the interplay of exogenous stimuli and transcriptional coactivators is highly complex and should be investigated in more detail in subsequent studies.

Besides TAZ, YAP is another transcriptional coactivator that is regulated via the Hippo signaling pathway.[251] If vioprolide A influences general signaling events that regulate Hippo signaling-mediated activation and MAML1-dependent nuclear retention of transcriptional coactivators, nuclear translocation of YAP should be impaired, too. Thus, to distinguish a general effect of vioprolide A on the Hippo signaling pathway from a selective action on the transcriptional coactivator TAZ, YAP as well as Hippo signaling molecules like LATS1/2 and MST1/2 should be subjected to further investigations.

5. The involvement of the cellular target NOP14 in the anti-inflammatory and anti-angiogenic actions of vioprolide A

Since vioprolide A was shown to interact with NOP14 in endothelial cells, a relation between the biological actions of vioprolide A and NOP14 was investigated by performing siRNA-mediated knockdown. Importantly, the protein expression of NOP14 was not completely knocked out but only reduced to approx. 50 %, which might explain intraexperimental differences regarding the effect size of NOP14 knockdown versus vioprolide A.

NOP14 has been reported as potential marker of sepsis, indicating a general involvement in the immune response.[323] Nevertheless, the role of NOP14 in the response towards inflammatory stimuli has not been elucidated, yet. Considering that vioprolide A exerts strong anti-inflammatory actions and targets NOP14 in endothelial cells, a potential connection between these two events is likely. Hence, by performing siRNA-mediated knockdown of NOP14, its influence on inflammatory actions in endothelial cells was analyzed. Like vioprolide A, NOP14 knockdown evoked anti-inflammatory actions in endothelial cells, including downregulation of TNF-induced THP-1 cell adhesion, *ICAM1* expression, p65 nuclear translocation and reduction of the KPNA2 protein expression. Importantly, vioprolide A treatment did not further increase the effect of NOP14 knockdown.

In particular, the expression of cell adhesion molecules, which mediate leukocyte adhesion, is highly inducible and strongly relies on *de novo* protein synthesis.[49, 60] As discussed in section VI.3.1, vioprolide A seems to reduce the ICAM-1 protein expression by a dual mechanism consisting of the inhibition of NF-κB signaling and *de novo* protein biosynthesis. Moreover, vioprolide A reduced the total protein level of the importin KPNA2 based on an inhibition of mRNA translation. Hence, reducing the process of ribosome biogenesis, thereby providing less mature ribosomes for the translation of mRNA into protein, is a logical explanation for the effects observed on THP-1 cell adhesion, p65 nuclear translocation and *ICAM1* mRNA expression. Nevertheless, further observations regarding the effect of vioprolide A on the NF-κB signaling pathway question that the inhibition of protein synthesis is the sole underlying cause for the anti-inflammatory actions of the natural product (see section VI.3.2). In concert with this suggestion, the effect of NOP14 knockdown alone on the abovementioned inflammatory processes was slightly less potent compared to vioprolide A treatment. Of course, this observation could be explained by the effectiveness of the siRNA-mediated knockdown of NOP14, which was only approximately 50 %, but could also suggest that vioprolide A affects additional intracellular events besides targeting NOP14.

In various studies NOP14 has been demonstrated to influence the Wnt/GSK-3β/β-catenin signaling pathway.[320-322] Wnt signaling is engaged in diverse biological actions, including inflammatory processes like Th2 differentiation or T cell adhesion, through stabilizing β-catenin and enhancing its nuclear recruitment.[537, 538] However, Wnt signaling has also been described as negative regulator of NF-κB signaling.[539] In this context, β-catenin builds a complex with NF-κB, which leads to a reduced NF-κB DNA binding and transcription activity.[540, 541] PI3K is a main upstream regulator of β-catenin-dependent inhibition of NF-κB: In cells with low β-catenin protein levels, PI3K induces NF-B activity, whereas in cells with high β-catenin protein expression PI3K lowers NF-κB activity. This effect has been underlined by the finding that inhibition of PI3K prevents the formation of an inhibitory complex between the PI3K subunit p85, β-catenin and NF-κB.[541] Further investigations regarding a potential involvement of the Wnt/β-catenin signaling pathway – in addition to the effect on *de novo* protein synthesis – in vioprolide A- and NOP14 knockdown-evoked anti-inflammatory effects should be conducted.

Considering that ribosome biogenesis and mRNA translation are frequently deregulated in cancer cells, it seems not surprising that alterations in the protein expression of NOP14 have been connected to tumor angiogenesis.[357] Surprising, however, is the fact that both overexpression as well as deletion of NOP14 in cancer cells have been reported to halt their angiogenic and invasive properties.[316-318, 321] Like for inflammatory processes, the involvement of NOP14 in angiogenic processes in normal, non-cancerous cells has remained unexplored to date. In this study, siRNA-mediated NOP14 knockdown in HUVECs revealed an inhibition of cell migration and proliferation but an increase in cell sprouting. NOP14 knockdown

significantly reduced VEGF-induced activation of MAPKs and TAZ nuclear translocation in sparse cells, while VEGF-dependent and -independent Akt activation was enhanced. Thus, vioprolide A treatment and NOP14 knockdown evoke the same effects on the respective signaling intermediates, whereas their effect on angiogenic functions varies regarding the VEGF-dependent and -independent sprouting.

It has been shown that deletion of the transcriptional repressor B-cell lymphoma 6 (Bcl-6) enhances basal sprouting of endothelial cell spheroids, while hindering cell proliferation through altering the cell cycle distribution by reducing the percentage of cells in the S phase as well as the expression of cyclin A and cyclin B1. This observation has been traced back to an alteration of tip and stalk cell selection through changing the expression of the Notch signaling components Dll4, Hairy Enhancer of Split 1 (HES1) and the Hes-related transcription factor HEY1.[542] Furthermore, it has been reported that cytosolic retention of the nuclear corepressors SMRT and NCoR leads to an upregulation of Notch- and tip cell dependent genes.[543] In general, transcriptional activators and repressors bind to specific sites on the DNA, thereby enhancing or impeding transcription of nearby genes.[544] Transcriptional cofactors, like coactivators or corepressors, again regulate the activity of the transcription factors, for example by influencing histone-modifying enzymes that change the chromatin structure and modifications.[545-547] Hence, NOP14 knockdown could evoke a cytosolic retention of transcription factors or transcriptional coactivators, thereby influencing epigenetic modulations that regulate the phenotype and gene expression profile of endothelial cells.

β-catenin is another transcriptional activator for the transcription factors T-cell factor (TCF)/Lef and RBP-J, which is regulated by the Wnt signaling pathway, a major target of NOP14 in cancer cells.[548, 549] Wnt signaling is not only involved in inflammatory actions but also regulates angiogenic processes in endothelial cells.[550] Interestingly, β-catenin in combination with its coactivator Pygopus 2 has been shown to maintain a repressed chromatin state at the Notch3 locus, thereby restricting Notch signaling. Downregulation of β-catenin and Pygopus 2 have been demonstrated to increase the expression of Notch signaling components like DLL4 and Hes1.[551, 552] Hence, Wnt and Notch signaling can crosstalk with each other, thereby regulating cell differentiation. Through interacting with the Wnt signaling, NOP14 might impair Notch signaling. NOP14 knockdown and reduced Wnt signaling could vice versa induce Notch signaling, thereby influencing tip and stalk cell selection and angiogenic functions of endothelial cells.

One major difference between vioprolide A targeted NOP14 and siRNA-mediated knockdown of NOP14 is the fact that vioprolide A did not impair NOP14 protein level but rather led to a redistribution of the nucleolar protein to the whole cell instead of only the nucleoli. Considering that NOP14 has been shown to both induce and reduce angiogenic processes, it might be possible that vioprolide A targets and inhibits one specific function of NOP14 but enables,

through the cellular redistribution, another function and protein-protein interaction of NOP14. The observation that vioprolide A treatment and NOP14 knockdown did not coincide on their effects on the VEGF-dependent and -independent endothelial cell sprouting, however, could also imply that vioprolide A accounts for more than just targeting NOP14 in endothelial cells.

6. The pro-survival effects of vioprolide A

Ribosome biogenesis and protein biosynthesis are fundamental processes of the cell, which are elementary for the adoption to environmental alterations and maintenance of homeostasis. In this regard, it is not surprising that inhibition of ribosome biogenesis and mRNA translation is cytotoxic and increases apoptosis.[553] Increased cytotoxicity might be beneficial in rapidly cycling cells with abnormally increased translation rates, like tumour cells. Increased apoptosis due to an inhibition of protein synthesis in normal cells, however, represents an enormous obstacle for the approval of mRNA translation inhibitors for clinical application.[342, 554] Indeed, vioprolide A was shown to reduce the amount of viable Jurkat cells with an IC_{50} of only 4.4 nM. Moreover, vioprolide A increased the percentage of apoptotic cancer cells with an EC_{50} ranging between 15.8 and 134 nM.[311] Surprisingly, vioprolide A considerably lowered the starvation-induced apoptosis of endothelial cells in a concentration-dependent manner, while the same concentrations also lowered *de novo* protein biosynthesis.

In-depth investigations further revealed that both the VEGF-dependent and VEGF-independent activation of the pro-survival kinase Akt was increased upon vioprolide A treatment despite impaired VEGF/VEGFR2-signaling. Akt participates in the regulation of ribosome biogenesis and protein biosynthesis through activating mTOR, which eventually upregulates translation initiation.[219, 555] Interestingly, besides being part of the initiation step of mRNA translation, eIF4E amplifies survival signaling through upregulating the PI3K/Akt upstream activator Nijmegen breakage syndrome 1 (NBS1).[556] Considering that in our study vioprolide A lowered mRNA translation, surplus eIF4E might switch from its role as translation initiation factor to initiating apoptotic rescue. Thus, the overactivation of Akt by vioprolide A might be a feedback mechanism of the translational inhibition. In favor of this hypothesis is on the one hand the observation that NOP14 knockdown enhances Akt activation and on the other hand the finding that differing inhibitors of protein biosynthesis, including cycloheximide and NSC119889, induce Akt phosphorylation in a PI3K-dependent mechanism.[469]

Akt acts as pro-survival kinase that prevents the cleavage of procaspase-3 into its active form.[557] Activation of caspase-3 is frequently observed after DNA damage. Doxorubicin is a DNA damaging agent, which strongly upregulates procaspase-3 cleavage. Consistent with its effect on Akt activation, vioprolide A profoundly inhibited doxorubicin-induced caspase-3 activation, while pretreatment with Ly294002 rescued caspase-3 activation. DNA damage-

induced activation of caspase-3 is commonly governed by p53.[558-560] Although vioprolide A strongly decreased the nuclear accumulation of p53 as well as expression of its pro-apoptotic, caspase cleavage-inducing target genes, inhibition of PI3K was not able to reverse these effects. Thus, vioprolide A seems to inhibit caspase-3 activation via two distinct mechanisms: on the one hand a hyperactivation of Akt and on the other hand the prevention of p53-induced apoptosis. In quiescent cells, constant ubiquitination and subsequent degradation keeps the protein level of p53 low. In activated and stressed cells, on the contrary, the degradation of p53 is inhibited and the de novo protein synthesis of p53 is enhanced, which evokes a rapid increase in the p53 protein level.[561] In this study, vioprolide A decreased the basal level of p53 in a time dependent manner. Thus it is likely that the inhibition of mRNA translation also prevents the DNA damage-induced p53 protein synthesis.

7. Conclusion and future perspective

7.1 Conclusion

The present study aimed to examine the effects of the myxobacteria-derived metabolite vioprolide A on inflammatory and angiogenic processes and to clarify the respective underlying mechanisms of action. Vioprolide A strongly reduced both inflammation and angiogenesis *in vivo* as determined by a laser-induced choroidal neovascularization assay. Intravital microscopy of the murine TNF-activated cremaster muscle underlined a strong impairment of the leukocyte-endothelial cell interaction during the inflammatory response.

In vitro experiments further underlined that the effect of vioprolide A on the leukocyte-endothelial cell interaction is mediated by a reduction of the TNF-induced cell adhesion molecules expression on the cell surface of the endothelial monlayer. The influence on cell adhesion molecules contributed to a dual mechanism of action of vioprolide A: On the one hand, vioprolide A reduced the general *de novo* protein synthesis in endothelial cells through interacting with the nucleolar protein NOP14, which is involved in the ribosomal biogenesis. Hence, the protein expression of short-lived proteins involved in the inflammatory response, including the TNFR1, was strongly lowered. On the other hand, the vioprolide A downregulated the TNF-induced activation and transcriptional activity of NF-κB including subsequent pro-inflammatory target gene expression through interfering with the importin-dependent nuclear translocation of the NF-κB subunit p65. Furthermore, we could for the first time show a general involvement of NOP14 in inflammatory actions in endothelial cells, since NOP14 knockdown evoked a reduction in TNF-induced inflammatory processes like leukocyte cell adhesion, cell adhesion molecule expression and p65 nuclear translocation.

Moreover, *in vitro* experiments revealed that vioprolide A declines all important angiogenic key features, including sprouting, migration and proliferation of endothelial cells. Mechanistically,

vioprolide A targeted two pivotal signaling pathways involved in angiogenic processes: On the one hand, protein expression of short-lived mediators of pro-angiogenic signaling, including the tyrosine kinase receptors VEGFR2, FGFR1 and EGFR, was significantly declined through targeting *de novo* protein synthesis. Consequently, the growth factor-induced activation of downstream signaling components including MAPKs was diminished. Surprisingly, however, vioprolide A increased rather than decreased the activation of the pro-survival kinase Akt and the NO-producing enzyme eNOS. On the other hand, the transcriptional coactivator TAZ, which is mainly regulated by the conserved Hippo signaling pathway, was kept from translocating to the nucleus and inducing the expression of pro-angiogenic target genes. Comparative studies with the cellular target of vioprolide A, NOP14, showed that NOP14 knockdown evoked the same effects on MAPKs and Akt activation and TAZ nuclear translocation than vioprolide A. Nevertheless, NOP14 knockdown exhibited opposing effects regarding the sprouting of endothelial cell spheroids. Hence, it is very likely that the actions of vioprolide A are only in part attributed to an inhibition of NOP14 and that differential mechanisms of action underly the pharmacological properties of the natural product.

Although the hindrance of ribosome biogenesis has previously been linked to an increase in apoptotic cell death, the inhibition of *de novo* protein synthesis as well as the anti-angiogenic actions of vioprolide A up to concentrations of 10 nM were not critical for the cell viability of endothelial cells.[553] On the contrary, vioprolide A induced pro-survival effects in endothelial cells based on an Akt-dependent and -independent inhibition of caspase-3 activation and prevention of DNA damage-induced p53-dependent apoptosis. In ALL cell lines and ALL patient-derived tumor xenografts, however, the same concentrations of vioprolide A induced specific apoptosis.[311]

In summary, this study provides insight into the pharmacological activities of vioprolide A, including potent anti-inflammatory, anti-angiogenic and pro-survival actions and introduces ribosome biogenesis and, in this context, the nucleolar protein NOP14 as promising cellular target in endothelial cells.

In many pathological conditions, chronic inflammation and angiogenesis are interrelated and reinforce each other.[262] Furthermore, it has been shown that an inflammatory microenvironment initiates tumor-dependent angiogenic processes including proliferation and metastasis.[562, 563] Considering that vioprolide A reduced both inflammatory and angiogenic actions in endothelial cells and, moreover, exhibited selective cytotoxicity towards cancer cells at concentrations that were not critical for endothelial cell viability, the natural product represents a promising lead compound for the treatment of different pathologies, including rheumatoid arthritis, psoriasis and cancer. Hence, the potential of vioprolide A should be further characterized in preclinical studies.

7.2 Future perspective

In this study, we examined the effects of vioprolide A on inflammatory and angiogenic actions with a special focus on endothelial cells. Numerous studies over the past decades have underlined that endothelial cells are key players of inflammation and angiogenesis under both physiological and pathological conditions. Nevertheless, different cell types including immune cells, mural cells and cancer cells participate in or evoke an inflammatory and angiogenic response, too. Immune cells initiate the inflammatory response through secreting pro-inflammatory cytokines and induce the resolution of inflammation to restore tissue homeostasis.[41, 42, 51] Mural cells are critically involved in the process of angiogenesis by stabilizing blood vessels and preventing the formation of an abnormal leaky vascular network.[564] In contrast to healthy, highly organized vasculature, the tumor vascular network is disorganized, immature and characterized by increased vessel permeability. Especially the lack of pericytes and intracellular junctions in the tumor vascular endothelium contributes to increased vessel permeability.[565, 566] It would be of high interest to investigate what effect the natural compound exerts on endothelial cells in pathological settings, for example a tumor microenvironment or chronic inflammatory situations. Therefore, co-cultures of endothelial cells and cancer cells in a two- or three-dimensional setup as well as addition of cancer cell spheroids to endothelial monolayers could be used.[567] Several *in vivo* models specifically address the investigation of a tumor environment, for example by implanting human tumor xenografts into mice or zebrafish embryos.[568, 569] *In vivo* models in mice have, moreover, been shown to mimic chronic inflammatory diseases including atherosclerosis by infecting the mice with the pathogen *Porphyromonas gingivalis*.[570] While in all *in vitro* experiments only endothelial cells were treated with vioprolide A, such a discrimination between the different cell types is not possible *in vivo*. Considering that in both the laser-induced CNV and the intravital microscopy of the murine cremaster muscle, also other cell types like macrophages, microglia, neutrophils and monocytes are crucially involved, the effect of vioprolide A could be potentiated when different cell types are sensitive to the treatment with the natural product. Hence, it would be interesting to observe whether the treatment of leukocytes instead of endothelial cells with vioprolide A impairs the leukocyte-endothelial cell interaction and leukocyte tissue infiltration in a comparable way as treating endothelial cells.

Cancer cells induce the endothelial cell-dependent formation of new vessels to ensure ongoing growth. However, metastasis is another important characteristic of cancer cells, which leads to the establishment of secondary tumors in distant tissue sections. Therefore, it is crucial that cancer cells mimic leukocytes, thereby initializing rolling on, adhesion to, and transmigration through the endothelial monolayer into the blood stream.[259] In this regard, it would be of high value to examine the effect of vioprolide A on features of cancer cell metastasis, including

adhesion molecule expression of the cancer cell surface, cancer-endothelial cell interactions and cancer cell migration.

In general, the study provided first insights into the underlying mechanisms responsible for the anti-inflammatory and anti-angiogenic actions of vioprolide A. Thus, further in-depth characterization of the underlying modes of action of vioprolide A is needed. Regarding the anti-inflammatory mechanism of action, our study mainly focused on the impact of vioprolide A on the TNF-induced inflammatory response. Nevertheless, several other cytokines induce inflammatory actions in endothelial cells as well, including lipopolysaccharide (LPS) or thrombin.[571] Hence, it should be evaluated if vioprolide A promotes specific anti-inflammatory actions on TNF-induced inflammation or also prevents the inflammatory response towards differing cytokines. Moreover, a potential inhibitory action of vioprolide A on other proteins involved in the leukocyte diapedesis, including P-selectin, PECAM-1 and CD99 would be beneficial to provide a complete image of the influence on the leukocyte-endothelial cell interaction. It would further be interesting to examine the precise mechanism underlying the reduction of IκBα protein level and importin-dependent inhibition of p65 nuclear translocation. Addition of proteasome-inhibiting agents, like MG132, as well as studies regarding the ubiquitination level of IκBα could be informative regarding the question whether vioprolide A prevents IκBα protein synthesis or induces its proteasomal degradation.[462, 572] Through siRNA-mediated knockdown experiments the influence of KPNA2 on the nuclear import of p65 and potential substitution by other importin alpha isoforms in endothelial cells could be evaluated in more detail.[483]

Regarding the anti-angiogenic actions of vioprolide A, we only focused on the VEGF-induced angiogenic processes. However, differing growth factors, including EGF and bFGF, also enhance angiogenic processes.[573, 574] Thus, it would be interesting to see whether – besides VEGFR2 – also EGFR and FGFR1 are involved in the anti-angiogenic actions of vioprolide A. We could identify the Hippo signaling pathway as target of vioprolide A. Nevertheless, the exact mechanism underlying the reduced TAZ nuclear localization remains unknown. It would be advantageous to conduct more in-depth investigations regarding cytosolic and nuclear effectors, which are involved in the translocation of TAZ to the nucleus. In our study, we observed a strong induction of the VEGF-dependent and -independent Akt activation, which seemed to be PI3K-dependent. Considering that the induction of Akt was involved in the pro-survival effects of vioprolide A, it would be interesting to elucidate the exact mechanism of Akt activation and to compare the effects observed in endothelial cells with cancer cells.

The actin cytoskeleton is connected to various biological functions and participates in intracellular protein transport. An increase of F-actin can alter the cell morphology, thereby influencing cellular processes and signaling pathways.[575] Cell morphology plays a crucial role during angiogenic processes like cell migration and contributes to the efficiency of p65 nuclear

translocation.[489, 497] Considering that stress fiber formation is tightly connected to protein biosynthesis and that other inhibitors of mRNA translation have been shown to target actin or induce F-actin formation, it should be evaluated if vioprolide A evokes such effects on the actin cytoskeleton as well.[490, 499] The structure of vioprolide A resembles actin-specific reagents and contains a Michael acceptor, which could interact with cystine residues of actin. Hence, a direct interaction between actin and vioprolide A could be investigated by mass spectrometry. Furthermore, the translation elongation factor eEF1A is involved in stress fibre formation.[491] Through inhibiting protein biosynthesis in a step prior to the initiation step of mRNA translation, vioprolide A could lead to an accumulation of unemployed translation factors, which in the following carry out cellular functions different of supporting mRNA translation.

NOP14 is plays an important role in ribosome biogenesis through interacting with EMG1.[312] Several studies have indicated that NOP14 is frequently overexpressed or deleted in abnormal cells. This indicates that different cell types have diverging sensitivities towards an inhibition of NOP14.[316-322] An increasing number of studies over the past years has furthermore linked deregulations in the ribosome assembly pathway to severe pathological conditions, including ribosomopathies.[375] Ribosomopathies, in turn, have been shown to increase the overall risk of cancer development.[576] Considering that vioprolide A is the only compound known to influence NOP14 to date, the natural compound could serve as chemical tool for the exploration of upstream and downstream signaling events connected to NOP14 and EMG1.[305] Moreover, the biological effects of vioprolide A partially differ from the ones observed for NOP14 knockdown. Especially the vioprolide A-evoked reduction of VEGF-induced sprouting could not be reproduced by NOP14 knockdown. Moreover, the effects of NOP14 knockdown on both inflammatory and angiogenic actions in endothelial cells were less potent compared to vioprolide A treatment. This could be due to the knockdown efficiency but could also indicate that vioprolide A promotes its effects not only through targeting NOP14. In cancer cells, various studies have outlined a connection between NOP14 and the Wnt/β-catenin signaling pathway.[321, 322] Although Wnt signaling partially regulates inflammatory and angiogenic processes, our study focused on more prominent angiogenic signaling pathways including the VEGFR2 and Hippo signaling. Nevertheless, investigating the Wnt signaling upon vioprolide treatment and NOP14 knockdown would be important on the one to hand verify Wnt signaling as target of NOP14 in endothelial cells and on the other hand to draw a potential connection to vioprolide A-dependent actions. In summary, more in-depth investigations regarding NOP14 and its cellular actions are needed to fully understand the role of NOP14 in vioprolide A-evoked effects and to uncover differences in the intracellular signaling events targeted by vioprolide A versus NOP14 knockdown.

VII REFERENCES

[1] Kruger-Genge, A., Blocki, A. *et al.* Vascular Endothelial Cell Biology: An Update. *Int J Mol Sci.* **20**, (2019).
[2] Rubanyi, G. M. The role of endothelium in cardiovascular homeostasis and diseases. *J Cardiovasc Pharmacol.* **22 Suppl 4**, S1-14 (1993).
[3] Hirschi, K. K. Hemogenic endothelium during development and beyond. *Blood.* **119**, 4823-4827 (2012).
[4] Shalaby, F., Rossant, J. *et al.* Failure of blood-island formation and vasculogenesis in Flk-1-deficient mice. *Nature.* **376**, 62-66 (1995).
[5] Eichmann, A., Corbel, C. *et al.* Ligand-dependent development of the endothelial and hemopoietic lineages from embryonic mesodermal cells expressing vascular endothelial growth factor receptor 2. *Proc Natl Acad Sci U S A.* **94**, 5141-5146 (1997).
[6] Lancrin, C., Sroczynska, P. *et al.* The haemangioblast generates haematopoietic cells through a haemogenic endothelium stage. *Nature.* **457**, 892-895 (2009).
[7] Aird, W. C. Phenotypic heterogeneity of the endothelium: I. Structure, function, and mechanisms. *Circ Res.* **100**, 158-173 (2007).
[8] Esmon, C. T. Thrombomodulin as a model of molecular mechanisms that modulate protease specificity and function at the vessel surface. *FASEB J.* **9**, 946-955 (1995).
[9] Girard, T. J., Tuley, E. *et al.* TFPIbeta is the GPI-anchored TFPI isoform on human endothelial cells and placental microsomes. *Blood.* **119**, 1256-1262 (2012).
[10] Ihrcke, N. S., Wrenshall, L. E. *et al.* Role of heparan sulfate in immune system-blood vessel interactions. *Immunol Today.* **14**, 500-505 (1993).
[11] Rondaij, M. G., Bierings, R. *et al.* Dynamics and plasticity of Weibel-Palade bodies in endothelial cells. *Arterioscler Thromb Vasc Biol.* **26**, 1002-1007 (2006).
[12] Giri, H., Panicker, S. R. *et al.* Thrombomodulin is essential for maintaining quiescence in vascular endothelial cells. *Proc Natl Acad Sci U S A.* **118**, (2021).
[13] Lilly, B. We have contact: endothelial cell-smooth muscle cell interactions. *Physiology (Bethesda).* **29**, 234-241 (2014).
[14] Baeyens, N., Bandyopadhyay, C. *et al.* Endothelial fluid shear stress sensing in vascular health and disease. *J Clin Invest.* **126**, 821-828 (2016).
[15] Bevan, J. A. and Henrion, D. Pharmacological implications of the flow-dependence of vascular smooth muscle tone. *Annu Rev Pharmacol Toxicol.* **34**, 173-190 (1994).
[16] Sandoo, A., van Zanten, J. J. *et al.* The endothelium and its role in regulating vascular tone. *Open Cardiovasc Med J.* **4**, 302-312 (2010).
[17] Feletou, M., Huang, Y. *et al.* Endothelium-mediated control of vascular tone: COX-1 and COX-2 products. *Br J Pharmacol.* **164**, 894-912 (2011).
[18] Masaki, T. Possible role of endothelin in endothelial regulation of vascular tone. *Annu Rev Pharmacol Toxicol.* **35**, 235-255 (1995).
[19] Stevens, T., Garcia, J. G. *et al.* Mechanisms regulating endothelial cell barrier function. *Am J Physiol Lung Cell Mol Physiol.* **279**, L419-422 (2000).
[20] Bazzoni, G. and Dejana, E. Endothelial cell-to-cell junctions: molecular organization and role in vascular homeostasis. *Physiol Rev.* **84**, 869-901 (2004).
[21] Minshall, R. D. and Malik, A. B. Transport across the endothelium: regulation of endothelial permeability. *Handb Exp Pharmacol.* 107-144 (2006).
[22] Ley, K. and Reutershan, J. Leucocyte-endothelial interactions in health and disease. *Handb Exp Pharmacol.* 97-133 (2006).
[23] Muller, W. A. Leukocyte-endothelial-cell interactions in leukocyte transmigration and the inflammatory response. *Trends Immunol.* **24**, 327-334 (2003).
[24] Munoz-Chapuli, R., Quesada, A. R. *et al.* Angiogenesis and signal transduction in endothelial cells. *Cell Mol Life Sci.* **61**, 2224-2243 (2004).
[25] Tonnesen, M. G., Feng, X. *et al.* Angiogenesis in wound healing. *J Investig Dermatol Symp Proc.* **5**, 40-46 (2000).
[26] Jia, G., Aroor, A. R. *et al.* Endothelial cell senescence in aging-related vascular dysfunction. *Biochim Biophys Acta Mol Basis Dis.* **1865**, 1802-1809 (2019).
[27] Golbidi, S., Edvinsson, L. *et al.* Smoking and Endothelial Dysfunction. *Curr Vasc Pharmacol.* **18**, 1-11 (2020).
[28] Engin, A. Endothelial Dysfunction in Obesity. *Adv Exp Med Biol.* **960**, 345-379 (2017).

[29] Cozma, A., Orasan, O. *et al.* Endothelial dysfunction in metabolic syndrome. *Rom J Intern Med.* **47**, 133-140 (2009).
[30] Hemanthakumar, K. A., Fang, S. *et al.* Cardiovascular disease risk factors induce mesenchymal features and senescence in mouse cardiac endothelial cells. *Elife.* **10**, (2021).
[31] Bernard, I., Limonta, D. *et al.* Endothelium Infection and Dysregulation by SARS-CoV-2: Evidence and Caveats in COVID-19. *Viruses.* **13**, (2020).
[32] Park, K. H. and Park, W. J. Endothelial Dysfunction: Clinical Implications in Cardiovascular Disease and Therapeutic Approaches. *J Korean Med Sci.* **30**, 1213-1225 (2015).
[33] Su, J. B. Vascular endothelial dysfunction and pharmacological treatment. *World J Cardiol.* **7**, 719-741 (2015).
[34] Medzhitov, R. Origin and physiological roles of inflammation. *Nature.* **454**, 428-435 (2008).
[35] Parke, D. V. and Parke, A. L. Chemical-induced inflammation and inflammatory diseases. *Int J Occup Med Environ Health.* **9**, 211-217 (1996).
[36] Medzhitov, R. and Janeway, C. A., Jr. Innate immunity: the virtues of a nonclonal system of recognition. *Cell.* **91**, 295-298 (1997).
[37] Gerullis, H., Georgas, E. *et al.* Inflammatory reaction as determinant of foreign body reaction is an early and susceptible event after mesh implantation. *Biomed Res Int.* **2014**, 510807 (2014).
[38] Roh, J. S. and Sohn, D. H. Damage-Associated Molecular Patterns in Inflammatory Diseases. *Immune Netw.* **18**, e27 (2018).
[39] Calhoun, K. N., Luckett-Chastain, L. R. *et al.* Associations Between Immune Phenotype and Inflammation in Murine Models of Irritant Contact Dermatitis. *Toxicol Sci.* **168**, 179-189 (2019).
[40] Brusilovsky, M., Rochman, M. *et al.* Environmental allergens trigger type 2 inflammation through ripoptosome activation. *Nat Immunol.* **22**, 1316-1326 (2021).
[41] Zedler, S. and Faist, E. The impact of endogenous triggers on trauma-associated inflammation. *Curr Opin Crit Care.* **12**, 595-601 (2006).
[42] Zuliani-Alvarez, L., Marzeda, A. M. *et al.* Mapping tenascin-C interaction with toll-like receptor 4 reveals a new subset of endogenous inflammatory triggers. *Nat Commun.* **8**, 1595 (2017).
[43] Abdulkhaleq, L. A., Assi, M. A. *et al.* The crucial roles of inflammatory mediators in inflammation: A review. *Vet World.* **11**, 627-635 (2018).
[44] Suvas, S. Role of Substance P Neuropeptide in Inflammation, Wound Healing, and Tissue Homeostasis. *J Immunol.* **199**, 1543-1552 (2017).
[45] Markiewski, M. M. and Lambris, J. D. The role of complement in inflammatory diseases from behind the scenes into the spotlight. *Am J Pathol.* **171**, 715-727 (2007).
[46] Claesson-Welsh, L. Vascular permeability--the essentials. *Ups J Med Sci.* **120**, 135-143 (2015).
[47] Hunt, B. J. and Jurd, K. M. Endothelial cell activation. A central pathophysiological process. *BMJ.* **316**, 1328-1329 (1998).
[48] Nourshargh, S. and Alon, R. Leukocyte migration into inflamed tissues. *Immunity.* **41**, 694-707 (2014).
[49] McIntyre, T. M., Prescott, S. M. *et al.* Cell-cell interactions: leukocyte-endothelial interactions. *Curr Opin Hematol.* **10**, 150-158 (2003).
[50] Nathan, C. Neutrophils and immunity: challenges and opportunities. *Nat Rev Immunol.* **6**, 173-182 (2006).
[51] Serhan, C. N. Resolution phase of inflammation: novel endogenous anti-inflammatory and proresolving lipid mediators and pathways. *Annu Rev Immunol.* **25**, 101-137 (2007).
[52] Franscini, N., Bachli, E. B. *et al.* Gene expression profiling of inflamed human endothelial cells and influence of activated protein C. *Circulation.* **110**, 2903-2909 (2004).

[53] Pober, J. S. and Sessa, W. C. Evolving functions of endothelial cells in inflammation. *Nat Rev Immunol.* **7**, 803-815 (2007).
[54] Smith, C. W. Endothelial adhesion molecules and their role in inflammation. *Can J Physiol Pharmacol.* **71**, 76-87 (1993).
[55] Radi, Z. A., Kehrli, M. E., Jr. *et al.* Cell adhesion molecules, leukocyte trafficking, and strategies to reduce leukocyte infiltration. *J Vet Intern Med.* **15**, 516-529 (2001).
[56] Vachino, G., Chang, X. J. *et al.* P-selectin glycoprotein ligand-1 is the major counter-receptor for P-selectin on stimulated T cells and is widely distributed in non-functional form on many lymphocytic cells. *J Biol Chem.* **270**, 21966-21974 (1995).
[57] Zarbock, A., Ley, K. *et al.* Leukocyte ligands for endothelial selectins: specialized glycoconjugates that mediate rolling and signaling under flow. *Blood.* **118**, 6743-6751 (2011).
[58] Ley, K., Laudanna, C. *et al.* Getting to the site of inflammation: the leukocyte adhesion cascade updated. *Nat Rev Immunol.* **7**, 678-689 (2007).
[59] McEver, R. P. Regulation of function and expression of P-selectin. *Agents Actions Suppl.* **47**, 117-119 (1995).
[60] Yu, G., Rux, A. H. *et al.* Endothelial expression of E-selectin is induced by the platelet-specific chemokine platelet factor 4 through LRP in an NF-kappaB-dependent manner. *Blood.* **105**, 3545-3551 (2005).
[61] Langer, H. F. and Chavakis, T. Leukocyte-endothelial interactions in inflammation. *J Cell Mol Med.* **13**, 1211-1220 (2009).
[62] Muller, W. A., Weigl, S. A. *et al.* PECAM-1 is required for transendothelial migration of leukocytes. *J Exp Med.* **178**, 449-460 (1993).
[63] Dufour, E. M., Deroche, A. *et al.* CD99 is essential for leukocyte diapedesis in vivo. *Cell Commun Adhes.* **15**, 351-363 (2008).
[64] Petri, B. and Sanz, M. J. Neutrophil chemotaxis. *Cell Tissue Res.* **371**, 425-436 (2018).
[65] Vestweber, D. How leukocytes cross the vascular endothelium. *Nat Rev Immunol.* **15**, 692-704 (2015).
[66] Abadi, A. T. B. Strategies used by helicobacter pylori to establish persistent infection. *World J Gastroenterol.* **23**, 2870-2882 (2017).
[67] Simmons, J. D., Stein, C. M. *et al.* Immunological mechanisms of human resistance to persistent Mycobacterium tuberculosis infection. *Nat Rev Immunol.* **18**, 575-589 (2018).
[68] Guidotti, L. G. and Chisari, F. V. Immunobiology and pathogenesis of viral hepatitis. *Annu Rev Pathol.* **1**, 23-61 (2006).
[69] Hobbs, C. A., Bobay, B. G. *et al.* NMR solution structure and DNA-binding model of the DNA-binding domain of competence protein A. *J Mol Biol.* **398**, 248-263 (2010).
[70] Nathan, C. Points of control in inflammation. *Nature.* **420**, 846-852 (2002).
[71] Brazil, J. C., Louis, N. A. *et al.* The role of polymorphonuclear leukocyte trafficking in the perpetuation of inflammation during inflammatory bowel disease. *Inflamm Bowel Dis.* **19**, 1556-1565 (2013).
[72] Suthahar, N., Meijers, W. C. *et al.* From Inflammation to Fibrosis-Molecular and Cellular Mechanisms of Myocardial Tissue Remodelling and Perspectives on Differential Treatment Opportunities. *Curr Heart Fail Rep.* **14**, 235-250 (2017).
[73] Leuti, A., Fazio, D. *et al.* Bioactive lipids, inflammation and chronic diseases. *Adv Drug Deliv Rev.* **159**, 133-169 (2020).
[74] Nathan, C. and Ding, A. Nonresolving inflammation. *Cell.* **140**, 871-882 (2010).
[75] Borish, L. C. and Steinke, J. W. 2. Cytokines and chemokines. *J Allergy Clin Immunol.* **111**, S460-475 (2003).
[76] Ruddle, N. H. Tumor necrosis factor (TNF-alpha) and lymphotoxin (TNF-beta). *Curr Opin Immunol.* **4**, 327-332 (1992).
[77] Horiuchi, T., Mitoma, H. *et al.* Transmembrane TNF-alpha: structure, function and interaction with anti-TNF agents. *Rheumatology (Oxford).* **49**, 1215-1228 (2010).
[78] Edwards, D. R., Handsley, M. M. *et al.* The ADAM metalloproteinases. *Mol Aspects Med.* **29**, 258-289 (2008).
[79] Eck, M. J. and Sprang, S. R. The structure of tumor necrosis factor-alpha at 2.6 A resolution. Implications for receptor binding. *J Biol Chem.* **264**, 17595-17605 (1989).

[80] Idriss, H. T. and Naismith, J. H. TNF alpha and the TNF receptor superfamily: structure-function relationship(s). *Microsc Res Tech.* **50**, 184-195 (2000).
[81] Medler, J. and Wajant, H. Tumor necrosis factor receptor-2 (TNFR2): an overview of an emerging drug target. *Expert Opin Ther Targets.* **23**, 295-307 (2019).
[82] Thornberry, N. A., Bull, H. G. *et al.* A novel heterodimeric cysteine protease is required for interleukin-1 beta processing in monocytes. *Nature.* **356**, 768-774 (1992).
[83] Palomo, J., Dietrich, D. *et al.* The interleukin (IL)-1 cytokine family--Balance between agonists and antagonists in inflammatory diseases. *Cytokine.* **76**, 25-37 (2015).
[84] Boraschi, D., Italiani, P. *et al.* The family of the interleukin-1 receptors. *Immunol Rev.* **281**, 197-232 (2018).
[85] Schluter, T., Schelmbauer, C. *et al.* Regulation of IL-1 signaling by the decoy receptor IL-1R2. *J Mol Med (Berl).* **96**, 983-992 (2018).
[86] Oeckinghaus, A. and Ghosh, S. The NF-kappaB family of transcription factors and its regulation. *Cold Spring Harb Perspect Biol.* **1**, a000034 (2009).
[87] Pahl, H. L. Activators and target genes of Rel/NF-kappaB transcription factors. *Oncogene.* **18**, 6853-6866 (1999).
[88] Israel, A. The IKK complex, a central regulator of NF-kappaB activation. *Cold Spring Harb Perspect Biol.* **2**, a000158 (2010).
[89] Poyet, J. L., Srinivasula, S. M. *et al.* Activation of the Ikappa B kinases by RIP via IKKgamma /NEMO-mediated oligomerization. *J Biol Chem.* **275**, 37966-37977 (2000).
[90] Delhase, M., Hayakawa, M. *et al.* Positive and negative regulation of IkappaB kinase activity through IKKbeta subunit phosphorylation. *Science.* **284**, 309-313 (1999).
[91] Karin, M. How NF-kappaB is activated: the role of the IkappaB kinase (IKK) complex. *Oncogene.* **18**, 6867-6874 (1999).
[92] Phelps, C. B., Sengchanthalangsy, L. L. *et al.* Mechanism of I kappa B alpha binding to NF-kappa B dimers. *J Biol Chem.* **275**, 29840-29846 (2000).
[93] Beg, A. A., Ruben, S. M. *et al.* I kappa B interacts with the nuclear localization sequences of the subunits of NF-kappa B: a mechanism for cytoplasmic retention. *Genes Dev.* **6**, 1899-1913 (1992).
[94] Brignall, R., Moody, A. T. *et al.* Considering Abundance, Affinity, and Binding Site Availability in the NF-kappaB Target Selection Puzzle. *Front Immunol.* **10**, 609 (2019).
[95] Liu, Y. C., Penninger, J. *et al.* Immunity by ubiquitylation: a reversible process of modification. *Nat Rev Immunol.* **5**, 941-952 (2005).
[96] Chiao, P. J., Miyamoto, S. *et al.* Autoregulation of I kappa B alpha activity. *Proc Natl Acad Sci U S A.* **91**, 28-32 (1994).
[97] Werner, S. L., Kearns, J. D. *et al.* Encoding NF-kappaB temporal control in response to TNF: distinct roles for the negative regulators IkappaBalpha and A20. *Genes Dev.* **22**, 2093-2101 (2008).
[98] Ghosh, S. and Hayden, M. S. New regulators of NF-kappaB in inflammation. *Nat Rev Immunol.* **8**, 837-848 (2008).
[99] Rout, M. P., Aitchison, J. D. *et al.* The yeast nuclear pore complex: composition, architecture, and transport mechanism. *J Cell Biol.* **148**, 635-651 (2000).
[100] Lange, A., Mills, R. E. *et al.* Classical nuclear localization signals: definition, function, and interaction with importin alpha. *J Biol Chem.* **282**, 5101-5105 (2007).
[101] Steggerda, S. M. and Paschal, B. M. Regulation of nuclear import and export by the GTPase Ran. *Int Rev Cytol.* **217**, 41-91 (2002).
[102] Gorlich, D., Seewald, M. J. *et al.* Characterization of Ran-driven cargo transport and the RanGTPase system by kinetic measurements and computer simulation. *EMBO J.* **22**, 1088-1100 (2003).
[103] Miyamoto, Y., Yamada, K. *et al.* Importin alpha: a key molecule in nuclear transport and non-transport functions. *J Biochem.* **160**, 69-75 (2016).
[104] Pumroy, R. A. and Cingolani, G. Diversification of importin-alpha isoforms in cellular trafficking and disease states. *Biochem J.* **466**, 13-28 (2015).
[105] Oka, M. and Yoneda, Y. Importin alpha: functions as a nuclear transport factor and beyond. *Proc Jpn Acad Ser B Phys Biol Sci.* **94**, 259-274 (2018).

[106] Gorlich, D., Henklein, P. *et al.* A 41 amino acid motif in importin-alpha confers binding to importin-beta and hence transit into the nucleus. *EMBO J.* **15**, 1810-1817 (1996).
[107] Herold, A., Truant, R. *et al.* Determination of the functional domain organization of the importin alpha nuclear import factor. *J Cell Biol.* **143**, 309-318 (1998).
[108] Kutay, U., Bischoff, F. R. *et al.* Export of importin alpha from the nucleus is mediated by a specific nuclear transport factor. *Cell.* **90**, 1061-1071 (1997).
[109] Chi, N. C. and Adam, S. A. Functional domains in nuclear import factor p97 for binding the nuclear localization sequence receptor and the nuclear pore. *Mol Biol Cell.* **8**, 945-956 (1997).
[110] Liu, S. M. and Liu, W. M. Recent developments in the understanding of nuclear protein import. *Protein Pept Lett.* **14**, 723-733 (2007).
[111] Goldfarb, D. S., Corbett, A. H. *et al.* Importin alpha: a multipurpose nuclear-transport receptor. *Trends Cell Biol.* **14**, 505-514 (2004).
[112] Kamei, Y., Yuba, S. *et al.* Three distinct classes of the alpha-subunit of the nuclear pore-targeting complex (importin-alpha) are differentially expressed in adult mouse tissues. *J Histochem Cytochem.* **47**, 363-372 (1999).
[113] Yasuhara, N., Shibazaki, N. *et al.* Triggering neural differentiation of ES cells by subtype switching of importin-alpha. *Nat Cell Biol.* **9**, 72-79 (2007).
[114] Kohler, M., Fiebeler, A. *et al.* Differential expression of classical nuclear transport factors during cellular proliferation and differentiation. *Cell Physiol Biochem.* **12**, 335-344 (2002).
[115] Cai, Y., Shen, Y. *et al.* Karyopherin Alpha 2 Promotes the Inflammatory Response in Rat Pancreatic Acinar Cells Via Facilitating NF-kappaB Activation. *Dig Dis Sci.* **61**, 747-757 (2016).
[116] Fagerlund, R., Kinnunen, L. *et al.* NF-{kappa}B is transported into the nucleus by importin {alpha}3 and importin {alpha}4. *J Biol Chem.* **280**, 15942-15951 (2005).
[117] Tao, R., Xu, X. *et al.* KPNA2 interacts with P65 to modulate catabolic events in osteoarthritis. *Exp Mol Pathol.* **99**, 245-252 (2015).
[118] Yang, F., Li, S. *et al.* Karyopherin alpha 2 promotes proliferation, migration and invasion through activating NF-kappaB/p65 signaling pathways in melanoma cells. *Life Sci.* **252**, 117611 (2020).
[119] Zhuo, Y., Guo, Z. *et al.* African Swine Fever Virus MGF360-12L Inhibits Type I Interferon Production by Blocking the Interaction of Importin alpha and NF-kappaB Signaling Pathway. *Virol Sin.* **36**, 176-186 (2021).
[120] Hume, D. A. and Fairlie, D. P. Therapeutic targets in inflammatory disease. *Curr Med Chem.* **12**, 2925-2929 (2005).
[121] Munoz, L. and Ammit, A. J. Targeting p38 MAPK pathway for the treatment of Alzheimer's disease. *Neuropharmacology.* **58**, 561-568 (2010).
[122] Stark, A. K., Sriskantharajah, S. *et al.* PI3K inhibitors in inflammation, autoimmunity and cancer. *Curr Opin Pharmacol.* **23**, 82-91 (2015).
[123] Yeung, Y. T., Aziz, F. *et al.* Signaling Pathways in Inflammation and Anti-inflammatory Therapies. *Curr Pharm Des.* **24**, 1449-1484 (2018).
[124] Johnson, D. E., O'Keefe, R. A. *et al.* Targeting the IL-6/JAK/STAT3 signalling axis in cancer. *Nat Rev Clin Oncol.* **15**, 234-248 (2018).
[125] Wang, W. Y., Tan, M. S. *et al.* Role of pro-inflammatory cytokines released from microglia in Alzheimer's disease. *Ann Transl Med.* **3**, 136 (2015).
[126] Koul, H. K., Pal, M. *et al.* Role of p38 MAP Kinase Signal Transduction in Solid Tumors. *Genes Cancer.* **4**, 342-359 (2013).
[127] Lupia, E., Pigozzi, L. *et al.* Role of phosphoinositide 3-kinase in the pathogenesis of acute pancreatitis. *World J Gastroenterol.* **20**, 15190-15199 (2014).
[128] Hawkins, P. T. and Stephens, L. R. PI3K signalling in inflammation. *Biochim Biophys Acta.* **1851**, 882-897 (2015).
[129] Lin, L., Hron, J. D. *et al.* Regulation of NF-kappaB, Th activation, and autoinflammation by the forkhead transcription factor Foxo3a. *Immunity.* **21**, 203-213 (2004).
[130] Ohtsubo, H., Ichiki, T. *et al.* Involvement of Mst1 in tumor necrosis factor-alpha-induced apoptosis of endothelial cells. *Biochem Biophys Res Commun.* **367**, 474-480 (2008).

[131] Karin, M. and Greten, F. R. NF-kappaB: linking inflammation and immunity to cancer development and progression. *Nat Rev Immunol.* **5**, 749-759 (2005).
[132] Bollrath, J. and Greten, F. R. IKK/NF-kappaB and STAT3 pathways: central signalling hubs in inflammation-mediated tumour promotion and metastasis. *EMBO Rep.* **10**, 1314-1319 (2009).
[133] Mankan, A. K., Canli, O. *et al.* TNF-alpha-dependent loss of IKKbeta-deficient myeloid progenitors triggers a cytokine loop culminating in granulocytosis. *Proc Natl Acad Sci U S A.* **108**, 6567-6572 (2011).
[134] Nagashima, K., Sasseville, V. G. *et al.* Rapid TNFR1-dependent lymphocyte depletion in vivo with a selective chemical inhibitor of IKKbeta. *Blood.* **107**, 4266-4273 (2006).
[135] Greten, F. R., Arkan, M. C. *et al.* NF-kappaB is a negative regulator of IL-1beta secretion as revealed by genetic and pharmacological inhibition of IKKbeta. *Cell.* **130**, 918-931 (2007).
[136] Dinarello, C. A., Simon, A. *et al.* Treating inflammation by blocking interleukin-1 in a broad spectrum of diseases. *Nat Rev Drug Discov.* **11**, 633-652 (2012).
[137] Mitoma, H., Horiuchi, T. *et al.* Molecular mechanisms of action of anti-TNF-alpha agents - Comparison among therapeutic TNF-alpha antagonists. *Cytokine.* **101**, 56-63 (2018).
[138] Owczarczyk-Saczonek, A., Owczarek, W. *et al.* Secondary failure of TNF-alpha inhibitors in clinical practice. *Dermatol Ther.* **32**, e12760 (2019).
[139] Risau, W. Mechanisms of angiogenesis. *Nature.* **386**, 671-674 (1997).
[140] Risau, W. and Flamme, I. Vasculogenesis. *Annu Rev Cell Dev Biol.* **11**, 73-91 (1995).
[141] Potente, M. and Carmeliet, P. The Link Between Angiogenesis and Endothelial Metabolism. *Annu Rev Physiol.* **79**, 43-66 (2017).
[142] Breier, G. Angiogenesis in embryonic development--a review. *Placenta.* **21 Suppl A**, S11-15 (2000).
[143] Baldwin, H. S. Early embryonic vascular development. *Cardiovasc Res.* **31 Spec No**, E34-45 (1996).
[144] Nyberg, P., Xie, L. *et al.* Endogenous inhibitors of angiogenesis. *Cancer Res.* **65**, 3967-3979 (2005).
[145] Reynolds, L. P., Grazul-Bilska, A. T. *et al.* Angiogenesis in the female reproductive organs: pathological implications. *Int J Exp Pathol.* **83**, 151-163 (2002).
[146] Reynolds, L. P., Grazul-Bilska, A. T. *et al.* Angiogenesis in the corpus luteum. *Endocrine.* **12**, 1-9 (2000).
[147] DiPietro, L. A. Angiogenesis and wound repair: when enough is enough. *J Leukoc Biol.* **100**, 979-984 (2016).
[148] Yoo, S. Y. and Kwon, S. M. Angiogenesis and its therapeutic opportunities. *Mediators Inflamm.* **2013**, 127170 (2013).
[149] Ribatti, D., Nico, B. *et al.* The history of the angiogenic switch concept. *Leukemia.* **21**, 44-52 (2007).
[150] Haase, V. H. The VHL tumor suppressor: master regulator of HIF. *Curr Pharm Des.* **15**, 3895-3903 (2009).
[151] Semenza, G. L. Regulation of mammalian O2 homeostasis by hypoxia-inducible factor 1. *Annu Rev Cell Dev Biol.* **15**, 551-578 (1999).
[152] Semenza, G. L. Hypoxia-inducible factor 1: master regulator of O2 homeostasis. *Curr Opin Genet Dev.* **8**, 588-594 (1998).
[153] Hahn, C. and Schwartz, M. A. Mechanotransduction in vascular physiology and atherogenesis. *Nat Rev Mol Cell Biol.* **10**, 53-62 (2009).
[154] Shyu, K. G. Cellular and molecular effects of mechanical stretch on vascular cells and cardiac myocytes. *Clin Sci (Lond).* **116**, 377-389 (2009).
[155] Buchanan, C. F., Verbridge, S. S. *et al.* Flow shear stress regulates endothelial barrier function and expression of angiogenic factors in a 3D microfluidic tumor vascular model. *Cell Adh Migr.* **8**, 517-524 (2014).
[156] Galie, P. A., Nguyen, D. H. *et al.* Fluid shear stress threshold regulates angiogenic sprouting. *Proc Natl Acad Sci U S A.* **111**, 7968-7973 (2014).

[157] Eberhardt, W. and Pfeilschifter, J. Nitric oxide and vascular remodeling: spotlight on the kidney. *Kidney Int Suppl.* S9-S16 (2007).
[158] Hayashi, S., Watanabe, N. *et al.* Roles of P-selectin in inflammation, neointimal formation, and vascular remodeling in balloon-injured rat carotid arteries. *Circulation.* **102**, 1710-1717 (2000).
[159] Kholia, S., Ranghino, A. *et al.* Extracellular vesicles as new players in angiogenesis. *Vascul Pharmacol.* **86**, 64-70 (2016).
[160] Todorova, D., Simoncini, S. *et al.* Extracellular Vesicles in Angiogenesis. *Circ Res.* **120**, 1658-1673 (2017).
[161] Gai, C., Carpanetto, A. *et al.* Extracellular vesicle-mediated modulation of angiogenesis. *Histol Histopathol.* **31**, 379-391 (2016).
[162] Ribatti, D., Conconi, M. T. *et al.* Nonclassic endogenous novel [corrected] regulators of angiogenesis. *Pharmacol Rev.* **59**, 185-205 (2007).
[163] Naito, H., Iba, T. *et al.* Mechanisms of new blood-vessel formation and proliferative heterogeneity of endothelial cells. *Int Immunol.* **32**, 295-305 (2020).
[164] Abhinand, C. S., Raju, R. *et al.* VEGF-A/VEGFR2 signaling network in endothelial cells relevant to angiogenesis. *J Cell Commun Signal.* **10**, 347-354 (2016).
[165] Blanco, R. and Gerhardt, H. VEGF and Notch in tip and stalk cell selection. *Cold Spring Harb Perspect Med.* **3**, a006569 (2013).
[166] Gerhardt, H., Golding, M. *et al.* VEGF guides angiogenic sprouting utilizing endothelial tip cell filopodia. *J Cell Biol.* **161**, 1163-1177 (2003).
[167] Ristimae, T., Huikuri, H. V. *et al.* Heart rate variability in patients with the first and recurrent myocardial infarction. *Clin Auton Res.* **8**, 195-199 (1998).
[168] Scharpfenecker, M., Fiedler, U. *et al.* The Tie-2 ligand angiopoietin-2 destabilizes quiescent endothelium through an internal autocrine loop mechanism. *J Cell Sci.* **118**, 771-780 (2005).
[169] Jakobsson, L., Franco, C. A. *et al.* Endothelial cells dynamically compete for the tip cell position during angiogenic sprouting. *Nat Cell Biol.* **12**, 943-953 (2010).
[170] Phng, L. K. and Gerhardt, H. Angiogenesis: a team effort coordinated by notch. *Dev Cell.* **16**, 196-208 (2009).
[171] Potente, M., Gerhardt, H. *et al.* Basic and therapeutic aspects of angiogenesis. *Cell.* **146**, 873-887 (2011).
[172] Iruela-Arispe, M. L. and Davis, G. E. Cellular and molecular mechanisms of vascular lumen formation. *Dev Cell.* **16**, 222-231 (2009).
[173] Andrae, J., Gallini, R. *et al.* Role of platelet-derived growth factors in physiology and medicine. *Genes Dev.* **22**, 1276-1312 (2008).
[174] Davis, S. and Yancopoulos, G. D. The angiopoietins: Yin and Yang in angiogenesis. *Curr Top Microbiol Immunol.* **237**, 173-185 (1999).
[175] van Groningen, J. P., Wenink, A. C. *et al.* Myocardial capillaries: increase in number by splitting of existing vessels. *Anat Embryol (Berl).* **184**, 65-70 (1991).
[176] Djonov, V. G., Kurz, H. *et al.* Optimality in the developing vascular system: branching remodeling by means of intussusception as an efficient adaptation mechanism. *Dev Dyn.* **224**, 391-402 (2002).
[177] Djonov, V., Baum, O. *et al.* Vascular remodeling by intussusceptive angiogenesis. *Cell Tissue Res.* **314**, 107-117 (2003).
[178] Yamazaki, Y. and Morita, T. Molecular and functional diversity of vascular endothelial growth factors. *Mol Divers.* **10**, 515-527 (2006).
[179] Peach, C. J., Mignone, V. W. *et al.* Molecular Pharmacology of VEGF-A Isoforms: Binding and Signalling at VEGFR2. *Int J Mol Sci.* **19**, (2018).
[180] Koch, S., Tugues, S. *et al.* Signal transduction by vascular endothelial growth factor receptors. *Biochem J.* **437**, 169-183 (2011).
[181] Shibuya, M. Vascular Endothelial Growth Factor (VEGF) and Its Receptor (VEGFR) Signaling in Angiogenesis: A Crucial Target for Anti- and Pro-Angiogenic Therapies. *Genes Cancer.* **2**, 1097-1105 (2011).
[182] Roskoski, R., Jr. VEGF receptor protein-tyrosine kinases: structure and regulation. *Biochem Biophys Res Commun.* **375**, 287-291 (2008).

[183] Ullrich, A. and Schlessinger, J. Signal transduction by receptors with tyrosine kinase activity. *Cell.* **61**, 203-212 (1990).
[184] Nolen, B., Taylor, S. *et al.* Regulation of protein kinases; controlling activity through activation segment conformation. *Mol Cell.* **15**, 661-675 (2004).
[185] Stuttfeld, E. and Ballmer-Hofer, K. Structure and function of VEGF receptors. *IUBMB Life.* **61**, 915-922 (2009).
[186] Shibuya, M. Vascular endothelial growth factor and its receptor system: physiological functions in angiogenesis and pathological roles in various diseases. *J Biochem.* **153**, 13-19 (2013).
[187] Olsson, A. K., Dimberg, A. *et al.* VEGF receptor signalling - in control of vascular function. *Nat Rev Mol Cell Biol.* **7**, 359-371 (2006).
[188] Kazi, J. U. and Ronnstrand, L. FMS-like Tyrosine Kinase 3/FLT3: From Basic Science to Clinical Implications. *Physiol Rev.* **99**, 1433-1466 (2019).
[189] Lindsey, S. and Langhans, S. A. Epidermal growth factor signaling in transformed cells. *Int Rev Cell Mol Biol.* **314**, 1-41 (2015).
[190] Xie, Y., Su, N. *et al.* FGF/FGFR signaling in health and disease. *Signal Transduct Target Ther.* **5**, 181 (2020).
[191] Sabbah, D. A., Hajjo, R. *et al.* Review on Epidermal Growth Factor Receptor (EGFR) Structure, Signaling Pathways, Interactions, and Recent Updates of EGFR Inhibitors. *Curr Top Med Chem.* **20**, 815-834 (2020).
[192] Martin, V., Liu, D. *et al.* Tie2: a journey from normal angiogenesis to cancer and beyond. *Histol Histopathol.* **23**, 773-780 (2008).
[193] Ramazani, Y., Knops, N. *et al.* Connective tissue growth factor (CTGF) from basics to clinics. *Matrix Biol.* **68-69**, 44-66 (2018).
[194] Keshet, Y. and Seger, R. The MAP kinase signaling cascades: a system of hundreds of components regulates a diverse array of physiological functions. *Methods Mol Biol.* **661**, 3-38 (2010).
[195] Qi, M. and Elion, E. A. MAP kinase pathways. *J Cell Sci.* **118**, 3569-3572 (2005).
[196] Tanoue, T. and Nishida, E. Molecular recognitions in the MAP kinase cascades. *Cell Signal.* **15**, 455-462 (2003).
[197] Keyse, S. M. Protein phosphatases and the regulation of mitogen-activated protein kinase signalling. *Curr Opin Cell Biol.* **12**, 186-192 (2000).
[198] McKay, M. M. and Morrison, D. K. Integrating signals from RTKs to ERK/MAPK. *Oncogene.* **26**, 3113-3121 (2007).
[199] Roskoski, R., Jr. ERK1/2 MAP kinases: structure, function, and regulation. *Pharmacol Res.* **66**, 105-143 (2012).
[200] Roberts, P. J. and Der, C. J. Targeting the Raf-MEK-ERK mitogen-activated protein kinase cascade for the treatment of cancer. *Oncogene.* **26**, 3291-3310 (2007).
[201] Johnson, G. L. and Nakamura, K. The c-jun kinase/stress-activated pathway: regulation, function and role in human disease. *Biochim Biophys Acta.* **1773**, 1341-1348 (2007).
[202] Ichijo, H. From receptors to stress-activated MAP kinases. *Oncogene.* **18**, 6087-6093 (1999).
[203] Weston, C. R. and Davis, R. J. The JNK signal transduction pathway. *Curr Opin Cell Biol.* **19**, 142-149 (2007).
[204] Kumar, A., Singh, U. K. *et al.* JNK pathway signaling: a novel and smarter therapeutic targets for various biological diseases. *Future Med Chem.* **7**, 2065-2086 (2015).
[205] Cuadrado, A. and Nebreda, A. R. Mechanisms and functions of p38 MAPK signalling. *Biochem J.* **429**, 403-417 (2010).
[206] Yong, H. Y., Koh, M. S. *et al.* The p38 MAPK inhibitors for the treatment of inflammatory diseases and cancer. *Expert Opin Investig Drugs.* **18**, 1893-1905 (2009).
[207] Liu, Y., Shepherd, E. G. *et al.* MAPK phosphatases--regulating the immune response. *Nat Rev Immunol.* **7**, 202-212 (2007).
[208] Franke, T. F., Kaplan, D. R. *et al.* PI3K: downstream AKTion blocks apoptosis. *Cell.* **88**, 435-437 (1997).

[209] Nave, B. T., Ouwens, M. *et al.* Mammalian target of rapamycin is a direct target for protein kinase B: identification of a convergence point for opposing effects of insulin and amino-acid deficiency on protein translation. *Biochem J.* **344 Pt 2**, 427-431 (1999).
[210] Zhang, Y., Wang, X. *et al.* Kinase AKT controls innate immune cell development and function. *Immunology.* **140**, 143-152 (2013).
[211] Ackah, E., Yu, J. *et al.* Akt1/protein kinase Balpha is critical for ischemic and VEGF-mediated angiogenesis. *J Clin Invest.* **115**, 2119-2127 (2005).
[212] Kim, D. and Chung, J. Akt: versatile mediator of cell survival and beyond. *J Biochem Mol Biol.* **35**, 106-115 (2002).
[213] Vanhaesebroeck, B., Guillermet-Guibert, J. *et al.* The emerging mechanisms of isoform-specific PI3K signalling. *Nat Rev Mol Cell Biol.* **11**, 329-341 (2010).
[214] Alessi, D. R., Andjelkovic, M. *et al.* Mechanism of activation of protein kinase B by insulin and IGF-1. *EMBO J.* **15**, 6541-6551 (1996).
[215] Sarbassov, D. D., Guertin, D. A. *et al.* Phosphorylation and regulation of Akt/PKB by the rictor-mTOR complex. *Science.* **307**, 1098-1101 (2005).
[216] Bozulic, L., Surucu, B. *et al.* PKBalpha/Akt1 acts downstream of DNA-PK in the DNA double-strand break response and promotes survival. *Mol Cell.* **30**, 203-213 (2008).
[217] Persad, S., Attwell, S. *et al.* Regulation of protein kinase B/Akt-serine 473 phosphorylation by integrin-linked kinase: critical roles for kinase activity and amino acids arginine 211 and serine 343. *J Biol Chem.* **276**, 27462-27469 (2001).
[218] Rodgers, S. J., Ferguson, D. T. *et al.* Regulation of PI3K effector signalling in cancer by the phosphoinositide phosphatases. *Biosci Rep.* **37**, (2017).
[219] Manning, B. D. and Toker, A. AKT/PKB Signaling: Navigating the Network. *Cell.* **169**, 381-405 (2017).
[220] Hoxhaj, G. and Manning, B. D. The PI3K-AKT network at the interface of oncogenic signalling and cancer metabolism. *Nat Rev Cancer.* **20**, 74-88 (2020).
[221] Alessi, D. R., Caudwell, F. B. *et al.* Molecular basis for the substrate specificity of protein kinase B; comparison with MAPKAP kinase-1 and p70 S6 kinase. *FEBS Lett.* **399**, 333-338 (1996).
[222] Manning, B. D. and Cantley, L. C. AKT/PKB signaling: navigating downstream. *Cell.* **129**, 1261-1274 (2007).
[223] Dimmeler, S., Fleming, I. *et al.* Activation of nitric oxide synthase in endothelial cells by Akt-dependent phosphorylation. *Nature.* **399**, 601-605 (1999).
[224] Gordan, J. D. and Simon, M. C. Hypoxia-inducible factors: central regulators of the tumor phenotype. *Curr Opin Genet Dev.* **17**, 71-77 (2007).
[225] Morbidelli, L., Donnini, S. *et al.* Role of nitric oxide in the modulation of angiogenesis. *Curr Pharm Des.* **9**, 521-530 (2003).
[226] Szymonowicz, K., Oeck, S. *et al.* New Insights into Protein Kinase B/Akt Signaling: Role of Localized Akt Activation and Compartment-Specific Target Proteins for the Cellular Radiation Response. *Cancers (Basel).* **10**, (2018).
[227] Brognard, J., Clark, A. S. *et al.* Akt/protein kinase B is constitutively active in non-small cell lung cancer cells and promotes cellular survival and resistance to chemotherapy and radiation. *Cancer Res.* **61**, 3986-3997 (2001).
[228] Fruman, D. A. and Rommel, C. PI3K and cancer: lessons, challenges and opportunities. *Nat Rev Drug Discov.* **13**, 140-156 (2014).
[229] Song, M. S., Salmena, L. *et al.* The functions and regulation of the PTEN tumour suppressor. *Nat Rev Mol Cell Biol.* **13**, 283-296 (2012).
[230] Pan, D. The hippo signaling pathway in development and cancer. *Dev Cell.* **19**, 491-505 (2010).
[231] Sudol, M., Bork, P. *et al.* Characterization of the mammalian YAP (Yes-associated protein) gene and its role in defining a novel protein module, the WW domain. *J Biol Chem.* **270**, 14733-14741 (1995).
[232] Kanai, F., Marignani, P. A. *et al.* TAZ: a novel transcriptional co-activator regulated by interactions with 14-3-3 and PDZ domain proteins. *EMBO J.* **19**, 6778-6791 (2000).

[233] Zhao, B., Wei, X. *et al.* Inactivation of YAP oncoprotein by the Hippo pathway is involved in cell contact inhibition and tissue growth control. *Genes Dev.* **21**, 2747-2761 (2007).
[234] Lei, Q. Y., Zhang, H. *et al.* TAZ promotes cell proliferation and epithelial-mesenchymal transition and is inhibited by the hippo pathway. *Mol Cell Biol.* **28**, 2426-2436 (2008).
[235] Murakami, M., Nakagawa, M. *et al.* A WW domain protein TAZ is a critical coactivator for TBX5, a transcription factor implicated in Holt-Oram syndrome. *Proc Natl Acad Sci U S A.* **102**, 18034-18039 (2005).
[236] Strano, S., Munarriz, E. *et al.* Physical interaction with Yes-associated protein enhances p73 transcriptional activity. *J Biol Chem.* **276**, 15164-15173 (2001).
[237] Zhao, B., Ye, X. *et al.* TEAD mediates YAP-dependent gene induction and growth control. *Genes Dev.* **22**, 1962-1971 (2008).
[238] Varelas, X., Sakuma, R. *et al.* TAZ controls Smad nucleocytoplasmic shuttling and regulates human embryonic stem-cell self-renewal. *Nat Cell Biol.* **10**, 837-848 (2008).
[239] Varelas, X., Samavarchi-Tehrani, P. *et al.* The Crumbs complex couples cell density sensing to Hippo-dependent control of the TGF-beta-SMAD pathway. *Dev Cell.* **19**, 831-844 (2010).
[240] Yagi, R., Chen, L. F. *et al.* A WW domain-containing yes-associated protein (YAP) is a novel transcriptional co-activator. *EMBO J.* **18**, 2551-2562 (1999).
[241] Wang, Y., Xu, X. *et al.* Comprehensive Molecular Characterization of the Hippo Signaling Pathway in Cancer. *Cell Rep.* **25**, 1304-1317 e1305 (2018).
[242] Choi, H. J., Zhang, H. *et al.* Yes-associated protein regulates endothelial cell contact-mediated expression of angiopoietin-2. *Nat Commun.* **6**, 6943 (2015).
[243] Neto, F., Klaus-Bergmann, A. *et al.* YAP and TAZ regulate adherens junction dynamics and endothelial cell distribution during vascular development. *Elife.* **7**, (2018).
[244] Wang, X., Freire Valls, A. *et al.* YAP/TAZ Orchestrate VEGF Signaling during Developmental Angiogenesis. *Dev Cell.* **42**, 462-478 e467 (2017).
[245] Kim, J., Kim, Y. H. *et al.* YAP/TAZ regulates sprouting angiogenesis and vascular barrier maturation. *J Clin Invest.* **127**, 3441-3461 (2017).
[246] Azad, T., Janse van Rensburg, H. J. *et al.* A LATS biosensor screen identifies VEGFR as a regulator of the Hippo pathway in angiogenesis. *Nat Commun.* **9**, 1061 (2018).
[247] Callus, B. A., Verhagen, A. M. *et al.* Association of mammalian sterile twenty kinases, Mst1 and Mst2, with hSalvador via C-terminal coiled-coil domains, leads to its stabilization and phosphorylation. *FEBS J.* **273**, 4264-4276 (2006).
[248] Chan, E. H., Nousiainen, M. *et al.* The Ste20-like kinase Mst2 activates the human large tumor suppressor kinase Lats1. *Oncogene.* **24**, 2076-2086 (2005).
[249] Praskova, M., Xia, F. *et al.* MOBKL1A/MOBKL1B phosphorylation by MST1 and MST2 inhibits cell proliferation. *Curr Biol.* **18**, 311-321 (2008).
[250] Hergovich, A., Schmitz, D. *et al.* The human tumour suppressor LATS1 is activated by human MOB1 at the membrane. *Biochem Biophys Res Commun.* **345**, 50-58 (2006).
[251] Hao, Y., Chun, A. *et al.* Tumor suppressor LATS1 is a negative regulator of oncogene YAP. *J Biol Chem.* **283**, 5496-5509 (2008).
[252] Hansen, C. G., Moroishi, T. *et al.* YAP and TAZ: a nexus for Hippo signaling and beyond. *Trends Cell Biol.* **25**, 499-513 (2015).
[253] Kim, J., Kwon, H. *et al.* MAML1/2 promote YAP/TAZ nuclear localization and tumorigenesis. *Proc Natl Acad Sci U S A.* **117**, 13529-13540 (2020).
[254] Varelas, X. The Hippo pathway effectors TAZ and YAP in development, homeostasis and disease. *Development.* **141**, 1614-1626 (2014).
[255] Dupont, S., Morsut, L. *et al.* Role of YAP/TAZ in mechanotransduction. *Nature.* **474**, 179-183 (2011).
[256] Breier, G., Chavakis, T. *et al.* Angiogenesis in metabolic-vascular disease. *Thromb Haemost.* **117**, 1289-1295 (2017).
[257] Chung, A. S. and Ferrara, N. Developmental and pathological angiogenesis. *Annu Rev Cell Dev Biol.* **27**, 563-584 (2011).
[258] Jeong, J. H., Ojha, U. *et al.* Pathological angiogenesis and inflammation in tissues. *Arch Pharm Res.* **44**, 1-15 (2021).

[259] Wirtz, D., Konstantopoulos, K. *et al.* The physics of cancer: the role of physical interactions and mechanical forces in metastasis. *Nat Rev Cancer.* **11**, 512-522 (2011).
[260] Maishi, N., Annan, D. A. *et al.* Tumor Endothelial Heterogeneity in Cancer Progression. *Cancers (Basel).* **11**, (2019).
[261] Lugano, R., Ramachandran, M. *et al.* Tumor angiogenesis: causes, consequences, challenges and opportunities. *Cell Mol Life Sci.* **77**, 1745-1770 (2020).
[262] Costa, C., Incio, J. *et al.* Angiogenesis and chronic inflammation: cause or consequence? *Angiogenesis.* **10**, 149-166 (2007).
[263] Murdoch, C., Muthana, M. *et al.* Hypoxia regulates macrophage functions in inflammation. *J Immunol.* **175**, 6257-6263 (2005).
[264] Xue, Q., Yan, Y. *et al.* Regulation of iNOS on Immune Cells and Its Role in Diseases. *Int J Mol Sci.* **19**, (2018).
[265] Mor, F., Quintana, F. J. *et al.* Angiogenesis-inflammation cross-talk: vascular endothelial growth factor is secreted by activated T cells and induces Th1 polarization. *J Immunol.* **172**, 4618-4623 (2004).
[266] Gong, Y. and Koh, D. R. Neutrophils promote inflammatory angiogenesis via release of preformed VEGF in an in vivo corneal model. *Cell Tissue Res.* **339**, 437-448 (2010).
[267] Grenier, A., Chollet-Martin, S. *et al.* Presence of a mobilizable intracellular pool of hepatocyte growth factor in human polymorphonuclear neutrophils. *Blood.* **99**, 2997-3004 (2002).
[268] Schruefer, R., Sulyok, S. *et al.* The proangiogenic capacity of polymorphonuclear neutrophils delineated by microarray technique and by measurement of neovascularization in wounded skin of CD18-deficient mice. *J Vasc Res.* **43**, 1-11 (2006).
[269] Ribatti, D. and Crivellato, E. Immune cells and angiogenesis. *J Cell Mol Med.* **13**, 2822-2833 (2009).
[270] Smolen, J. S., Aletaha, D. *et al.* Rheumatoid arthritis. *Lancet.* **388**, 2023-2038 (2016).
[271] Heidenreich, R., Rocken, M. *et al.* Angiogenesis drives psoriasis pathogenesis. *Int J Exp Pathol.* **90**, 232-248 (2009).
[272] Chu, H. and Wang, Y. Therapeutic angiogenesis: controlled delivery of angiogenic factors. *Ther Deliv.* **3**, 693-714 (2012).
[273] Zirlik, K. and Duyster, J. Anti-Angiogenics: Current Situation and Future Perspectives. *Oncol Res Treat.* **41**, 166-171 (2018).
[274] Bethel, A., Kirsch, J. R. *et al.* Intravenous basic fibroblast growth factor decreases brain injury resulting from focal ischemia in cats. *Stroke.* **28**, 609-615; discussion 615-606 (1997).
[275] Takeshita, S., Zheng, L. P. *et al.* Therapeutic angiogenesis. A single intraarterial bolus of vascular endothelial growth factor augments revascularization in a rabbit ischemic hind limb model. *J Clin Invest.* **93**, 662-670 (1994).
[276] Gupta, R., Tongers, J. *et al.* Human studies of angiogenic gene therapy. *Circ Res.* **105**, 724-736 (2009).
[277] Nagai, M. K. and Embil, J. M. Becaplermin: recombinant platelet derived growth factor, a new treatment for healing diabetic foot ulcers. *Expert Opin Biol Ther.* **2**, 211-218 (2002).
[278] Losordo, D. W. and Dimmeler, S. Therapeutic angiogenesis and vasculogenesis for ischemic disease: part II: cell-based therapies. *Circulation.* **109**, 2692-2697 (2004).
[279] Melincovici, C. S., Bosca, A. B. *et al.* Vascular endothelial growth factor (VEGF) - key factor in normal and pathological angiogenesis. *Rom J Morphol Embryol.* **59**, 455-467 (2018).
[280] Ferrara, N., Hillan, K. J. *et al.* Bevacizumab (Avastin), a humanized anti-VEGF monoclonal antibody for cancer therapy. *Biochem Biophys Res Commun.* **333**, 328-335 (2005).
[281] Yamasaki, M., Murakami, I. *et al.* Carboplatin plus Weekly Paclitaxel Combined with Bevacizumab as First-line Treatment for Non-small Cell Lung Cancer. *Anticancer Res.* **37**, 923-928 (2017).

[282] Tiseo, M., Boni, L. *et al.* Italian, Multicenter, Phase III, Randomized Study of Cisplatin Plus Etoposide With or Without Bevacizumab as First-Line Treatment in Extensive-Disease Small-Cell Lung Cancer: The GOIRC-AIFA FARM6PMFJM Trial. *J Clin Oncol.* **35**, 1281-1287 (2017).
[283] Jiao, Q., Bi, L. *et al.* Advances in studies of tyrosine kinase inhibitors and their acquired resistance. *Mol Cancer.* **17**, 36 (2018).
[284] Finger, R. P., Fleckenstein, M. *et al.* [Therapeutic anti-VEGF in ophthalmology: physiopathology and treatment of age-related macular degeneration]. *Pharm Unserer Zeit.* **36**, 424-430 (2007).
[285] Titchenell, P. M. and Antonetti, D. A. Using the past to inform the future: anti-VEGF therapy as a road map to develop novel therapies for diabetic retinopathy. *Diabetes.* **62**, 1808-1815 (2013).
[286] Cai, S. and Bressler, N. M. Aflibercept, bevacizumab or ranibizumab for diabetic macular oedema: recent clinically relevant findings from DRCR.net Protocol T. *Curr Opin Ophthalmol.* **28**, 636-643 (2017).
[287] Garweg, J. G., Traine, P. G. *et al.* Continued anti-VEGF treatment does not prevent recurrences in eyes with stable neovascular age-related macular degeneration using a treat-and-extend regimen: a retrospective case series. *Eye (Lond).* (2021).
[288] Usui-Ouchi, A. and Friedlander, M. Anti-VEGF therapy: higher potency and long-lasting antagonism are not necessarily better. *J Clin Invest.* **129**, 3032-3034 (2019).
[289] Escalante, C. P. and Zalpour, A. Vascular endothelial growth factor inhibitor-induced hypertension: basics for primary care providers. *Cardiol Res Pract.* **2011**, 816897 (2011).
[290] Chen, Z. I. and Ai, D. I. Cardiotoxicity associated with targeted cancer therapies. *Mol Clin Oncol.* **4**, 675-681 (2016).
[291] Izumiya, Y., Shiojima, I. *et al.* Vascular endothelial growth factor blockade promotes the transition from compensatory cardiac hypertrophy to failure in response to pressure overload. *Hypertension.* **47**, 887-893 (2006).
[292] Kinch, M. S., Haynesworth, A. *et al.* An overview of FDA-approved new molecular entities: 1827-2013. *Drug Discov Today.* **19**, 1033-1039 (2014).
[293] Giddings, L. A. and Newman, D. J. Microbial natural products: molecular blueprints for antitumor drugs. *J Ind Microbiol Biotechnol.* **40**, 1181-1210 (2013).
[294] Katz, L. and Baltz, R. H. Natural product discovery: past, present, and future. *J Ind Microbiol Biotechnol.* **43**, 155-176 (2016).
[295] Butler, M. S., Robertson, A. A. *et al.* Natural product and natural product derived drugs in clinical trials. *Nat Prod Rep.* **31**, 1612-1661 (2014).
[296] Zhang, L., Song, J. *et al.* The strategies and techniques of drug discovery from natural products. *Pharmacol Ther.* **216**, 107686 (2020).
[297] Niu, G. Genomics-Driven Natural Product Discovery in Actinomycetes. *Trends Biotechnol.* **36**, 238-241 (2018).
[298] Reichenbach, H. Myxobacteria, producers of novel bioactive substances. *J Ind Microbiol Biotechnol.* **27**, 149-156 (2001).
[299] Wenzel, S. C. and Muller, R. The biosynthetic potential of myxobacteria and their impact in drug discovery. *Curr Opin Drug Discov Devel.* **12**, 220-230 (2009).
[300] Weissman, K. J. and Muller, R. Myxobacterial secondary metabolites: bioactivities and modes-of-action. *Nat Prod Rep.* **27**, 1276-1295 (2010).
[301] Kunze, B., Jansen, R. *et al.* Chondramides A approximately D, new antifungal and cytostatic depsipeptides from Chondromyces crocatus (myxobacteria). Production, physico-chemical and biological properties. *J Antibiot (Tokyo).* **48**, 1262-1266 (1995).
[302] Braig, S., Wiedmann, R. M. *et al.* Pretubulysin: a new option for the treatment of metastatic cancer. *Cell Death Dis.* **5**, e1001 (2014).
[303] Bader, C. D., Panter, F. *et al.* In depth natural product discovery - Myxobacterial strains that provided multiple secondary metabolites. *Biotechnol Adv.* **39**, 107480 (2020).
[304] Schummer, D., Forche, E. *et al.* Antibiotics from gliding bacteria .76. Vioprolides: New antifungal and cytotoxic peptolides from Cystobacter violaceus. *Liebigs Annalen.* 971-978 (1996).

[305] Wu, G., Nielson, J. R. *et al.* Bonnevillamides, Linear Heptapeptides Isolated from a Great Salt Lake-Derived Streptomyces sp. *Mar Drugs.* **15**, (2017).
[306] Hoffmann, T., Krug, D. *et al.* Correlating chemical diversity with taxonomic distance for discovery of natural products in myxobacteria. *Nat Commun.* **9**, 803 (2018).
[307] Butler, E., Florentino, L. *et al.* Synthesis of macrocyclic precursors of the vioprolides. *Org Biomol Chem.* **16**, 6935-6960 (2018).
[308] Yan, F., Auerbach, D. *et al.* Biosynthesis and Heterologous Production of Vioprolides: Rational Biosynthetic Engineering and Unprecedented 4-Methylazetidinecarboxylic Acid Formation. *Angew Chem Int Ed Engl.* **57**, 8754-8759 (2018).
[309] Yan, F. and Muller, R. Class I Methyltransferase VioH Catalyzes Unusual S-Adenosyl-l-methionine Cyclization Leading to 4-Methylazetidinecarboxylic Acid Formation during Vioprolide Biosynthesis. *ACS Chem Biol.* **14**, 99-105 (2019).
[310] Chauhan, D., Bartok, E. *et al.* BAX/BAK-Induced Apoptosis Results in Caspase-8-Dependent IL-1beta Maturation in Macrophages. *Cell Rep.* **25**, 2354-2368 e2355 (2018).
[311] Kirsch, V. C., Orgler, C. *et al.* The Cytotoxic Natural Product Vioprolide A Targets Nucleolar Protein 14, Which Is Essential for Ribosome Biogenesis. *Angew Chem Int Ed Engl.* **59**, 1595-1600 (2020).
[312] Liu, P. C. and Thiele, D. J. Novel stress-responsive genes EMG1 and NOP14 encode conserved, interacting proteins required for 40S ribosome biogenesis. *Mol Biol Cell.* **12**, 3644-3657 (2001).
[313] Chauvin, C., Koka, V. *et al.* Ribosomal protein S6 kinase activity controls the ribosome biogenesis transcriptional program. *Oncogene.* **33**, 474-483 (2014).
[314] Hein, N., Hannan, K. M. *et al.* The nucleolus: an emerging target for cancer therapy. *Trends Mol Med.* **19**, 643-654 (2013).
[315] Boisvert, F. M., van Koningsbruggen, S. *et al.* The multifunctional nucleolus. *Nat Rev Mol Cell Biol.* **8**, 574-585 (2007).
[316] Zhou, B., Wu, Q. *et al.* NOP14 promotes proliferation and metastasis of pancreatic cancer cells. *Cancer Lett.* **322**, 195-203 (2012).
[317] Du, Y., Liu, Z. *et al.* Pancreatic Cancer Progression Relies upon Mutant p53-Induced Oncogenic Signaling Mediated by NOP14. *Cancer Res.* **77**, 2661-2673 (2017).
[318] Ying, Y., Li, J. *et al.* CCND1, NOP14 and DNMT3B are involved in miR-502-5p-mediated inhibition of cell migration and proliferation in bladder cancer. *Cell Prolif.* **53**, e12751 (2020).
[319] Fan, X., Liu, L. *et al.* Integrated analysis of RNA-binding proteins in human colorectal cancer. *World J Surg Oncol.* **18**, 222 (2020).
[320] Zhu, X., Jia, W. *et al.* NOP14 regulates the growth, migration, and invasion of colorectal cancer cells by modulating the NRIP1/GSK-3beta/beta-catenin signaling pathway. *Eur J Histochem.* **65**, (2021).
[321] Li, J., Fang, R. *et al.* NOP14 inhibits melanoma proliferation and metastasis by regulating Wnt/beta-catenin signaling pathway. *Braz J Med Biol Res.* **52**, e7952 (2018).
[322] Lei, J. J., Peng, R. J. *et al.* NOP14 suppresses breast cancer progression by inhibiting NRIP1/Wnt/beta-catenin pathway. *Oncotarget.* **6**, 25701-25714 (2015).
[323] Li, Y., Zhang, F. *et al.* Identification of potential genes and miRNAs associated with sepsis based on microarray analysis. *Mol Med Rep.* **17**, 6227-6234 (2018).
[324] Bassler, J. and Hurt, E. Eukaryotic Ribosome Assembly. *Annu Rev Biochem.* **88**, 281-306 (2019).
[325] Rabl, J., Leibundgut, M. *et al.* Crystal structure of the eukaryotic 40S ribosomal subunit in complex with initiation factor 1. *Science.* **331**, 730-736 (2011).
[326] Klinge, S., Voigts-Hoffmann, F. *et al.* Crystal structure of the eukaryotic 60S ribosomal subunit in complex with initiation factor 6. *Science.* **334**, 941-948 (2011).
[327] Scheer, U. and Hock, R. Structure and function of the nucleolus. *Curr Opin Cell Biol.* **11**, 385-390 (1999).
[328] Venema, J. and Tollervey, D. Ribosome synthesis in Saccharomyces cerevisiae. *Annu Rev Genet.* **33**, 261-311 (1999).

[329] Stokes, J. M. and Brown, E. D. Chemical modulators of ribosome biogenesis as biological probes. *Nat Chem Biol.* **11**, 924-932 (2015).
[330] Kressler, D., Linder, P. *et al.* Protein trans-acting factors involved in ribosome biogenesis in Saccharomyces cerevisiae. *Mol Cell Biol.* **19**, 7897-7912 (1999).
[331] Watkins, N. J. and Bohnsack, M. T. The box C/D and H/ACA snoRNPs: key players in the modification, processing and the dynamic folding of ribosomal RNA. *Wiley Interdiscip Rev RNA.* **3**, 397-414 (2012).
[332] Kobayashi, J. and Matsuura, Y. Structural basis for cell-cycle-dependent nuclear import mediated by the karyopherin Kap121p. *J Mol Biol.* **425**, 1852-1868 (2013).
[333] Holzer, S., Ban, N. *et al.* Crystal structure of the yeast ribosomal protein rpS3 in complex with its chaperone Yar1. *J Mol Biol.* **425**, 4154-4160 (2013).
[334] Caesar, S., Greiner, M. *et al.* Kap120 functions as a nuclear import receptor for ribosome assembly factor Rpf1 in yeast. *Mol Cell Biol.* **26**, 3170-3180 (2006).
[335] Rout, M. P., Blobel, G. *et al.* A distinct nuclear import pathway used by ribosomal proteins. *Cell.* **89**, 715-725 (1997).
[336] Pillet, B., Mitterer, V. *et al.* Hold on to your friends: Dedicated chaperones of ribosomal proteins: Dedicated chaperones mediate the safe transfer of ribosomal proteins to their site of pre-ribosome incorporation. *Bioessays.* **39**, 1-12 (2017).
[337] Panse, V. G. Getting ready to translate: cytoplasmic maturation of eukaryotic ribosomes. *Chimia (Aarau).* **65**, 765-769 (2011).
[338] Strunk, B. S., Novak, M. N. *et al.* A translation-like cycle is a quality control checkpoint for maturing 40S ribosome subunits. *Cell.* **150**, 111-121 (2012).
[339] Gadal, O., Strauss, D. *et al.* Nuclear export of 60s ribosomal subunits depends on Xpo1p and requires a nuclear export sequence-containing factor, Nmd3p, that associates with the large subunit protein Rpl10p. *Mol Cell Biol.* **21**, 3405-3415 (2001).
[340] Occhipinti, L., Chang, Y. *et al.* Non-FG mediated transport of the large pre-ribosomal subunit through the nuclear pore complex by the mRNA export factor Gle2. *Nucleic Acids Res.* **41**, 8266-8279 (2013).
[341] Hackmann, A., Gross, T. *et al.* The mRNA export factor Npl3 mediates the nuclear export of large ribosomal subunits. *EMBO Rep.* **12**, 1024-1031 (2011).
[342] Burgers, L. D. and Furst, R. Natural products as drugs and tools for influencing core processes of eukaryotic mRNA translation. *Pharmacol Res.* **170**, 105535 (2021).
[343] Sonenberg, N. and Hinnebusch, A. G. Regulation of translation initiation in eukaryotes: mechanisms and biological targets. *Cell.* **136**, 731-745 (2009).
[344] Pestova, T. V., Kolupaeva, V. G. *et al.* Molecular mechanisms of translation initiation in eukaryotes. *Proc Natl Acad Sci U S A.* **98**, 7029-7036 (2001).
[345] Hashem, Y., des Georges, A. *et al.* Structure of the mammalian ribosomal 43S preinitiation complex bound to the scanning factor DHX29. *Cell.* **153**, 1108-1119 (2013).
[346] Hinnebusch, A. G. The scanning mechanism of eukaryotic translation initiation. *Annu Rev Biochem.* **83**, 779-812 (2014).
[347] Konikkat, S. and Woolford, J. L., Jr. Principles of 60S ribosomal subunit assembly emerging from recent studies in yeast. *Biochem J.* **474**, 195-214 (2017).
[348] Dever, T. E., Dinman, J. D. *et al.* Translation Elongation and Recoding in Eukaryotes. *Cold Spring Harb Perspect Biol.* **10**, (2018).
[349] Hellen, C. U. T. Translation Termination and Ribosome Recycling in Eukaryotes. *Cold Spring Harb Perspect Biol.* **10**, (2018).
[350] Chartier-Harlin, M. C., Dachsel, J. C. *et al.* Translation initiator EIF4G1 mutations in familial Parkinson disease. *Am J Hum Genet.* **89**, 398-406 (2011).
[351] Correddu, D. and Leung, I. K. H. Targeting mRNA translation in Parkinson's disease. *Drug Discov Today.* **24**, 1295-1303 (2019).
[352] Laguesse, S. and Ron, D. Protein Translation and Psychiatric Disorders. *Neuroscientist.* **26**, 21-42 (2020).
[353] Hansen, J., Etchison, D. *et al.* Association of cap-binding protein with eucaryotic initiation factor 3 in initiation factor preparations from uninfected and poliovirus-infected HeLa cells. *J Virol.* **42**, 200-207 (1982).

[354] Wu, G. Q., Xu, Y. M. *et al.* Recent insights into eukaryotic translation initiation factors 5A1 and 5A2 and their roles in human health and disease. *Cancer Cell Int.* **20**, 142 (2020).
[355] Gonzalez-Teran, B., Cortes, J. R. *et al.* Eukaryotic elongation factor 2 controls TNF-alpha translation in LPS-induced hepatitis. *J Clin Invest.* **123**, 164-178 (2013).
[356] Kapur, M. and Ackerman, S. L. mRNA Translation Gone Awry: Translation Fidelity and Neurological Disease. *Trends Genet.* **34**, 218-231 (2018).
[357] Silvera, D., Formenti, S. C. *et al.* Translational control in cancer. *Nat Rev Cancer.* **10**, 254-266 (2010).
[358] Getz, M. J., Elder, P. K. *et al.* Effect of cell proliferation on levels and diversity of poly(A)-containing mRNA. *Cell.* **7**, 255 -265 (1976).
[359] Larsson, O., Li, S. *et al.* Eukaryotic translation initiation factor 4E induced progression of primary human mammary epithelial cells along the cancer pathway is associated with targeted translational deregulation of oncogenic drivers and inhibitors. *Cancer Res.* **67**, 6814-6824 (2007).
[360] Koromilas, A. E., Lazaris-Karatzas, A. *et al.* mRNAs containing extensive secondary structure in their 5' non-coding region translate efficiently in cells overexpressing initiation factor eIF-4E. *EMBO J.* **11**, 4153-4158 (1992).
[361] Wang, S., Lloyd, R. V. *et al.* Expression of eukaryotic translation initiation factors 4E and 2alpha correlates with the progression of thyroid carcinoma. *Thyroid.* **11**, 1101-1107 (2001).
[362] Wang, S., Rosenwald, I. B. *et al.* Expression of the eukaryotic translation initiation factors 4E and 2alpha in non-Hodgkin's lymphomas. *Am J Pathol.* **155**, 247-255 (1999).
[363] Rosenwald, I. B., Koifman, L. *et al.* Expression of the translation initiation factors eIF-4E and eIF-2* is frequently increased in neoplastic cells of Hodgkin lymphoma. *Hum Pathol.* **39**, 910-916 (2008).
[364] Tejada, S., Lobo, M. V. *et al.* Eukaryotic initiation factors (eIF) 2alpha and 4E expression, localization, and phosphorylation in brain tumors. *J Histochem Cytochem.* **57**, 503-512 (2009).
[365] Zheng, J., Li, X. *et al.* eIF4E Overexpression Is Associated with Poor Prognoses of Ovarian Cancer. *Anal Cell Pathol (Amst).* **2020**, 8984526 (2020).
[366] Truitt, M. L., Conn, C. S. *et al.* Differential Requirements for eIF4E Dose in Normal Development and Cancer. *Cell.* **162**, 59-71 (2015).
[367] Xie, D., Ma, N. F. *et al.* Overexpression of EIF-5A2 is associated with metastasis of human colorectal carcinoma. *Hum Pathol.* **39**, 80-86 (2008).
[368] Luo, J. H., Hua, W. F. *et al.* Overexpression of EIF-5A2 predicts tumor recurrence and progression in pTa/pT1 urothelial carcinoma of the bladder. *Cancer Sci.* **100**, 896-902 (2009).
[369] Mathews, M. B. and Hershey, J. W. The translation factor eIF5A and human cancer. *Biochim Biophys Acta.* **1849**, 836-844 (2015).
[370] Tahmasebi, S., Khoutorsky, A. *et al.* Translation deregulation in human disease. *Nat Rev Mol Cell Biol.* **19**, 791-807 (2018).
[371] Knight, J. R. P., Garland, G. *et al.* Control of translation elongation in health and disease. *Dis Model Mech.* **13**, (2020).
[372] Biterge-Sut, B. Alterations in Eukaryotic Elongation Factor complex proteins (EEF1s) in cancer and their implications in epigenetic regulation. *Life Sci.* **238**, 116977 (2019).
[373] Gandin, V., Miluzio, A. *et al.* Eukaryotic initiation factor 6 is rate-limiting in translation, growth and transformation. *Nature.* **455**, 684-688 (2008).
[374] Golob-Schwarzl, N., Wodlej, C. *et al.* Eukaryotic translation initiation factor 6 overexpression plays a major role in the translational control of gallbladder cancer. *J Cancer Res Clin Oncol.* **145**, 2699-2711 (2019).
[375] Turi, Z., Lacey, M. *et al.* Impaired ribosome biogenesis: mechanisms and relevance to cancer and aging. *Aging (Albany NY).* **11**, 2512-2540 (2019).
[376] Freed, E. F., Bleichert, F. *et al.* When ribosomes go bad: diseases of ribosome biogenesis. *Mol Biosyst.* **6**, 481-493 (2010).

[377] Shenoy, N., Kessel, R. *et al.* Alterations in the ribosomal machinery in cancer and hematologic disorders. *J Hematol Oncol.* **5**, 32 (2012).
[378] Narla, A. and Ebert, B. L. Ribosomopathies: human disorders of ribosome dysfunction. *Blood.* **115**, 3196-3205 (2010).
[379] Amsterdam, A., Sadler, K. C. *et al.* Many ribosomal protein genes are cancer genes in zebrafish. *PLoS Biol.* **2**, E139 (2004).
[380] Donadieu, J., Leblanc, T. *et al.* Analysis of risk factors for myelodysplasias, leukemias and death from infection among patients with congenital neutropenia. Experience of the French Severe Chronic Neutropenia Study Group. *Haematologica.* **90**, 45-53 (2005).
[381] Taskinen, M., Ranki, A. *et al.* Extended follow-up of the Finnish cartilage-hair hypoplasia cohort confirms high incidence of non-Hodgkin lymphoma and basal cell carcinoma. *Am J Med Genet A.* **146A**, 2370-2375 (2008).
[382] Dong, J., Liao, W. *et al.* Ribosomal protein S3 gene silencing protects against experimental allergic asthma. *Br J Pharmacol.* **174**, 540-552 (2017).
[383] Nishiura, H., Shibuya, Y. *et al.* Monocyte chemotactic factor in rheumatoid arthritis synovial tissue. Probably a cross-linked derivative of S19 ribosomal protein. *J Biol Chem.* **271**, 878-882 (1996).
[384] Yamamoto, T. Molecular mechanism of monocyte predominant infiltration in chronic inflammation: mediation by a novel monocyte chemotactic factor, S19 ribosomal protein dimer. *Pathol Int.* **50**, 863-871 (2000).
[385] Poddar, D., Basu, A. *et al.* An extraribosomal function of ribosomal protein L13a in macrophages resolves inflammation. *J Immunol.* **190**, 3600-3612 (2013).
[386] Basu, A., Poddar, D. *et al.* Ribosomal protein L13a deficiency in macrophages promotes atherosclerosis by limiting translation control-dependent retardation of inflammation. *Arterioscler Thromb Vasc Biol.* **34**, 533-542 (2014).
[387] Jones, D. T., Lechertier, T. *et al.* Endogenous ribosomal protein L29 (RPL29): a newly identified regulator of angiogenesis in mice. *Dis Model Mech.* **6**, 115-124 (2013).
[388] Guo, P., Wang, Y. *et al.* Ribosomal protein S15a promotes tumor angiogenesis via enhancing Wnt/beta-catenin-induced FGF18 expression in hepatocellular carcinoma. *Oncogene.* **37**, 1220-1236 (2018).
[389] Ruf, M. T., Andreoli, A. *et al.* Ribosomal protein S6 is hyperactivated and differentially phosphorylated in epidermal lesions of patients with psoriasis and atopic dermatitis. *Br J Dermatol.* **171**, 1533-1536 (2014).
[390] Cho, S. M., Lee, H. J. *et al.* Daptomycin suppresses tumor migration and angiogenesis via binding to ribosomal protein S19 in humans. *J Antibiot (Tokyo).* **74**, 726-733 (2021).
[391] Catez, F., Dalla Venezia, N. *et al.* Ribosome biogenesis: An emerging druggable pathway for cancer therapeutics. *Biochem Pharmacol.* **159**, 74-81 (2019).
[392] Pal, I., Safari, M. *et al.* Targeting Translation of mRNA as a Therapeutic Strategy in Cancer. *Curr Hematol Malig Rep.* **14**, 219-227 (2019).
[393] Laham-Karam, N., Pinto, G. P. *et al.* Transcription and Translation Inhibitors in Cancer Treatment. *Front Chem.* **8**, 276 (2020).
[394] Dastidar, S. G., Pham, M. T. *et al.* 4E-BP1 Protects Neurons from Misfolded Protein Stress and Parkinson's Disease Toxicity by Inducing the Mitochondrial Unfolded Protein Response. *J Neurosci.* **40**, 8734-8745 (2020).
[395] Tain, L. S., Mortiboys, H. *et al.* Rapamycin activation of 4E-BP prevents parkinsonian dopaminergic neuron loss. *Nat Neurosci.* **12**, 1129-1135 (2009).
[396] Hao, P., Yu, J. *et al.* Eukaryotic translation initiation factors as promising targets in cancer therapy. *Cell Commun Signal.* **18**, 175 (2020).
[397] Malina, A., Mills, J. R. *et al.* Emerging therapeutics targeting mRNA translation. *Cold Spring Harb Perspect Biol.* **4**, a012377 (2012).
[398] Assouline, S., Culjkovic, B. *et al.* Molecular targeting of the oncogene eIF4E in acute myeloid leukemia (AML): a proof-of-principle clinical trial with ribavirin. *Blood.* **114**, 257-260 (2009).
[399] Bronstrup, M. and Sasse, F. Natural products targeting the elongation phase of eukaryotic protein biosynthesis. *Nat Prod Rep.* **37**, 752-762 (2020).

[400] Jaffe, E. A., Nachman, R. L. *et al.* Culture of human endothelial cells derived from umbilical veins. Identification by morphologic and immunologic criteria. *J Clin Invest.* **52**, 2745-2756 (1973).
[401] Boyum, A. Isolation of lymphocytes, granulocytes and macrophages. *Scand J Immunol.* **Suppl 5**, 9-15 (1976).
[402] Ades, E. W., Candal, F. J. *et al.* HMEC-1: establishment of an immortalized human microvascular endothelial cell line. *J Invest Dermatol.* **99**, 683-690 (1992).
[403] Tsuchiya, S., Yamabe, M. *et al.* Establishment and characterization of a human acute monocytic leukemia cell line (THP-1). *Int J Cancer.* **26**, 171-176 (1980).
[404] Abraham, R. T. and Weiss, A. Jurkat T cells and development of the T-cell receptor signalling paradigm. *Nat Rev Immunol.* **4**, 301-308 (2004).
[405] Nicoletti, I., Migliorati, G. *et al.* A rapid and simple method for measuring thymocyte apoptosis by propidium iodide staining and flow cytometry. *J Immunol Methods.* **139**, 271-279 (1991).
[406] Lomakina, G. Y., Modestova, Y. A. *et al.* Bioluminescence assay for cell viability. *Biochemistry (Mosc).* **80**, 701-713 (2015).
[407] Naylor, L. H. Reporter gene technology: the future looks bright. *Biochem Pharmacol.* **58**, 749-757 (1999).
[408] Potter, H. Electroporation in biology: methods, applications, and instrumentation. *Anal Biochem.* **174**, 361-373 (1988).
[409] Shao, Z., Friedlander, M. *et al.* Choroid sprouting assay: an ex vivo model of microvascular angiogenesis. *PLoS One.* **8**, e69552 (2013).
[410] Liang, C. C., Park, A. Y. *et al.* In vitro scratch assay: a convenient and inexpensive method for analysis of cell migration in vitro. *Nat Protoc.* **2**, 329-333 (2007).
[411] Boyden, S. The chemotactic effect of mixtures of antibody and antigen on polymorphonuclear leucocytes. *J Exp Med.* **115**, 453-466 (1962).
[412] Falasca, M., Raimondi, C. *et al.* Boyden chamber. *Methods Mol Biol.* **769**, 87-95 (2011).
[413] Mahmood, T. and Yang, P. C. Western blot: technique, theory, and trouble shooting. *N Am J Med Sci.* **4**, 429-434 (2012).
[414] Smith, P. K., Krohn, R. I. *et al.* Measurement of protein using bicinchoninic acid. *Anal Biochem.* **150**, 76-85 (1985).
[415] Laemmli, U. K. Cleavage of structural proteins during the assembly of the head of bacteriophage T4. *Nature.* **227**, 680-685 (1970).
[416] Thorpe, G. H. and Kricka, L. J. Enhanced chemiluminescent reactions catalyzed by horseradish peroxidase. *Methods Enzymol.* **133**, 331-353 (1986).
[417] Livak, K. J. and Schmittgen, T. D. Analysis of relative gene expression data using real-time quantitative PCR and the 2(-Delta Delta C(T)) Method. *Methods.* **25**, 402-408 (2001).
[418] Miller, M. W. and Nowakowski, R. S. Use of bromodeoxyuridine-immunohistochemistry to examine the proliferation, migration and time of origin of cells in the central nervous system. *Brain Res.* **457**, 44-52 (1988).
[419] Crowley, L. C., Chojnowski, G. *et al.* Measuring the DNA Content of Cells in Apoptosis and at Different Cell-Cycle Stages by Propidium Iodide Staining and Flow Cytometry. *Cold Spring Harb Protoc.* **2016**, (2016).
[420] Liu, J., Xu, Y. *et al.* Imaging protein synthesis in cells and tissues with an alkyne analog of puromycin. *Proc Natl Acad Sci U S A.* **109**, 413-418 (2012).
[421] Jafari, R., Almqvist, H. *et al.* The cellular thermal shift assay for evaluating drug target interactions in cells. *Nat Protoc.* **9**, 2100-2122 (2014).
[422] Mempel, T. R., Moser, C. *et al.* Visualization of leukocyte transendothelial and interstitial migration using reflected light oblique transillumination in intravital video microscopy. *J Vasc Res.* **40**, 435-441 (2003).
[423] Lambert, V., Lecomte, J. *et al.* Laser-induced choroidal neovascularization model to study age-related macular degeneration in mice. *Nat Protoc.* **8**, 2197-2211 (2013).
[424] Campos, M., Amaral, J. *et al.* A novel imaging technique for experimental choroidal neovascularization. *Invest Ophthalmol Vis Sci.* **47**, 5163-5170 (2006).

[425] Alroy, J., Goyal, V. *et al.* Lectin histochemistry of mammalian endothelium. *Histochemistry.* **86**, 603-607 (1987).
[426] Utans, U., Arceci, R. J. *et al.* Cloning and characterization of allograft inflammatory factor-1: a novel macrophage factor identified in rat cardiac allografts with chronic rejection. *J Clin Invest.* **95**, 2954-2962 (1995).
[427] Martinez Molina, D., Jafari, R. *et al.* Monitoring drug target engagement in cells and tissues using the cellular thermal shift assay. *Science.* **341**, 84-87 (2013).
[428] Stark, A., Schwenk, R. *et al.* Narciclasine exerts anti-inflammatory actions by blocking leukocyte-endothelial cell interactions and down-regulation of the endothelial TNF receptor 1. *FASEB J.* **33**, 8771-8781 (2019).
[429] Yamada, Y., Taketani, S. *et al.* Cytotrienin A, a translation inhibitor that induces ectodomain shedding of TNF receptor 1 via activation of ERK and p38 MAP kinase. *Eur J Pharmacol.* **667**, 113-119 (2011).
[430] Huang, Y., Fu, Z. *et al.* Serum starvation-induces down-regulation of Bcl-2/Bax confers apoptosis in tongue coating-related cells in vitro. *Mol Med Rep.* **17**, 5057-5064 (2018).
[431] Hasan, N. M., Adams, G. E. *et al.* Effect of serum starvation on expression and phosphorylation of PKC-alpha and p53 in V79 cells: implications for cell death. *Int J Cancer.* **80**, 400-405 (1999).
[432] Goyeneche, A. A., Harmon, J. M. *et al.* Cell death induced by serum deprivation in luteal cells involves the intrinsic pathway of apoptosis. *Reproduction.* **131**, 103-111 (2006).
[433] Romorini, L., Garate, X. *et al.* AKT/GSK3beta signaling pathway is critically involved in human pluripotent stem cell survival. *Sci Rep.* **6**, 35660 (2016).
[434] Pilco-Ferreto, N. and Calaf, G. M. Influence of doxorubicin on apoptosis and oxidative stress in breast cancer cell lines. *Int J Oncol.* **49**, 753-762 (2016).
[435] Yang, F., Chen, H. *et al.* Doxorubicin caused apoptosis of mesenchymal stem cells via p38, JNK and p53 pathway. *Cell Physiol Biochem.* **32**, 1072-1082 (2013).
[436] Hassan, M., Alaoui, A. *et al.* The BH3-only member Noxa causes apoptosis in melanoma cells by multiple pathways. *Oncogene.* **27**, 4557-4568 (2008).
[437] Zhu, H. Q., Zhang, C. *et al.* Oridonin induces Mdm2-p60 to promote p53-mediated apoptosis and cell cycle arrest in neuroblastoma. *Cancer Med.* **8**, 5313-5326 (2019).
[438] Mikami, S., Kobayashi, T. *et al.* Cell-free protein synthesis systems with extracts from cultured human cells. *Methods Mol Biol.* **607**, 43-52 (2010).
[439] Leulliot, N., Bohnsack, M. T. *et al.* The yeast ribosome synthesis factor Emg1 is a novel member of the superfamily of alpha/beta knot fold methyltransferases. *Nucleic Acids Res.* **36**, 629-639 (2008).
[440] Bernstein, K. A., Gallagher, J. E. *et al.* The small-subunit processome is a ribosome assembly intermediate. *Eukaryot Cell.* **3**, 1619-1626 (2004).
[441] Campa, C., Costagliola, C. *et al.* Inflammatory mediators and angiogenic factors in choroidal neovascularization: pathogenetic interactions and therapeutic implications. *Mediators Inflamm.* **2010**, (2010).
[442] Staton, C. A., Reed, M. W. *et al.* A critical analysis of current in vitro and in vivo angiogenesis assays. *Int J Exp Pathol.* **90**, 195-221 (2009).
[443] Stryker, Z. I., Rajabi, M. *et al.* Evaluation of Angiogenesis Assays. *Biomedicines.* **7**, (2019).
[444] Malinda, K. M. In vivo matrigel migration and angiogenesis assay. *Methods Mol Biol.* **467**, 287-294 (2009).
[445] Patil, K. R., Mahajan, U. B. *et al.* Animal Models of Inflammation for Screening of Anti-inflammatory Drugs: Implications for the Discovery and Development of Phytopharmaceuticals. *Int J Mol Sci.* **20**, (2019).
[446] Duarte, D. B., Vasko, M. R. *et al.* Models of Inflammation: Carrageenan Air Pouch. *Curr Protoc Pharmacol.* **72**, 5 6 1-5 6 9 (2016).
[447] Baez, S. An open cremaster muscle preparation for the study of blood vessels by in vivo microscopy. *Microvasc Res.* **5**, 384-394 (1973).
[448] Harwig, J. and Scott, P. M. Brine shrimp (Artemia salina L.) larvae as a screening system for fungal toxins. *Appl Microbiol.* **21**, 1011-1016 (1971).

[449] Osborn, L., Hession, C. *et al.* Direct expression cloning of vascular cell adhesion molecule 1, a cytokine-induced endothelial protein that binds to lymphocytes. *Cell.* **59**, 1203-1211 (1989).
[450] Kleiveland, C. R. Peripheral Blood Mononuclear Cells. In: K. Verhoeckx, P. Cotter, I. Lopez-Exposito, C. Kleiveland, T. Lea, A. Mackie, T. Requena, D. Swiatecka and H. Wichers, editors. The Impact of Food Bioactives on Health: in vitro and ex vivo models. Cham (CH)2015. p. 161-167.
[451] Robertson, M. J., Caligiuri, M. A. *et al.* Human natural killer cell adhesion molecules. Differential expression after activation and participation in cytolysis. *J Immunol.* **145**, 3194-3201 (1990).
[452] Privratsky, J. R. and Newman, P. J. PECAM-1: regulator of endothelial junctional integrity. *Cell Tissue Res.* **355**, 607-619 (2014).
[453] Ghosh, S., May, M. J. *et al.* NF-kappa B and Rel proteins: evolutionarily conserved mediators of immune responses. *Annu Rev Immunol.* **16**, 225-260 (1998).
[454] Wajant, H. and Scheurich, P. TNFR1-induced activation of the classical NF-kappaB pathway. *FEBS J.* **278**, 862-876 (2011).
[455] Yamada, Y., Tashiro, E. *et al.* Mycotrienin II, a translation inhibitor that prevents ICAM-1 expression induced by pro-inflammatory cytokines. *J Antibiot (Tokyo).* **64**, 361-366 (2011).
[456] Hirano, S. and Kataoka, T. Deoxynivalenol induces ectodomain shedding of TNF receptor 1 and thereby inhibits the TNF-alpha-induced NF-kappaB signaling pathway. *Eur J Pharmacol.* **701**, 144-151 (2013).
[457] Hirano, S., Quach, H. T. *et al.* Irciniastatin A, a pederin-type translation inhibitor, promotes ectodomain shedding of cell-surface tumor necrosis factor receptor 1. *J Antibiot (Tokyo).* **68**, 417-420 (2015).
[458] Tanigaki, R., Takahashi, R. *et al.* 4-Hydroxypanduratin A and Isopanduratin A Inhibit Tumor Necrosis Factor alpha-Stimulated Gene Expression and the Nuclear Factor kappaB-Dependent Signaling Pathway in Human Lung Adenocarcinoma A549 Cells. *Biol Pharm Bull.* **42**, 26-33 (2019).
[459] Ogura, H., Tsukumo, Y. *et al.* Ectodomain shedding of TNF receptor 1 induced by protein synthesis inhibitors regulates TNF-alpha-mediated activation of NF-kappaB and caspase-8. *Exp Cell Res.* **314**, 1406-1414 (2008).
[460] Kataoka, T. Translation inhibitors and their unique biological properties. *Eur J Pharmacol.* **676**, 1-5 (2012).
[461] Levine, S. J. Mechanisms of soluble cytokine receptor generation. *J Immunol.* **173**, 5343-5348 (2004).
[462] Krishnathas, G. M., Strodke, B. *et al.* C81-evoked inhibition of the TNFR1-NFkappaB pathway during inflammatory processes for stabilization of the impaired vascular endothelial barrier for leukocytes. *FASEB J.* **35**, e21656 (2021).
[463] Baumann, B., Bohnenstengel, F. *et al.* Rocaglamide derivatives are potent inhibitors of NF-kappa B activation in T-cells. *J Biol Chem.* **277**, 44791-44800 (2002).
[464] Wang, C., Deng, L. *et al.* TAK1 is a ubiquitin-dependent kinase of MKK and IKK. *Nature.* **412**, 346-351 (2001).
[465] Yang, J., Lin, Y. *et al.* The essential role of MEKK3 in TNF-induced NF-kappaB activation. *Nat Immunol.* **2**, 620-624 (2001).
[466] Bai, D., Ueno, L. *et al.* Akt-mediated regulation of NFkappaB and the essentialness of NFkappaB for the oncogenicity of PI3K and Akt. *Int J Cancer.* **125**, 2863-2870 (2009).
[467] Mathes, E., O'Dea, E. L. *et al.* NF-kappaB dictates the degradation pathway of IkappaBalpha. *EMBO J.* **27**, 1357-1367 (2008).
[468] Tergaonkar, V., Bottero, V. *et al.* IkappaB kinase-independent IkappaBalpha degradation pathway: functional NF-kappaB activity and implications for cancer therapy. *Mol Cell Biol.* **23**, 8070-8083 (2003).
[469] Dai, C. L., Shi, J. *et al.* Inhibition of protein synthesis alters protein degradation through activation of protein kinase B (AKT). *J Biol Chem.* **288**, 23875-23883 (2013).
[470] Plas, D. R. and Thompson, C. B. Akt activation promotes degradation of tuberin and FOXO3a via the proteasome. *J Biol Chem.* **278**, 12361-12366 (2003).

[471] Xu, D., Shan, B. *et al.* Phosphorylation and activation of ubiquitin-specific protease-14 by Akt regulates the ubiquitin-proteasome system. *Elife.* **4**, e10510 (2015).
[472] Bräutigam, J. Narciclasine inhibits angiogenic processes by activation of Rho kinase and by downregulation of the VEGF receptor 2 [Dissertation]. Frankfurt: Johann Wolfgang Goethe-University (2019).
[473] Campbell, K. J. and Perkins, N. D. Post-translational modification of RelA(p65) NF-kappaB. *Biochem Soc Trans.* **32**, 1087-1089 (2004).
[474] Huang, B., Yang, X. D. *et al.* Posttranslational modifications of NF-kappaB: another layer of regulation for NF-kappaB signaling pathway. *Cell Signal.* **22**, 1282-1290 (2010).
[475] Sakurai, H., Chiba, H. *et al.* IkappaB kinases phosphorylate NF-kappaB p65 subunit on serine 536 in the transactivation domain. *J Biol Chem.* **274**, 30353-30356 (1999).
[476] Buss, H., Dorrie, A. *et al.* Constitutive and interleukin-1-inducible phosphorylation of p65 NF-{kappa}B at serine 536 is mediated by multiple protein kinases including I{kappa}B kinase (IKK)-{alpha}, IKK{beta}, IKK{epsilon}, TRAF family member-associated (TANK)-binding kinase 1 (TBK1), and an unknown kinase and couples p65 to TATA-binding protein-associated factor II31-mediated interleukin-8 transcription. *J Biol Chem.* **279**, 55633-55643 (2004).
[477] Bohuslav, J., Chen, L. F. *et al.* p53 induces NF-kappaB activation by an IkappaB kinase-independent mechanism involving phosphorylation of p65 by ribosomal S6 kinase 1. *J Biol Chem.* **279**, 26115-26125 (2004).
[478] Mahipal, A. and Malafa, M. Importins and exportins as therapeutic targets in cancer. *Pharmacol Ther.* **164**, 135-143 (2016).
[479] Sun, X., He, S. *et al.* Systemic delivery of microRNA-181b inhibits nuclear factor-kappaB activation, vascular inflammation, and atherosclerosis in apolipoprotein E-deficient mice. *Circ Res.* **114**, 32-40 (2014).
[480] Leonard, A., Rahman, A. *et al.* Importins alpha and beta signaling mediates endothelial cell inflammation and barrier disruption. *Cell Signal.* **44**, 103-117 (2018).
[481] Rachidi, S. M., Qin, T. *et al.* Molecular profiling of multiple human cancers defines an inflammatory cancer-associated molecular pattern and uncovers KPNA2 as a uniform poor prognostic cancer marker. *PLoS One.* **8**, e57911 (2013).
[482] Liu, Z., Zhang, D. *et al.* KPNA2 Contributes to the Inflammatory Processes in Synovial Tissue of Patients with Rheumatoid Arthritis and SW982 Cells. *Inflammation.* **38**, 2224-2234 (2015).
[483] Liang, P., Zhang, H. *et al.* KPNB1, XPO7 and IPO8 mediate the translocation ofNF-kappaB/p65 into the nucleus. *Traffic.* **14**, 1132-1143 (2013).
[484] Bayliss, R., Corbett, A. H. *et al.* The molecular mechanism of transport of macromolecules through nuclear pore complexes. *Traffic.* **1**, 448-456 (2000).
[485] Kohler, M., Speck, C. *et al.* Evidence for distinct substrate specificities of importin alpha family members in nuclear protein import. *Mol Cell Biol.* **19**, 7782-7791 (1999).
[486] Appert-Rolland, C., Ebbinghaus, M. *et al.* Intracellular transport driven by cytoskeletal motors: General mechanisms and defects. *Phys Rep.* **593**, 1-59 (2015).
[487] Nemeth, Z. H., Deitch, E. A. *et al.* Disruption of the actin cytoskeleton results in nuclear factor-kappaB activation and inflammatory mediator production in cultured human intestinal epithelial cells. *J Cell Physiol.* **200**, 71-81 (2004).
[488] Goldblum, S. E., Ding, X. *et al.* TNF-alpha induces endothelial cell F-actin depolymerization, new actin synthesis, and barrier dysfunction. *Am J Physiol.* **264**, C894-905 (1993).
[489] Mitra, A., Venkatachalapathy, S. *et al.* Cell geometry dictates TNFalpha-induced genome response. *Proc Natl Acad Sci U S A.* **114**, E3882-E3891 (2017).
[490] Brautigam, J., Bischoff, I. *et al.* Narciclasine inhibits angiogenic processes by activation of Rho kinase and by downregulation of the VEGF receptor 2. *J Mol Cell Cardiol.* **135**, 97-108 (2019).
[491] Snape, N., Li, D. *et al.* The eukaryotic translation elongation factor 1A regulation of actin stress fibers is important for infectious RSV production. *Virol J.* **15**, 182 (2018).
[492] Hesketh, J. Translation and the cytoskeleton: a mechanism for targeted protein synthesis. *Mol Biol Rep.* **19**, 233-243 (1994).

[493] Hovland, R., Hesketh, J. E. *et al.* The compartmentalization of protein synthesis: importance of cytoskeleton and role in mRNA targeting. *Int J Biochem Cell Biol.* **28**, 1089-1105 (1996).
[494] Lobov, I. and Mikhailova, N. The Role of Dll4/Notch Signaling in Normal and Pathological Ocular Angiogenesis: Dll4 Controls Blood Vessel Sprouting and Vessel Remodeling in Normal and Pathological Conditions. *J Ophthalmol.* **2018**, 3565292 (2018).
[495] Faa, G., Messana, I. *et al.* Proteomics applied to pediatric medicine: opportunities and challenges. *Expert Rev Proteomics.* **13**, 883-894 (2016).
[496] Petrie, R. J., Doyle, A. D. *et al.* Random versus directionally persistent cell migration. *Nat Rev Mol Cell Biol.* **10**, 538-549 (2009).
[497] SenGupta, S., Parent, C. A. *et al.* The principles of directed cell migration. *Nat Rev Mol Cell Biol.* **22**, 529-547 (2021).
[498] Holzinger, A. Jasplakinolide: an actin-specific reagent that promotes actin polymerization. *Methods Mol Biol.* **586**, 71-87 (2009).
[499] Sorensen, P. M., Iacob, R. E. *et al.* The natural product cucurbitacin E inhibits depolymerization of actin filaments. *ACS Chem Biol.* **7**, 1502-1508 (2012).
[500] Vinals, F. and Pouyssegur, J. Confluence of vascular endothelial cells induces cell cycle exit by inhibiting p42/p44 mitogen-activated protein kinase activity. *Mol Cell Biol.* **19**, 2763-2772 (1999).
[501] Derenzini, M., Pasquinelli, G. *et al.* Structural and functional organization of ribosomal genes within the mammalian cell nucleolus. *J Histochem Cytochem.* **54**, 131-145 (2006).
[502] Wang, X., Bove, A. M. *et al.* Molecular Bases of VEGFR-2-Mediated Physiological Function and Pathological Role. *Front Cell Dev Biol.* **8**, 599281 (2020).
[503] Brant-Zawadzki, P. B., Schmid, D. I. *et al.* Translational control in endothelial cells. *J Vasc Surg.* **45 Suppl A**, A8-14 (2007).
[504] Zhang, Y., Wang, P. *et al.* eIF3i activity is critical for endothelial cells in tumor induced angiogenesis through regulating VEGFR and ERK translation. *Oncotarget.* **8**, 19968-19979 (2017).
[505] Qi, J. W., Qin, T. T. *et al.* TNFSF15 inhibits vasculogenesis by regulating relative levels of membrane-bound and soluble isoforms of VEGF receptor 1. *Proc Natl Acad Sci U S A.* **110**, 13863-13868 (2013).
[506] Harrington, L. S., Sainson, R. C. *et al.* Regulation of multiple angiogenic pathways by Dll4 and Notch in human umbilical vein endothelial cells. *Microvasc Res.* **75**, 144-154 (2008).
[507] de Vries, C., Escobedo, J. A. *et al.* The fms-like tyrosine kinase, a receptor for vascular endothelial growth factor. *Science.* **255**, 989-991 (1992).
[508] Sawano, A., Takahashi, T. *et al.* Flt-1 but not KDR/Flk-1 tyrosine kinase is a receptor for placenta growth factor, which is related to vascular endothelial growth factor. *Cell Growth Differ.* **7**, 213-221 (1996).
[509] Waltenberger, J., Claesson-Welsh, L. *et al.* Different signal transduction properties of KDR and Flt1, two receptors for vascular endothelial growth factor. *J Biol Chem.* **269**, 26988-26995 (1994).
[510] Seetharam, L., Gotoh, N. *et al.* A unique signal transduction from FLT tyrosine kinase, a receptor for vascular endothelial growth factor VEGF. *Oncogene.* **10**, 135-147 (1995).
[511] Takahashi, T., Yamaguchi, S. *et al.* A single autophosphorylation site on KDR/Flk-1 is essential for VEGF-A-dependent activation of PLC-gamma and DNA synthesis in vascular endothelial cells. *EMBO J.* **20**, 2768-2778 (2001).
[512] Chevalier, D., Thorin, E. *et al.* Simultaneous measurement of ERK, p38, and JNK MAP kinase cascades in vascular smooth muscle cells. *J Pharmacol Toxicol Methods.* **44**, 429-439 (2000).
[513] Bonny, C., Oberson, A. *et al.* IB1 reduces cytokine-induced apoptosis of insulin-secreting cells. *J Biol Chem.* **275**, 16466-16472 (2000).
[514] Dickens, M., Rogers, J. S. *et al.* A cytoplasmic inhibitor of the JNK signal transduction pathway. *Science.* **277**, 693-696 (1997).

[515] Joneson, T., Fulton, J. A. *et al.* Kinase suppressor of Ras inhibits the activation of extracellular ligand-regulated (ERK) mitogen-activated protein (MAP) kinase by growth factors, activated Ras, and Ras effectors. *J Biol Chem.* **273**, 7743-7748 (1998).
[516] Schaeffer, H. J., Catling, A. D. *et al.* MP1: a MEK binding partner that enhances enzymatic activation of the MAP kinase cascade. *Science.* **281**, 1668-1671 (1998).
[517] Ebner, M., Lucic, I. *et al.* PI(3,4,5)P3 Engagement Restricts Akt Activity to Cellular Membranes. *Mol Cell.* **65**, 416-431 e416 (2017).
[518] Georgescu, M. M. PTEN Tumor Suppressor Network in PI3K-Akt Pathway Control. *Genes Cancer.* **1**, 1170-1177 (2010).
[519] Zhuang, L., Lin, J. *et al.* Cholesterol-rich lipid rafts mediate akt-regulated survival in prostate cancer cells. *Cancer Res.* **62**, 2227-2231 (2002).
[520] Calay, D., Vind-Kezunovic, D. *et al.* Inhibition of Akt signaling by exclusion from lipid rafts in normal and transformed epidermal keratinocytes. *J Invest Dermatol.* **130**, 1136-1145 (2010).
[521] Chen, J., Somanath, P. R. *et al.* Akt1 regulates pathological angiogenesis, vascular maturation and permeability in vivo. *Nat Med.* **11**, 1188-1196 (2005).
[522] Sun, J. F., Phung, T. *et al.* Microvascular patterning is controlled by fine-tuning the Akt signal. *Proc Natl Acad Sci U S A.* **102**, 128-133 (2005).
[523] Chen, Z. P., Mitchelhill, K. I. *et al.* AMP-activated protein kinase phosphorylation of endothelial NO synthase. *FEBS Lett.* **443**, 285-289 (1999).
[524] Fleming, I., Fisslthaler, B. *et al.* Phosphorylation of Thr(495) regulates Ca(2+)/calmodulin-dependent endothelial nitric oxide synthase activity. *Circ Res.* **88**, E68-75 (2001).
[525] Butt, E., Bernhardt, M. *et al.* Endothelial nitric-oxide synthase (type III) is activated and becomes calcium independent upon phosphorylation by cyclic nucleotide-dependent protein kinases. *J Biol Chem.* **275**, 5179-5187 (2000).
[526] Kim, J., Yang, G. *et al.* AMPK activators: mechanisms of action and physiological activities. *Exp Mol Med.* **48**, e224 (2016).
[527] Fleming, I., Bauersachs, J. *et al.* Ca2+-independent activation of the endothelial nitric oxide synthase in response to tyrosine phosphatase inhibitors and fluid shear stress. *Circ Res.* **82**, 686-695 (1998).
[528] Kim, S. A., Kang, O. H. *et al.* Cryptotanshinone Induces Cell Cycle Arrest and Apoptosis of NSCLC Cells through the PI3K/Akt/GSK-3beta Pathway. *Int J Mol Sci.* **19**, (2018).
[529] Shreberk-Shaked, M. and Oren, M. New insights into YAP/TAZ nucleo-cytoplasmic shuttling: new cancer therapeutic opportunities? *Mol Oncol.* **13**, 1335-1341 (2019).
[530] Yin, F., Yu, J. *et al.* Spatial organization of Hippo signaling at the plasma membrane mediated by the tumor suppressor Merlin/NF2. *Cell.* **154**, 1342-1355 (2013).
[531] Yu, J., Zheng, Y. *et al.* Kibra functions as a tumor suppressor protein that regulates Hippo signaling in conjunction with Merlin and Expanded. *Dev Cell.* **18**, 288-299 (2010).
[532] Zhao, B., Li, L. *et al.* Angiomotin is a novel Hippo pathway component that inhibits YAP oncoprotein. *Genes Dev.* **25**, 51-63 (2011).
[533] Panciera, T., Azzolin, L. *et al.* Mechanobiology of YAP and TAZ in physiology and disease. *Nat Rev Mol Cell Biol.* **18**, 758-770 (2017).
[534] Wada, K., Itoga, K. *et al.* Hippo pathway regulation by cell morphology and stress fibers. *Development.* **138**, 3907-3914 (2011).
[535] Yu, F. X. and Guan, K. L. The Hippo pathway: regulators and regulations. *Genes Dev.* **27**, 355-371 (2013).
[536] Benham-Pyle, B. W., Pruitt, B. L. *et al.* Cell adhesion. Mechanical strain induces E-cadherin-dependent Yap1 and beta-catenin activation to drive cell cycle entry. *Science.* **348**, 1024-1027 (2015).
[537] Notani, D., Gottimukkala, K. P. *et al.* Global regulator SATB1 recruits beta-catenin and regulates T(H)2 differentiation in Wnt-dependent manner. *PLoS Biol.* **8**, e1000296 (2010).
[538] Staal, F. J., Weerkamp, F. *et al.* Wnt target genes identified by DNA microarrays in immature CD34+ thymocytes regulate proliferation and cell adhesion. *J Immunol.* **172**, 1099-1108 (2004).

[539] Ma, B., Fey, M. *et al.* WNT/beta-catenin signaling inhibits CBP-mediated RelA acetylation and expression of proinflammatory NF-kappaB target genes. *J Cell Sci.* **128**, 2430-2436 (2015).
[540] Winston, J. T., Strack, P. *et al.* The SCFbeta-TRCP-ubiquitin ligase complex associates specifically with phosphorylated destruction motifs in IkappaBalpha and beta-catenin and stimulates IkappaBalpha ubiquitination in vitro. *Genes Dev.* **13**, 270-283 (1999).
[541] Liu, J., Liao, Y. *et al.* PI3K is required for the physical interaction and functional inhibition of NF-kappaB by beta-catenin in colorectal cancer cells. *Biochem Biophys Res Commun.* **434**, 760-766 (2013).
[542] Buchberger, E., Payrhuber, D. *et al.* Inhibition of the transcriptional repressor complex Bcl-6/BCoR induces endothelial sprouting but does not promote tumor growth. *Oncotarget.* **8**, 552-564 (2017).
[543] Espinosa, L., Ingles-Esteve, J. *et al.* IkappaBalpha and p65 regulate the cytoplasmic shuttling of nuclear corepressors: cross-talk between Notch and NFkappaB pathways. *Mol Biol Cell.* **14**, 491-502 (2003).
[544] Reynolds, N., O'Shaughnessy, A. *et al.* Transcriptional repressors: multifaceted regulators of gene expression. *Development.* **140**, 505-512 (2013).
[545] Naar, A. M., Lemon, B. D. *et al.* Transcriptional coactivator complexes. *Annu Rev Biochem.* **70**, 475-501 (2001).
[546] Maksour, S., Ooi, L. *et al.* More than a Corepressor: The Role of CoREST Proteins in Neurodevelopment. *eNeuro.* **7**, (2020).
[547] Perissi, V., Jepsen, K. *et al.* Deconstructing repression: evolving models of co-repressor action. *Nat Rev Genet.* **11**, 109-123 (2010).
[548] Graham, T. A., Weaver, C. *et al.* Crystal structure of a beta-catenin/Tcf complex. *Cell.* **103**, 885-896 (2000).
[549] Yamamizu, K., Matsunaga, T. *et al.* Convergence of Notch and beta-catenin signaling induces arterial fate in vascular progenitors. *J Cell Biol.* **189**, 325-338 (2010).
[550] Olsen, J. J., Pohl, S. O. *et al.* The Role of Wnt Signalling in Angiogenesis. *Clin Biochem Rev.* **38**, 131-142 (2017).
[551] Gu, B., Watanabe, K. *et al.* Pygo2 regulates histone gene expression and H3 K56 acetylation in human mammary epithelial cells. *Cell Cycle.* **11**, 79-87 (2012).
[552] Gu, B., Watanabe, K. *et al.* Chromatin effector Pygo2 mediates Wnt-notch crosstalk to suppress luminal/alveolar potential of mammary stem and basal cells. *Cell Stem Cell.* **13**, 48-61 (2013).
[553] Scala, F., Brighenti, E. *et al.* Direct relationship between the level of p53 stabilization induced by rRNA synthesis-inhibiting drugs and the cell ribosome biogenesis rate. *Oncogene.* **35**, 977-989 (2016).
[554] Lindqvist, L. M., Vikstrom, I. *et al.* Translation inhibitors induce cell death by multiple mechanisms and Mcl-1 reduction is only a minor contributor. *Cell Death Dis.* **3**, e409 (2012).
[555] Ruggero, D. and Sonenberg, N. The Akt of translational control. *Oncogene.* **24**, 7426-7434 (2005).
[556] Culjkovic, B., Tan, K. *et al.* The eIF4E RNA regulon promotes the Akt signaling pathway. *J Cell Biol.* **181**, 51-63 (2008).
[557] Yamaguchi, H. and Wang, H. G. The protein kinase PKB/Akt regulates cell survival and apoptosis by inhibiting Bax conformational change. *Oncogene.* **20**, 7779-7786 (2001).
[558] Oda, E., Ohki, R. *et al.* Noxa, a BH3-only member of the Bcl-2 family and candidate mediator of p53-induced apoptosis. *Science.* **288**, 1053-1058 (2000).
[559] Tait, S. W. and Green, D. R. Mitochondria and cell death: outer membrane permeabilization and beyond. *Nat Rev Mol Cell Biol.* **11**, 621-632 (2010).
[560] Kracikova, M., Akiri, G. *et al.* A threshold mechanism mediates p53 cell fate decision between growth arrest and apoptosis. *Cell Death Differ.* **20**, 576-588 (2013).
[561] Aubrey, B. J., Kelly, G. L. *et al.* How does p53 induce apoptosis and how does this relate to p53-mediated tumour suppression? *Cell Death Differ.* **25**, 104-113 (2018).
[562] Comen, E. A., Bowman, R. L. *et al.* Underlying Causes and Therapeutic Targeting of the Inflammatory Tumor Microenvironment. *Front Cell Dev Biol.* **6**, 56 (2018).

[563] Zhang, S., Yang, X. *et al.* Interplay between inflammatory tumor microenvironment and cancer stem cells. *Oncol Lett.* **16**, 679-686 (2018).
[564] Attwell, D., Mishra, A. *et al.* What is a pericyte? *J Cereb Blood Flow Metab.* **36**, 451-455 (2016).
[565] Schaaf, M. B., Garg, A. D. *et al.* Defining the role of the tumor vasculature in antitumor immunity and immunotherapy. *Cell Death Dis.* **9**, 115 (2018).
[566] Siemann, D. W. The unique characteristics of tumor vasculature and preclinical evidence for its selective disruption by Tumor-Vascular Disrupting Agents. *Cancer Treat Rev.* **37**, 63-74 (2011).
[567] Li, W., Khan, M. *et al.* Advances in tumor-endothelial cells co-culture and interaction on microfluidics. *J Pharm Anal.* **8**, 210-218 (2018).
[568] Nicoli, S., Ribatti, D. *et al.* Mammalian tumor xenografts induce neovascularization in zebrafish embryos. *Cancer Res.* **67**, 2927-2931 (2007).
[569] Richmond, A. and Su, Y. Mouse xenograft models vs GEM models for human cancer therapeutics. *Dis Model Mech.* **1**, 78-82 (2008).
[570] Hayashi, C., Viereck, J. *et al.* Porphyromonas gingivalis accelerates inflammatory atherosclerosis in the innominate artery of ApoE deficient mice. *Atherosclerosis.* **215**, 52-59 (2011).
[571] Mai, J., Virtue, A. *et al.* An evolving new paradigm: endothelial cells--conditional innate immune cells. *J Hematol Oncol.* **6**, 61 (2013).
[572] Kisselev, A. F. and Goldberg, A. L. Proteasome inhibitors: from research tools to drug candidates. *Chem Biol.* **8**, 739-758 (2001).
[573] van Cruijsen, H., Giaccone, G. *et al.* Epidermal growth factor receptor and angiogenesis: Opportunities for combined anticancer strategies. *Int J Cancer.* **117**, 883-888 (2005).
[574] Nakamichi, M., Akishima-Fukasawa, Y. *et al.* Basic Fibroblast Growth Factor Induces Angiogenic Properties of Fibrocytes to Stimulate Vascular Formation during Wound Healing. *Am J Pathol.* **186**, 3203-3216 (2016).
[575] Prasain, N. and Stevens, T. The actin cytoskeleton in endothelial cell phenotypes. *Microvasc Res.* **77**, 53-63 (2009).
[576] Goudarzi, K. M. and Lindstrom, M. S. Role of ribosomal protein mutations in tumor development (Review). *Int J Oncol.* **48**, 1313-1324 (2016).
[577] Schader, K. A. The cell cycle: a review. *Vet Pathol.* **35**, 461-478 (1998).

VIII APPENDIX

1. Declaration

Except where stated otherwise by reference or acknowledgement, the work presented was generated by myself under the supervision of my advisors during my doctoral studies. All contributions from colleagues are explicitly referenced in the thesis. The material listed below was obtained in the context of collaborative research:

Figure 22: Vioprolide A reduces the laser-induced CNV leakage *in vivo*. Conceptualization and performance of the *in vivo* experiment was performed by Yanfen Li and Prof. Dr. Stylianos Michalakis (Department of Ophthalmology, University Hospital, Ludwig Maximilians University of Munich (LMU), Munich, Germany). Data interpretation and figure preparation belong to my own contributions.

Figure 23: Vioprolide A attenuates the cell infiltration to CNV laser lesion areas *in vivo*. Conceptualization and performance of the *in vivo* experiment was performed by Yanfen Li and Prof. Dr. Stylianos Michalakis (Department of Ophthalmology, University Hospital, Ludwig Maximilians University of Munich (LMU), Munich, Germany). Data interpretation and figure preparation belong to my own contributions.

Figure 24: Vioprolide A lowers the leukocyte-endothelial cell interaction *in vivo*. Conceptualization and performance of the *in vivo* experiment was performed by Dr. Matthias P. Fabritius and Prof. Dr. Christoph A. Reichel (Department of Radiology, University Hospital, Ludwig Maximilians University of Munich (LMU), Munich, Germany and Department of Otorhinolaryngology and Walter Brendel Centre for Experimental Medicine, Clinical Centre of the Ludwig Maximilians University of Munich (LMU), Munich, Germany). Data interpretation and figure preparation belong to my own contributions.

Figure 25: Treatment of HUVECs with up to 10 nM of vioprolide A has no impact on cell viability. Performance of part (A, 24h+48h) was performed by Dr. Betty Luong (Institute of Pharmaceutical Biology, Goethe University, Frankfurt, Germany). Data interpretation and figure preparation belong to my own contributions.

Figure 26: Apoptotic cell death of HUVECs is not increased by vioprolide A up to 10 nM. Performance of part (A, 24h+48h) was performed by Dr. Betty Luong (Institute of Pharmaceutical Biology, Goethe University, Frankfurt, Germany). Data interpretation and figure preparation belong to my own contributions.

Figure 27: Concentrations below 30 nM of vioprolide A do not impair the membrane integrity of HUVECs. Performance of part (A, 24h+48h) was performed by Dr. Betty Luong (Institute of Pharmaceutical Biology, Goethe University, Frankfurt, Germany). Data interpretation and figure preparation belong to my own contributions.

Figure 51: Vioprolide A reduces the sprouting area of choroidal explant cultures. Conceptualization and performance of the *ex vivo* experiment was performed by Yanfen Li and Prof. Dr. Stylianos Michalakis (Department of Ophthalmology, University Hospital, Ludwig Maximilians University of Munich (LMU), Munich, Germany). Data interpretation and figure preparation belong to my own contributions.

Whenever a figure, table or text is identical to a previous publication, it is stated explicitly in the thesis that copyright permission and/or co-author agreement has been obtained. The following parts of the thesis have been previously published:

Figure 1: Differentiation of hemangioblasts into endothelial cells.

Figure 2: Phenotypes and permeability of the vascular endothelium.

Figure 3: Healthy and dysfunctional vascular endothelium.

Figure 4: Triggers and outcomes of inflammation.

Figure 5: The multistep cascade of leukocyte-endothelial cell interaction.

Figure 6: Triggers and pathological consequences of chronic inflammation.

Figure 7: Steps of the canonical NF-κB signaling pathway.

Figure 8: Model of the nuclear import and export system.

Figure 9: Steps of sprouting angiogenesis.

Figure 10: Schematic overview of the tip and stalk cell selection.

Figure 11: Activation cascade of the VEGFRs.

Figure 12: Overview of the MAPKs ERK, JNK, and p38 and their respective activation mechanism.

Figure 13: Activation and downstream processes of Akt.

Figure 14: Regulation of the transcriptional coactivator YAP/TAZ.

2. Publications

2.1. Original publications

Published:

Luisa D. Burgers, Betty Luong, Yanfen Li, Matthias P. Fabritius, Stylianos Michalakis, Christop A. Reichel, Rolf Müller, Robert Fürst. **The natural product vioprolide A exerts anti-inflammatory actions through inhibition of its cellular target NOP14 and downregulation of importin-dependent NF-κB p65 nuclear translocation.** Biomed Pharmacother. 2021; 144: 112255.

Anna Proschak, Giada Martinelli, Denia Frank, Marco J. Rotter, Steffen Brunst, Lilia Weizel, Luisa D. Burgers, Robert Fürst, Ewgenij Proschak, Izidor Sosič, Stanislav Gobec, Thomas A. Wichelhaus. **Nitroxoline and its derivatives are potent inhibitors of metallo-β-lactamases.** Eur. J. Med. Chem. 2021; DOI: 10.1016/j.ejmech.2021.113975

In preparation:

Luisa D. Burgers, Yanfen Li, Stylianos Michalakis, Sarah Ciurus, Stefan Zahler, Rolf Müller, Robert Fürst. **The protein synthesis inhibitor vioprolide A inhibits angiogenic processes through downregulating VEGF receptor 2- and Hippo-signaling.** In preparation.

2.2. Reviews

Luisa D. Burgers, Robert Fürst. **Natural products as drugs and tools for influencing core processes of eukaryotic mRNA translation.** Pharmacol Res. 2021; 170: 105535.

2.3. Poster presentations

Luisa D. Burgers, Yanfen Li, Stylianos Michalakis, Stefan Zahler, Robert Fürst. **The myxobacterial metabolite vioprolide A inhibits angiogenic processes through its cellular target NOP14.** Annual Meeting of the Deutsche Pharmazeutische Gesellschaft e.V. (DPhG), September 29 – October 1, 2021, virtual conference.

Luisa D. Burgers, Betty Luong, Christoph A. Reichel, Rolf Müller, Robert Fürst. **Vioprolide A reduces pro-inflammatory processes in human endothelial cells – inhibition of protein translation as central mechanism?** Annual Meeting of the Deutsche Pharmazeutische Gesellschaft e.V. (DPhG), September 1 – 4, 2019, Heidelberg, Germany.

2.4. Oral presentations

Luisa D. Burgers, Betty Luong, Yanfen Li, Matthias P. Fabritius, Stylianos Michalakis, Christoph A. Reichel, Rolf Müller, Robert Fürst. **Vioprolide A exerts anti-inflammatory actions in endothelial cells through inhibiting NOP14 and downregulating KPNA2.** 69th International Congress and Annual Meeting of the Society for Medicinal Plant and Natural Product Research (GA), September 6 – 8, 2021, virtual conference.

Luisa D. Burgers, Betty Luong, Matthias P. Fabritius, Christoph A. Reichel, Yanfen Li, Stylianos Michalakis, Rolf Müller, Robert Fürst. **Vioprolide A reduces pro-inflammatory processes in human endothelial cells – inhibition of protein translation as central mechanism?** 6th Germany Pharm-Tox Summit and 87th Annual Meeting of the German Society for Experimental and Clinical Pharmacology and Toxicology (DGPT), March 1 – 3, 2021, virtual conference.

Luisa D. Burgers, Betty Luong, Stefan Zahler, Rolf Müller, Robert Fürst. **Vioprolide A impairs angiogenic processes in human endothelial cells *in vitro* – inhibition of protein translation as central mechanism?** 5th Germany Pharm-Tox Summit and 86th Annual Meeting of the German Society for Experimental and Clinical Pharmacology and Toxicology (DGPT), March 2 – 5, 2020, Leipzig, Germany.

3. Acknowledgement/Danksagung

An erster Stelle möchte ich Prof. Dr. Robert Fürst meinen tiefsten Dank aussprechen, für die Möglichkeit meine Promotion am Institut für Pharmazeutische Biologie durchführen zu können und Teil seiner Arbeitsgruppe sein zu dürfen. Vielen Dank für deine hervorragende, individuell gestaltete Betreuung, regelmäßige fruchtbare Diskussionen, wissenschaftlichen Rat und Unterstützung während der gesamten Promotionszeit. Du hast mich immer dazu motiviert über meine eigenen Grenzen hinauszugehen, mehr zu wagen, neue Ideen zu entwickeln und vor allem nicht aufzugeben. Weiterhin danke ich dir für die Möglichkeit an mehreren Fachtagungen teilzunehmen, sodass ich dort meine Arbeit vorstellen und Kontakte zu anderen Wissenschaftlern knüpfen konnte. Ich habe während meiner gesamten Promotionszeit das motivierende und respektvolle Miteinander sehr geschätzt und bin stolz darauf ein Teil des Arbeitskreises Fürst zu sein.

Ein weiterer großer Dank gilt Prof. Dr. Rolf Marschalek für die freundliche Übernahme des Zweitgutachtens meiner Dissertation sowie für die Arbeit und Zeit beim Erstellen des Gutachtens. Ich danke dir vielmals für die hochinteressanten Diskussionen und deinen wissenschaftlichen Input während der gemeinsamen Instituts-Seminare.

Außerdem möchte ich mich bei meinen Kooperationspartnern bedanken, die durch ihre fachliche Unterstützung maßgeblich am Fortschritt meiner Arbeit beteiligt waren und zu einer schönen Fachpublikation geführt haben. Vielen Dank an Prof. Dr. Rolf Müller für die freundliche Bereitstellung von Vioprolide A, an Yanfen Li und Prof. Dr. Stylianos Michalakis für die Durchführung des laser-induzierten choroidalen Neovaskularisations-Experiments und an Dr. Matthias P. Fabritius und Prof. Dr. Christoph A. Reichel für die Durchführung der Intravitalmikroskopie. Ein besonderer Dank geht auch an Dr. Ilse Zündorf für die große Unterstützung bei Anfertigung von Abbildungen für mein Review und meine Fachpublikation.

Ein großer Dank geht an alle ehemaligen und aktuellen Mitglieder des Instituts für Pharmazeutische Biologie für die angenehme Arbeitsatmosphäre und die gute Zusammenarbeit. Danke an Anna Stark, Anna Siemund, Becci, Betty, Claus, Freia, Ilse, Isabell, Iris, Jaqueline, Jule, Laura, Lea, Mareike, Melissa, Sarah, Sebastian, Thomas, Tobi, Tom, Vanessa, Valerie und alle nicht namentlich genannten Mitarbeiter und Masteranden.
Ein besonders großer Dank geht an meine zwei Sonnenscheine Mareike und Melissa. Mit euch habe ich zwei wundervolle Freundinnen dazugewonnen. Melissa, ich werde deine Gesangseinlagen und deine quirlige Art so sehr vermissen. Meine Antwort auf deine Frage: “I love you, I love you, you love me?” wird immer „yes, I do!” sein. Mareike, du hast mir immer Halt gegeben und ich bin sehr froh, dass wir die Möglichkeit haben, unsere gemeinsamen

Kaffee-und Schoki-Pausen in Zukunft fortzusetzen. Ihr habt mich ab dem ersten Tag auf meiner Reise begleitet und ohne euch wäre meine Zeit im und außerhalb des Labors nicht halb so schön gewesen.
Ich möchte außerdem Anna Stark danken für die spaßigen ersten gemeinsamen Monate im Labor. Du hast mich an die Hand genommen, mir so viel beigebracht und meinen Start in Frankfurt durch deine Herzlichkeit perfekt gemacht.
Danke auch an Sebastian, dafür dass du mit deiner tollen und witzigen Art immer die Stimmung im Labor aufgehellt hast.
Danke weiterhin an Sarah und Lea, dafür dass ihr mein letztes Jahr als Doktorandin im Labor so schön, verrückt und einzigartig gemacht habt und für die schönen After-Work-Erlebnisse bei Lea im Garten. Ein großer Dank geht auch an meine ehemalige Masterandin Jule. Es hat mir großen Spaß bereitet mit dir zusammenzuarbeiten.

Zu guter Letzt möchte ich mich gerne bei meinen Freunden und meiner Familie bedanken.
Liebe Miri, ich danke dir für deine Zuversicht und dein Verständnis, wenn ich mich vor lauter Arbeit und Stress mal länger nicht gemeldet habe. Du hast mir sehr viel Kraft gegeben und ich bin froh, dass du meine beste Freundin bist.
Lieber Tom, ich bin dir zutiefst dankbar für deine unendliche Liebe, Geduld, gute Laune und Aufmunterung in den richtigen Momenten. Du warst immer für mich da, wenn ich an mir selber gezweifelt habe und hast mir einen festen Halt gegeben. Ich bin glücklich und stolz dich an meiner Seite zu haben.
Ein besonderer Dank geht außerdem an Paula und Arek. Ihr habt mich mit gemeinsamen Ausflügen, Balkon- Koch- und Spieleabenden immer wieder daran erinnert, dass es neben der Arbeit auch noch ein Leben gibt.
Mein wichtigster Dank gilt meinen Eltern, Danielle und Jan Willem. Bedankt voor jullie onbeperkte steun en jullie vertrouwen in mijn eigen beslissingen. Jullie hebben altijd in me geloofd en me de vrijheid gegeven om mijn eigen weg te gaan. Bedankt dat jullie altijd naast me staan. Zonder jullie was dit alles nooit mogelijk geweest. Dit werk is aan jullie opgedragen.
Diese Arbeit ist euch gewidmet.